UNIVERSIDADE FEDERAL DE JUIZ DE FORA
FACULDADE DE MEDICINA
PROGRAMA DE PÓS-GRADUAÇÃO EM SAÚDE

Luiz Gustavo de Oliveira

Avaliação do efeito anti-inflamatório e anti-proliferativo de Condroitim sulfato e/ou Glucosamina em células RAW 264.7, IEC-6 e Caco-2.

Juiz de Fora - MG
2019

Luiz Gustavo de Oliveira

Avaliação do efeito anti-inflamatório e anti-proliferativo de Condroitim sulfato e/ou Glucosamina em células RAW 264.7, IEC-6 e Caco-2.

Tese apresentada ao Programa de Pós-graduação em Saúde, da Universidade Federal de Juiz de Fora como requisito para a obtenção do título de Doutor em Saúde.

Orientador: Julio Maria Fonseca Chebli
Co-orientador: Jair Adriano Kopke de Aguiar

Juiz de Fora – MG
2019

Ficha catalográfica elaborada através do programa de geração
automática da Biblioteca Universitária da UFJF,
com os dados fornecidos pelo(a) autor(a)

Oliveira, Luiz Gustavo de .
Avaliação do efeito anti-inflamatório e anti-proliferativo de Condroitim sulfato e/ou Glucosamina em células RAW 264.7, IEC-6 e Caco-2. / Luiz Gustavo de Oliveira. – 2019.
156 f. : il.

Orientador: Júlio Maria Fonseca Chebli
Coorientador: Jair Adriano Kopke de Aguiar
Tese (doutorado) - Universidade Federal de Juiz de Fora, Faculdade de Medicina. Programa de Pós-Graduação em Saúde Brasileira, 2019.

1. Anti-inflamatório. 2. Condroitim sulfato. 3. Glucosamina. 4. Lipopolissacarídeo. 5. RAW 264.7. I. Chebli, Júlio Maria Fonseca, orient. II. Aguiar, Jair Adriano Kopke de, coorient. III. Título.

LUIZ GUSTAVO DE OLIVEIRA

AVALIAÇÃO DO EFEITO ANTI-INFLAMATÓRIO E ANTI-PROLIFERATIVO DE CONDROITIM SULFATO E/OU GLUCOSAMINA EM CÉLULAS RAW 264.7, IEC-6 E CACO-2

Tese apresentada ao Programa de Pós-Graduação em Saúde, da Faculdade de Medicina da Universidade Federal de Juiz de Fora, como requisito parcial para obtenção do título de Doutor em Saúde - Área de Concentração: Saúde Brasileira

Aprovada em: 05 / 08 / 2019

BANCA EXAMINADORA

Prof. Dr. Júlio Maria Fonseca Chebli – Orientador
Universidade Federal de Juiz de Fora

Prof. Dr. Jair Adriano Kopke de Aguiar - Coorientador
Universidade Federal de Juiz de Fora

Profa. Dra. Tarsila Campanha da Rocha Ribeiro
Universidade Federal de Juiz de Fora

Prof. Dr. César Augusto Caneschi
Fundação Presidente Antônio Carlos - Ubá

Profa. Dra. Katia das Neves Gomes
Hospital de Força Aérea do Galeão

Profa. Dra. Roberta Reis Soares
Hospital de Força Aérea do Galeão

Dedico este trabalho à minha MÃE, um presente, um anjo, que ganhei de Deus. Exemplo de ser humano, que com todas as dificuldades encontradas antes de iniciar essa jornada, esteve meu lado me incentivando e dando apoio sempre, pois sem o esforço dela no início de tudo, nada teria acontecido.

AGRADECIMENTOS

Agradeço em primeiro lugar à Deus, por tudo que me proporcionou em minha vida, pois nada é por acaso. E também por ter colocado pessoas especiais em toda trajetória percorrida até aqui.

Agradecer, ao meu orientador, amigo e ‘’pai’’, por essa trajetória que se iniciou em 2006 durante a graduação, com projetos de iniciação científica e continua até hoje com essa Tese de Doutorado. Agradecer também por todas as oportunidades que me proporcionou, pela confiança depositada em mim, além da enorme paciência. Serei eternamente grato a você, meu amigo e orientador.

Agradeço o apoio ao Prof. Júlio Chebli por acreditar em meu projeto desde o mestrado e pela oportunidade de concluir mais esta etapa na minha vida.

Aos professores membros da banca, por terem aceitado analisar o trabalho.

A todos os Professores do programa de pós-graduação em Saúde Brasileira.

A todos os amigos do laboratório de Glicoconjugados, que de forma direta ou indireta contribuíram para a realização do trabalho

Aos demais professores de todo o departamento de Bioquímico, em especial a Valquíria Medeiros e a Elita Scio.

A professora Yara Michelacci, por abrir as portas de seu laboratório na UNIFESP e contribuir com o trabalho.

Ao grande amigo e técnico do laboratório de Bioquímica, Geraldinho pela amizade criada nesse período que perdura até hoje.

Ao meu grande amigo e irmão André, que o destino nos fez encontrar, pelo apoio e incentivo no laboratório desde o inicio na graduação em Juiz de Fora e até este trabalho com os experimentos realizados na UNIFESP.

Aos amigos Júlio e Viviane por todo incentivo e apoio, além dos momentos de descontração nos momentos mais difíceis desse período, obrigado por tudo de coração.

A Julianna, minha namorada e grande amiga, pela paciência, compreensão e incentivo durante todo este tempo.

Aos meus irmãos Felippe e Carlos Henrique (Kaique), pelo exemplo de pessoas, pelo apoio contínuo e incentivo durante toda trajetória desde o mestrado.

A minha avó, que se tornou minha Mãe em vida, pelos puxões de orelha, e preocupação comigo, além de todo apoio e incentivo para finalizar mais essa etapa.

A minha Mãe e ‘’Pai’’, Cidinha, que não está mais presente em vida, mas está ao meu lado em todos as minhas decisões, me iluminando e apoiando, que fez questão antes de partir para um lugar melhor, ver minha inscrição e matrícula no Doutorado. Não tenho palavras para descrever a falta que me faz, mas agradeço a cada dia por ter conhecido uma pessoa tão iluminada.

Por fim agradeço à UFJF e as agências de fomento, CNPQ e CAPES pelos financiamentos disponibilizado à pesquisa e as bolsas de estudo concedida.

“A mente que se abre a uma nova idéia, jamais voltará ao seu tamanho original”

(Albert Einstein)

RESUMO

Condroitim sulfato (CS) e Glucosamina (GlcN) são atualmente indicados para o tratamento de doenças inflamatórias, como osteoartrite, por reduzir em condrócitos a ação do fator de transcrição nuclear NF-kB, atividade de metaloproteinases (MMP), interleucinas, óxido nítrico sintase induzível (iNOS) entre outros mediadores inflamatórios. O objetivo do presente trabalho, foi investigar os efeitos de CS, GlcN e CS/GlcN sobre modelo de inflamação agudo induzido por lipopolissacarídio (LPS) em linhagens celulares RAW 267.4, IEC-6 e Caco-2) bem como entender o mecanismo molecular deste efeito sobre essas linhagens celulares. CS, GlcN e CS/GlcN, foram caracterizados pordiferentes métodos, entre eles, eletroforese em gel de agarose e em gel de poliacrilamida, *fluorophore-assisted carbohydrate electrophoresis* (FACE), e ^{13}C RMN. A atividade anti-inflamatória de CS e GlcN associados ou não foi avaliada pela produção de óxido nítrico (NO), atividade de metaloproteases (MMP-9 e -2), liberação de TNF-α, IL-6 e IL-1β por ELISA. Além do deslocamento nuclear do NF-kB por microscopia confocal de imunofluorescência e expressão de IL-1β e iNOS. As análises demonstraram que o CS utilizado nos testes é caracterizado por ser do tipo 4 sulfatado. CS, GlcN e CS/GlcN foram capazes de reduzir a expressão de iNOS e a produção de NO, além de reduzir os níveis de produção de TNF-α nos macrófagos RAW 264.7. Já CS/GlcN e GlcN reduziram a atividade de MMP-9, e a produção de IL-1β, mantendo uma maior expressão de pro-IL-1β. CS, GlcN e CS/GlcN também diminuiram o deslocamento nuclear do fator de transcrição NF-kB. Dessa forma, esses resultados indicam que CS e GlcN associados ou não apresentam uma atividade anti-inflamatória frente à macrófagos RAW 264.7. Com relação à resposta dos compostos estudados frente as células IEC-6 e Caco-2, não foi possível avaliar nas condições disponíveis, uma vez, que foi possível estimular um processo inflamatório nas mesmas.

Palavras-chave: Anti-inflamatório. Condroitim sulfato. Glucosamina. RAW 264.7. Lipopolissacarídeo. NF-kB.

ABSTRACT

Chondroitin Sulfate (CS) and Glucosamine (GlcN) are currently indicated for the treatment of inflammatory diseases, such as osteoarthritis, by reducing the action of nuclear transcription factor NF-kB, metalloproteinase activity (MMP), interleukins, nitric oxide synthase inducible (iNOS) among other inflammatory mediators. The objective of the present study was to investigate the effects of CS, GlcN,and CS/GlcN on the model of acute inflammation induced by lipopolysaccharide (LPS) in cell lines RAW 267.4, IEC-6 and Caco-2, as well as, to understand the molecular mechanism of this effect on macrophages RAW 264.7, IEC-6 and Caco-2. CS and GlcN were characterized by agarose gel electrophoresis, polyacrylamide gel for molecular weight, fluorophore-assisted carbohydrate electrophoresis (FACE), and 13C NMR. The anti-inflammatory activity of CS and GlcN associated or not was evaluated by the production of nitric oxide (NO), metalloproteinases activity (MMP-9 and -2), TNF-α, IL-6 and IL-1β by ELISA. In addition, translocation of NF-κB by confocal immunofluorescence microscopy, and expression of IL-1b and iNOS. The analyzes showed that the CS used in the tests is characterized as a chondroitin 4-sulfate. CS, GlcN and CS/GlcN were able to reduce iNOS expression and NO production. In addition to reducing levels of TNF-α in RAW 264.7 macrophages. Already CS/GlcN and GlcN reduced the activity of MMP-9, and the production of IL-1β, maintaining a higher pro-IL-1β expression. Cs, GlcN and CS/GlcN also decreased the nuclear translocationt of the NF-kB. Thus, these results indicate that CS and GlcN associated or not, present an anti-inflammatory activity against RAW 264.7 macrophages. With regard to the response of the compounds studied to IEC-6 and Caco-2 cells, it was not possible to evaluate in the available conditions, once, that we can not stimulate an inflammatory process in them.

Keywords: Anti-inflammatory. Chondroitin sulfate. Glucosamine. RAW 264.7. Lipopolysaccharide. NF-kB.

LISTA DE FIGURAS

LISTA DE TABELAS

LISTA DE ABREVIATURAS E SÍMBOLOS

Δ	presença de insaturação
ΔDi0S	2-acetamido-2-deoxi-3-*O*-(ácido β-D-gluco-4-enepiranosil urônico)-D-galactose, ou dissacarídeo insaturado não sulfatado
ΔDi2S	2-acetamido-2-deoxi-3-*O*-(ácido 2-*O*-sulfo- β-D-gluco-4-enepiranosil urônico)-D-galactose, ou dissacarídeo insaturado 2-sulfatado
ΔDi4S	2-acetamido-2-deoxi-3-*O*-(ácido β-D-gluco-4-enepiranosil urônico)-4-*O*-sulfo-D-galactose, ou dissacarídeo insaturado 4-sulfatado
ΔDi6S	2-acetamido-2-deoxi-3-*O*-(ácido β-D-gluco-4-enepiranosil urônico)-6-*O*-sulfo-D-galactose, ou dissacarídeo insaturado 6-sulfatado
ΔDi2,4S	2-acetamido-2-deoxi-3-*O*-(ácido 2-*O*-sulfo- β-D-gluco-4-enepiranosil urônico)-4-*O*-sulfo-D-galactose, ou dissacarídeo insaturado 2,4-dissulfatado
ΔDi2,6S	2-acetamido-2-deoxi-3-*O*-(ácido 2-*O*-sulfo- β-D-gluco-4-enepiranosil urônico)-6-*O*-sulfo-D-galactose, ou dissacarídeo insaturado 2,6-dissulfatado
ΔDi4,6S	2-acetamido-2-deoxi-3-*O*-(ácido β-D-gluco-4-enepiranosil urônico)-4,6-di-*O*-sulfo-D-galactose, ou dissacarídeo insaturado 4,6-dissulfatado
ΔDi2,4,6S	2-acetamido-2-deoxi-3-*O*-(ácido 2-*O*-sulfo- β-D-gluco-4-enepiranosil urônico)-4,6-di-*O*-sulfo-D-galactose, ou dissacarídeo insaturado 2,4,6-trissulfatado
ΔDiHA	2-acetamido-2-deoxi-3-*O*-(ácido β-D-gluco-4-enepiranosil urônico)-D-glicose, ou dissacarídeo insaturado de ácido hialurônico
μ	micro
Abs	absorbância
Ac	acetato ou acetil
AMAC	2-aminoacridona
C4S	condroitim 4-sulfato
C6S	condroitim 6-sulfato
Cetavlon	brometo de *N*-cetil-*N,N,N*-trimetilamônio

Chase ABC	condroitinase ABC
Chase AC	condroitinase AC
CS	condroitim sulfato
D_2O	óxido de deutério ou água deuterada
DMEM	Dulbeco's
DMSO	dimetil sulfóxido
DS	dermatam sulfato
EBSS	Earle's balanced salt solution
FACE	fluorophore assisted carbohydrate electrophoresis
GAG	glicosaminoglicano
GalNAc	*N*-acetil-D-galactosamina
GlcA	ácido β-D-glucurônico
GlcN	glucosamina
GlcNAc	*N*-acetil-D-glucosamina
Hep	heparina
$HBSS^{++}$	Hank's balanced salt solution, contendo Ca^{2+} e Mg^{2+}
HPLC	high performance liquid chromatography
HS	heparam sulfato
IdoA	ácido α-L-idurônico
IL	interleucina
kDa	quilo Daltons
KS	Keratam sulfato
M	molar
$NaCNBH_3$	cianoborohidreto de sódio
NFkB	fator de transcrição nuclear-kB
PAGE	polyacrylamide gel electrophoresis
PBS	salina tamponada com fosfato

RMN	ressonância magnética nuclear
PG	Proteoglicano
SFB	soro fetal bovino
Tris	Tris hidroximetil aminometano
UV	ultra violeta
Xil	xilose

SUMÁRIO

1 INTRODUÇÃO

1.1 PROTEOGLICANOS E GLICOSAMINOGLICANOS

Proteoglicanos (PGs) são importantes componentes celulares, sendo caracterizados como macromoléculas que possuem pelo menos uma cadeia de glicosaminoglicano ligada covalentemente a um núcleo proteico (KJELLEN; LINDAHL, 1991).

Os glicosaminoglicanos (GAGs) por sua vez, são heteropolissacarídeos de cadeias lineares que consistem de unidades dissacarídicas repetitivas. Tipicamente são polidispersos tendo cadeias com peso molecular variando entre 10-50 kDa. As unidades dissacarídicas são constituídas por uma hexosamina (glucosamina ou galactosamina) e açúcar não nitrogenado (ácido D-glucurônico, ácido L-idurônico ou D-galactose), unidos entre si por ligações glicosídicas. Esses monossacarídeos pode estar sulfatados em diferentes graus e posições, que juntamente com os grupamentos carboxílicos dos ácidos urônicos, conferem alta densidade de cargas negativas a esses polímeros (JACKSON; BUSCH; CARDIN, 1991).

De acordo com o tipo de hexosamina, os GAGs podem ser divididos em galactosaminoglicanos, que incluem condroitim sulfato e dermatam sulfato, e em glucosaminoglicanos, a exemplo de heparam sulfato, heparina, queratam sulfato e ácido hialurônico (MEYER et al., 1982; SAMPAIO; NADER, 2006).

A hexosamina é sempre *N*-acetilada em condroitim sulfato (CS), dermatam sulfato (DS), ácido hialurônico (HA) e queratam sulfato (KS), enquanto na heparina (Hep) a glucosamina é geralmente *N*-sulfatada, e no heparam sulfato (HS) as duas substituições podem ocorrer (MEYER et al., 1982; SAMPAIO; NADER, 2006).

Além da classificação de acordo com o tipo de hexosamina, os GAGs ainda podem ser distinguidos de acordo com o açúcar não nitrogenado. Ácido D-glucurônico é o único encontrado em CS e HA, enquanto KS apresenta galactose. Já em DS, HS e Hep, ácido D-glucurônico e ácido L-idurônico coexistem em proporções variadas (MEYER et al., 1982; SAMPAIO; NADER, 2006).

A presença de grupamentos sulfato em diferentes posições, bem como o tipo de ligação glicosídica intradissacarídica e interdissacarídica aumentam ainda

mais a complexidade destas moléculas (MEYER et al., 1982; SAMPAIO; NADER, 2006).

Com exceção do ácido hialurônico (HA), o único não sulfatado, os GAGs são formados por dois ou mais tipos de unidades dissacarídicas. Diferentes proporções entre esses dissacarídeos são encontradas nos GAGs de diferentes origens e, por isso, cada um deles se constitui numa família. A Figura 1 apresenta as unidades mais frequentes de cada uma dessas famílias de heteropolissacarídeos (ESKO; KIMATA; LINDAHL, 2009).

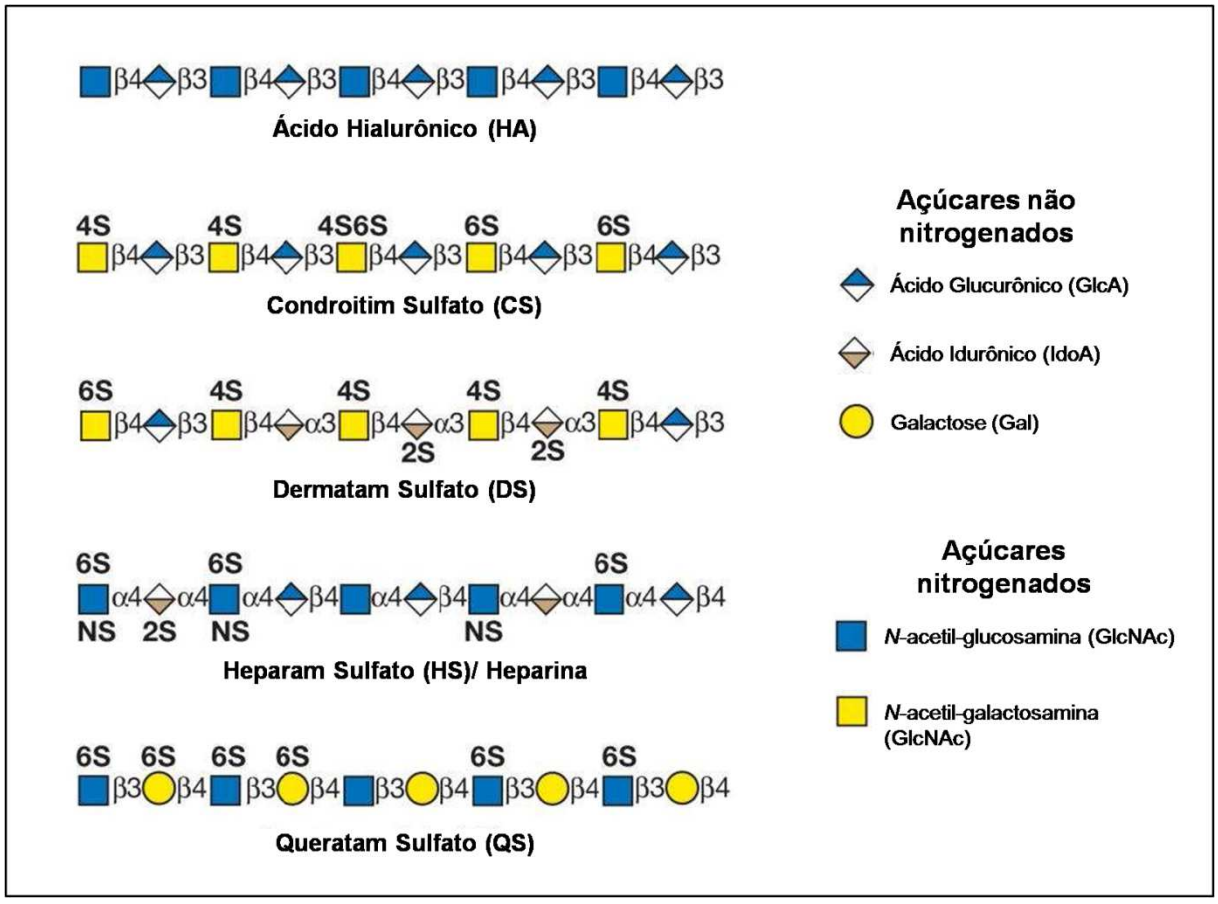

Figura 1. Esquema da composição típica de diferentes famílias de glicosaminoglicanos. GAGs consistem de unidades dissacarídicas repetitivas. Ácido hialurônico não tem grupamentos sulfato, mas os GAGs restantes contêm sulfatos em várias posições. Como descrito no texto, ocorre considerável variação no grau e nas posições de sulfatação, bem como na quantidade de resíduos de ácido idurônico e nas ligações intra e interdissacarídicas. Fonte: Adaptado de ESKO, KIMATA, LINDAHL, 2009

Os GAGs desempenham um papel crítico na sinalização de uma variedade de processos fisiológicos incluindo interação célula-célula, adesão célula-

matriz, proliferação celular, divisão celular, morfogênese, regulação e sinalização molécula (MIKAMI; KITAGAWA, 2013; SAMPAIO; NADER, 2006; SCOTT, 1992; SUGAHARA et al., 1996; TAIPALE; KESKI-OJA, 1997).

Os GAGs são encontrados tanto em animais vertebrados quanto em invertebrados. Estudos pioneiros reportaram a diversidade estrutural de CS, DS e HS em vertebrados, em que foi demonstrado que cada tecido analisado possuía uma composição característica, diferindo entre si quanto à quantidade relativa, tipo e tamanho molecular dos GAGs constituintes, nesses estudos ainda foi visualizado que um mesmo tecido de diferentes vertebrados possuem em geral, o mesmo glicosaminoglicano (DIETRICH; SAMPAIO; TOLEDO, 1976; GOMES; DIETRICH, 1982; TOLEDO; DIETRICH, 1977).

Em 1977, (CASSARO; DIETRICH, 1977) publicaram o primeiro estudo sistemático da distribuição de GAG em todas as classes de invertebrados.

Entretanto, somente a partir do isolamento e caracterização da especificidade de várias liases, sulfatases e glucuronidases bacterianas foi possível realizar a determinação estrutural dos diferentes GAGs. Novas tecnologias têm sido empregadas na determinação estrutural destes compostos, tais como, Ressonância Magnética Nuclear (RMN), Cromatografia Líquida de Alta Eficiência (HPLC), Espectroscopia RAMAN e Eletroforese Capilar (EC) (DESAIRE; LEARY, 2000; KARAMANOS et al., 1994; MAINRECK et al., 2011; MICHELACCI; DIETRICH, 1975, 1976b; MITROPOULOU; STAGIANNIS, 2004; VOLPI, 2007a).

A biossíntese da complexa estrutura dos GAGs é regulada, e os diversos padrões de sulfatação tem demonstrado uma relação tecido e organismo específicos, podendo ainda ter alterações durante o crescimento e desenvolvimento. Mutações em muitos genes de enzimas biosintéticas de GAGs em vertebrados conduzem a severas consequências, indicando que a expressão de específicas estruturas sulfatadas de GAGs desempenham um papel importante na vida (YAMADA; SUGAHARA; ÖZBEK, 2011).

O HA é o GAG estruturalmente mais simples, uma vez que não é sulfatado, sendo constituído por um tipo de unidade dissacarídica (DiHA), constituída por ácido β-D-glucurônico e por *N*-acetilgalactosamina. Este é o único GAG presente como cadeia polissacarídica livre nos tecidos (LAURENT; FRASER, 1992). Essas propriedades estruturais são responsáveis por suas funções fisiológicas, como manutenção da viscoelasticidade do líquido sinovial e do humor vítreo, hidratação e

reparo de tecidos e organização de proteoglicanos na matriz extracelular (COWMAN; MATSUOKA, 2005).

CS, o primeiro GAG a ser isolado (KRUKENBERG, 1884), é constituído por ácido β-D-glucurônico e por *N*-acetilgalactosamina. No entanto, o grau de sulfatação, as posições a que se ligam os grupamentos sulfato e o tamanho do polímero variam de acordo com a espécie animal, o tecido e o estado fisiológico (MICHELACCI et al., 1979; MICHELACCI; DIETRICH, 1986). Suas unidades dissacarídicas podem ser não sulfatadas (Di0S), sulfatadas na posição 4 ou 6 do resíduo de hexosamina (Di4S e Di6S, respectivamente), dissulfatadas na galactosamina ou na galactosamina e na posição 2 do ácido urônico (Di2,4S, Di2,6S, Di4,6S), e em alguns casos podem estar presentes ainda dissacarídeos trissulfatados (Di2,4,6S) ou outros dissacarídeos atípicos em baixas proporções (LAMARI; KARAMANOS, 2006).

DS também é constituído também por ácido β-D-glucurônico e *N*-acetilgalactosamina, mas apresenta também ácido α-L-idurônico, o que o diferencia do CS (FRANSSON; MALMSTROM, 1971). A proporção entre ácido β-D-glucurônico e ácido α-L-idurônico varia conforme a espécie e tecido, assim como o peso molecular (POBLACIÓN; MICHELACCI, 1986).

KS já possui como constituinetes a D-galactose e *N*-acetilgalactosamina, podendo ser sulfatado na posição 6 desses dois resíduos de monossacarídeos. Assim, KS pode possuir unidades dissacarídicas não sulfatadas, monossulfatadas e dissulfatadas (OEBEN et al., 1987). O seu perfil de sulfatação e peso molecular podem variar conforme a origem, e há indícios da presença de outros açúcares em menores proporções, como ácido siálico e fucose (MATHEWS; CIFONELLI, 1965).

HS e Hep são constituídos por D-glucosamina, que pode estar N-sulfatada ou N-acetilada, e tanto por ácido β-D-glucurônico quanto ácido α-L-idurônico. Hep é mais sulfatada, sendo o GAG com maior densidade de cargas aniônicas, além de apresentar alta proporção de ácido α-L-idurônico (70 a 80%) (LINDAHL; AXELSSON, 1971), sendo que a maioria desses resíduos estão sulfatados na posição C2 (SILVA; DIETRICH, 1975), enquanto a hexosamina é geralmente sulfata nas posições N- e C6 (DIETRICH, 1968).

Já HS, apresenta a hexosamina mais *N*-acetilada que sulfatada e possui maior proporção de ácido β-D-glucurônico que a heparina (DIETRICH et al., 1998; GALLAGHER; WALKER, 1985). Em relação ao tamanho dos polímeros,

normalmente o HS é maior, podendo chegar a 50 kDa, enquanto Hep apresenta em média 20 kDa (MENEGHETTI et al., 2015; MULLOY; GRAY; BARROWCLIFFE, 2000).

Tabela 1. Composição dissacarídica dos GAGs e peso molecular modal

	Açúcar não nitrogenado	Ligação	Hexosamina	Ligação	P.M.*
Ácido hialurônico (HA)	Ácido β-D-glucurônico	β(1→3)	β-D-*N*-acetilglucosamina	β(1→4)	5-50 x10^5
Condroitim sulfato (CS)	Ácido β-D-glucurônico	β(1→3)	β-D-*N*-acetilgalactosamina	β(1→4)	2-10 x10^4
Dermatam sulfato (DS)	Ácido α-L-idurônico	α(1→3)	β-D-*N*-acetilgalactosamina	β(1→4)	2-5 x10^4
	Ácido β-D-glucurônico	β(1→3)			
Heparam sulfato (HS) e Heparina (Hep)	Ácido α-L-idurônico	α(1→4)	α-D-glucosamina (N-acetilada ou N-sulfatada)	α(1→4)	0,5-5 x10^4
	Ácido β-D-glucurônico	β(1→4)			
Queratam sulfato (KS)	β-D-galactose	β(1→4)	β-D-*N*-acetilglucosamina	β(1→3)	1-3 x10^4

* O peso molecular modal varia nessa faixa conforme a origem dos GAGs.

Com exceção do HA, os demais GAGs encontram-se ligados covalentemente a um esqueleto proteico nos tecidos, formandos os PGs. A ligação desses GAGs ao esqueleto proteico nos PGs, se faz por meio do tetrassacarídeo ácido glucurônico-galactosil-galactosil-xilose (GlcA-Gal-Gal-Xil), onde a extremidade redutora se une à proteína por uma ligação do tipo *O*-glicosídica entre a xilose do tetrassacarídeo e a hidroxila de um resíduo de serina/treonina. A extremidade não redutora se liga à cadeia de GAG (IOZZO; SCHAEFER, 2015; IOZZO, 1998; SAMPAIO; NADER, 2006).

Os PGs estão amplamente distribuídos em todos os tecidos de animais e apresentam grande diversidade estrutural, o que dificulta sua classificação. Um mesmo tipo de GAG pode estar associado a diferentes proteínas, formando PGs diferentes. Atualmente, a classificação de PGs mais utilizada baseia-se tanto na sua

localização quanto na estrutura do esqueleto proteico e nos tipos de GAGs presentes (IOZZO; SCHAEFER, 2015).

Os PGs podem estar localizados na região intracelular, geralmente em grânulos secretórios como o serglicim, na superfície celular encontram-se os sindecans e glipicans, na matriz extracelular intersticial estão presentes vários outros PGs, como agrecam e versicam (PGs de alto peso molecular), decorim e biglicam (PGs de baixo peso molecular) e na membrana basal encontramos o perlecam (IOZZO; SCHAEFER, 2015).

Os PGs são encontrados em vários tecidos, sendo particularmente abundantes no tecido cartilaginoso articular no qual desempenham uma importante atividade de regulação osmótica associada à presença das cadeias de GAG hidrofílicas, mantendo-o altamente hidratado. A cartilagem possui uma composição importante para a sua propriedade de compressão, onde contém 70-75% (p/p) de água, alto teor de colágeno fibrilar (~20% p/p) e também uma elevada porcentagem de PGs (5-7% p/p) (SEIBEL; ROBINS; BILEZIKIAN, 2006).

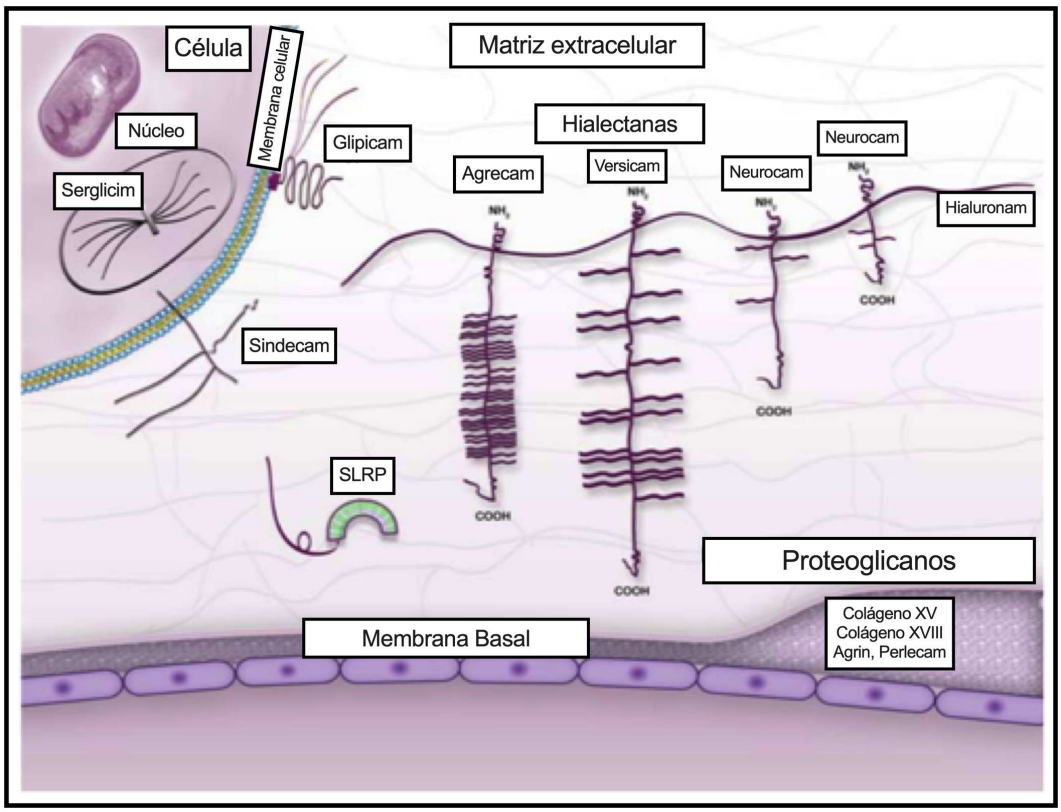

Figura 2. Classificação de Proteoglicanos (PGs) baseado em sua localização e ligação. O grupo heterogêneo de PGs incluem os de matriz extracelular, como os proteoglicanos ricos em Leucina (SLRP) e as Hialectanas, os de superfície celular como o Sindecam e os PGs intracelulares como o Serglicim.

1.2 CONDROITIM SULFATO

Condroitim sulfato é um glicosaminoglicano formado por unidades dissacarídicas repetitivas de ácido D-glucurônico (GlcA) e *N*-acetil-galactosamina (GalNAc), unidas por ligações glicosídicas β(1→3) e β(1→4), [→4GlcAβ1→3GalNAcβ1→]. De acordo com a sulfatação dos dissacarídeos, diferentes tipos de condroitim sulfato são conhecidos. Os principais tipos de condroitim sulfato são classificados como condroitim 4-sulfato (C4S), ou condroitim sulfato A (CS-A), rico em dissacarídeos sulfatados na posição 4 da *N*-acetil-galactosamina (~65% Di4S) e condroitim 6-sulfato (C6S), ou condroitim sulfato C (CS-C), que possui essencialmente *N*-acetil-galactosamina sulfatada na posição 6 (~90% Di6S). O DS, conhecido anteriormente como CS-B, possui uma estrutura hibrida devido à modificação do resíduo de ácido glucurônico, envolvendo epimerização do C-5 para formar ácido idurônico (LAMARI; KARAMANOS, 2006; VOLPI, 2007a).

A proporção relativa dos dissacarídeos na cadeia de condroitim sulfato varia de acordo com o tecido e a espécie. Por exemplo, condroitim sulfato extraído de plaquetas e tecidos cerebrais apresenta mais de 90% de unidades dissacarídicas 4-sulfatadas (DIETRICH et al., 1978; NADER, 1991). Já cartilagem humana normal de indivíduos adultos e cartilagem de tubarão apresentam maior proporção (85%) do dissacarídeo 6-sulfatado (MICHELACCI; HORTON, 1989).

Em animais de origem marinha são encontrados também outros tipos de unidades dissacarídicas. O dissacarídeo E extraído de cartilagem de lula (CS-E) apresenta dois grupos sulfato nas posições 4 e 6 da *N*-acetil-galactosamina (SUZUKI et al., 1968). A unidade dissacarídica D, encontrada em cartilagem de tubarão e arraias (CS-D), apresenta dissacarídeos di-sulfatados na posição 2 do ácido glucurônico e 6 da *N*-acetil-galactosamina (VOLPI, 2007a).

No ambiente marinho, em caranguejos, dissacarídeos conhecidos como tipo K (CS-K), que possuem sulfatação na posição 4 da GalNAc e também são 3-O-sulfatados em GlcA (LAMARI; KARAMANOS, 2006; SUGAHARA; YAMADA, 2000).

A Figura 3 mostra a estrutura de dissacarídeos que formam os diferentes tipos de condroitim sulfato e dermatam sulfato.

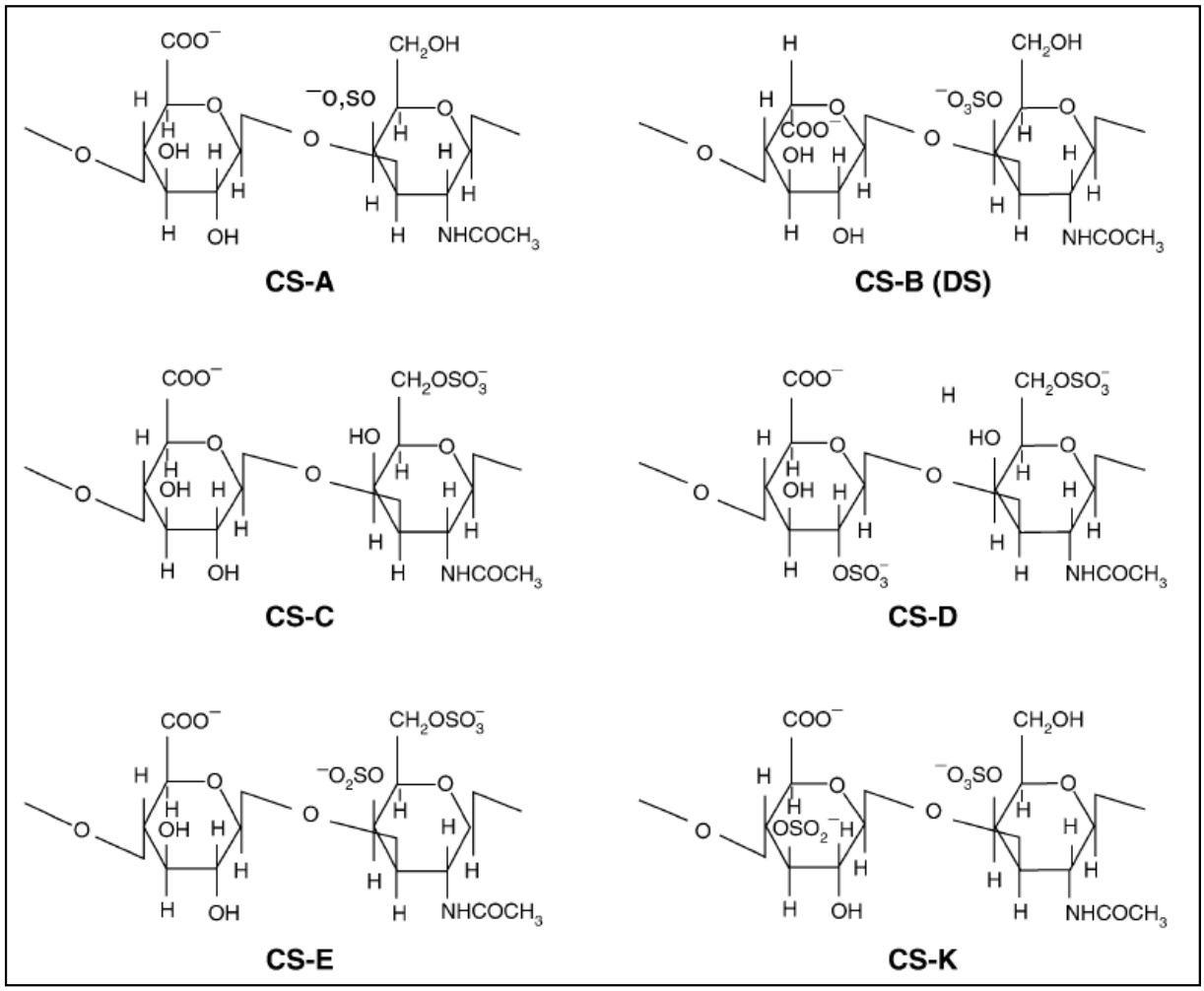

Figura 3. Estrutura química dos dissacarídeos que constituem diversos tipos de Condroitim Sulfato e Dermatam Sulfato. Fonte: STYLIANOU; TRIANTAPHYLLIDOU; VYNIOS, 2006.

A heterogeneidade de estruturas do condroitim sulfato é responsável pelas mais diversas e especializadas funções deste polissacarídeo. Na cartilagem articular, tecido conjuntivo que reveste os ossos, proteoglicanos de condroitim sulfato são os maiores responsáveis por retenção de água no tecido, o que pode ser atribuído às cargas negativas distribuídas na molécula (MARTEL-PELLETIER et al., 2008; STYLIANOU; TRIANTAPHYLLIDOU; VYNIOS, 2006).

Diversas evidências indicam que as cadeias de CS desempenham importantes funções biológicas na inflamação, proliferação celular, diferenciação, migração, morfogênese de tecidos, organogênese, infecção e reparo tecidual, devido a sua capacidade de interagir com diversas compostos tais como moléculas

de matriz, fatores de crescimento, inibidores de protease, citocinas, quimiocinas, moléculas de adesão e fatores de virulência, capacidade esta relacionada à grande densidade de cargas negativas, a suas longas cadeias e em domínios funcionais dependendo da combinação de dissacarídeos formadores (BANDTLOW et al., 2000; GEMBA et al., 2002; MARTEL-PELLETIER et al., 2008; VOLPI, 2011).

A compreensão abrangente dos mecanismos nos processos catabólicos e de biossíntese de CS são essenciais para o entendimento de suas funções no organismo. A biossíntese de CS inicia pela síntese da região de ligação GAG-proteína, GlcAβ1–3Galβ1–3Galβ1–4Xylβ1–O-Ser, que é covalentemente ligada a resíduos específicos de serina inseridos em diferentes núcleos proteicos (HAYES et al., 2018; MIKAMI; KITAGAWA, 2013; PRYDZ; DALEN, 2000; SILBERT; SUGUMARAN, 2002).

A estrutura do tetrassacarídeo da região de ligação é montada por adição sequencial progressiva de unidades monossacarídicas: uma Xil (xilose), duas Gal (galactose) sucessivas, e um resíduo de GlcA, pelas correspondentes glicosil-transferases específicas, XylT (xilosiltransferase), GalT-I (β1,4-galactosiltransferase I) , GalT-II (β1,3-galactosiltransferase II) e GlcAT-I (β1,3-glucuroniltransferase I), respectivamente (HAYES et al., 2018; MIKAMI; KITAGAWA, 2013; PRYDZ; DALEN, 2000; SILBERT; SUGUMARAN, 2002).

Após o término da formação do tetrassacarídeo da região de ligação, o primeiro resíduo de GalNAc é transferido para o terminal não-redutor do resíduo GlcA do tetrassacarídeo da região de ligação pela ação de GalNAc transferase I (GalNAcT I), desencadeando a síntese de CS. Em seguida resíduos de GlcA e GalNAc são alternadamente transferidos para as crescentes cadeias de CS pelas ações de enzimas GlcAT-II (glucuroniltransferase II) e GalNAcT-II (*N*-acetilgalactosaminiltransferase II) respectivamente. Glicosiltransferases com dupla atividade (glucuroniltransferase II e *N*-acetilgalactosaminiltransferase II) também têm sido descritas como responsáveis pela síntese das unidades dissacarídicas repetidas de CS, essas enzimas foram designadas como condroitim sintases (HAYES et al., 2018; MIKAMI; KITAGAWA, 2013; PRYDZ; DALEN, 2000; SILBERT; SUGUMARAN, 2002).

Modificações destas cadeias crescentes de CS são realizadas por enzimas, tais como GlcA C5-epimerase e uma série de sulfotransferases, construindo a diversidade estrutural de CS. As sulfotransferases catalisam a

transferência de um resíduo de sulfato de 3'-fosfoadenosina 5'-fosfosulfato (PAPS) para uma posição específica GalNAc, GlcA ou IdoA em CS/DS, formando desse modo padrões de sulfatação altamente heterogêneos. As sulfatações dos polímeros de CS podem compreender apenas GalNAc4S; somente GalNAc6S; tanto GalNAc4S e GalNAc6S no mesmo polissacarídeo e ainda GalNAc4,6S; GlcA 2- ou 3- sulfato e também GalNAc não sulfatada também podem ser formadas. No mecanismo de sulfatação de CS, uma unidade O não sulfatada é utilizada como um substrato aceptor comum de dois tipos de O-sulfotransferases, uma catalisa a sufatação na posição 4 da GalNAc formando GalNAc4S e outra realiza 6-O-sulfatação dos resíduos de GalNAc, originando GalNAc6S. Subsequentes sulfatações das unidades A e C formadas também podem ocorrer formando dissacarídeos dissulfatados D e E (BAENZIGER, 2003; HAYES et al., 2018; ITO; HABUCHI, 2000; MIKAMI; KITAGAWA, 2013; SAMPAIO; NADER, 2006).

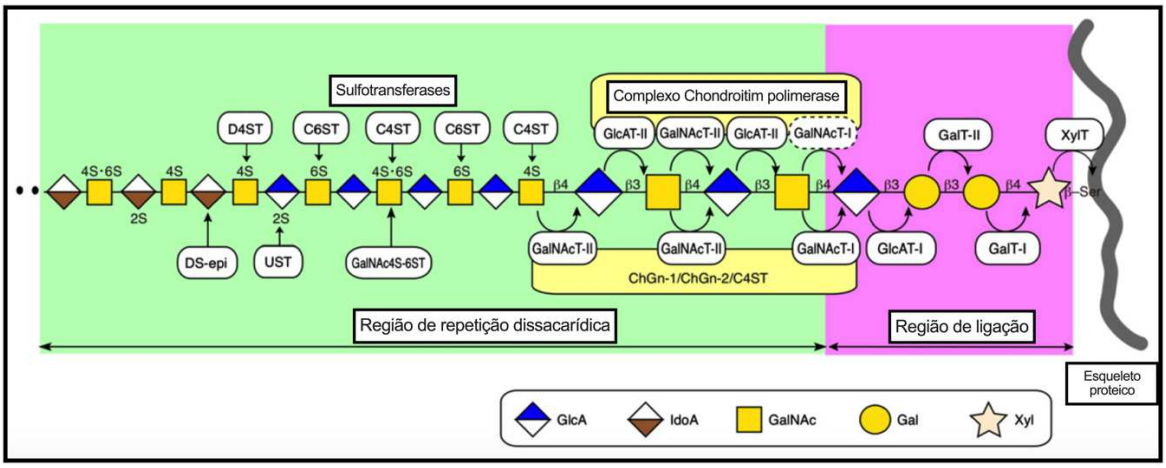

Figura 4. Mecanismo de biossíntese de CS. Fonte: HAYES et al., 2018.

1.3 USO FARMACOLÓGICO DO CONDROITIM SULFATO E GLUCOSAMINA

Atualmente, CS é prescrito como medicamento em países europeus, tendo sido classificado como evidência 1A pelas recomendações da EULAR (*European League Against Rheumatism*) para o tratamento de OA de joelho e de mão (JORDAN et al., 2003). A utilização de CS como adjuvante terapêutico para tratamento de OA permite reduzir o uso de AINEs (Anti-inflamatório não esteroidal), além de melhorar os sinais clínicos da doença (CLEGG et al., 2006).

No Brasil, o condroitim sulfato é registrado pela ANVISA como medicamento. Quanto à denominação dada a esse princípio ativo no país, pode-se encontrar sulfato de condroitina ou condroitina sulfato de sódio. Neste trabalho, este insumo farmacêutico será denominado condroitim sulfato, que é a tradução mais adequada do termo “chondroitin sulfate”. A utilização de condroitim sulfato no regime terapêutico da osteoartrite melhora a função das articulações, pois reduz a dor e o edema articular e impede o estreitamento do espaço articular. Além disso, a segurança e tolerância do fármaco mostram-se favoráveis ao uso (UEBELHART et al., 2006).

Entretanto, ainda são controversas as bases bioquímicas e fisiológicas que levam à melhora dos quadros clínicos de doenças articulares após tratamento com CS (LAMARI et al., 2006). Na busca deste entendimento, verificou-se que esta macromolécula apresenta certa ação anti-inflamatória, reduzindo a expressão de mediadores, como citocinas, na resposta induzida por LPS em condrócitos (CAMPO et al., 2009). Esta resposta parece ser mediada pelo fator de transcrição NF-κB (JOMPHE et al., 2008).

Além disso, outras ações farmacológicas do CS, que parecem depender de sua capacidade de interagir, por exemplo, com outras moléculas de matriz, fatores de crescimento, inibidores de protease, citocinas, quimiocinas, moléculas de adesão e fatores de virulência de patógenos, também vêm sendo investigadas (VOLPI, 2011).

Em experimentos *in vitro*, o CS reduziu a concentração de citocinas pró-inflamatórias, como fator de necrose tumoral (TNF-α) e interleucina-1β (IL-1β), e provocou ainda diminuição da concentração sistêmica e articular de óxido nítrico e espécies reativas de oxigênio possivelmente agindo sobre a translocação do NF-kB (DU SOUICH et al., 2009; IOVU; DUMAIS; DU SOUICH, 2008).

O CS reduziu também o nível de proteases de matriz mediado por IL-1β, como as metaloproteases de matriz (MMP-2, MMP-3, MMP-9, MMP-13 e MMP-14) (IMADA et al., 2010).

Estudo prévio realizado em nosso laboratório, utilizando modelo experimental de colite induzida por dextran sulfato de sódio (DSS), observamos que a administração de CS juntamente com Glucosamina (GlcN) promoveu um efeito protetor e anti-inflamatório nos animais (OLIVEIRA, 2013).

Estes compostos foram capazes de reduzir o índice de atividade da doença (IAD) nos animais do grupo colite tratado com CS e GlcN quando comparados ao grupo colite. Além de retardar os sinais clínicos, observamos melhoras nos parâmetros hematológicos, evitando a redução no número de eritrócitos (P<0,01 vs grupo colite), e a redução de hemoglobina (P<0,05 vs grupo colite) (OLIVEIRA, 2013).

CS e GlcN também evitou alterações histológicas significativas, como erosões da mucosa, destruição das células caliciformes e das criptas bem como infiltração de leucócitos observadas no grupo colite tanto pelas colorações com hematoxilina e eosina (HE) e azul de alcian. Estas moléculas ainda reduziram a atividade de mieloperoxidase (MPO; P<0,01 vs grupo colite) um importante marcador de infiltrado inflamatório. Comprovando os resultados observados na histologia (OLIVEIRA, 2013).

No mesmo trabalho, dosamos os níveis de NO tecidual no cólon dos animais e observamos que NO foram reduzidos quando houve a administração de CS e Glu no grupo colite (P<0.05 vs grupo colite), enquanto os grupos controles mantiveram um nível basal desta molécula (OLIVEIRA, 2013).

Análise da atividade de MMP-2 e MMP-9 realizada por zimografia mostrou no grupo colite, além do aumento da atividade de MMP-2 comparado aos grupos controles, o aparecimento da atividade de MMP-9. Já, o tratamento do grupo colite com CS e Glu, notamos que houve uma redução significativa da atividade de MMP-9 (P<0.05 vs grupo colite) e uma atividade menor de MMP-2 não significativa. Este resultado se destaca, pela importância do CS e GlcN participando da redução da atividade de MMP-9, responsável pelo dano tecidual e presente nos animais induzidos, e uma manutenção da atividade de MMP-2, envolvida no reparo tecidual. Portanto, de acordo com nossos resultados estas moléculas se mostram promissoras para o tratamento de DII, necessitando de estudos mais aprofundados no seu envolvimento com a resposta inflamatória (OLIVEIRA, 2013).

1.4 HOMEOSTASE INTESTINAL E IMUNOPATOGÊNESE

O trato gastrointestinal humano é colonizado por um grande número de microrganismos, responsáveis por garantir o funcionamento intestinal (NELL; SUERBAUM; JOSENHANS, 2010). Esta microbiota desempenha algumas funções,

como a manutenção da integridade da barreira epitelial, proteção contra toxinas nocivas e irritantes à mucosa intestinal, além de reduzir a susceptibilidade dos hospedeiros a infecções por organismos enteropatogênicos (YU; HUANG, 2013).

Porém um desequilíbrio no trato gastrointestinal, decorrente da alteração do número e da diversidade de microrganismos, pode resultar em aumento de patógenos capazes de desencadear uma resposta imune excessiva (BOUMA; STROBER, 2003).

O crescimento de bactérias patogênicas como a *Escherichia coli* enterohemorrágica, leva uma produção de metabólitos como o ácido sálico durante a inflamação intestinal, contribuindo com o aumento da resposta imune e consequente produção de citocinas pró-inflamatórias (HUANG et al., 2015).

Sabe-se que a flora intestinal humana é composta de espécies bacterianas pertencentes a alguns filos principais, Firmicutes, Bacteroidetes, Proteobacteria e Actinobacteria (MATIJASIC et al., 2016).

Estudos realizados em pacientes portadores de doença de Crohn e colite ulcerativa têm mostrado uma diminuição significativa de bactérias dos filos Bacteriodetes e Firmicutes, que ajudam na homeostase intestinal, e aumento de bactérias do filo Proteobacteria, que contribuem para a inflamação descontrolada na DII (NEMOTO et al., 2012; SHA et al., 2013).

Deste modo, os microrganismos presentes no intestino desempenham papel chave na regulação na resposta imune intestinal, por isso são considerados importantes no desenvolvimento das DII (ANDERSEN et al., 2012).

A mucosa intestinal coexiste em equilíbrio com um amplo espectro de espécies bacterianas e seus metabólitos presentes no lúmen intestinal. A manutenção do equilíbrio funcional, denominado homeostase intestinal, é fundamental para preservar a fisiologia normal da mucosa. Perturbações na homeostase intestinal podem contribuir para a fisiopatologia de muitos transtornos gastrointestinais, incluindo DII (KHOR; GARDET; XAVIER, 2011).

A preservação da homeostase da mucosa intestinal depende da complexa interação entre as células epiteliais intestinais (IECs), da microbiota intestinal e das células imune locais, como macrófagos, células dendríticas, linfócitos B, linfócitos T e células estromais. Desequilíbrios nessa dinâmica celular podem resultar em um processo inflamatório (MALOY; POWRIE, 2011).

A função do sistema imune intestinal é coordenar esse equilíbrio celular e garantir uma resposta eficiente contra as bactérias patogênicas, bem como manter uma tolerância a microbiota residente (GEREMIA et al., 2014). Para tal, o sistema imunológico utiliza diferentes mecanismos de defesa, divididos em imunidade inata e imunidade adquirida (HUANG; CHEN, 2016).

A imunidade inata é uma resposta mais rápida, sendo esta responsável pela proteção inicial do hospedeiro contra patógenos, enquanto a imunidade adquirida desenvolve-se mais lentamente, porém confere longa duração (memória imunológica). Ambas desempenham papéis chaves e interligados na patogênese das DII (SIEGMUND; ZEITZ, 2011).

Nesse contexto, a primeira linha de defesa da imunidade inata é fornecida pelas células epiteliais intestinais (IECs) que formam uma barreira física e bioquímica, a fim de manter a segregação entre as comunidades microbianas do lúmen e o sistema imunitário da mucosa intestinal (GOTO; IVANOV, 2013). Além disso, IECs especializadas apresentam outras funções que são essenciais para a homeostase intestinal, como a secreção de mucina, peptídeos antimicrobianos (isoenzimas, defensinas, lectinas entre outros), compostos que influenciam a colonização microbiana, modulação das respostas imune e detecção de microrganismos patogênicos e não-patogênicos (PETERSON; ARTIS, 2014).

Pacientes com DII podem apresentar disfunção em algumas IECs especializadas (célula de Paneth) e isso contribui para o aumento da inflamação intestinal por meio da redução da secreção de defensinas (KOSLOWSKI et al., 2010).

Esses indivíduos ainda possuem uma camada de IEC mais sensível e propensa à descamação durante o processo inflamatório, podendo ocorre apoptose destas células. Tais alterações proporcionam aumento da permeabilidade na barreira epitelial intestinal e induzem o tráfico antigênico do lúmen para a lâmina própria do intestino (GEROVA et al., 2011; KIESSLICH et al., 2012).

A partir do momento em que ocorre a translocação bacteriana pela barreira epitelial, as células imunitárias são ativadas para reagir contra o microrganismo invasor (NEURATH, 2014) (Figura 5).

Inicialmente por meio da expressão receptores de reconhecimento padrão (PRRs), principalmente receptores *Toll-Likes* (TLRs), na superfície de fagócitos (macrófagos e neutrófilos), capazes de reconhecer padrões moleculares associados

à patógenos (PAMPs) como, por exemplo, lipopolissacarídeos (LPS), peptideoglicanos e flagelinas, em grande parte derivadas de microrganismos que atravessaram a barreira epitelial intestinal (ABREU, 2010; GERSEMANN; WEHKAMP; STANGE, 2012).

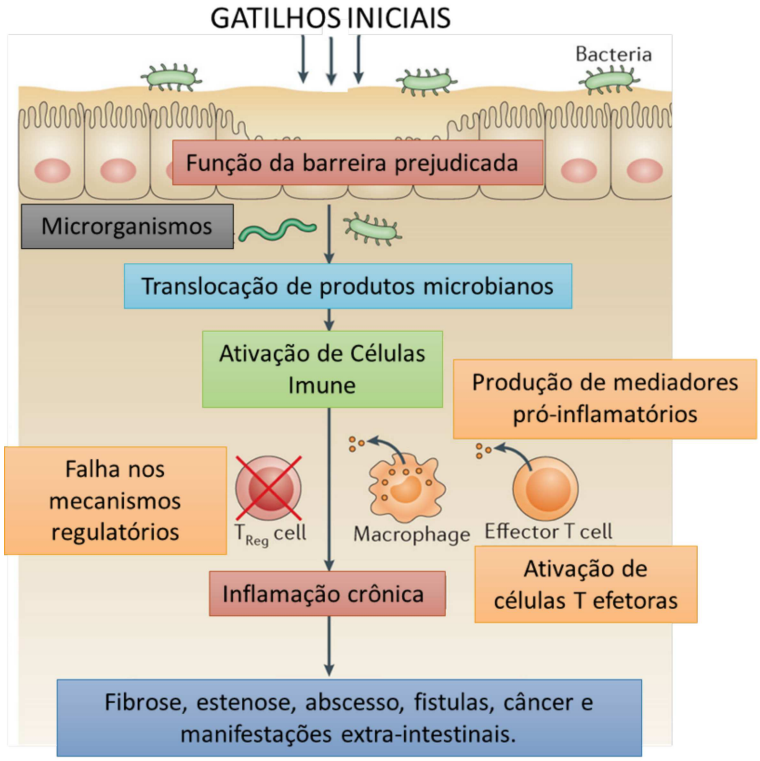

Figura 5. Mecanismo para a patogênese de DII. *Treg cell* (célula T reguladora), *Macrophage* (macrófagos), *Effector T cell* (célula T efetora). Fonte: Adaptado de NEURATH, 2014.

As células dendríticas e os macrófagos também atuam como células apresentadoras de antígenos (APCs - *antigen presenting cells*) e contribuem para a iniciação e regulação de fenômenos da imunidade adquirida (SIEGMUND; ZEITZ, 2011). De modo que, as APCs são fundamentais na diferenciação de linfócitos T virgem em células T efetoras (Th1, Th2, Th17) e T reguladoras (Treg ou Th3) (STROBER, 2013).

Estudos direcionados para a compreensão da imunopatogênese das DII demonstram que a disfunção da resposta imunológica, ocasiona a polarização de células da imunidade adquirida dos indivíduos portadores destas patologias (XU et al., 2014).

Na doença de Crohn há um predomínio de células Th1 secretoras de INF-γ, em virtude da diferenciação dos linfócitos T virgens em decorrência da produção

de IL-12 e TNF-α por células mononucleares. Enquanto na colite ulcerativa ocorre predomínio de resposta Th2 associada com aumento de IL-5, IL4 e produção de IL-13 (LARMONIER et al., 2015).

Os linfócitos T reg também são cruciais na resposta imune adquirida da mucosa intestinal, pois controlam a ativação exacerbada de reações inflamatórias em processos crônicos. A liberação de citocinas inibitórias, como IL-10 e TGF-β, estimulam a ativação de Treg, e consequentemente tem ação supressora sobre o processo inflamatório intestinal (HIMMEL et al., 2012).

Quando uma inflamação aguda da mucosa não é resolvida por mecanismos anti-inflamatórios ou pela supressão da resposta imune pró-inflamatória, um quadro de inflamação crônica desenvolve-se. Por sua vez, a inflamação crônica pode causar complicações nas DII e também a destruição dos tecidos (NEURATH, 2014).

Assim por meio de uma resposta imune exacerbada ocorre uma intensa síntese e liberação de diferentes mediadores inflamatórios, incluindo espécies reativas de oxigênio e nitrogênio e inúmeras citocinas pró-inflamatórias (MUZES et al., 2012).

Além disso, a destruição celular e ulceração da mucosa, observadas clinicamente ao longo processo inflamatório intestinal, ocorrem devido ao aumento da secreção e atividade enzimática de mieloperoxidases e proteases, especialmente as metaloproteases, que influenciam na remodelação tecidual e degradação de matriz extracelular da mucosa intestinal destes pacientes (DE BRUYN et al., 2016).

1.5 ATIVAÇÃO DE MACRÓFAGOS DA LINHAGEM RAW 264.7 POR LPS E MDP

Conforme demonstrado anteriormente, os fagócitos mononucleares, como os macrófagos, são fundamentais para manutenção da homeostase intestinal, portanto são potenciais células alvo na terapia anti-inflamatória em diversas patologias, como as DII.

A infecção de células por microrganismos, ativam a resposta inflamatória. A inflamação é uma resposta do corpo para remover esse estímulo bem como promover a cura e o reparo tecidual (MEDZHITOV, 2008; TAKEUCHI; AKIRA, 2010).

Os fagócitos mononucleares são uma das populações de leucócitos mais abundantes da mucosa intestinal saudável, e os macrófagos residentes estão

presentes ao longo de todo o trato gastrointestinal, localizados na lâmina própria próxima à monocamada de células epiteliais (BAIN; MOWAT, 2014).

Estes macrófagos desempenham várias funções que lhes permitam contribuir tanto para a tolerância imunológica via inércia seletiva, quanto em respostas imunes em quadros patológicos por meio de sua ativação (MANN; LI, 2014).

A ativação dos macrófagos, podem se dar, por meios de PRRs que são os responsáveis por reconhecerem a presença de microrganismos. Esse reconhecimento se dá por meio de estruturas conservadas, presentes em espécies microbianas, chamadas de PAMPs (CUI et al., 2014).

Além disso, evidências atuais indicam que os PRRs também reconhecem moléculas liberadas de células danificadas conhecidas como DAMPs (padrão molecular associado ao dano celular) (CUI et al., 2014; TAKEDA; AKIRA, 2015).

Atualmente quatro diferentes classes da família PRR são identificadas, entre elas, incluem proteínas transmebranas como os receptores Toll-like (TLRs) e receptores lecitina tipo-C (CLRs), bem como proteínas citoplasmáticas tais como gene indutor de Ácido retinóico (RLRs) e os receptores NOD-like (NLRs) (AKIRA; UEMATSU; TAKEUCHI, 2006; MOGENSEN, 2009; TAKEDA; AKIRA, 2004; TAKEUCHI; AKIRA, 2001).

Após a invasão de um patógeno, esses PRRs podem desencadear vias de sinalização para a ativação de NF-kB, Interferon tipo I (IFN) ou ativação de um complexo inflamasoma, o que resulta na produção de citocinas e quimiocinas pro-inflamatórias e consequente ativação da resposta imune adaptativa (CUI et al., 2014; IWASAKI; MEDZHITOV, 2004; TAKEDA; AKIRA, 2004).

Esses genes codificam citocinas pró-inflamatórias como, IFNs, quimiocinas e proteínas antimicrobianas, proteínas estas envolvidas na modulação da sinalização dos PRRs. Vale ressaltar que a expressão de proteínas dos genes induzidos varia com os receptores PRRs ativados (TAKEUCHI; AKIRA, 2001).

A resposta inflamatória é orquestrada por citocinas proinflamatórias como TNF-α, IL-1 e IL-6. Essas citocinas regulam a morte celular de tecidos inflamatórios, modificam a permeabilidade do endotélio vascular, recrutamento de células do sangue para o tecido inflamado e a produção de proteínas de fase aguda (TAKEUCHI; AKIRA, 2010).

Embora, TNF e IL-6 são principalmente reguladas em nível transcricional e translacional, a produção de IL-1β é regulada em dois passos. O primeiro passo é a expressão de um zimogênio, pro-IL-1β, o qual é regulado pela síntese de mRNA por receptores *Toll-like* principalmente (AKIRA; UEMATSU; TAKEUCHI, 2006; TAKEUCHI; AKIRA, 2010).

Porém, a maturação de IL-1β requer a clivagem da pro-IL-1β por uma protease, a caspase-1, a qual é ativada de forma independente da ativação de TLR. Pois o complexo que ativa capase-1, é chamado de inflamassoma, e é composto de receptores *NOD-like*, ASC e caspase-1 (HE; HARA; NÚÑEZ, 2016).

A família de TLR é uma das mais bem caracterizadas das famílias de PRRs, e é responsável por detectar patógenos invasores fora das células e em endossomos e lisossomos intracelulares (SATOH; AKIRA, 2016).

Diferentes TLRs podem reconhecer diversos padrões moleculares de microorganismos e seus próprios componentes, conforme tabela abaixo.

Tabela 2. Ligantes e localização dos receptores *Toll-like* e *NOD-like*.

PRRs	Localização	Ligante	Origem do ligante
TLR			
TLR1	Membrana plasmática	Lipoproteína Triacil	Bactéria
TLR2	Membrana plasmática	Lipoproteína	Bactéria, vírus, parasitas
TLR3	Endo-lisossoma	dsRNA	Vírus
TLR4	Membrana plasmática	LPS	Bactéria, vírus
TLR5	Membrana plasmática	Flagelina	Bactéria
TLR6	Membrana plasmática	Lipoproteína Diacil	Bactéria, vírus
TLR7 (humano TLR8)	Endo-lisossoma	ssRNA	Vírus, bactéria
TLR9	Endo-lisossoma	Cpg-DNA	Vírus, bactéria, protozoários
TLR10	Endo-lisossoma	Desconhecido	Desconhecido
TLR11	Membrana plasmática	Molécula tipo-Profilina	Protozoários
NLR			
NOD1	Citoplasma	iE-DAP	Bactéria
NOD2	Citoplasma	MDP	Bactéria

Fonte: Elaborado pelo autor, 2019.

Dentre os TLRs, o TLR4 expresso em macrófagos, reconhece lipopolissacarídeos (LPS) na superfície celular. O LPS é um componente derivado da membrana externa de bactérias Gram negativa capaz de ativar este receptor (COCHET; PERI, 2017).

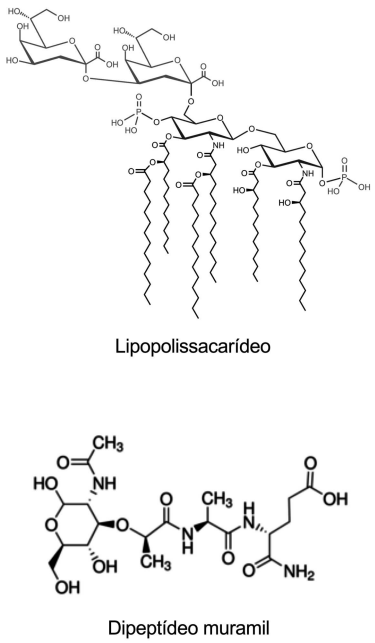

Figura 6. Estrutura química dos ligantes do TLR-4 (Lipopolissacarídeo) e NOD2 (Dipeptideo muramil). Fonte: Elaborado pelo autor, 2019.

Assim a sinalização dos TLRs, ocorrem a partir do reconhecimento de PAMPs levando a um aumento da transcrição de diferentes genes dependendo do tipo de receptor e célula estimulada. A diferença na via de sinalização na célula se deve a moléculas adaptadoras recrutadas pelo tipo de TLR ativado, podendo ser MyD88 e TRIF (AKIRA; UEMATSU; TAKEUCHI, 2006).

A sinalização do TLR2 e TLR4 necessita da interação do MyD88 com a quinase associada a IL-1R (IRAK)-4, uma quinase serina/treonina com um domínio *N*-terminal, a qual ativa outros membros da família IRAK, IRAK-1 e IRAK-2 (KAWAGOE et al., 2008). Estas irão dissociar da molécula adaptadora MyD88 e interagir com fator 6 associado-TNFR (TRAF6) (XIA et al., 2009).

TRAF6 irá fosforilar a quinase IkB (IKK)-β, e dessa forma, o complexo IKK, composto por IKK-α e IKK-β irá fosforilar IkB-α, que irá sofrer degradação,

liberando o NF-kB para migrar para o núcleo e ativar a expressão de citocinas pró-inflamatórias (AKIRA; UEMATSU; TAKEUCHI, 2006).

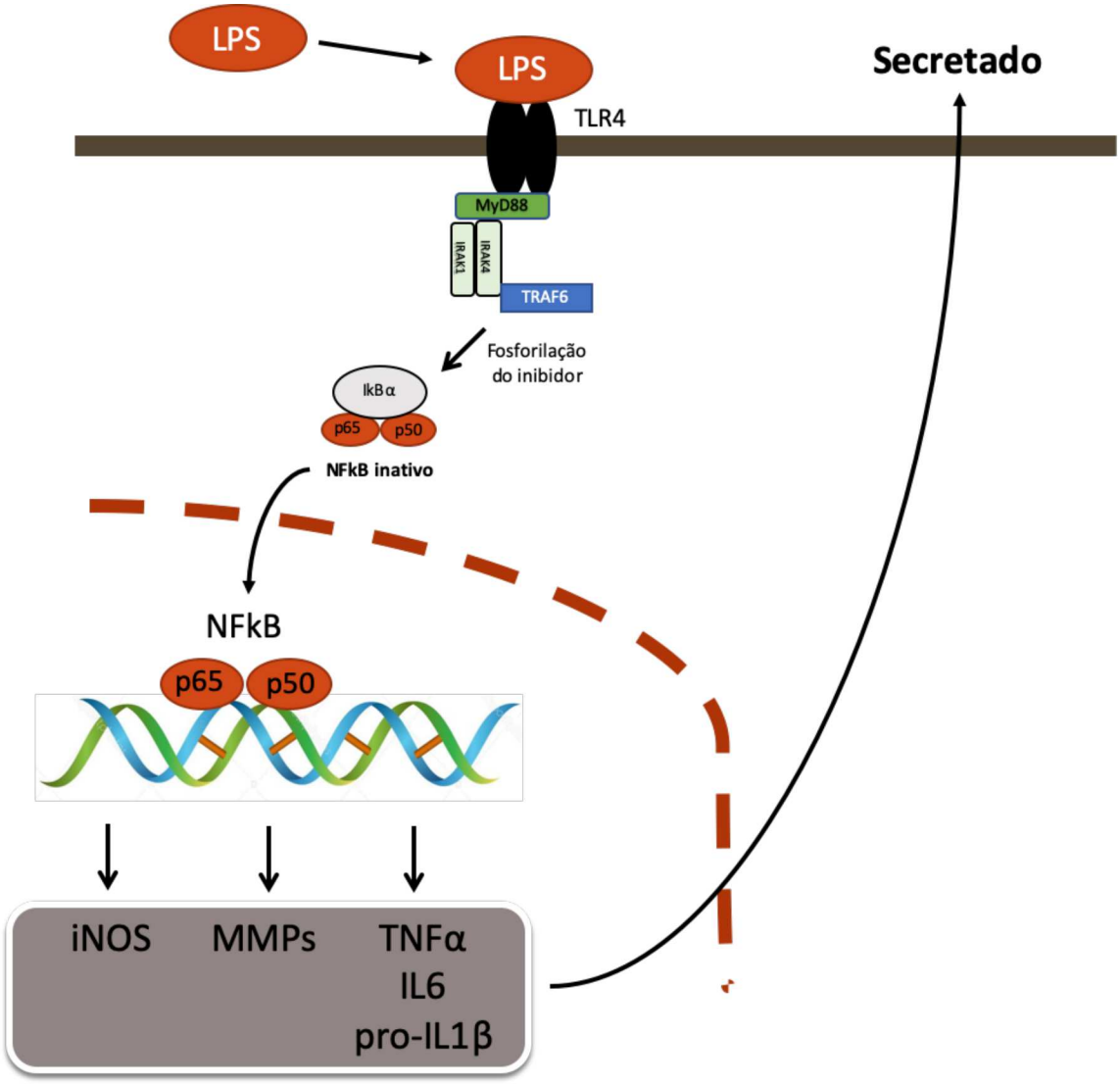

Figura 7. Via de sinalização após ativação do receptor TLR4 por LPS. Fonte: Elaborado pelo autor, 2019.

Já os receptores *NOD-like*, podem levar à formação de complexos proteicos denominados inflamassomas, entre eles, o inflamassoma NLRP3, formado por três estruturas básicas: receptores *NOD-like*, proteína adaptadora (ASC) e pró-caspase 1. Essa caspase ativa é responsável por realizar a maturação proteolítica de IL-1β, que então é liberada para o meio extracelular (HE; HARA; NÚÑEZ, 2016).

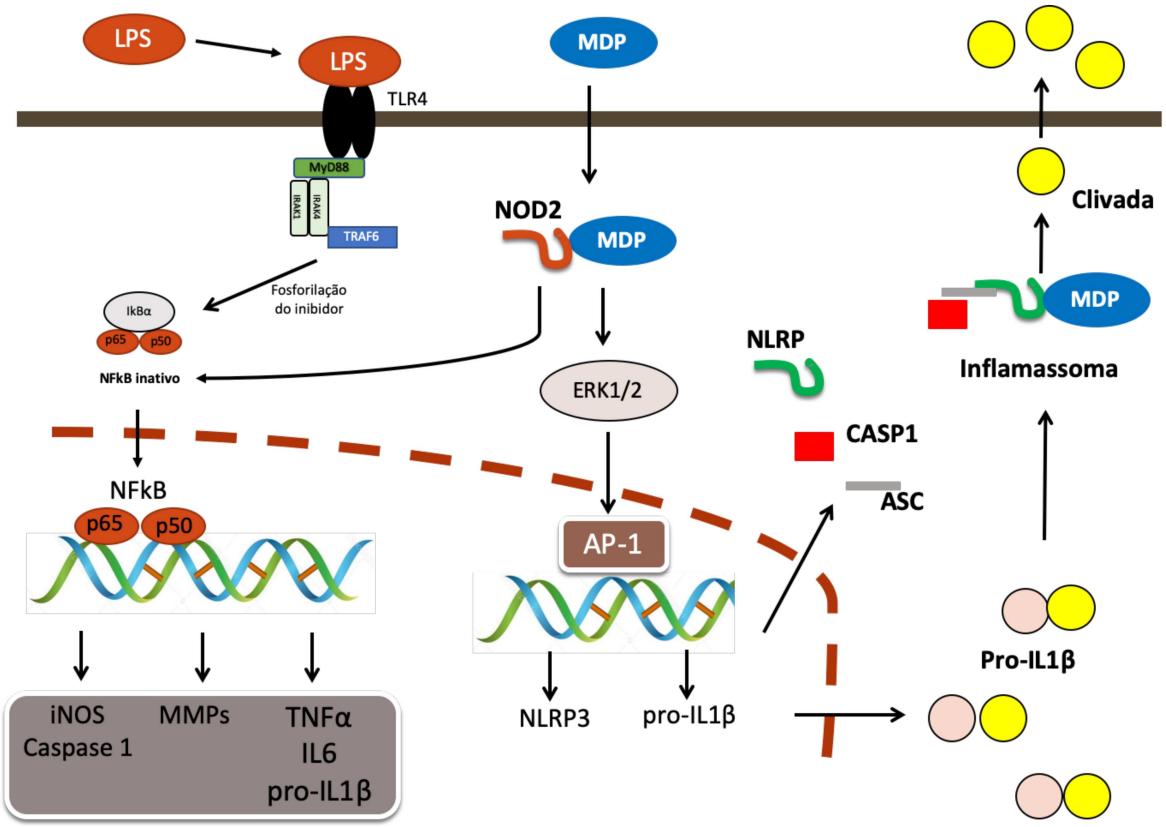

Figura 8. Via de sinalização após ativação simultânea do receptor TLR4 por LPS e ativação do receptor NOD2 por MDP, para formação do inflamassoma NLRP3 e clivagem da pro-IL1-β. Fonte: Elaborado pelo autor, 2019.

1.6 NF-KB E DOENÇA INFLAMATÓRIA INTESTINAL

O NF-κB tem papel fundamental na amplificação da resposta inflamatória, induzindo a expressão de mediadores pró-inflamatórios, como já visto (WULLAERT; BONNET; PASPARAKIS, 2011).

Em um processo inflamatório crônico o aumento da atividade de NF-κB, por células estimuladas, pode culminar com o aumento da transcrição de mediadores inflamatórios, tais como: óxido nítrico sintase induzida (iNOS), ciclooxigenases-2 (COX-2) e várias citocinas, incluindo TNF-α, proIL-1β, e IL-6 que podem provocar inúmeras doenças, dentre essas a DII (HUANG et al., 2015; PARK et al., 2012).

O NF-kB é um fator de transcrição que realiza importante papel, tanto em situações normais como na coordenação de respostas imunes e adaptáveis, regulando a expressão de mediadores inflamatórios (ZINGARELLI; SHEEHAN; WONG, 2003).

Por conta da habilidade de induzir a expressão de vários mediadores pró-inflamatórios, o NF-kB tem sido relacionado como um dos principais fatores de transcrição na fisiopatologia de várias doenças inflamatórias crônicas (HAYDEN; WEST; GHOSH, 2006).

Neste contexto, as indicações iniciais de que o NF-kB está envolvido na patogênese da DII veio com estudos utilizando biópsias de pacientes (WULLAERT, 2010).

Analisando o estado de ativação do NF-kB, pela ativação da subunidade p65 por imunofluorescência em biópsias intestinais com DII foi demonstrado que o NF-kB além de expresso, está ativo em macrófagos e em células epiteliais da mucosa intestinal. Interessante ressaltar que o nível de ativação do NF-kB teve correlação significativa com a severidade da inflamação intestinal (ROGLER et al., 1998).

A ativação de NF-kB é também encontrada em modelos experimentais de doença inflamatória intestinal, incluindo a colite induzida por DSS (ATREYA; ATREYA; NEURATH, 2008).

Dessa forma, por conta de relação do NF-kB com o aumento de citocinas pró-inflamatórias, MMPs, NO e outros mediadores inflamatórios afirma-se que a ativação do NF-kB contribui para uma disfunção ou destruição celular, portanto sua inibição pode melhorar o curso da doença pela redução destes mediadores inflamatórios.

As metaloproteases de matriz (MMPs) que podem estar aumentadas por conta da ativação do NF-kB, são endopeptidases dependentes de cálcio e zinco e consideradas as principais enzimas envolvidas no controle da homeostase de todas as proteínas da matriz extracelular (MEC) em vários níveis incluindo regulação da função, crescimento e divisão celular, regulação da resposta imune, controle da síntese de elementos da MEC. Elas são proteinases capazes de degradarem quase todos os componentes da MEC tais como colágeno, proteoglicanos, fibronectina, elastina e laminina (MEDINA; RADOMSKI, 2006; RAVI; GARG; SITARAMAN, 2007).

No grupo das metaloproteases, existem duas MMPs, MMP-2 e MMP-9, que estão envolvidas na DII. MMP-2 é expressa no cólon normal, principalmente nas células epiteliais e lâmina própria. Durante a DII, a MMP-2 é altamente regulada e seu papel essencial esta relacionada à cicatrização tecidual (RAVI; GARG; SITARAMAN, 2007).

Já MMP-9, como as outras metaloproteases, é sintetizada na sua forma inativa (pró-enzima) que requer uma ativação proteolítica. Porém a pró-MMP9 por si só é capaz de degradar certos tipos de colágeno. Esta gelatinase está ausente em todos os tecidos, exceto neutrófilos, macrófagos e osteoclastos (RAVI; GARG; SITARAMAN, 2007).

Embora estas enzimas apresentem similaridades estruturais possuem efeitos diferentes no desenvolvimento da inflamação intestinal. Expressão de MMP-2 e sua atividade estão aumentadas na colite induzida por DSS, o mesmo foi observado em pacientes com DII. Esse efeito da MMP-2 está relacionado à manutenção da barreira epitelial, já que em ratos *knockout*-MMP-2 os animais foram mais susceptíveis ao desenvolvimento de colite induzida por DSS, e apresentaram uma disfunção da barreira epitelial (GARG et al., 2006).

MMP-9 também se apresenta elevada tanto em atividade como na sua expressão na colite, porém os efeitos desta enzima são contrários aos da MMP-2 (MEDINA et al., 2003).

Outra enzima influenciada pela ativação do NF-kB, a óxido nítrico sintase induzida (iNOS) parece exercer ação direta no processo inflamatório. Existem vários estudos em relação ao papel do óxido nítrico (NO) produzido por esta enzima, como um possível fator na iniciação e propagação do processo inflamatório, isto porque o NO produzido em níveis elevados pela iNOS tem sido associado à desregulação da resposta imune e ao dano tecidual e celular (CROSS; WILSON, 2003).

Estudos mostram que a produção de NO é induzida na inflamação do trato gastrointestinal, sendo que a concentração no reto de pacientes com doença inflamatória intestinal está significativamente maior do que em pacientes saudáveis (HERULF et al., 1998; VERMEIREN et al., 2012).

Este aumento de NO foi atribuído ao aumento da atividade da iNOS no epitélio intestinal mostrando uma expressão maior desta proteína (CROSS; WILSON, 2003; OHTAKE et al., 2010; VERMEIREN et al., 2012).

Em modelo experimental a maioria dos estudos utilizando inibidores da iNOS ou em ratos *knockout*-iNOS mostraram melhoras na colite experimental, sugerindo o envolvimento da iNOS na progressão da DII (OHTAKE et al., 2010).

Portanto, devido aos danos provocados pelo processo inflamatório crônico das DII e a redução na eficácia dos regimes terapêuticos propostos pelos médicos, principalmente devido a dificuldade de adesão dos pacientes ao tratamento

pela presença dos efeitos colaterais, torna-se importante a busca por novos medicamentos para o tratamento da DII.

1.7 JUSTIFICATIVA DO TRABALHO

De acordo com as informações apresentadas, CS e GlcN apresentam atividade anti-inflamatória confirmada em diversos estudos, principalmente em modelos de osteoartrite. A grande maioria dos estudos envolvem a atividade anti-inflamatória destes compostos com uma redução da fosforilação do NF-kB.

Como descrevemos, o NF-kB exerce papel importante na DII, já que sua expressão e atividade estão aumentadas nesta patologia, e dessa forma uma variedade de mediadores envolvidos na inflamação, entre eles MMPs que podem estar envolvidas no reparo/dano tecidual e a iNOS enzima responsável pela produção de NO.

Assim, devido aos resultados já observados por nós, em modelo de colite *in vivo* da ação anti-inflamatória e protetora do CS e GlcN, e esta molécula mostrar-se promissora para o tratamento da DII, faz-se necessário aprofundarmos mais no estudo dos efeitos deste composto e sua possível via de ação, tanto em modelo de inflamação agudo em RAW 264.7, quanto em célula epitelial intestinal (IEC-6 e Caco-2) utilizando modelos *in vitro* de inflamação.

2 OBJETIVOS

2.1 OBJETIVO GERAL

Investigar os efeitos de Condroitim sulfato e ou Glucosamina sobre modelo de inflamação agudo induzido por LPS em linhagens celulares RAW 267.4, IEC-6 e Caco-2.

2.2 OBJETIVOS ESPECÍFICOS

- Avaliar a qualidade dos compostos utilizados, CS, GlcN e CS/GlcN para avaliar a atividade anti-inflamatória

- Investigar o efeito de CS, GlcN e CS/GlcN sobre a produção de óxido nítrico nas linhagens celulares RAW 267.4, IEC-6, Caco-2.

- Avaliar a ação de CS, GlcN e CS/GlcN sobre a produção e expressão de IL-1β, TNF-α, iNOS, MMP-2, MMP-9, em linhagens celulares RAW 267.4, IEC-6, Caco-2.

- Analisar a ação de CS, GlcN e CS/GlcN sobre o fator de transcrição NF-kB em linhagens celulares RAW 267.4, IEC-6, Caco-2.

3 MATERIAIS E MÉTODOS

3.1 MATERIAIS

3.1.1 Eletroforese em gel de agarose

- Câmara de eletroforese em gel de agarose horizontal, da Técnica Permatron Ind. Com. Ltda. (Joinvile, SC, Brasil)
- Lâminas de vidro de 1 mm de espessura, dimensões de 10 x 7,5 cm, 7,5 x 7,5 cm e 5 x 7,5 cm da Geo-Química Produtos Para Laboratórios Ltda (São Paulo, SP, Brasil)
- Agarose da Bio-Rad Laboratories Inc. (Richmond, CA, USA)
- 1,3-diaminopropano da Sigma-Aldrich Co. (St. Louis, MO, USA)
- Brometo de *N*-cetil-*N,N,N*-trimetilamônio (cetavlon) da Aldrich Chemical Co., Inc. (Millwauke, WI, USA)
- Azul de toluidina da Sigma-Aldrich Co. (St. Louis, MO, USA)

3.1.2 Dosagem de proteínas solúveis

- Pierce® BCA Protein Assay Kit, da Thermo Scientific (Rockford, IL, USA)

3.1.3 Eletroforese em gel de poliacrilamida

- Acrilamida e bis-acrilamida da Bio-Rad Laboratories Inc. (Richmond, CA, USA)
- Gelatina incolor da Gelco Gelatinas do Brasil Ltda. (Pedreira, SP, Brasil)
- Coomassie Brilliant Blue R-250 da Sigma-Aldrich Co. (St. Louis, MO, USA)
- Azul de bromofenol da Bio-Rad Laboratories Inc. (Richmond, CA, USA)

3.1.4 Fluorophore assisted carbohydrate electrophoresis

- Dissacarídeos insaturados de CS ΔDi0S, ΔDi4S e ΔDi6S, bem como tetrassacarídeos e oligossacarídeos de CS, foram produzidos por cromatografia em papel preparativa
- 2-aminoacridona (AMAC) da Sigma-Aldrich Co. (St. Louis, MO, USA)
- Cianoboro-hidreto de sódio da Sigma-Aldrich Co. (St. Louis, MO, USA)

3.1.5 Cultura de células

- EBSS (Earle's Balanced Salt Solution) foi preparada em nosso laboratório: cloreto de sódio 6,8 g/L, cloreto de potássio 0,4 g/L, hidrogenofosfato dissódico (Na_2HPO_4) 1,14 g/L, di-hidrogenofosfato de sódio (NaH_2PO_4) 0,12 g/L, di-hidrogenofosfato de potássio (KH_2PO_4) 0,2 g/L, hidrogenocarbonato de sódio ($NaHCO_3$) 2,2 g/L, D-glicose 1,0 g/L e vermelho de fenol 0,01 g/L
- Solução de tripsina 0,25% e EDTA 0,05% Gibco da Life Technologies Inc. (Nova York, NY, USA)
- Soro fetal bovino (SFB) da empresa Cultilab.
- Solução de penicilina (10.000 U/mL) e estreptomicina (10.000 µg/mL) Gibco da Life Technologies Inc. (Nova York, NY, USA)
- Hidrogenocarbonato de sódio, ou bicarbonato de sódio ($NaHCO_3$) da Sigma-Aldrich Co. (St. Louis, MO, USA)
- Meio de cultura DMEM (Dulbecco's Modified Eagle's Medium) alta glicose: glicose 4,5 g/L, com L-glutamina e piruvato de sódio, sem bicarbonato de sódio, da Cultilab.
- Filtros de acetato de celulose (0,22 µM) da Corning Incorporated (Corning, NY, USA)
- Membrana de filtração de 0,22 µM da Merck KGaA (Darmstadt, Alemanha)
- LPS (lipopolissacarídeos de *E. coli* 055:B5 e *Salmonella*), γ-irradiado, da Sigma-Aldrich Co. (St. Louis, MO, USA)
- Câmara de Neubauer da WR Research (São Paulo, SP, Brasil)
- Placas de cultura de 35, 60 e 100 mm da Corning Incorporated (Corning, NY, USA)
- Placas de cultura de 24 poços e 96 poços da Corning Incorporated (Corning, NY, USA)
- Linhagem de macrófagos de camundongo RAW 264.7, IEC6 e Caco-2 foram adquiridas no banco de células do Rio de Janeiro (BCRJ-UFRJ).
- Brometo de 3-(4,5-dimetiltiazolil-2)-2,5-difeniltetrazolium (MTT) foi obtido da Sigma-Aldrich Co. (St. Louis, MO, USA)

3.1.6 Kits de ELISA

Os seguintes kits foram adquiridos da R&D Systems, Inc. (Minneapolis, MN, USA):

- Mouse TNF-α DuoSet ELISA (#DY410)
- Mouse IL-6 DuoSet ELISA (#DY406)
- Mouse IL-1β/IL-1F2 DuoSet ELISA (#DY401)

3.1.7 Imunofluorescência

- Lamínulas de vidro de 13 mm para microscopia confocal da Perfecta Ind. e Com. de lâminas de vidro LTDA (São Paulo, SP, Brasil)
- Lâminas silanizadas da Dako Co. (Carpinteria, California, USA)
- HBSS^{++} (Hank's Balanced Salt Solution, contendo Ca^{2+} e Mg^{2+}) foi preparado em nosso laboratório: cloreto de sódio 0,137 M, cloreto de potássio 5,4 mM, cloreto de cálcio 1,3 mM, sulfato de magnésio 1,0 mM, hidrogenofosfato dissódico 0,25 mM, di-hidrogenofosfato de potássio 0,44 mM, bicarbonato de sódio 4,2 mM, glicose 0,1 g/L
- Solução de paraformaldeído 20% da Electron Microscopy Sciences (Hatfield, PA, USA)
- Anticorpo primário anti-p65 NF-κB, policlonal produzido em coelho, da abcam (Cambridge, MA, USA)
- Anticorpo secundário anti-IgG de coelho conjugado com Alexa Fluor® 488, DAPI (4',6-diamidino-2-fenilindol) e meio de montagem "*Prolong Gold antifade mountant"* da Thermo Fisher Scientific (Waltham, MA, USA)
-

3.1.8 Western blotting

- Membranas de PVDF da Bio-Rad Laboratories Inc. (Richmond, CA, USA)
- Anticorpo monoclonal contra iNOS, IL1-β e β-Actina da *Santa Cruz Biotechnology*, CA, EUA.
- Anticorpo secundário anti-IgG de camundongo produzido em cabra com conjugada com peroxidase foram obtidos da *Santa Cruz Biotechnology*, CA, EUA.

- Substrato quimioluminescente "*SuperSignal West Pico Chemiluminescent Substrate" (PIERCE)* da Thermo Scientific (Rockford, IL, EUA)

3.2 DELINEAMENTO EXPERIMENTAL

O trabalho foi dividido em duas partes, em que primeiramente foi realizado a análise estrutural dos compostos, e posteriormente, analisados os efeitos dos mesmos sobre linhagem de macrófago RAW 264.7, avaliando o potencial efeito anti-inflamatório.

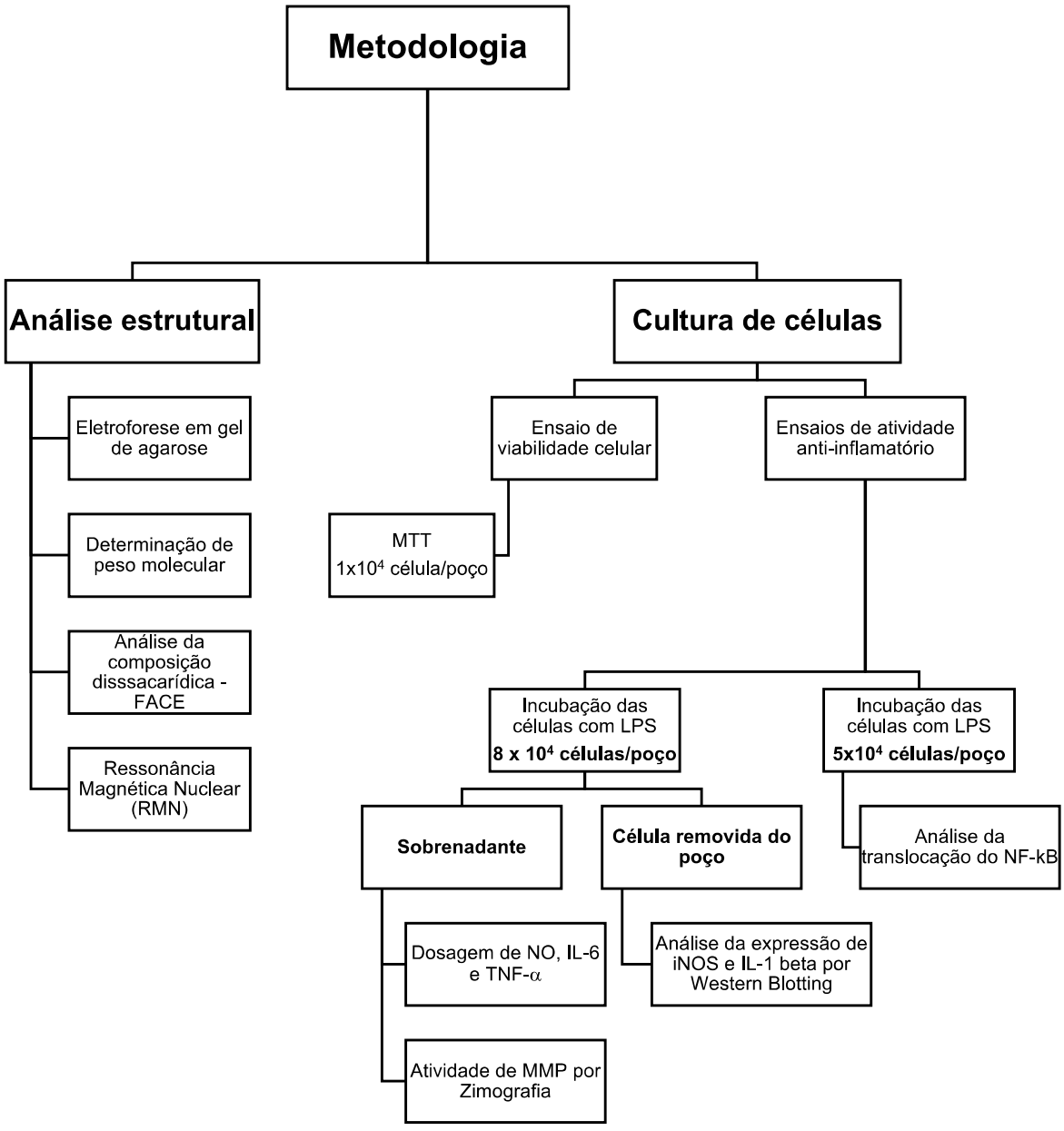

Figura 9. Delineamento experimental. Fonte: Elaborado pelo autor, 2019.

3.3 ANÁLISE ESTRUTURAL DO CONDROITIM SULFATO

3.3.1 Eletroforese em gel de agarose

O CS foi analisado por eletroforese em gel de agarose (0,5%) em tampão 1,3-diaminopropano (PDA) 0,05 M, pH 9,0 (DIETRICH; DIETRICH, 1976). Uma mistura padrão de glicosaminoglicanos (5 µL), contendo condroitim sulfato, dermatam sulfato e heparam sulfato, na concentração de 1 mg/mL cada, foi aplicada às lâminas como controle. A corrida eletroforética foi realizada em câmara refrigerada, submetida a uma diferença de potencial 100 V, por aproximadamente 1 hora. Após a corrida, o gel foi submerso em solução de brometo de cetiltrimetilamônio (CETAVLON) 0,1%, por 2 horas. Após esse período o gel foi seco em corrente de ar quente e corado com azul de toluidina 0,1% em solução de ácido acético 1%:etanol 50% por 20 minutos. O excesso de corante foi posteriormente removido com solução de ácido acético 1%/etanol 50%. O gel foi digitalizado e os glicosaminoglicanos quantificados por densitometria usando o programa TotalLab TL120 1D v 2009 (Nonlinear Dynamics Ltd.).

3.3.2 Determinação do peso molecular

Análise do peso molecular na amostra de CS foi determinada por eletroforese em gel de poliacrilamida adaptado como por Hilborn e Anastassiadis, (1971) (HILBORN; ANASTASSIADIS, 1971) e modificado por Dietrich e Nader, (1974) (DIETRICH et al., 1989).

Alíquotas (20 µg) foram dissolvidas em 10 µL de tampão de amostra (Tris 40 mM, NaCl 20 mM, EDTA 2 mM, glicerol 40%, vermelho de cresol 0,05%) e aplicadas em gel de poliacrilamida 7,5% em tampão Tris-HCl 20 mM. A eletroforese foi realizada em tampão de corrida contendo Tris 40 mM, NaCl 20 mM, EDTA 2 mM pH 8,3 (100 V), em sistema de eletroforese vertical. Após 1 hora de corrida o gel foi removido das placas e corado com azul de toluidina 0,1% em ácido acético 1%, por 10 minutos. O excesso de corante foi removido com solução de ácido acético 1%, e o gel digitalizado e submetido à análise densitomética pelo programa TotalLab TL120 1D v 2009 (Nonlinear Dynamics Ltd.)

3.3.3 Análise da composição dissacarídica

A análise dos dissacarídeos constituintes do CS foi realizada por método enzimático: alíquotas de 10 µL (10 mg/mL) de amostra foram incubadas com 10 mUE condrotinase AC de *Flavobacterium heparinum* à 37ºC no período de 18h. Após o período de incubação, o material foi colocado em banho a 100 ºC por 10 minutos para inativação da enzima, seco a vácuo e ressuspenso em água destilada. A partir desse ponto o material foi analisado pelo método *fluorophore assisted carbohydrate electrophoresis* (FACE).

3.3.3.1 Fluorophore assisted carbohydrate electrophoresis (FACE)

Alíquotas contendo 20 µg do produto da disgestão do CS e da amostra GlcN (monossacarídeo) foram secas à vácuo e derivatizadas com 5 µL de solução de 2-aminoacridona (AMAC) 20 mM (100nmol), na presença de 5 µL de cianoboro-hidreto de sódio 1M. Após 16h a 37ºC foram adicionados 5 µL de glicerol 60%. O material foi imediatamente analisado ou armazenado a -80ºC.

Alíquotas das amostras derivatizadas (2 µL) foram então analisadas em sistema de eletroforese vertical Mini-PROTEAN Tetra Cell com lâminas de 7,2 cm com espaçadores de 0,75. A corrida eletroforética foi realizada em gel de acrilamida-bisacrilamida 25%, preparados em sistema-tampão de Tris-glicina (1) e Tris-borato (2). Para o sistema tampão (1) Tris-glicina os géis foram preparados em tampão Tris-HCl, e foi usado como tampão de corrida Tris-glicina. Para o sistema tampão (2) Tris-borato os géis foram preparados em tampão Tris-borato, e a corrida foi realizada com tampão contendo Tris-borato-glicina (OONUKI et al., 2005).

Gel para Sistema Tris-glicina: Solução para dois géis de corrida foi preparada a partir de 5 mL de solução de acrilamida-bisacrilamida T 40%, C 5%; 1,5 mL de tampão Tris-HCl 1,5 M, pH 8,8 e 3,5 mL de água destilada. Solução para o gel de entrada foi preparado misturando 500 µL de solução de acrilamida-bisacrilamida T 40%, C 5%; 660 µL de tampão Tris-HCl 0,5 M, pH 6,7 e 3,0 mL de água destilada.

Géis para Sistema Tris-borato: Solução para dois géis de corrida foi preparada a partir de 5 mL de solução de acrilamida-bisacrilamida T 40%, C 5%; 2,5 mL de tampão Tris-borato (0,75 M/0,5 M), pH 7,0 e 2,5 mL de água destilada. Solução para o gel de entrada foi preparada com 2 mL de solução de acrilamida-

bisacrilamida T 10%, C 2,5%; 1,0 mL de tampão Tris-borato (0,5 M/0,5 M), pH 6,8 e 1,0 mL de água destilada.

Para eletroforese, 150 mL de tampão de corrida diluído (1X) em água destilada a 4 °C foram adicionados ao anodo. O tampão de corrida estoque (10x) para sistema Tris-glicina foi Tris-glicina (0,25 M/1,92 M), pH 8,3. O tampão de corrida estoque (5X) para sistema Tris-borato foi Tris-borato-glicina (0,6 M/0,5 M/0,5 M), pH 8,3. Após remoção dos pentes, as amostras foram aplicadas no gel, e o catodo foi preenchido com aproximadamente 500 mL de tampão de corrida diluído a 4 °C. O sistema foi submetido a uma diferença de potencial de 100 V, que após cerca de 20 minutos foi aumentada para 220 V. A migração dos sacarídeos derivatizados foi acompanhada durante a corrida usando luz UV320-400nm (luz negra). Após a corrida, as placas foram lavadas com água destilada e as imagens digitalizadas em GelDoc-It Imaging System (transluminador UV com filtro em 365 nm e Câmera scientific grade CCD GelCam 310), em diferentes tempos de exposição.

3.3.4 Ressonância Magnética Nuclear

Os experimentos de RMN de ^{13}C no estado sólido foram realizados em um espectrômetro Bruker Avance III HD 300 (7.04 T), operado a uma frequência de Larmor de 75,00 MHz. As análises foram executadas em uma sonda MAS, em rotores de ZrO2 (e tampas de Kel-F) de 4 mm. Os espectros foram obtidos numa frequência de giro de 10000 Hz, com tempo de relaxação de 2,0 s e um pulso de 90° de 2,5 μs utilizando giro-ao-ângulo mágico, e polarização cruzada. Os deslocamentos químicos foram padronizados de forma indireta através de uma amostra de Glicina, com sinal referente a carbonila em 176,00 ppm em relação ao TMS que é o padrão primário.

3.4 CULTURA DE CÉLULAS

3.4.1 Linhagens Celulares

A linhagem de macrófagos murinos (RAW 264.7), adenocarcinoma colorretal humano (Caco-2) e célula epitelial intestinal (IEC-6) foram adquiridas no banco de células do Rio de Janeiro (BCRJ-UFRJ). Células RAW 264.7, IEC-6 e

Caco-2 foram mantidas em meio de Eagle modificado por Dulbecco (DMEM, Cultilab) suplementado 10% de soro fetal bovino na presença de penicilina (100 UI/ml) e estreptomicina (100 μg/ml). Todas as linhagens foram mantidas a 37ºC sob tensão de 5% de CO_2.

O subcultivo foi realizado semanalmente, como descrito a seguir. Para a manutenção dos estoques celulares, inicialmente o meio foi removido da placa de células em semi-confluência e posteriormente lavadas com solução de EBSS. Em seguida, as células foram incubadas com uma solução de EDTA 5mM (4ml em cada placa de 100x10mm) mantendo-se a placa na incubadora a 37ºC durante o tempo necessário para que as células se desprendam da placa. A seguir, elas foram ressuspendidas, cuidadosamente, várias vezes com uma pipeta e transferidas (aproximadamente $2x10^5$ células) para uma nova placa contendo meio de cultura enriquecido com soro fetal bovino conforme descrito anteriormente e previamente equilibrado a 37ºC. O meio será substituído no dia seguinte ao subcultivo, e após cada 3 dias, até a sua semi-confluência.

3.4.2 Ensaios de atividade anti-inflamatório

Para a realização de ensaios de atividade anti-inflamatória, as células foram subcultivadas em placas de 96 poços (8×10^4 células/poço) ou placas de 10mm (1×10^6 células/placa). Após 24h, o sobrenadante foi removido e foi adicionado meio de ativação (DMEM suplementado com 2% SFB). As células foram incubadas com as substancias testadas e ao mesmo tempo estimuladas com LPS. A concentração de LPS variou de acordo com o tipo de experimento, bem como o tempo de estímulo ao qual as células foram submetidas (informações apresentadas ao longo da descrição dos resultados obtidos em cada experimento).

3.4.3 Ensaio de viabilidade

Atividade citotóxica foi avaliada pelo ensaio de MTT (MOSMANN; METHODS, 1983). Células (70 a 80% de confluência em placas P100) foram obtidas após subcultivo e transferidas para placas de 96 poços ($1X10^4$ célula/poço) e incubadas por 24 horas com 0,2 mL/poço de meio DMEM com 10% de soro fetal bovino, e mantidas em ambiente de 5% de CO_2, a 37ºC. Após esse período, as

placas foram lavadas com salina tamponada estéril (EBSS) e meio contendo as drogas testadas, adicionado. A solução estoque das drogas foi diluída com DMEM sem soro fetal bovino em variadas concentrações. Após 44 horas de incubação, 20 µL de solução (5 mg/mL) de MTT (3-(4,5-dimethylthiazol-2-yl)-2,5-diphenyl tetrazolium bromide - Sigma) foi adicionado a cada poço e incubado a 37°C por 4 horas. O meio foi aspirado, e o produto formado (cristais de formazam) solubilizados com DMSO 100%. A quantidade de MTT-formazam obtida é diretamente proporcional ao número de células vivas (viáveis) e foi determinada pela medida da densidade ótica (OD) a 540 nm em leitor de placas Multiskan Ascent (Thermo Electron Corporation). As determinações foram realizadas em triplicatas ou hexaplicatas.

3.4.4 Análise de marcadores inflamatórios

3.4.4.1 Dosagem de óxido nítrico (NO)

A produção de óxido nítrico (NO) em RAW 264.7, IEC-6 e Caco-2, foi quantificada indiretamente pela dosagem de nitrito no sobrenadante da cultura, pelo do método de Griess, uma vez que, o NO é composto de meia vida curta (TSIKAS, 2007).

Desta forma, as células acima foram cultivados em placas de 96 poços na concentração de $8x10^4$ células/poço (RAW 264.7) e $5x10^4$ ou $100x10^4$ células/poço (Caco-2 e IEC-6) e incubados por 24 horas. Em seguida, as células foram estimuladas com 100 ng/mL de lipopolissacarídeo de *E.coli* (LPS) para linhagens de macrófagos, enquanto nas células IEC e Caco-2 foram utilizadas diferentes concentrações. Concomitante, as células foram tratadas com as amostras em diferentes concentrações, por 48 horas. Ao sobrenadante da cultura celular (100 µl) foi adicionado 100 µl do reagente de Griess (1% sulfanilamida em ácido fosfórico 5% e 0.1% de *N*-[1-nafitil] etilenodiaminadiidroclorídrico em água - Sigma-Aldrich Co, St. Louis, MO, EUA). Após 10 minutos de incubação a absorbância da reação foi determinada por leitura em 540 nm em leitor de microplacas (Thermo Scientific - MULTISKAN GO, Waltham, MA, USA). Um padrão de $Na(NO_2)$ (Sigma-Aldrich Co, St. Louis, MO, EUA) foi utilizado para elaboração de uma curva padrão, e a equação

da reta obtida foi aplicada no cálculo da concentração (µM) de nitrito presente nas amostras.

3.4.4.2 Dosagem de Citocinas

O efeito anti-inflamatório das amostras *in vitro*, foi analisado pela quantificação de citocinas pró-inflamatórias produzidas pelas células citadas acima, induzidas com LPS. As células foram semeadas em placas de 96 poços na concentração de $8x10^4$ células/poço e incubadas por 24 horas. As células foram estimuladas com 100 ng/mL de LPS, e concomitante, tratadas com as amostras em diferentes concentrações por até 84 horas. A dosagem das citocinas, TNF-α, IL-6, IL-10 e IL-1β presentes nos sobrenadantes da cultura celular foi realizada pelo método de ELISA do tipo sanduíche, de acordo com as instruções do fabricante dos kits (Duo Set Kit, RD Systems, Minneapolis, MN, EUA).

3.4.4.3 Atividade de Metaloproteases (Gelatinases)

O efeito das drogas sobre a atividade das metaloproteases de matriz, sintetizadas por células RAW 264.7 induzidas com LPS, foi avaliado por zimografia em gel de poliacrilamida com gelatina. As células foram semeadas em placas de 96 poços, na concentração de $8x10^4$ células/poço. A cultura foi então estimulada com 100 ng/mL de LPS, e concomitante tratada com as drogas em diferentes concentrações por 48 horas. Os sobrenadantes da cultura foram submetidos a quantificação proteica, pelo método BCA, de acordo com as informações do fabricante do Kit, (ThermoScientific® - Kit PRICE BCA, Waltham, MA, USA), tais amostras foram reservadas em freezer -80°C. Posteriormente, foram preparados géis de 0,75 mm com solução de acrilamida-bisacrilamida, e como substrato foi adicionada gelatina à 2,5%. Volumes equivalentes a 10 µg de proteína de cada amostra, previamente quantificadas, foram aplicadas ao gel para migração eletroforética (30 mA à 4ºC) em tampão de Tris-glicina (25mM/192mM). Após a migração, os géis foram lavados com 100 mL de Triton X-100 2% e incubados com 100 mL de tampão de incubação (50 mM Tris-HCl, pH 8.2, 5mM $CaCl_2$ e 1µM $ZnCl_2$) por 24 horas à 37ºC. Em seguida, os géis foram corados com Coomassie Blue R250 (0,5% de corante, 30% de metanol e 10% ácido acético) e descorados com solução

descorante (30% de metanol e 10% ácido acético). A atividade das gelatinases foi evidenciada pela presença de regiões claras nos géis (MIURA et al., 1995; SHAPIRO; KELLEY; KOBAYASHI, 2001).

Para medir a intensidade dessas bandas foi utilizado o programa TotalLab Quant® (England, UK).

3.4.4.4 Análise por Western Blotting

A linhagem celular (RAW 264.7) foram mantidas em placas de petri 100x10 mm. Após atingirem a semi-confluência as células foram subcultivadas para placas de 96 poços e após 24h foram estimuladas com LPS (100 ng/ml) por 48 horas na presença ou ausência das drogas. Após incubação, as células foram coletadas e lavadas por duas vezes em tampão PBS em banho de gelo e em seguida foram rompidas com tampão de lise (50 mM Tris-HCl – pH 7,5, 150 mM NaCl, 1% Nonidet P-40, 2 mM EDTA, 1 mM EGTA, 1 mM $NaVO_3$, 10 mM NaF, 1 mM ditiotreitol, 1 mM PMSF, 25 µg/ml aprotinina e 25 µg/ml leupeptina) e mantidas em gelo por 30 minutos. As células lisadas foram lavadas e a concentração de proteína determinada pelo kit BCA (ThermoScientific® - Kit PRICE BCA, Waltham, MA, USA). Foram aplicados 30 µg de proteína em gel de poliacrilamida-SDS (10%) e submetidas a SDS-PAGE (60mA por 2 h, Bio-rad). Após a corrida eletroforética as proteínas do gel serão transferidas para uma membrana de PVDF em sistema úmido, em tampão Tris 25 mM, glicina 200 mM e metanol 4% a 400mA por 1 h e 30 minutos de eletroforese. Após a transferência das proteínas, as membranas de PVDF serão incubadas com uma solução de leite Molico desnatado 5% em TBS (0,1 M, pH 7,4), Tween 20 0,05% sob agitação branda por 1 h, a temperatura ambiente, a fim de bloquear os sítios inespecíficos da membrana. Cada membrana contendo as proteínas foram incubadas com anticorpos primários monoclonais (iNOS, MMP-9, MMP-2, diluição 1:1000, Santa Cruz Biotechnology, CA, EUA) de acordo com as instruções do fabricante. A expressão proteica será visualizada usando um anticorpo secundário conjugado com peroxidase diluído em TBS-Tween 0,05%, Molico 5%, por 1 h a temperatura ambiente (1:10.000, Santa Cruz Biotechnology). Para a visualização do complexo antígeno-anticorpo a membrana será revelada por quimioluminescência. Após as lavagens com TBS as membranas serão incubadas com o reagente SuperSignal West Pico por no mínimo 5 minutos e então, em

câmara escura a membrana será exposta a um filme de raio-X. O filme será revelado em solução reveladora Kodak, lavado rapidamente em água e fixado em solução fixadora Kodak. A seguir, o filme será lavado em água corrente e seco a temperatura ambiente. Comparação da intensidade das bandas será realizada por análise densitométrica e normalizada pela β-Actina (1:20.000, Santa Cruz Biotechnology).

3.4.4.5 Análise por imunofluorescência confocal do deslocamento nuclear NF- κB

A análise do deslocamento nuclear do NF-κB foi realizada por microscopia de imunofluorescência confocal. RAW 264.7 foi subcultivada sobre lamínulas de 12mm em placas de 24 poços ($5x10^4$ células/poço). Depois de 12h de incubação, o meio foi removido e as células foram tradadas com as amostras em diferentes concentrações e induzidas com LPS (10 ng/mL). Após, 30 minutos, células foram lavadas duas vezes com HBSS ($HBSS^{++}$, HBSS contendo Ca^{+2} e Mg^{+2}), fixadas com paraformaldeído 4% (15 minutos), lavadas três vezes com $HBSS^{++}$, e permeabilizada com metanol -20°C por 15 minutos. Após lavagens ($HBSS^{++}$ 2 x, e 0,1 M glicina in $HBSS^{++}$, 30 min em banho de gelo), as lamínulas foram incubadas sequencialmente com solução de bloqueio (1% BSA, 0,1% Triton X-100 in $HBSS^{++}$, 1 h), anticorpo primário (mouse anti-p65 NF-κB antibody, diluído 1:500 em tampão de bloqueio, 24h, 4ºC), e anticorpo secundário (Alexa Fluor 488-conjugado donkey anti-mouse Igg, diluído 1:250 em tampão de bloqueio. Núcleo foi corado com DAPI (1:5000 em tampão de bloqueio, 30 minutos). Após cada coloração as células foram lavadas com $HBSS^{++}$ para remover os anticorpos não ligados. As lamínulas foram montadas em lâminas de vidro usando meio de montagem Prolong Gold e as imagens de fluorescência foram capturadas por microscópio confocal Leica TCS SP8. Os controlos negativos, preparados sem anticorpo primário, foram utilizados para correção de fundo.

3.4.5 Análise estatística

Os resultados foram apresentados como média ± desvio padrão dos experimentos realizados. A análise estatística foi realizada por análise de variância (ANOVA) seguida de um teste de Dunnet. Resultados de $p<0,05$ foram considerados estatisticamente significativas.

4 RESULTADOS E DISCUSSÃO

4.1 ANÁLISE ESTRUTURAL DO CONDROITIM SULFATO

A caracterização estrutural, físico química e a pureza dos CS (Artrolive® e Extrasul) utilizados nos experimentos foram determinadas por eletroforese em gel de agarose em tampão 1,3 propilenodiamino-acetato (PDA) 0,05M, pH 9,0, eletroforese em gel de poliacrilamida em tampão Tris-Glicina 20mM, pH 7,4, análise do padrão de dissacarídeos com condroitinases de *Flavobacterium heparinum* por FACE e análise espectroscópica por RMN de fase sólida.

Essa análise prévia é importante, pois, o CS pode ser extraído de diferentes fontes animais como de aves, suína, bovina e peixes cartilaginosos para depois ser submetidos a técnicas de purificação para uso comercial (VOLPI, 2019, 2007b, 2009).

Nesse processo uma mistura de CS de diferentes fontes podem ocorrer, produzindo um produto final com diferentes características e propriedades, além do uso de matérias primas não controladas como osso e tecidos moles (MARTEL-PELLETIER et al., 2015; VOLPI, 2019). Isso pode gerar uma substancia com uma estrutura não definida e com baixa reprodutibilidade, tendo como consequência variações no grau de pureza, dos efeitos biológicos, na presença de contaminantes e na segurança e eficácia clínica (VOLPI, 2019).

Além disso, preparações finais de CS podem ser adulteradas adicionando sacarídeos mais baratos e demais substâncias orgânicas que não são capazes de ser determinada com os métodos de controle de qualidade utilizadas pelas industrias farmacêuticas (DA CUNHA et al., 2015; ZHANG et al., 2014).

A seguir apresentamos os resultados obtidos em cada um desses experimentos.

4.1.1 Eletroforese em gel de agarose

As soluções de CS utilizadas nos experimentos apresentaram uma única banda metacromática na eletroforese em gel de agarose em tampão PDA com migração semelhante à do CS presente na mistura padrão de glicosaminoglicanos (Figura 10). Porém, pequena diferença de migração fica evidente na solução de C6S devido à posição dos grupamentos sulfatos.

O método de eletroforese em gel de agarose utilizado neste trabalho, desenvolvido por (DIETRICH; DIETRICH, 1976) Dietrich & Dietrich (1976), é utilizado para a separação de diferentes GAGs, baseando-se na interação entre a diamina presente no tampão e as cargas negativas dos GAGs. Neste método, GAGs mais sulfatados (contendo maior densidade de cargas negativas), como heparam sulfato e heparina, interagem mais com a diamina do tampão e migram menos. Já condroitim sulfato (CS) e dermatam sulfato (DS), por apresentar menor densidade de carga, apresentam maior migração eletroforética. A diferença na migração entre estes dois GAGs, se deve principalmente à conformação espacial do ácido urônico (β-D-glucurônico para CS e α-L-idurônico para DS).

Após a corrida eletroforética, os GAGs são corados por azul de toluidina, um corante que se complexa com os grupamentos sulfato destes compostos produzindo metacromasia, corando-os em roxo. Dessa forma, pode-se afirmar que as soluções utilizadas com CS não estão contaminadas por DS, HS ou heparina.

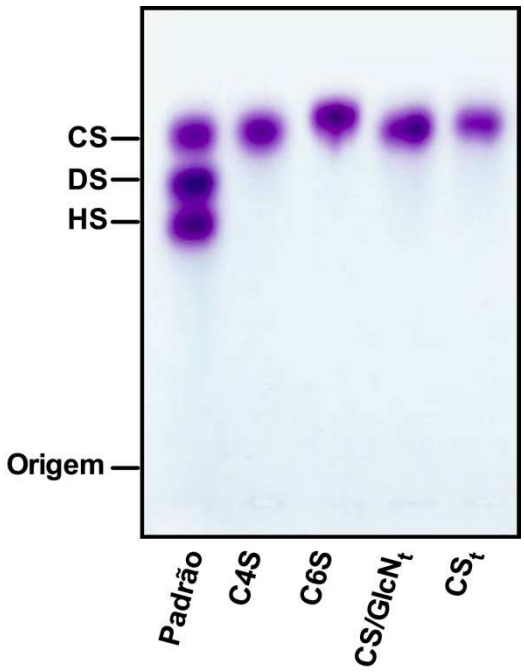

Figura 10. Eletroforese em gel de agarose em tampão PDA, do CS utilizado nos experimentos. Padrão, mistura padrão de glicosaminoglicanos contendo: CS, condroitim sulfato; DS, dermatam sulfato; HS, heparan sulfato; C4S, condroitim 4 sulfato; C6S, condroitim 6 sulfato; $CS/GlcN_t$ (Artrolive®); condroitin sulfato associado à glucosamina usados no experimento; CS_t (Extrasul): condroitim sulfato utilizado nos experimentos.

4.1.2 Determinação do peso molecular

O peso molecular do CS utilizado nos experimentos, foram determinados por eletroforese em gel de poliacrilamida, como descrito em métodos. Todos os CS apresentaram uma dispersão no gel de eletroforese como pode ser observado na Figura 11. A velocidade de migração é inversamente proporcional ao logarítmico do peso molecular.

A

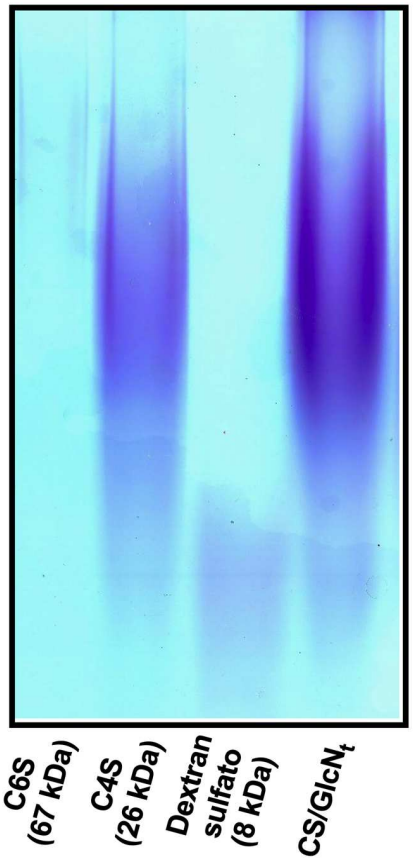

B

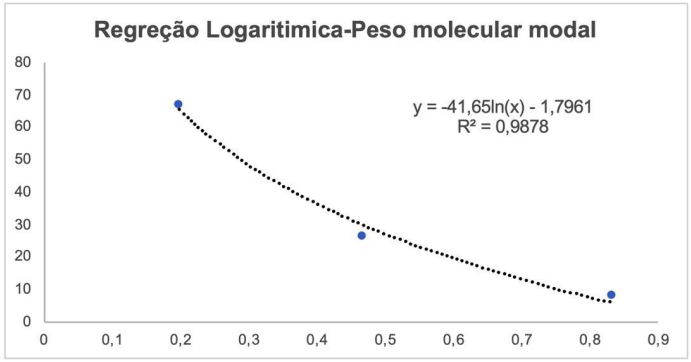

C

	rf	kDa
Dextran sulfato	0,835	8
C4S	0,468	26
C6S	0,199	67
CS/GlcN t	0,462	30,4

Figura 11. Eletroforese em gel de poliacrilamida de CS utilizada nos experimentos. Após corrida eletroforética, o gel foi corado com azul de toluidina 0,1% em ácido acético 1% (A). A distância de migração é inversamente proporcional ao logaritmo do peso molecular dos compostos (B). Os géis foram submetidos a densitometria, e as distâncias de migração foram medidas. O peso modal do polímero foi determinado com base nos padrões, C6S; condroitim 6 sulfato; C4S; condroitim 4 sulfato; Dextran sulfato (C).

O peso molecular modal das amostras foi estimado por meio de regressão logarítmica, comparando-se a distância de migração das amostras testadas com os valores obtidos das amostras de peso molecular já estabelecido (Dextran sulfato, C4S, C6S).

Considerando os aspectos estruturais, uma vez que pode haver diferença no tamanho entre os CSs, devido à fonte de obtenção e diferenças no processo de extração e purificação, o CS purificado de fonte terrestre como cartilagem de ave, suína e bovina geralmente apresenta peso molecular entre 13 e 26kDa (VOLPI, 2007b). Porém, CS de cartilagem de peixe, tubarão e arraia possuem peso molecular maior entre 50-70 kDa (VOLPI, 2007b) . Nosso resultado demonstrou que o CS utilizado nos experimentos apresentou peso molecular modal de 30 kDa, que está próximo dos pesos encontrados em CS extraído de animais terrestres.

4.1.3 Análise da composição do Condroitim Sulfato e Glucosamina por FACE

A análise da composição dissacarídica do CS foi realizada pela técnica *Fluorophore Assisted Carbohydrate Electrophoresis (FACE)* após a degradação dos compostos com condroitinase AC *de Flavobacterium heparinum* (liase bacteriana).

Estas enzimas são importantes ferramentas na identificação e análise estrutural de GAGs. Condroitinases (ou condroitim liases) de *Flavobacterium heparinum* são endoglicosidases que reconhecem ligações glicosídicas presentes em condroitim sulfato, dermatam sulfato e ainda ácido hialurônico. De acordo com sua especificidade são denominadas como: condroitinase AC (*N*-acetilgalactosamina ou *N*-acetilglucosamina e ácido D-glucurônico), condroitinase B (*N*-acetilgalactosamina e ácido L-idurônico), condroitinase C (*N*-acetilgalactosamina 6S ou não sulfatada e ácido D-glucurônico). Condroitinase ABC quebra ligações β-glicosídicas em CS, DS e HA (MICHELACCI; DIETRICH, 1976a, 1976b).

A condroitinase AC quebra ligações β-glicosídicas entre *N*-acetilgalactosamina e ácido glucurônico, degradrando CS agindo sobre regiões 4, 6-sulfatadas e não sulfatadas, produzindo como produtos finais dissacarídeos contendo uma instauração entre C4-C5 do resíduo de ácido urônico, conforme Figura 12 (AGUIAR et al., 2003; MICHELACCI; DIETRICH, 1976b).

A FACE foi incialmente estabelecida por Peter Jackson para análises de diversos sacarídeos em géis de alta densidade (JACKSON, 1990, 1991, 1994), posteriormente adaptado para análise de dissacarídeos glicosaminoglicanos (CALABRO et al., 2001; CALABRO; HASCALL; MIDURA, 2000). Recentemente essa técnica tem sido utilizada para identificar possíveis contaminantes em

preparações farmacêuticas de CS, além de analisar a composição disssacarídica do CS (DA CUNHA et al., 2015).

É uma técnica que consiste na derivatização de sacarídeos com grupo aldeído redutor livre (Figura 12 A) com um composto fluorescente como a 2-aminoacridona (AMAC), formando uma base de Schiff que é reduzida por cianoboro-hidreto de sódio, obtendo como produto final na reação, derivados sacarídeos-fluoróforo estáveis, podendo estes, ser separados por eletroforese em gel de poliacrilamida em géis de alta densidade, conforme esquema abaixo

A Figura 12 (C) mostra um gel de FACE com a análise dissacarídicas de cada CS. No CS utilizado nos experimentos, os principais dissacarídeos formados foram os monossulfatados ΔDi4S e ΔDi6S com pequena quantidade de dissacarídeos não sulfatado ΔDi0S. Além disso, C6S (Sigma Aldrich) contêm pequenas quantidade de oligo/tetra sacarídeos.

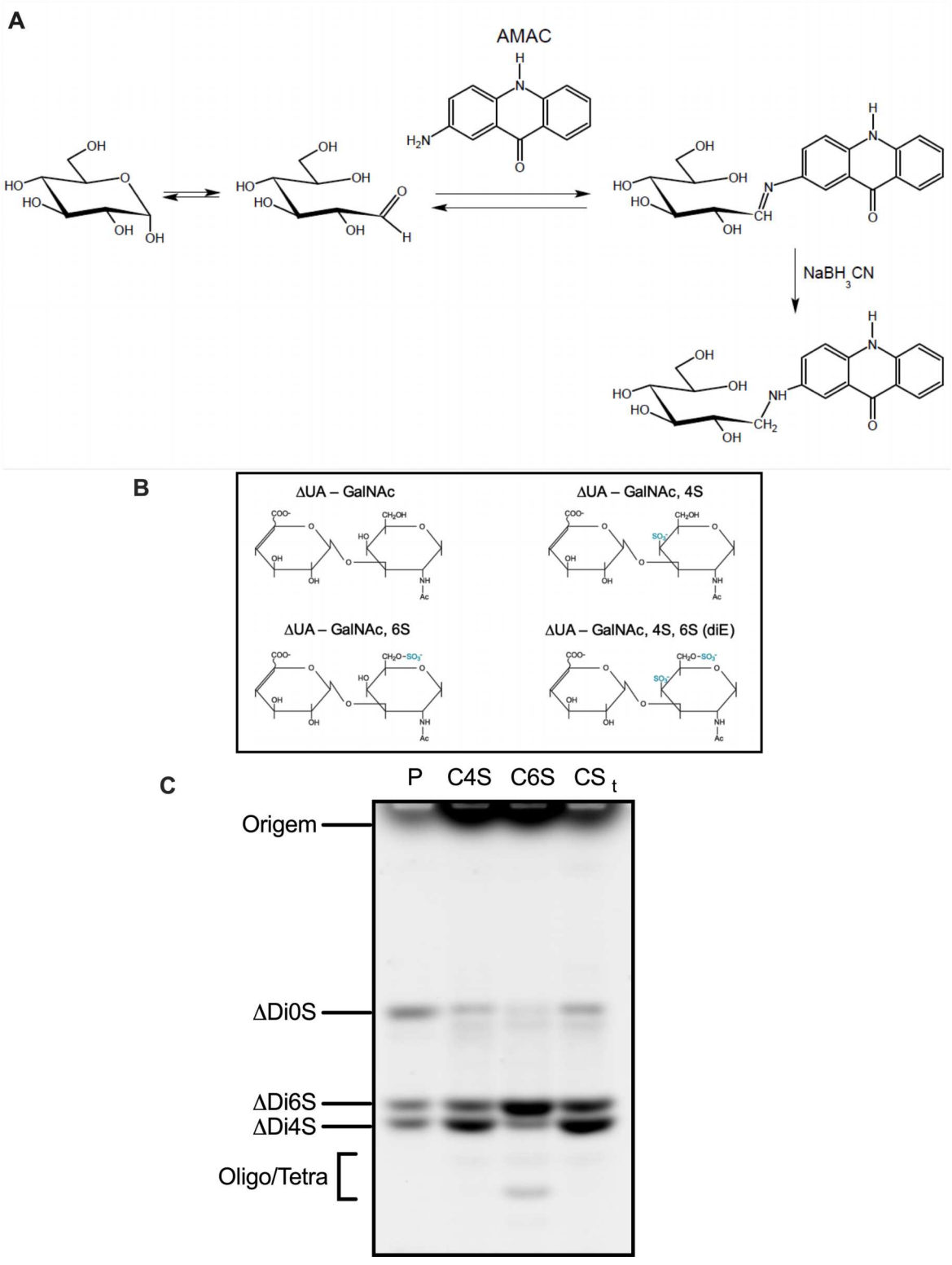

Figura 12. Esquema representativo de derivatização de sacarídeos por AMAC (A), dissacarídeos constituintes do CS após degradação enzimática (B) e eletrofluorograma (FACE) de produtos da digestão do CS utilizado nos experimentos por condroitinase AC de *F. heparinum*. Imagens dos géis foram obtidas em sistema de foto documentação equipado com câmera e transluminador UV (λ= 365nm). P: mistura padrão ΔDi0S, ΔDi4S, ΔDi6S; C6S; condroitim 6 sulfato; C4S; condroitim 4 sulfato; CS_t; condroitim sulfato teste.

Podemos observar que os dissacarídeos monossulfatados predominam nos CS analisados (Tabela 3), sendo a maioria (≅ 46%) unidades 4 sulfatadas (Di4S) do CS utilizado em nossos experimentos, valor correspondente no C4S (Sigma Aldrich), portanto classificado como ‘’condroitim 4-sulfato’’. O C6S (Sigma Aldrich) é predominantemente 6-sulfato, formado por ≅ 58% destas unidades dissacarídicas. Além disso todos os CS contêm pequenas quantidades de dissacarídeos não sulfatados (7-12%).

Diversas evidências indicam que as cadeias de CS desempenham importantes funções biológicas na inflamação, proliferação celular, diferenciação, migração, morfogênese de tecidos, organogênese, infecção e reparo tecidual, devido a sua capacidade de interagir com diversas compostos tais como moléculas de matriz, fatores de crescimento, inibidores de protease, citocinas, quimiocinas, moléculas de adesão e fatores de virulência, capacidade esta ligada à grande densidade de cargas negativas, a suas longas cadeias e em seus domínios funcionais dependendo da combinação de dissacarídeos formadores do CS (BANDTLOW et al., 2000; GEMBA et al., 2002; MARTEL-PELLETIER et al., 2008; VOLPI, 2019, 2011).

Corroborando com a afirmações acima, estudos com C4S em modelos inflamatórios *in vivo* e *in vitro*, como em condrócitos estimulados com IL-1β (DA CUNHA et al., 2017) e LPS (CAMPO et al., 2009) e modelo animal de pancreatite aguda (CAMPO et al., 2008) e hepatite aguda (CAMPO et al., 2004) o C4S foi capaz de atuar como uma substância anti-inflamatória.

Tabela 3. Composição relativa de dissacarídeos do CS utilizado nos experimentos.

	Composição dissacarídica %			
	ΔDi0S	**ΔDi4S**	**ΔDi6S**	**Oligo/Tetra Não determinado**
C4S padrão	11,94	46,07	30,45	11,54
C6S padrão	7,14	18,01	57,97	16,88
CS teste	11,33	46,58	34,65	7,45

C4S: condroitim 4 sulfato; C6S: condroitim 6 sulfato; CS teste, condroitim sulfato utilizado nos experimentos.

Já para identificação da presença de Glucosamina, foi utilizado o sistema de Tampão Tris-Borato, uma vez que os monossacarídeos neutros (GalNAc e

GlcNAc) apresentam migração, devido à complexação de íons borato com os derivados sacarídeo-AMAC neutros, que passam a apresentar carga negativa.

A glucosamina é um monossacarídeo que penetra pouco no gel de corrida e é visualizada no topo do eletrofluorograma como banda difusa. Já *N*-acetil-glucosamina apresenta maior penetração no gel de corrida, de acordo com a Figura 13.

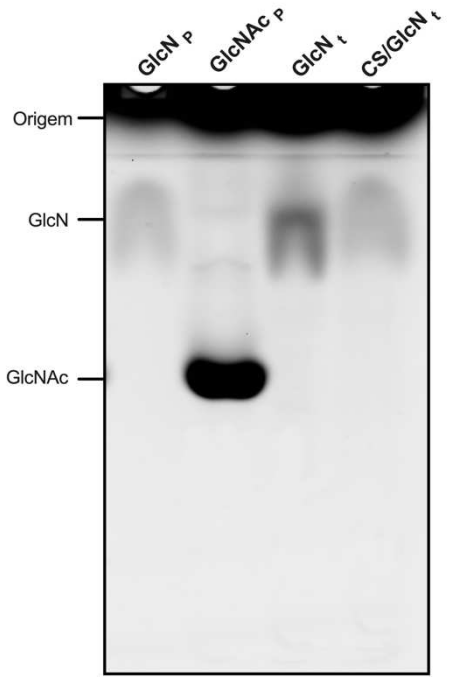

Figura 13. Eletrofluorograma (FACE) de GlcN em Tris-Borato utilizado nos experimentos. Imagens dos géis foram obtidas em sistema de foto documentação equipado com câmera e transluminador UV (λ= 365nm). P: GlcN (Glucosamina) e GlcNAc (*N*-acetil-glucosamina) e Teste: GlcN (Glucosamina) e CS/GlcN (Condroitim sulfato e glucosamina).

4.1.4 Método espectroscópico

4.1.4.1 Análise por Ressonância Magnética Nuclear

Os espectros obtidos de CS (C4S padrão, C6S padrão, amostra teste CS_t) estão ilustrados na Figura 14.

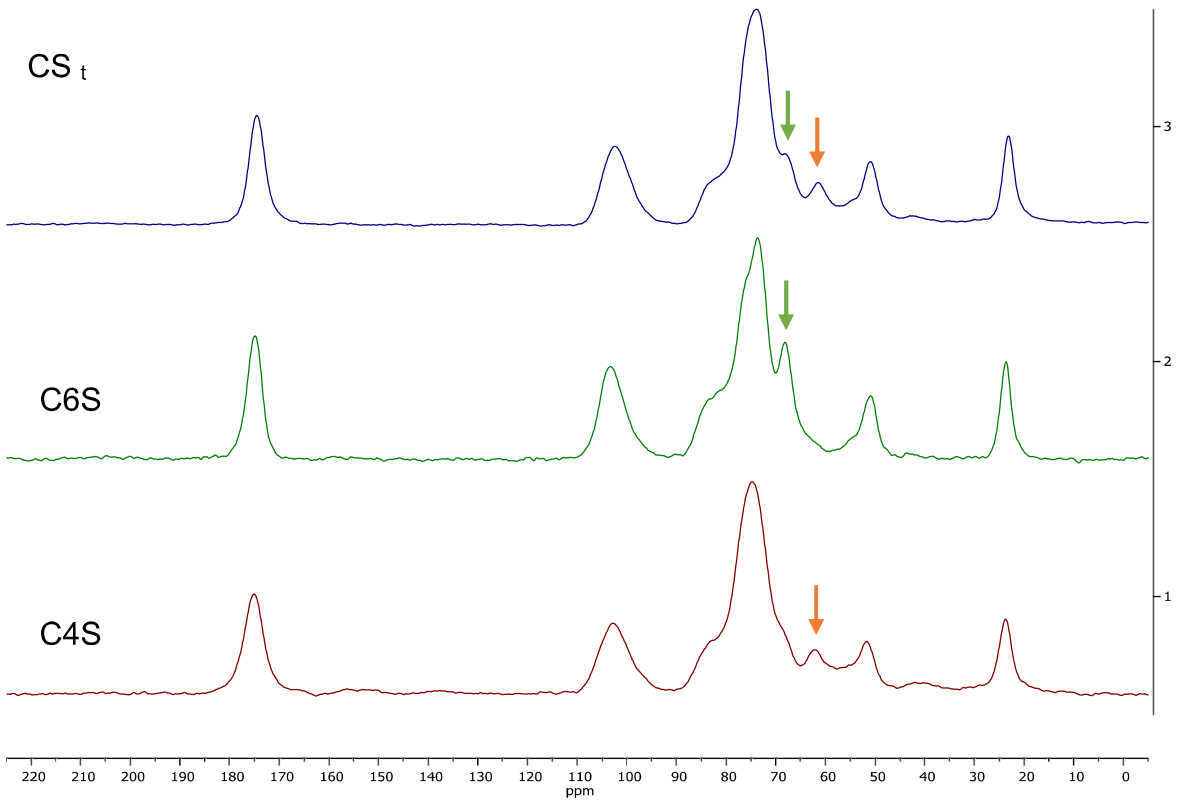

Figura 14. Espectro de ressonância magnética nuclear de ^{13}C dos padrões de C6S e C4S e CS utilizado nos experimentos.

Na figura acima, o CS utilizado nos experimentos (CS_t), apresenta sinais característicos de sulfatação tanto na posição 4, sinal de 62 ppm, quanta na posição 6, sinal em 68 ppm corroborando com os resultados obtidos por Mucci e colaboradores (2000). Portanto, o CS utilizado nos experimentos possui sulfatação na posição 4 e 6 da amostra, como o resultado visualizado e quantificado pela FACE.

Na análise do Condroitim Sulfato associado a Glucosamina (CS/GlcN) utilizada nos experimentos, os espectros obtidos são observados na Figura 15.

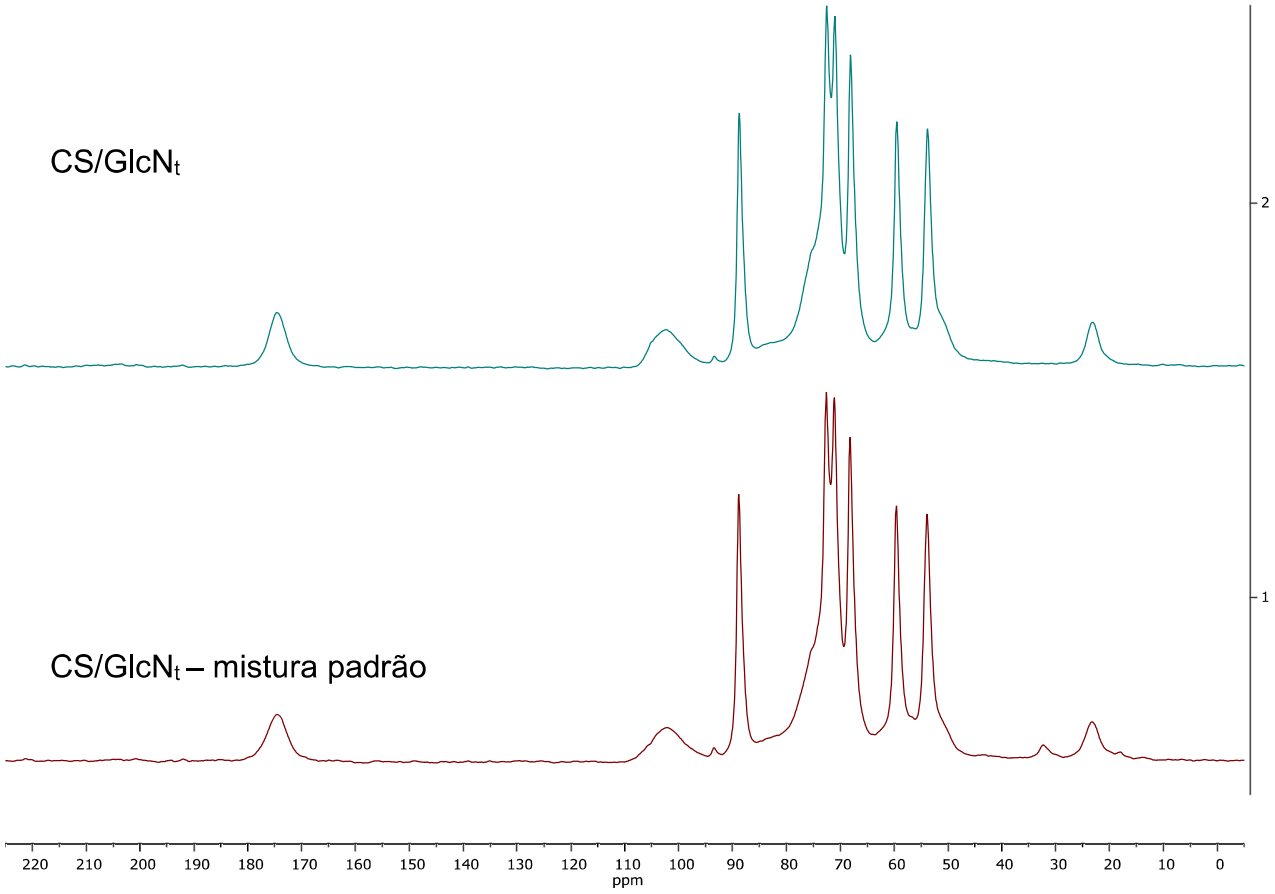

Figura 15. Espectro de ressonância magnética nuclear de ^{13}C da mistura padrão de CS associado à Glucosamina e a associação utilizada nos experimentos.

O espectro de RMN de sólido de ^{13}C do ($CS/GlcN_t$) apresenta os mesmos sinais observados no espectro da mistura de padrões Condroitim 4-Sulfato e Glucosamina acetilada, confirmando o conteúdo de princípios ativo e a qualidade das substâncias utilizadas nos testes.

Quando, é analisado o padrão de sulfatação da solução utilizada nos testes de $CS/GlcN_t$, não foi possível identificar, através da técnica de RMN de sólido de ^{13}C quais regiões de sulfatação estão presentes na formulação, uma vez que, os sinais referentes a glucosamina apresentam-se na mesma região que os carbonos contendo os grupos sulfatos (Figura 16).

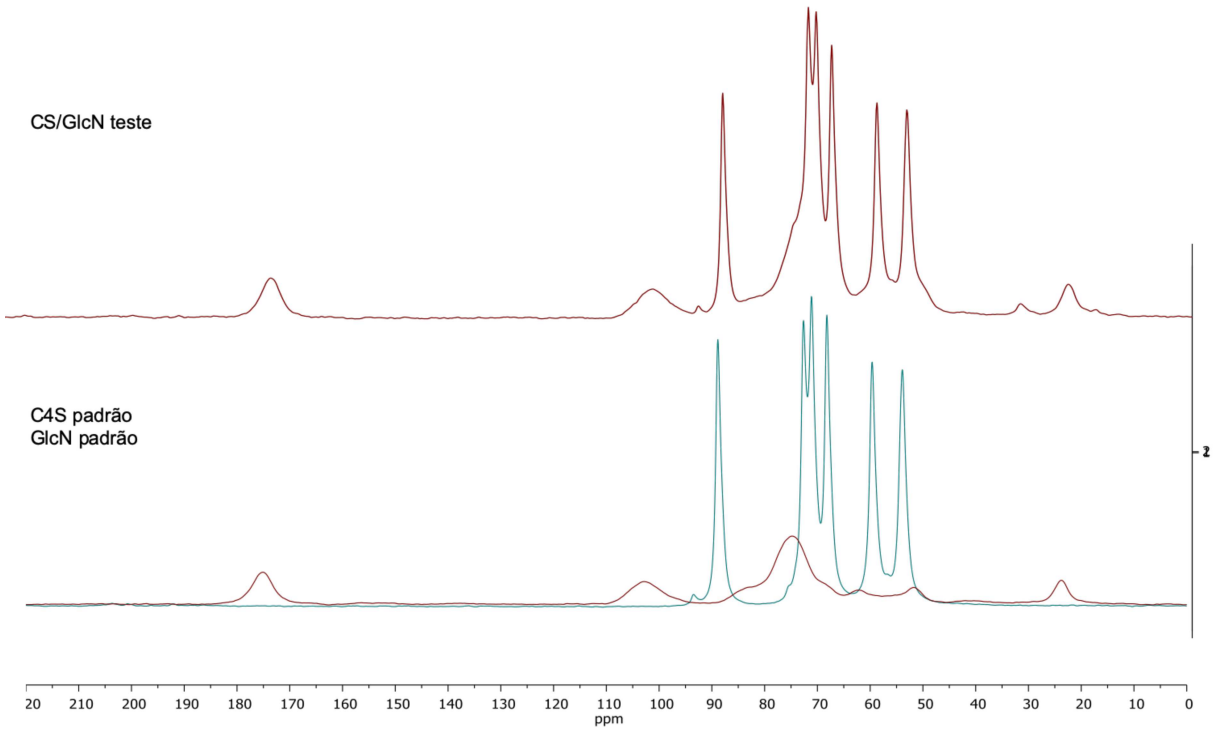

Figura 16. Espectro de ressonância magnética nuclear de ^{13}C do CS/GlcN teste e a sobreposição dos espectros do padrão de C4S e Glucosamina.

4.2 CULTURA DE CÉLULAS

4.2.1 Avaliação da concentração de LPS para indução de processo inflamatório

Após a caracterização das amostras utilizadas, realizou-se testes para definir a melhor concentração dos diferentes tipos de LPS (*Escherichia coli* O55:B5 e *Salmonella entérica typhimurium* – Sigma Aldrich) para induzir o processo inflamatório nas células da linhagem, RAW 264.7, IEC-6 e Caco-2.

4.2.1.1 Efeito de LPS sobre macrófagos da linhagem RAW 264.7

Para realizar a indução das células RAW 264.7, verificamos protocolos descritos na literatura, em que se utilizam diferentes concentrações de LPS como estímulo inflamatório (CAMPO et al., 2009; DA CUNHA et al., 2017; FENTON et al., 2000; GRISHIN et al., 2006).

Antes de iniciar os testes com LPS, foi avaliado a viabilidade dos macrófagos após incubação com LPS em diferentes concentrações por 48 horas,

em seguida foi realizado o ensaio de viabilidade (MTT) confirmando, que as concentrações de LPS (10 ng/mL até 1000 ng/mL) não alterou a viabilidade na célula testada.

Dessa forma, inicialmente, analisamos o perfil de liberação de NO em macrófagos da linhagem (RAW 264.7) desafiadas por LPS em diferentes concentrações no período de 48 horas (Figura 17).

O maior nível de produção de NO pelas células estimuladas foi obtido com 100ng/mL de LPS. Acima dessa concentração, não foi observada diferença estatística para a liberação de NO no período de 48 horas.

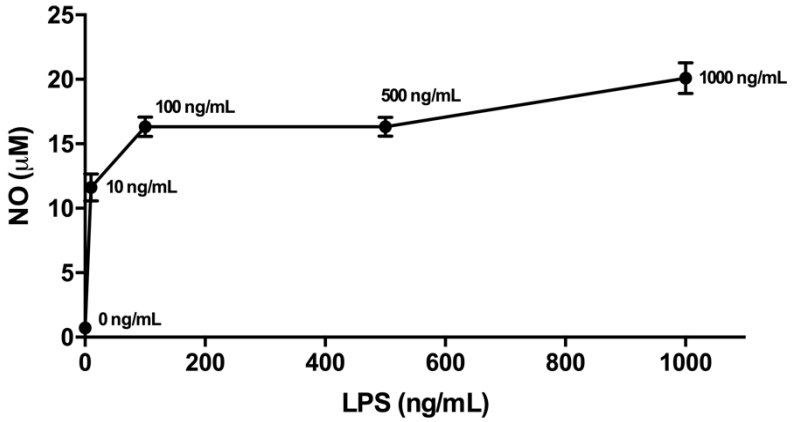

Figura 17. Efeito da concentração de LPS na ativação e produção de NO em macrófagos da linhagem RAW 264.7 no período de 48 horas. Macrófagos da linhagem RAW 264.7 foram cultivados em placas de cultura de 96 poços (80.000 células por poço) utilizando DMEM suplementado com 10% de soro fetal bovino (SFB). Após 24 horas o sobrenadante foi removido e foi adicionado novo meio contendo LPS em diferentes concentrações (10, 100, 500 e 1000ng/mL) contendo SFB 2%. Condição controle (basal) foi realizada incubando-se às células em meio suplementado com DMEM/SBF 2%. Após 48 horas de estímulo os meios foram coletados e realizada a dosagem de NO conforme descrito em Métodos. Os valores representam média de triplicatas experimentais, e as barras desvio padrão.

Uma vez determinada a concentração ideal para estímulo da RAW 264.7, as células foram desafiadas com LPS 100 ng/mL em diferentes tempos de exposição, a fim de obter-se a cinética de produção de NO em relação ao período da exposição (Figura 18).

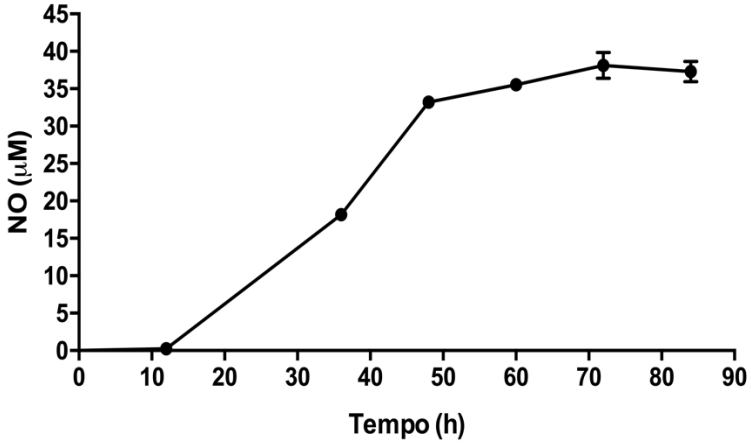

Figura 18. Cinética de liberação de NO em macrófagos da linhagem RAW 264.7 desafiadas com LPS 100ng/mL. Macrófagos da linhagem RAW 264.7 foram cultivados em placas de cultura de 96 poços (80.000 células por poço) utilizando DMEM suplementado com 10% de soro fetal bovino (SFB). Após 24 horas o sobrenadante foi removido e foi adicionado novo meio contendo LPS 100ng/mL contendo SFB 2%. Condição controle (basal) foi realizada incubando-se às células em meio suplementado com DMEM/SBF 2%. Os meios foram coletados em diferentes tempos (12, 36, 48, 60, 72 e 84 horas) e realizada a dosagem de NO conforme descrito em Métodos. Os valores representam média de triplicatas experimentais, e as barras desvio padrão

Com base nesses resultados, adotou-se o tempo de 48 horas para realizar os testes de estímulo com LPS 100 ng/mL, uma vez que a produção de NO tende a se manter após 48 horas de indução, com pequenos aumentos/variações nos tempos superiores.

Observou-se também, que nessa concentração, o LPS induziu mudanças morfológicas significativas nas células (Figura 21).

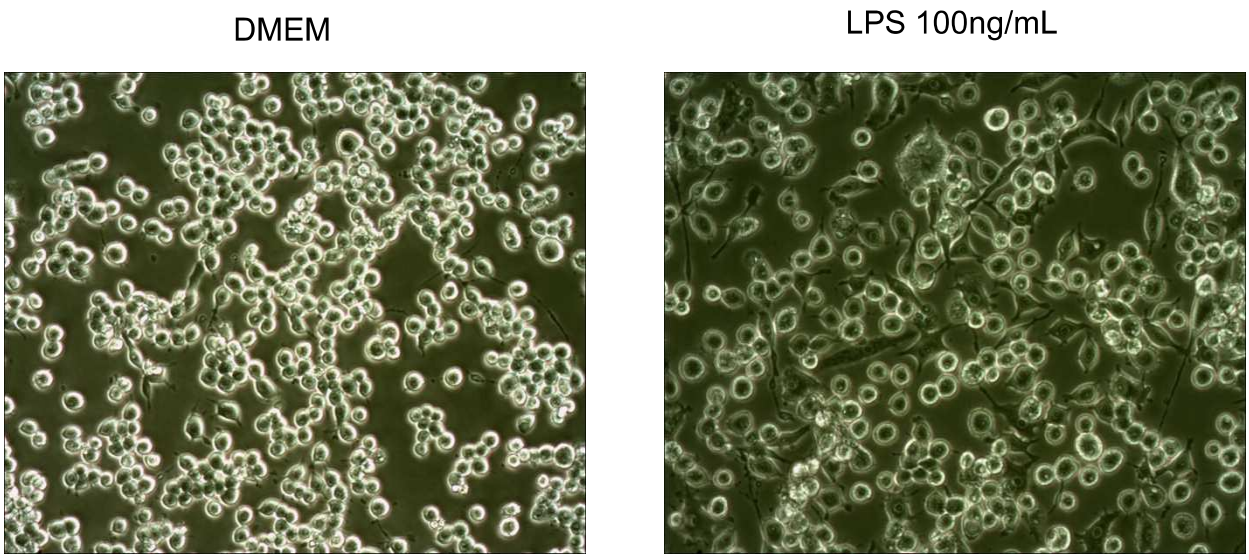

Figura 19. Efeito do LPS sobre a morfologia em macrófagos da linhagem RAW 264.7 no tempo de 48 horas. Macrófagos da linhagem RAW 264.7 foram cultivadas em placas de cultura de 24 poços ($10x10^5$ células por poço). Após 24 horas de exposição o meio foi removido e as células foram incubadas com novo meio suplementado com DMEM/SFB 2% na ausência ou presença de LPS 100ng/mL. Aumento de 100x.

Em outro momento, foi avaliado o efeito da presença de SFB 2% sobre a ativação de macrófagos. A Figura 20 mostra que as células desafiadas com LPS 100 ng/mL com ou sem SFB 2% não tiveram alteração na liberação de NO.

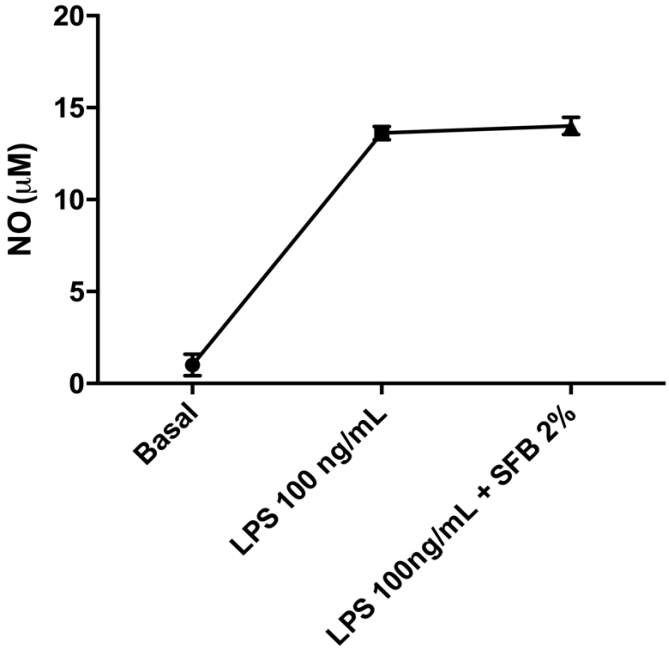

Figura 20. Efeito da concentração de SFB à 2% na ativação de macrófagos da linhagem RAW 264.7 no período de 48h. Macrófagos da linhagem RAW 264.7 foram cultivados em placas de cultura de 96 poços (80.000 células por poço) utilizando DMEM suplementado com 10% de soro fetal bovino (SFB). Após 24 horas o sobrenadante foi removido e foi adicionado novo meio contendo LPS 100ng/mL contendo ou não SFB 2%. Condição controle (basal) foi realizada incubando-se às células em meio suplementado com DMEM. Após 48 horas de estímulo os meios foram coletados e realizada a dosagem de NO conforme descrito em Métodos. Os valores representam média de triplicatas experimentais, e as barras desvio padrão.

Os estudos realizados acima para definição da melhor concentração de LPS, o tempo de exposição da linhagem celular ao mesmo, e o uso de soro ou não no meio de cultura utilizado para indução do processo inflamatório, teve como parâmetro as dosagens de NO pelo seu importante papel no processo inflamatório.

O NO é uma importante substancia com diversos papéis no resposta imune inata e adaptativa (LEE et al., 2017). Foi identificada primeiramente no processo de vasodilatação arterial (FURCHGOTT; ZAWADZKI, 1980; IGNARRO et al., 1987; PALMER; FERRIGE; MONCADA, 1987). Já no sistema imune sua expressão foi observada em macrófagos após estímulos com citocinas e partículas microbianas, sugerindo o seu papel na defesa contra patógenos (MARLETTA et al., 1988; NATHAN, 1992).

A produção de NO, ocorre por meio de três enzimas identificadas, sendo elas a óxido nítrico sintase neuronal (nNOS), endotelial (eNOS) e a induzida (iNOS),

sendo que a produção pode ocorrer por varias células do sistema imune (BREDT; SNYDER, 1990; LAMAS et al., 1992; LOWENSTEIN et al., 1992). Macrófagos, neutrófilos, linfócitos T podem induzir a expressão da iNOS, e o NO produzido pode atuar como efetor da inflamação (LEE et al., 2017).

No processo inflamatório e na resposta imune há uma perda no equilíbrio da enzima iNOS e produção de NO que está envolvida na patogênese de doenças inflamatórias, interferindo na integridade da barreira epitelial em doenças crônicas e formação de radicais livres (LEE et al., 2017).

Dando continuidade no comportamento da linhagem celular RAW 264.7 desafiadas com LPS (100ng/mL), foi avaliado o perfil de produção de outros mediadores pró inflamatórios ao longo do tempo. Em que, se observa o aumento gradativo de TNF-α e IL-6 ao longo do tempo (Figura 21), enquanto a produção de IL-1β não foi detectada (Figura 22).

O estudo de citocinas em condições inflamatórias não está relacionado somente no entendimento da imunopatogênese, mas também em avaliar o potencial para diagnóstico e aplicações terapêuticas (BAMIAS; COMINELLI, 2016).

TNF-α é uma citocina com importante funções na homeostasia e nas doenças inflamatórias. TNF-α induz inflamação por meio do recrutamento de células inflamatórias (por meio do aumento de moléculas de adesão e ativação de células endoteliais), indução de mediadores inflamatórios e a degeneração tecidual pela indução de enzimas capazes de promover a degradação tecidual (KALLIOLIAS; IVASHKIV, 2016).

Já a IL-6 é um citocina com importante papel na defesa do hospedeiro, pois quando uma infecção ou dano tecidual ocorre, IL-6 é produzida prontamente por monócitos e macrófagos para remover o agente infeccioso e restaurar o dano tecidual através da ativação do sistema imune, hematológico e da síntese de proteínas de fase aguda. Porém a persistência e a produção excessiva de IL-6 exercem papel patológico no desenvolvimento de várias doenças inflamatórias e câncer (KANG; TANAKA; KISHIMOTO, 2015; TANAKA et al., 2016; TANAKA; NARAZAKI; KISHIMOTO, 2012, 2014). Por exemplo em casos de doenças inflamatórias crônica como artrite reumatoide, em que a concentração de IL-6 está constantemente elevada (TANAKA et al., 2016; TANAKA; NARAZAKI; KISHIMOTO, 2012).

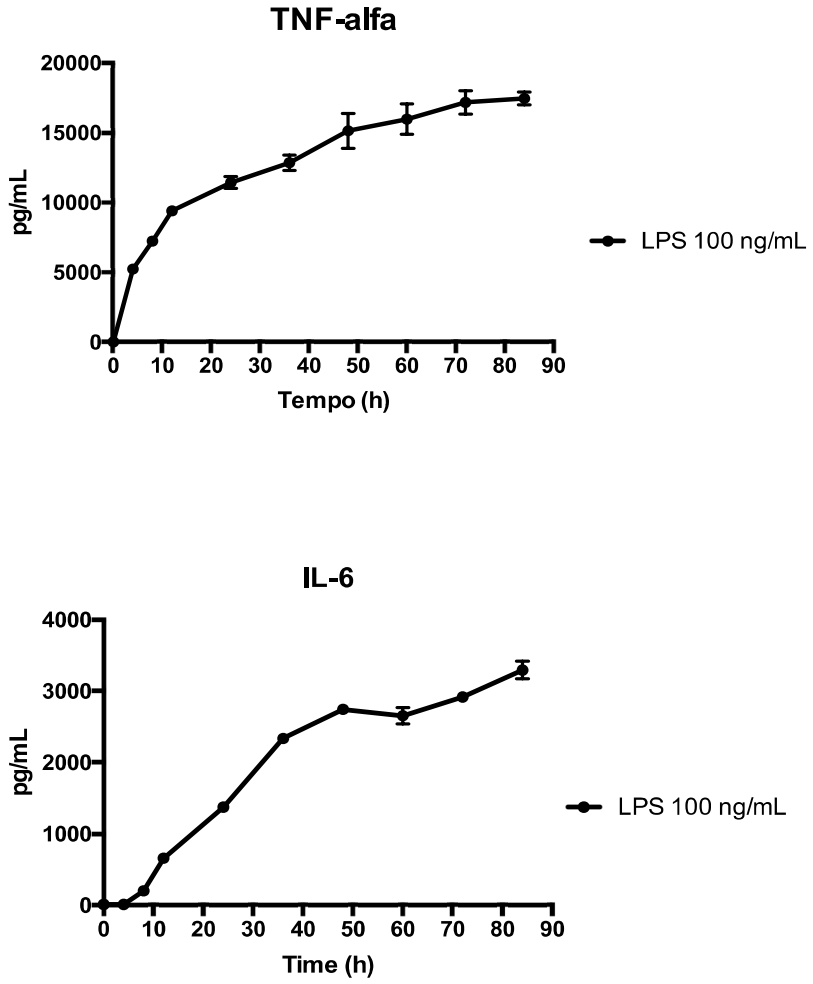

Figura 21. Cinética de liberação de TNF-α e IL-6 em macrófagos da linhagem RAW 264.7 desafiadas com LPS 100ng/mL. Macrófagos da linhagem RAW 264.7 foram cultivados em placas de cultura de 96 poços (80.000 células por poço) utilizando DMEM suplementado com 10% de soro fetal bovino (SFB). Após 24 horas o sobrenadante foi removido e foi adicionado novo meio contendo LPS 100ng/mL. Os meios foram coletados após diferentes tempos (0-84h) e realizada a dosagem de TNF-α e IL-6, conforme descrito em Métodos. Os valores representam média de triplicatas experimentais, e as barras desvio padrão.

Com relação a produção de IL-1β, uma vez que não houve a liberação e detecção de produção dessa interleucina no meio de cultura. Para avaliar a produção de IL1-β na linhagem RAW 264.7, foi necessário a utilização de MDP 10μg/mL, molécula responsável por ativar complexo de inflamassoma no macrófago (HIROTA et al., 2011; LEE et al., 2015).

Uma vez ativado o complexo inflamasoma, pelo MDP, foi possível a detecção e quantificação de IL-1β por conta da clivagem da pro-IL-1β e sua liberação para o meio de cultura, conforme o resultado apresentado na Figura 22.

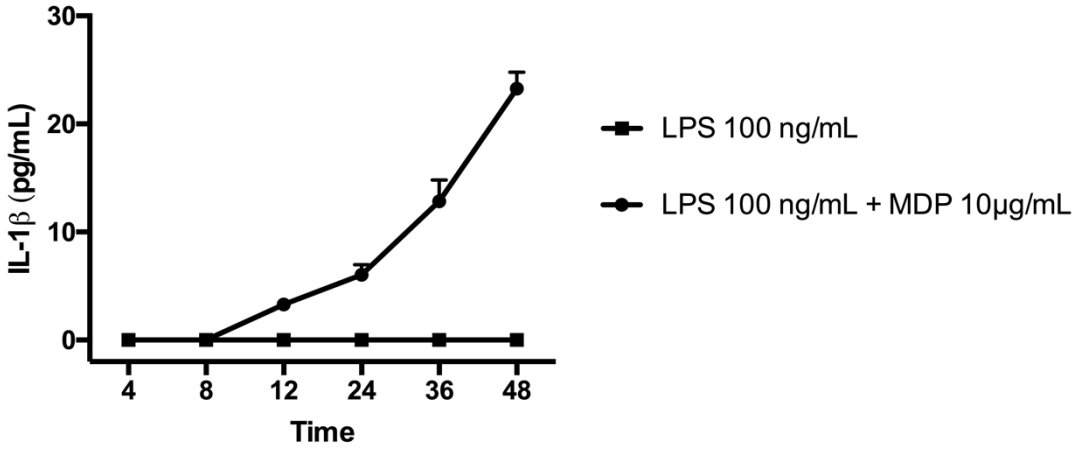

Figura 22. Cinética de liberação de IL1-β em macrófagos da linhagem RAW 264.7 desafiadas com LPS 100ng/mL e LPS 100ng/mL + MDP 10μg/mL. Macrófagos da linhagem RAW 264.7 foram cultivados em placas de cultura de 96 poços (80.000 células por poço) utilizando DMEM suplementado com 10% de soro fetal bovino (SFB). Após 24 horas o sobrenadante foi removido e foi adicionado novo meio contendo LPS 100ng/mL e LPS 100ng/mL + MDP 10μg/mL. Os meios foram coletados após diferentes tempos (0-48h) e realizada a dosagem de IL-1β, conforme descrito em Métodos. Os valores representam média de triplicatas experimentais, e as barras desvio padrão.

O estudo da produção e liberação de IL-1β possui grande importância, pois, essa interleucina exerce efeitos em varias células e possui papel chave na inflamação aguda e crônica. Além de possuir importantes funções homeostáticas como regulação da fome, sono e temperatura (DINARELLO, 1996).

IL-1β é membro da família de todas IL-1 que compreendem 11 membros no total, em que todos são expressos como zimogênio e requerem uma quebra por proteínas para adquirir sua forma ativa biologicamente (BENT et al., 2018).

A produção excessiva de IL-1β atua na amplificação de reações imunes e está envolvida na patogênese durante diferentes estágios de doenças, como artrite reumatoide, doença inflamatória intestinal, osteoartrite, doenças vasculares, esclerose múltipla e doença de Alzheimer (BENT et al., 2018; REN; TORRES, 2009).

Por esse motivo a importância de estudar o perfil de liberação dessas citocinas pelos macrófagos da linhagem RAW 264.7.

4.2.1.2 Efeito de CS, GlcN e CS/GlcN sobre macrófagos da linhagem RAW 264.7

Para analisar o efeito de CS, GlcN e CS/GlcN, foi realizado ensaio de viabilidade dos macrófagos após incubação da linhagem celular com os compostos CS, GlcN e CS/GlcN, para avaliar a concentração de trabalho, desejável, para cada substância (Figura 23).

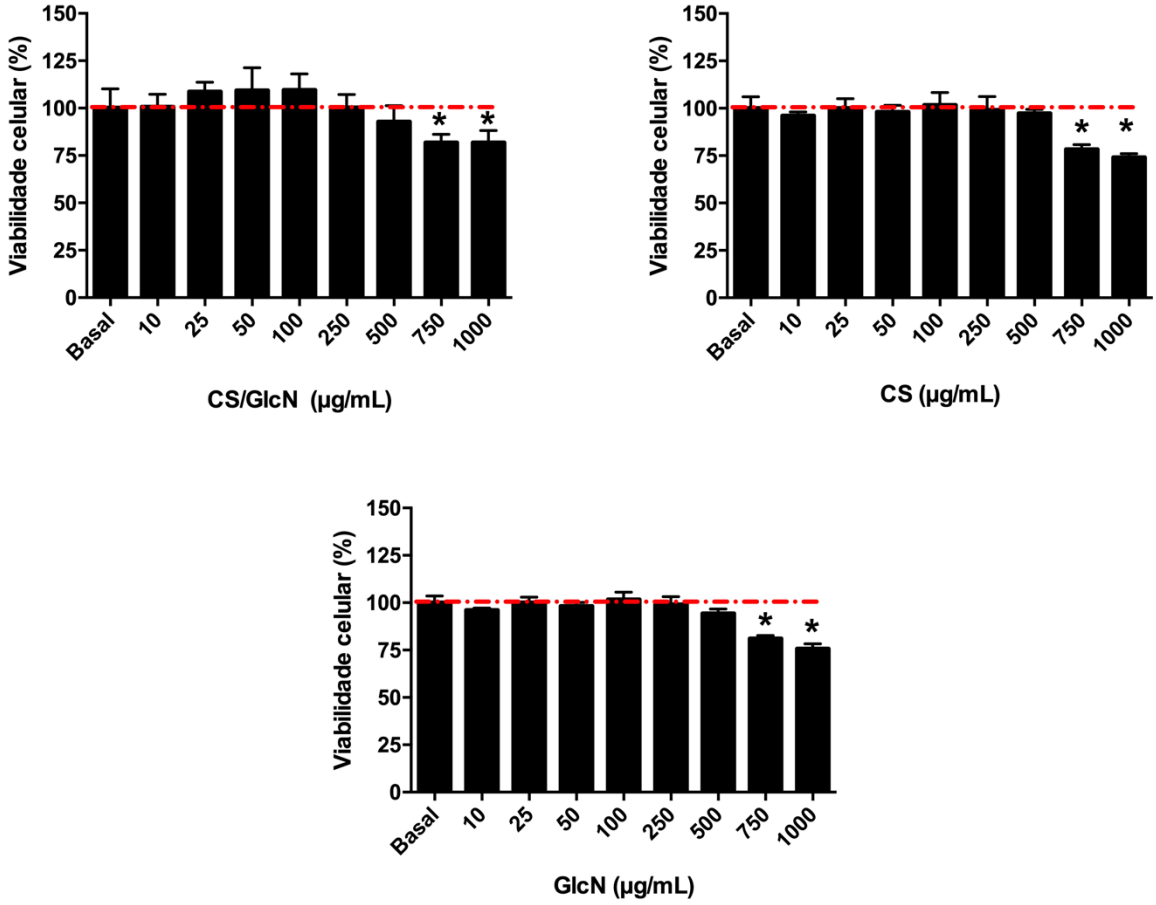

Figura 23. Ensaio de viabilidade em macrófagos da linhagem RAW 264.7 tratadas com CS, GlcN e CS/GlcN. Macrófagos da linhagem RAW 264.7 foram cultivados em placas de cultura de 96 poços ($10x10^3$ células por poço). Após 24 horas o sobrenadante foi removido e as células foram incubadas com novo meio suplementado com 2% de SFB e diferentes concentrações de CS, GlcN e

CS/GlcN (10, 25, 50, 100, 250, 500, 750, 1000μg/mL). Os meios condicionados foram coletados após 48 horas de cultivo, e as células foram incubadas com solução MTT (0,5 mg/mL, concentração final) por mais 4 horas. O sobrenadante foi então descratado e os cristais de formazan foram solubilizados pela adição de 200μg/mL de dimetilsulfóxido (DMSO) e a absorbância (λ=540nm) foi medida em leitor de microplaca. Os valores representam média de triplicatas experimentais, e as barras desvio padrão. ∗ p<0,05 comparado ao grupo basal.

De acordo com os resultados apresentados na figura anterior, a linhagem celular RAW 264.7 incubada após 48h, com CS, GlcN, CS/GlcN, possui alteração em sua viabilidade apenas com concentração acima de 750 μg/mL.

Após confirmação do resultado, foi realizado um teste para determinar a concentração de NO no período de 48h após desafiar as células com LPS + CS/GlcN (Figura 24), com a finalidade de se chegar a uma concentração com melhor resultado na produção desse parâmetro inflamatório

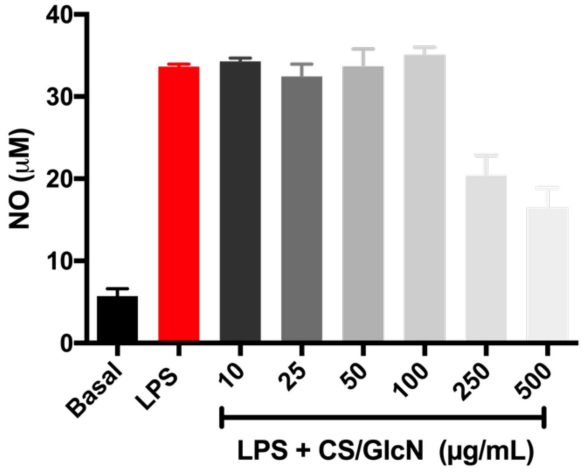

Figura 24. Efeito do CS/GlcN sobre a produção de NO em macrófagos da linhagem RAW 264.7 desafiadas com LPS 100ng/mL após 48 horas de exposição. Macrófagos da linhagem RAW 264.7 foram cultivados em placas de cultura de 96 poços (80.000 células por poço) utilizando DMEM suplementado com 10% de soro fetal bovino (SFB). Após 24 horas o sobrenadante foi removido e foi adicionado novo meio com SFB 2%, contendo LPS 100ng/mL contendo CS/GlcN em diferentes concentrações (10, 25, 50, 100, 250, 500μg/mL) . Os meios foram coletados após após 48 horas, conforme descrito em Métodos. Os valores representam média de triplicatas experimentais, e as barras desvio padrão.

Avaliando a produção de NO na Figura 24, CS/GlcN foi capaz de provocar redução desse mediador inflamatório a partir da concentração de 250 μg/mL, sendo a redução na concentração de 500 μg/mL a mais relevante.

Portanto, a concentração de CS/GlcN, CS e GlcN estabelecida para os demais testes foi de 500 μg/mL, levando em consideração também que essas concentrações não alteraram a viabilidade sobre os macrófagos, pelo ensaio de MTT.

Após a definição da concentração de trabalho, foi realizado teste com as demais substâncias, e foi observado que todas as amostras foram capazes de reduzir a produção de NO de forma significativa, sendo a associação de CS/GlcN possuindo a redução relevante (Figura 25).

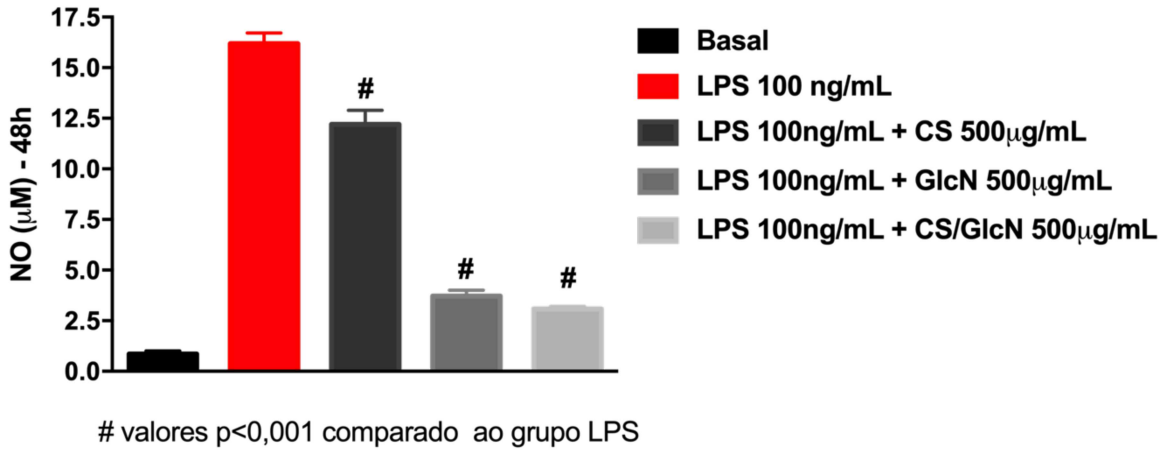

Figura 25. Efeito do CS, GlcN e CS/GlcN sobre a produção de NO em macrófagos da linhagem RAW 264.7 desafiadas com LPS 100ng/mL após 48 horas de exposição. Macrófagos da linhagem RAW 264.7 foram cultivados em placas de cultura de 96 poços (80.000 células por poço) utilizando DMEM suplementado com 10% de soro fetal bovino (SFB). Após 24 horas o sobrenadante foi removido e foi adicionado novo meio com SFB 2%, contendo LPS 100ng/mL contendo CS, GlcN, CS/GlcN 500μg/mL. Os meios foram coletados após após 48 horas, e dosados conforme descrito em Métodos. Os valores representam média de triplicatas experimentais, e as barras desvio padrão.

Com os resultados obtidos, foi investigada a produção de mediadores inflamatórios (TNF-α, IL-6 e IL-1β) produzidos pelos macrófagos, após serem desafiados com LPS 100 ng/mL concomitante com CS, GlcN e CS/GlcN.

Os efeitos das moléculas testadas na produção de TNF-α após desafiadas com LPS 100ng/mL, mostram que todos os compostos foram capazes de reduzir a produção desse mediador inflamatório após um período de 48 horas de forma significativa (Figura 26).

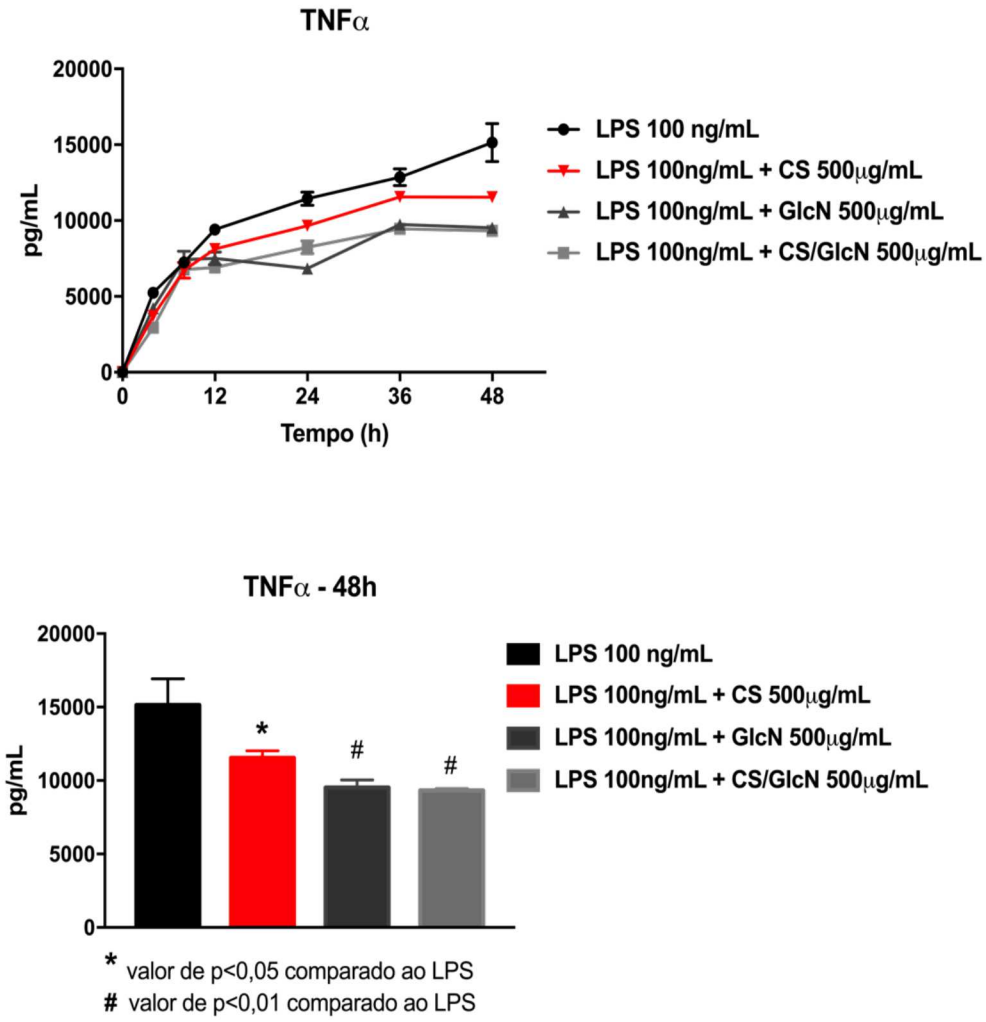

Figura 26. Efeito do CS, GlcN e CS/GlcN sobre a produção de TNF-α em macrófagos da linhagem RAW 264.7 desafiadas com LPS 100ng/mL no período de 48 horas. Macrófagos da linhagem RAW 264.7 foram cultivados em placas de cultura de 96 poços (80.000 células por poço) utilizando DMEM suplementado com 10% de soro fetal bovino (SFB). Após 24 horas o sobrenadante foi removido e foi adicionado novo meio contendo LPS 100ng/mL e LPS 100ng/mL acrescidos de CS, GlcN e CS/GlcN (500μg/mL). Os meios foram coletados após diferentes tempos (0-48h) e realizada a dosagem de TNF-α, conforme descrito em Métodos. Foi realizada a análise dos resultados no tempo de 48 horas para avaliar a liberação de TNF-α. Os valores representam média de triplicatas experimentais, e as barras desvio padrão.

De acordo com estudos recentes, que corrobora com nossos resultados, foi observado em diferentes modelos inflamatórios a redução de TNF-α, como em modelo animal de osteoartrite (LI et al., 2018) e condrócitos humano (SCOTTO D'ABUSCO et al., 2007) pela GlcN.

Já o CS também foi capaz de reduzir a mesma citocina em mastócitos humanos estimulados por IL-33 (GROSS; THEOHARIDES, 2019) bem como a associação dos dois compostos em modelo animal de osteoartrite produzindo efeitos protetores (TERENCIO et al., 2016).

Na Figura 27 é apresentado o efeito de CS, GlcN e CS/GlcN sobre a produção de IL-6. Foi verificado que apenas o CS não foi capaz de reduzir a produção da mesma, em valores significativos.

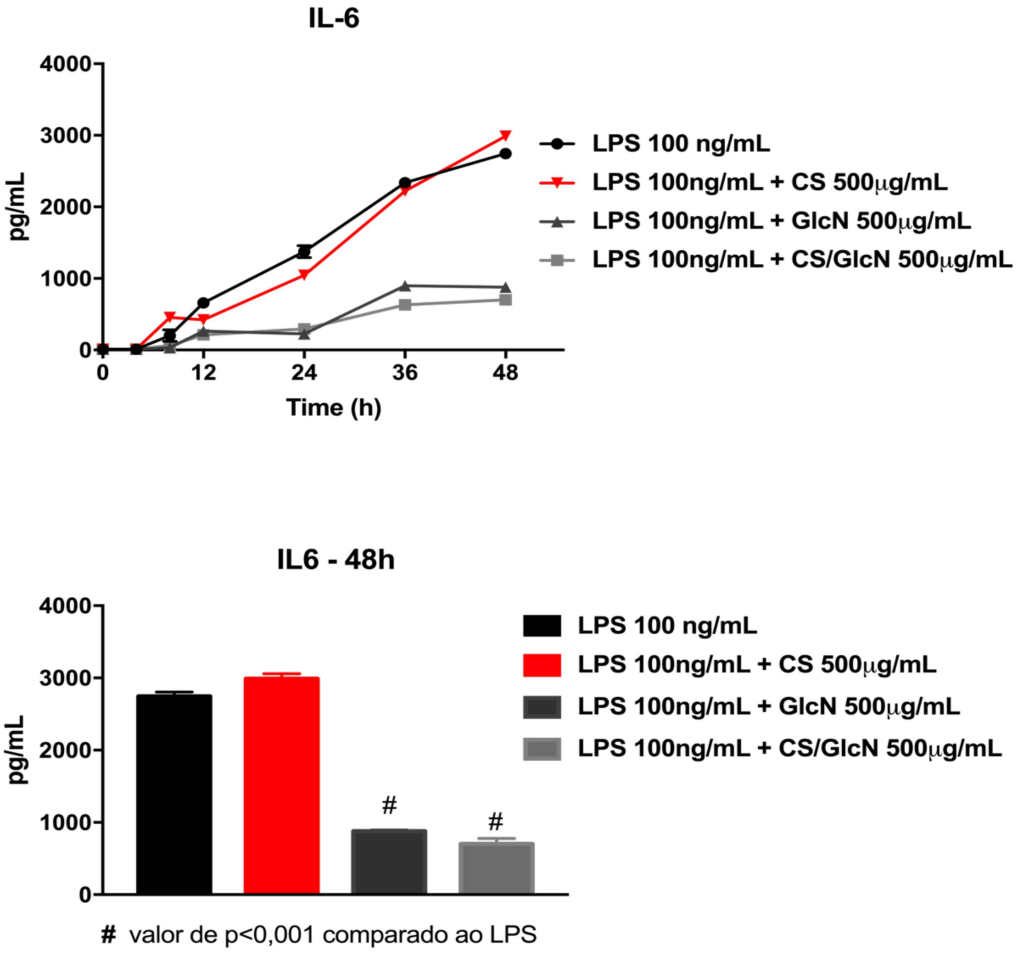

Figura 27. Efeito do CS, GlcN e CS/GlcN sobre a produção de IL-6 em macrófagos da linhagem RAW 264.7 desafiadas com LPS 100ng/mL no período de 48 horas. Macrófagos da linhagem RAW 264.7 foram cultivados em placas de cultura de 96 poços (80.000 células por poço) utilizando DMEM suplementado com 10% de soro fetal bovino (SFB). Após 24 horas o sobrenadante foi removido e foi adicionado novo meio contendo LPS 100ng/mL e LPS 100ng/mL acrescidos de CS, GlcN e CS/GlcN (500µg/mL). Os meios foram coletados após diferentes tempos (0-48h) e realizada a dosagem de IL-6, conforme descrito em Métodos. Foi realizada a análise dos resultados no tempo de 48 horas para avaliar a liberação de IL-6. Os valores representam média de triplicatas experimentais, e as barras desvio padrão.

Da Cunha e colaboradores (2017), em trabalho semelhante com macrófagos da linhagem RAW 264.7 obteve resultado semelhante, em que tanto o C4S e C6S não foram capazes de diminuir a produção de IL-6.

Enquanto isso, a GlcN e associação desta com CS, obtiveram valores próximos e significativos na redução de IL-6. Provavelmente, essa redução semelhante com a associação dos compostos, se deve mais ao efeito da GlcN, pois estudos principalmente em condrócitos e modelos animais de osteoartrite mostram que esse composto possui uma boa capacidade de redução da IL-6 (SOMEYA et al., 2016).

Para investigação da produção de IL-1β (Figura 28), foi necessário a utilização de uma solução de MDP, capaz de ativar o complexo de inflamassoma, possibilitando a clivagem da pro-IL-1β e assim permitir sua liberação para o meio de cultura em que foi dosada.

De forma semelhante à produção de IL-6, apenas CS não foi capaz de reduzir de forma significativa a produção de IL-1β, porém resultado diferente foi observado em linhagem de monócitos THP-1 estimuladas com urato monossódico no qual CS inibiu significativamente IL-1β (ORLOWSKY et al., 2014).

Já a GlcN e CS/GlcN reduziram os níveis dessa interleucina em níveis relevantes. Estudo recente em macrófagos humanos e de camundongos, mostrou que a GlcN é capaz de reduzir a dosagem de IL-1β, ao inibir o complexo inflamassoma NLRP3, importante na liberação da forma ativa dessa interleucina (CHIU et al., 2019).

Estudos do efeito da associação de CS/GlcN sobre o NLRP3 inflamasoma não são observados na literatura, abrindo uma possibilidade de estudo dessa associação sobre esse complexo inflamasoma e sua ativação.

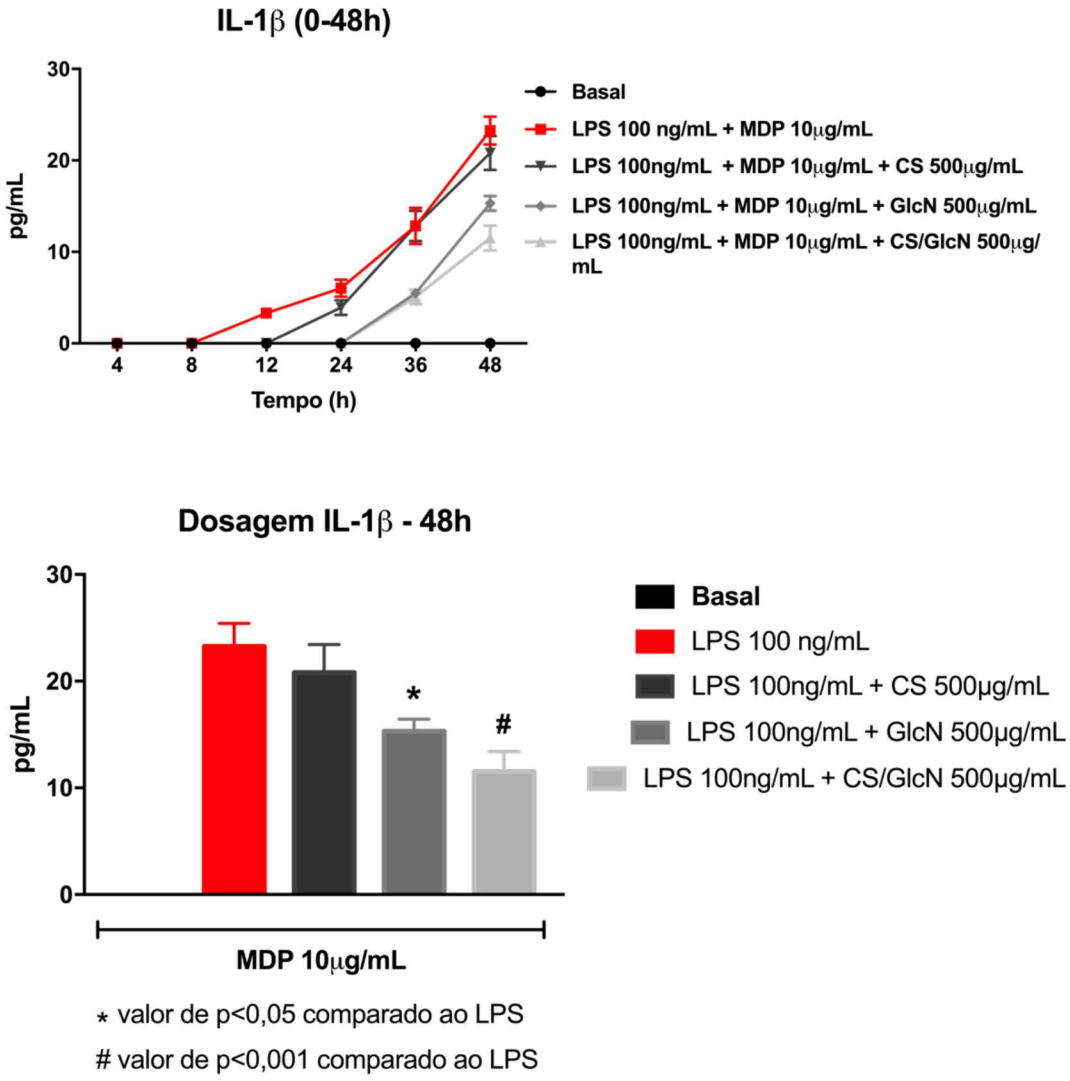

Figura 28. Efeito do CS, GlcN e CS/GlcN sobre a produção de IL-1β em macrófagos da linhagem RAW 264.7 desafiadas com LPS 100ng/mL + MDP 10μg/mL no período de 48 horas. Macrófagos da linhagem RAW 264.7 foram cultivados em placas de cultura de 96 poços (80.000 células por poço) utilizando DMEM suplementado com 10% de soro fetal bovino (SFB). Após 24 horas o sobrenadante foi removido e foi adicionado novo meio contendo e LPS 100ng/mL + MDP 10μg/mL e LPS 100ng/mL + MDP 10μg/mL acrescidos de CS, GlcN e CS/GlcN (500μg/mL). Os meios foram coletados após diferentes tempos (0-48h) e realizada a dosagem de IL-1β, conforme descrito em Métodos. Foi realizada a análise dos resultados no tempo de 48 horas para avaliar a liberação de IL-1β. Os valores representam média de triplicatas experimentais, e as barras desvio padrão.

4.2.1.3 Efeito de CS, GlcN e CS/GlcN sobre a atividade de metaloproteases em macrófagos da linhagem RAW 264.7.

Para avaliar a atividade de metaloproteases, MMP-2 e MMP-9, foi realizada análise por zimografia no sobrenadante da cultura de macrófagos da linhagem RAW 264.7, após estímulo com LPS 100ng/mL e incubadas de forma simultânea com CS, GlcN ou CS/GlcN nas concentrações padronizadas por um período de 48h.

A atividade enzimática destas gelatinases foi evidenciada pelas regiões claras dos géis.

Conforme ilustrado na Figura 29 os sobrenadantes dos macrófagos incubados somente com CS não apresentaram atividade reduzida da relação MMP-9/MMP-2. Apenas, com a adição de GlcN ou CS/GlcN, foi verificada a redução proteolítica desta enzima no zimograma, de forma significativa.

Resultado semelhante foi obtido por Chou e colaboradores (2005) em modelo de artrite em ratos, em que foi observado efeito da associação dos compostos enquanto a administração apenas de CS não reduziu MMP-9.

A redução de MMP-9 pela GlcN e sua associação com CS mostra-se importante pois existe uma correlação positiva do aumento da atividade desta enzima com o estágio da doença (OLIVEIRA, 2013).

Além disso, é importante o resultado obtido no presente trabalho, pois MMP-9, está envolvida em processos carcinogênicos que inclui invasão, metástase e angiogênese, promovendo o desenvolvimento e a progressão do câncer, por isso a importância da descoberta de inibidores de MMP-9 (HUANG, 2018).

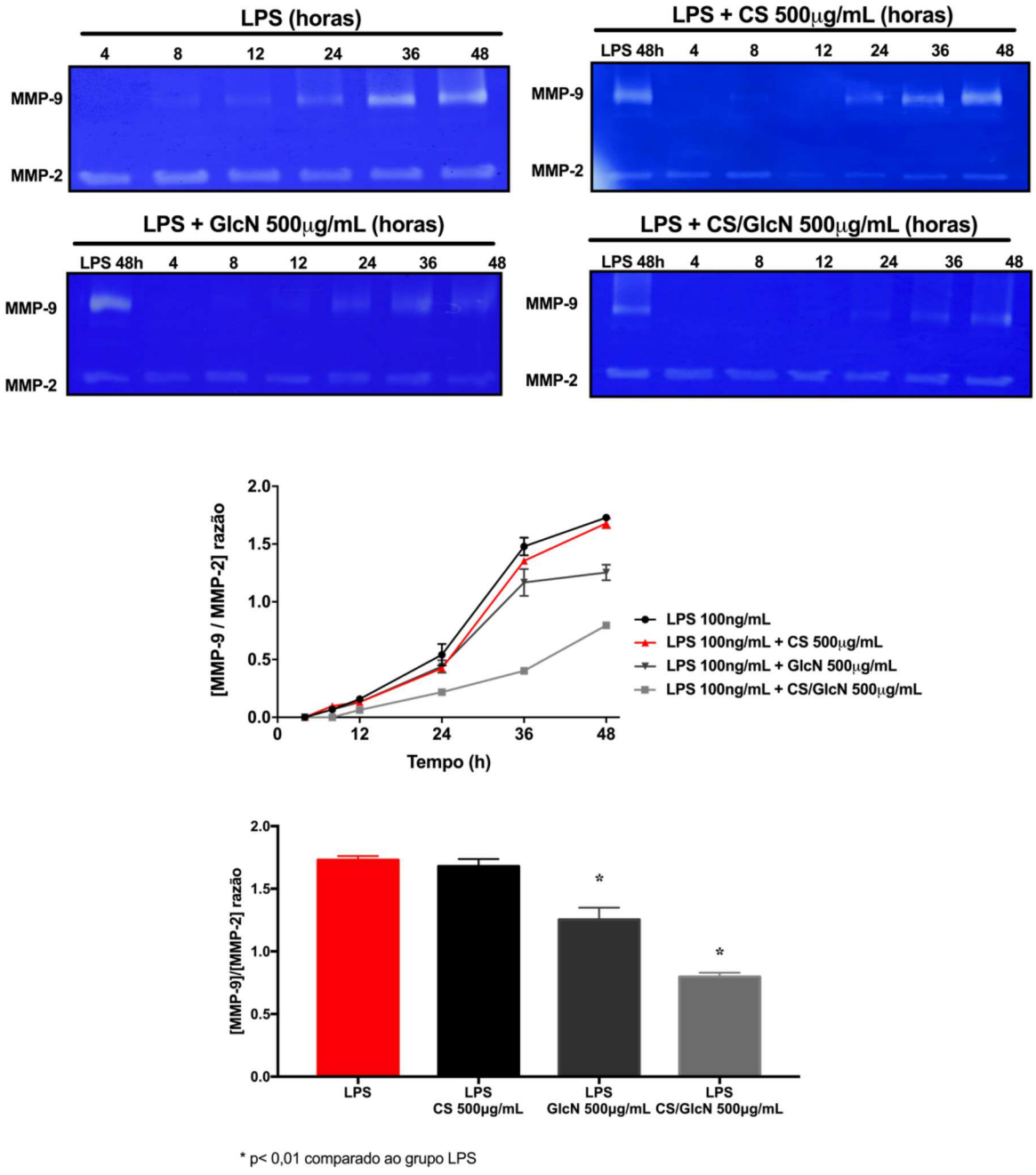

Figura 29. Efeito do CS, GlcN e CS/GlcN sobre a atividade de gelatinases produzidas por macrófagos da linhagem RAW 264.7 desafiadas com LPS 100ng/mL no período de 48h de exposição. Macrófagos da linhagem RAW 264.7 foram cultivados em placas de cultura de 96 poços (80.000 células por poço) utilizando DMEM suplementado com 10% de soro fetal bovino (SFB). Após 24 horas o sobrenadante foi removido e foi adicionado novo meio contendo LPS 100ng/mL e LPS 100ng/mL acrescidos de CS, GlcN e CS/GlcN (500µg/mL). Os meios foram coletados em diferentes tempos (0-48h) e realizada zimograma, conforme descrito em Métodos. Foi realizada a análise dos resultados no perío co de 48 horas e no tempo de 48 horas para avaliar a atividade das gelatinases. Os valores foram expressos pela razão MMP-9/MMP-2, representam média de triplicatas experimentais, e as barras o desvio padrão.

4.2.1.4 Análise por imunofluorescência confocal do deslocamento nuclear de NF-kB

O deslocamento nuclear do fator de transcrição NF-kB foi estimado com base na razão entre a intensidade de fluorescência de NF-kB no núcleo pela intensidade de fluorescência no citoplasma (NF-kB núcleo/citoplasma).

A Figura 30 mostra, imagens representativas da marcação do núcleo (DAPI) e de NF-kB, bem como a sobreposição (*Merge*) em macrófagos estimulados por 30 minutos com LPS 10 ng/mL.

Nos macrófagos não estimulados (basal), a marcação de NF-kB é menor no núcleo das células e maior no citoplasma. No entanto, com LPS 10ng/mL é possível notar maior marcação de NF-kB no núcleo, evidenciando o deslocamento nuclear do fator de transcrição, ou seja, sua ativação.

Os macrófagos estimulados por LPS 10 ng/mL com CS, GlcN e CS/GlcN, conforme metodologia, mostraram redução significativa do deslocamento nuclear em comparação com LPS 10ng/mL.

Diferentes estudos com CS, GlcN e a associação, mostram resultados semelhantes em que todos os compostos foram capazes de reduzir a translocação do NFkB (CANAS et al., 2010; CHAN; CARON; ORTH, 2006; DA CUNHA et al., 2017; IMAGAWA et al., 2011; LARGO et al., 2003; STABLER et al., 2017)

Estes resultados são importantes, pois, a redução da translocação do NFkB reflete na expressão de proteínas pró-inflamatórias e a liberação de citocinas, analisadas neste trabalho. Assim, esse resultado confirma os resultados anteriores em que há uma diminuição significativa dos parâmetros pro-inflamatórios analisados para quase todos os compostos testados.

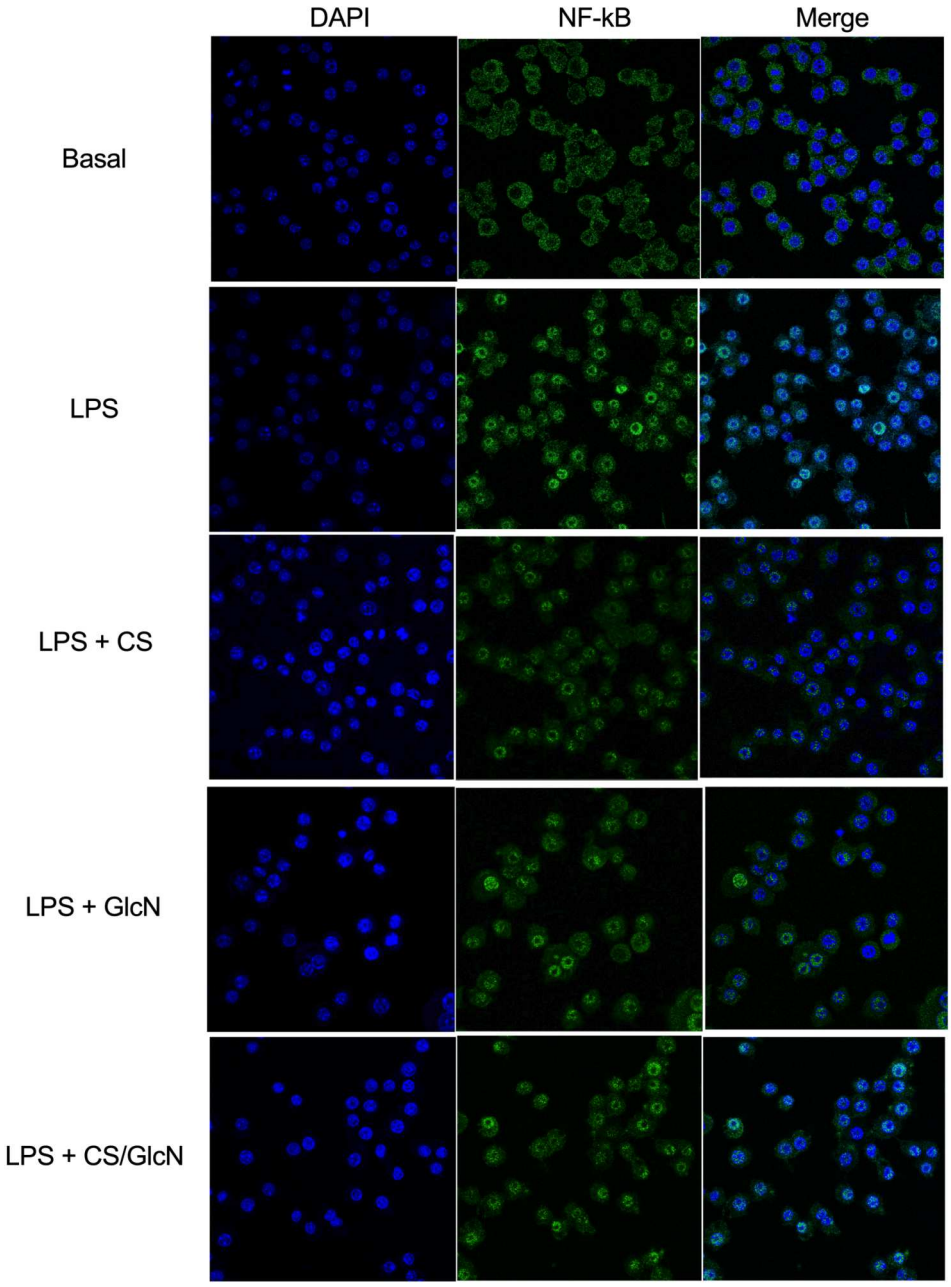
DAPI
NF-kB
Merge
Basal
LPS
LPS + CS
LPS + GlcN
LPS + CS/GlcN

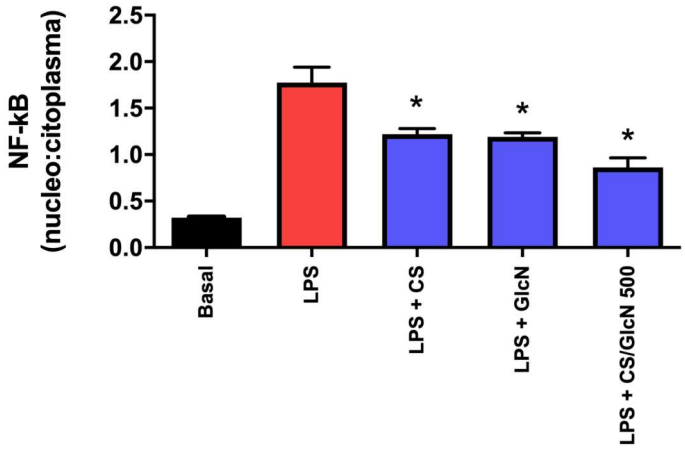
NF-kB
(nucleo:citoplasma)
2.5
2.0
1.5
1.0
0.5
0.0
*
*
*
Basal
LPS
LPS + CS
LPS + GlcN
LPS + CS/GlcN 500

Figura 30. Efeito do CS, GlcN e CS/GlcN sobre o deslocamento nuclear de NF-kB em macrófagos da linhagem RAW 264.7. Macrófagos da linhagem RAW 264.7 foram cultivadas sobre lamínula de 13mm para miscroscopia confocal ($5x10^5$ células/lamínula), conforme descrito em Métodos. As células foram tratadas com CS/GlcN 500μg/mL e desafiadas com LPS 10ng/mL. Após 30 minutos, os meios condicionados foram removidos e as células foram submetidas a protocolo de imunofluorescência. As intensidades de fluorescência do NF-kB no núcleo e citoplasma foram analizasadas utilizando o programa FIJI. A razão entre a intensidade de fluorescência de NF-kB no núcleo e a marcação nuclear (DAPI) foi utilizada como medida relativa do deslocamento do fator de transcrição para o núcleo.

4.2.1.5 Análise da expressão de iNOS, IL-1β

Após análise da produção de NO e de IL-1β por macrófagos da linhagem RAW 264.7, foi realizado um experimento para avaliar a expressão proteica de iNOS e de IL-1β por *Western Blotting* (Figura 31).

De acordo com os resultados, observamos que CS, GlcN e CS/GlcN foram capazes de reduzir a expressão de iNOS de forma significativa. O que reflete o resultado também obtido na produção e liberação de NO para o meio de cultura quando incubados com CS, GlcN e CS/GlcN.

Com relação a produção de IL-1β, após estímulo com LPS e MDP que é capaz de promover a clivagem da pro-IL-1β e sua liberação para o meio de cultura. Observamos que tanto CS, GlcN e CS/GlcN foram capazes de retardar a clivagem da pro-IL-1β (presente na célula) e a liberação de IL-1β para o meio de cultura, onde é dosada. Corroborando com os dados obtidos na dosagem desta interleucina.

Li e colaboradores (2019), obtiveram resultados semelhantes com CS em condrócitos em que observou uma redução na expressão de iNOS bem como a expressão de IL-1β.

Outro trabalho, usando cartilagem articular bovina estimulada por IL-1, observou que a associação de CS/GlcN e a GlcN foram capazes de reduzir a expressão de iNOS (CHAN et al., 2005).

Portanto, os resultados obtidos neste trabalho, reforçam a importância destas moléculas na atividade anti-inflamatória.

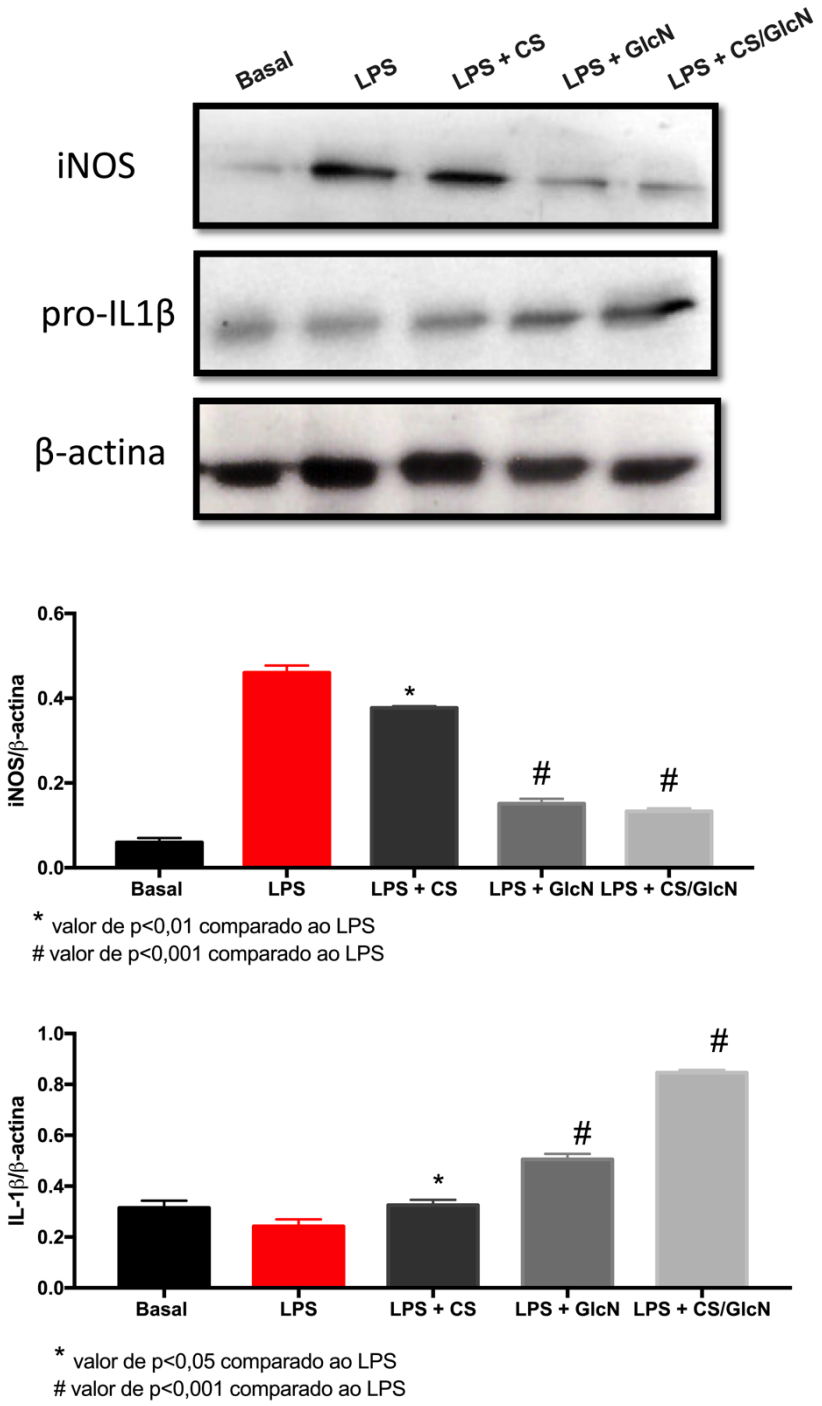

Figura 31. Expressão de iNOS e IL-1b em nas células de macrófagos da linhagem RAW 264.7. Macrófagos da linhagem RAW 264.7 foram cultivadas em placas de 10 mm ($1x10^6$ células/placas), conforme descrito em Métodos. As células foram desafiadas com LPS 100ng/mL e tratadas com CS, GlcN e CS/GlcN 500μg/mL. Após 48 horas, os meios condicionados foram removidos e as células foram submetidas a protocolo de lise celular, foram aplicados 30μg de proteína e realizada corrida de eletroforese e transferência para membrana de PVDF. Após incubação com os anticorpos na membrana o complexo antígeno-anticorpo foi revelado por quimiolumenescência.

4.3 AVALIAÇÃO DA CONCENTRAÇÃO DE LPS PARA INDUÇÃO DE PROCESSO INFLAMATÓRIO NAS CÉLULAS IEC-6 E CACO-2

Para avaliar a indução de processo inflamatório nas células IEC-6, foram testadas, em diferentes concentrações de LPS de diferentes origens (*E. coli* e *Salmonella*).

Inicialmente foi analisada, o perfil de liberação de NO nas células IEC-6 desafiadas por LPS (*E. coli)* em diferentes concentrações até 50 e 100μg/mL no período de 48 horas após testarem concentrações menores (Figura 32).

A produção de NO pelas células IEC-6 desafiadas com LPS não foi capaz de produzir NO de forma significativa comparada a produção de macrófagos.

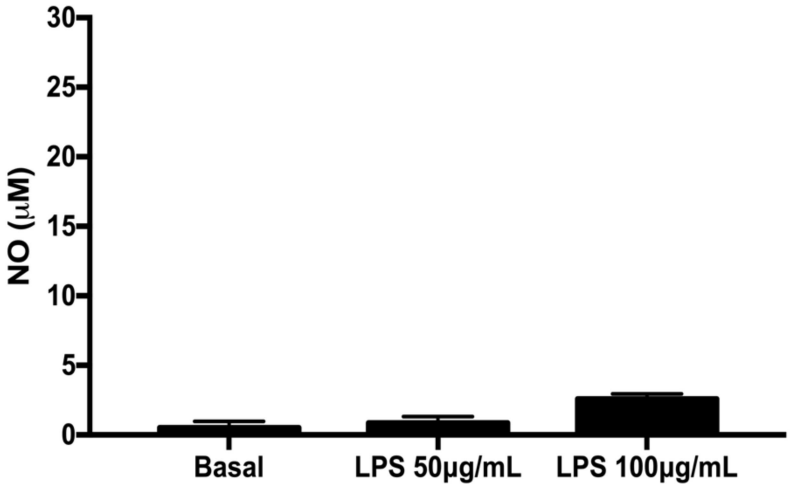

Figura 32. Efeito do LPS *E. coli* na produção de NO. Células de endotélio intestinal (IEC-6) foram cultivadas em placas de cultura de 96 poços (100.000 células por poço) utilizando DMEM suplementado com 10% de soro fetal bovino (SFB). Após 24 horas o sobrenadante foi removido e foi adicionado novo meio contendo e LPS *E. coli* (50 e 100μg/mL). Os meios foram coletados após 48 horas e realizada a dosagem de NO, conforme descrito em Métodos. Os valores representam média de triplicatas experimentais, e as barras desvio padrão.

Para avaliar se a fonte do LPS obtido poderia interferir no estimulo de LPS na produção de NO. Foi testado, LPS em diferentes concentrações provenientes de cepas de *E. coli* e *Salmonella* nos tempos de 48 horas e 72 horas (Figura 33). Porém não foi obtido êxito com o experimento e a produção de NO continuou próximo da produção basal da célula.

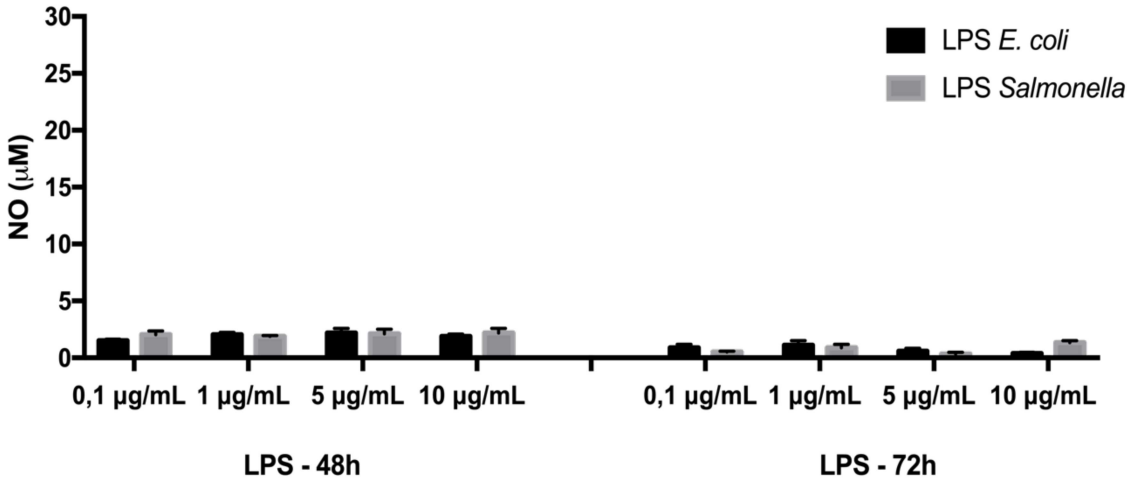

Figura 33. Efeito do LPS *E. coli* e de *Salmonella* na produção de NO no tempo de 48 horas e 72 horas. Células de endotélio intestinal (IEC-6) foram cultivadas em placas de cultura de 96 poços (100.000 células por poço) utilizando DMEM suplementado com 10% de soro fetal bovino (SFB). Após 24 horas o sobrenadante foi removido e foi adicionado novo meio contendo e LPS *E. coli* e *Salmonella* (0,1-10μg/mL). Os meios foram coletados após 48 horas e realizada a dosagem de NO, conforme descrito em Métodos. Os valores representam média de triplicatas experimentais, e as barras desvio padrão.

Os resultados observados se justificam, pois, no trato gastrointestinal, milhares de microrganismos coexistem com células mantendo um ambiente mutualista (BACKHED et al., 2005; DHEER et al., 2016; HOOPER; MIDTVEDT; GORDON, 2002). E o epitélio intestinal, juntamente com o muco secretado por essas células, forma a barreira física para esses microrganismos comensais. Além disso os receptores Toll-like estão expressos nas células epiteliais para regular essas bactérias comensais (JANEWAY; GOODNOW; MEDZHITOV, 1996; LIEVIN-LE MOAL; SERVIN, 2006).

Por conta dessa bactérias presentes no ambiente intestinal, a expressão de receptores Tool-like é reduzida, principalmente o TLR4 nas células epiteliais e da lâmina própria do intestino (ABREU, 2010; OTTE; CARIO; PODOLSKY, 2004). Assim, mesmo expondo as células IEC-6 e Caco-2 aos diferentes tipos de LPS, a produção de NO seria baixa, pois não há números suficientes de TLR4 para ser ativado e desencadear a produção de NO.

5 CONCLUSÃO

- O CS sulfato das amostras utilizadas após caracterização confirmou ser do tipo 4-sulfato, com peso molecular modal de 30kDa;
- Nenhum dos compostos analisados possuíam qualquer tipo de contaminação;
- CS, GlcN e CS/GlcN na concentração estudada foram capazes de reduzir a produção de NO de forma significativa;
- CS, GlcN e CS/GlcN na concentração estudada foram capazes de reduzir a produção e liberação de TNF-α de forma significativa;
- Somente GlcN e CS/GlcN reduziram a produção e liberação de IL-6 bem como IL-1β;
- A redução da relação MMP-9/MMP-2 foi observada pela GlcN e sua associação com CS;
- A translocação do NFkB e a expressão de iNOS foi diminuída por todos os compostos de forma significativa;
- Houve uma regulação na clivagem da proteína inativa, pro-IL-1β, pelo CS, GlcN e CS/GlcN impedindo sua clivagem e liberação para o meio de cultura;

Portanto, verificamos que os compostos analisados neste trabalho possuem uma importante atividade anti-inflamatória, visto que, todos eles reduziram a translocação do NFkB, importante fator de transcrição envolvido na sinalização celular para amplificar uma resposta inflamatória. Sendo essa redução da translocação, confirmada com as dosagens realizadas de fatores pro-inflamatórios estimulados por essa via do NFkB, em que quase todas foram reduzidas pelas substancias estudadas.

Além disso, pudemos observar que a GlcN e CS/GlcN reduzem a clivagem da pro-IL-1β de forma mais significativa, sugerindo que estes compostos podem atuar no mecanismo de ativação do NLRP3 inflamassoma, conforme Figura 34.

Para isso, estudos sobre essa via de sinalização com estes compostos devem ser realizados.

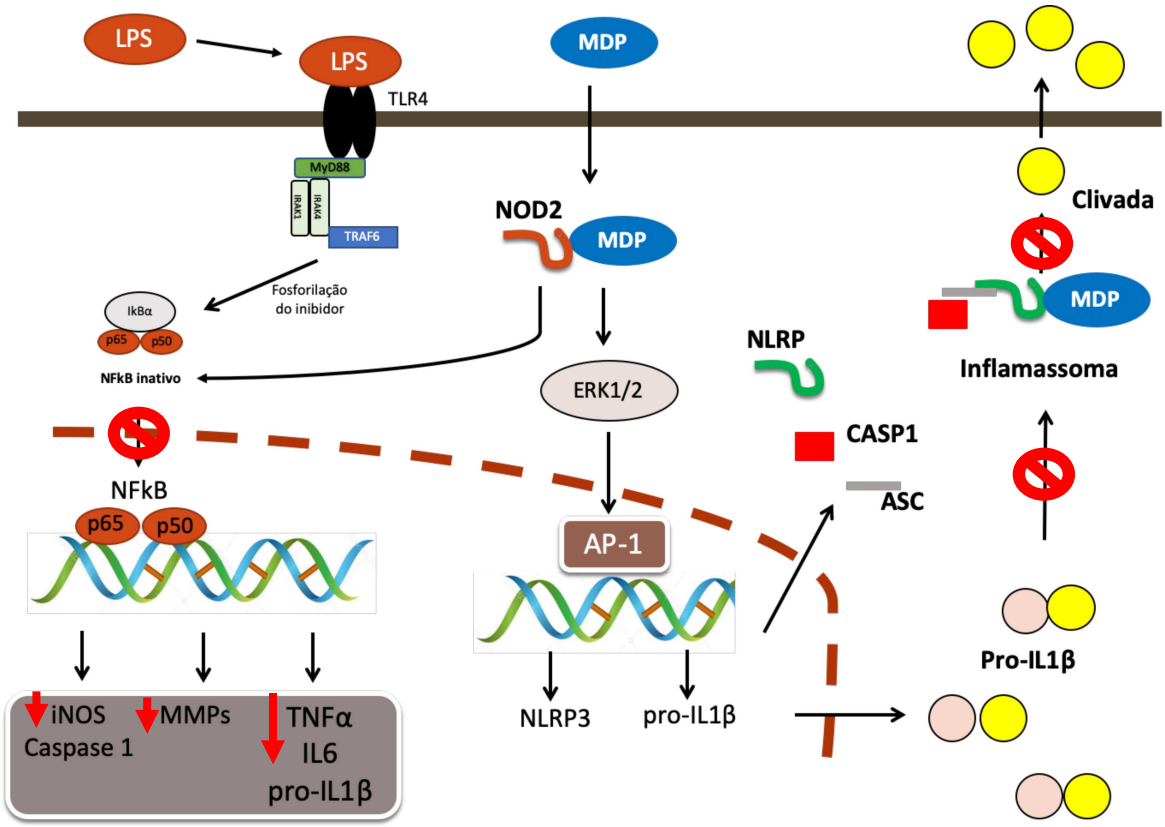

Figura 34. Modelo do mecanismo de ação de CS, GlcN e CS/GlcN baseados nos resultados obtidos no presente trabalho. Redução da translocação do NFkB e consequente redução da expressão de iNOS e produção de NO, redução da atividade de MMP9 e da liberação de TNF-α e IL-6. Ação sobre a clivagem da pro-IL-1β em IL-1β (sua forma ativa

REFERÊNCIAS

ABREU, M. T. Toll-like receptor signalling in the intestinal epithelium: How bacterial recognition shapes intestinal functionNature Reviews Immunology, 2010.

AGUIAR, J. A. et al. An improved methodology to produce Flavobacterium heparinum chondroitinases, important instruments for diagnosis of diseases. **Biotechnol Appl Biochem**, 2003.

AKIRA, S.; UEMATSU, S.; TAKEUCHI, O. Pathogen Recognition and Innate Immunity. **Cell**, v. 124, n. 4, p. 783–801, 24 fev. 2006.

ANDERSEN, V. et al. Diet and risk of inflammatory bowel diseaseDigestive and Liver Disease, 2012.

ATREYA, I.; ATREYA, R.; NEURATH, M. F. NF-kappaB in inflammatory bowel disease. **J Intern Med**, v. 263, n. 6, p. 591–596, 2008.

BACKHED, F. et al. Host-Bacterial Mutualism in the Human Intestine. **Science**, v. 307, n. 5717, p. 1915–1920, 25 mar. 2005.

BAENZIGER, J. U. Glycoprotein hormone GalNAc-4-sulphotransferase. **Biochemical Society transactions**, v. 31, n. 2, p. 326–330, abr. 2003.

BAIN, C. C.; MOWAT, A. M. Macrophages in intestinal homeostasis and inflammation. **Immunological reviews**, v. 260, n. 1, p. 102–117, jul. 2014.

BAMIAS, G.; COMINELLI, F. Cytokines and intestinal inflammation. **Current Opinion in Gastroenterology**, v. 32, n. 6, p. 437–442, nov. 2016.

BANDTLOW, C. E. et al. Proteoglycans in the developing brain: new conceptual insights for old proteins. **Physiological reviews**, 2000.

BENT, R. et al. Interleukin-1 Beta—A Friend or Foe in Malignancies? **International Journal of Molecular Sciences**, v. 19, n. 8, p. 2155, 24 jul. 2018.

BOUMA, G.; STROBER, W. The immunological and genetic basis of inflammatory bowel disease. **Nat Rev Immunol**, v. 3, n. 7, p. 521–533, 2003.

BREDT, D. S.; SNYDER, S. H. Isolation of nitric oxide synthetase, a calmodulin-requiring enzyme. **Proceedings of the National Academy of Sciences**, v. 87, n. 2, p. 682–685, 1 jan. 1990.

CALABRO, A. et al. Fluorophore-assisted carbohydrate electrophoresis (FACE) of glycosaminoglycans. **Osteoarthritis and Cartilage**, v. 9, p. 16–22, 2001.

CALABRO, A.; HASCALL, V. C.; MIDURA, R. J. Adaptation of FACE methodology for microanalysis of total hyaluronan and chondroitin sulfate composition from cartilage. **Glycobiology**, v. 10, n. 3, p. 283–93, 1 mar. 2000.

CAMPO, G. M. et al. Hyaluronic acid and chondroitin-4-sulphate treatment reduces damage in carbon tetrachloride-induced acute rat liver injury. **Life Sci**, v. 74, n. 10, p. 1289–1305, 2004.

CAMPO, G. M. et al. Chondroitin-4-Sulphate Reduced Oxidative Injury in Caerulein-Induced Pancreatitis in Mice: The Involvement of NF-κB Translocation and Apoptosis Activation. **Experimental Biology and Medicine**, v. 233, n. 6, p. 741–752, jun. 2008.

CAMPO, G. M. et al. Glycosaminoglycans modulate inflammation and apoptosis in LPS-treated chondrocytes. **J Cell Biochem**, v. 106, n. 1, p. 83–92, 2009.

CANAS, N. et al. Chondroitin sulfate inhibits lipopolysaccharide-induced inflammation in rat astrocytes by preventing nuclear factor kappa B activation. **Neuroscience**, v. 167, n. 3, p. 872–879, 2010.

CASSARO, C. M.; DIETRICH, C. P. Distribution of sulfated mucopolysaccharides in invertebrates. **The Journal of biological chemistry**, v. 252, n. 7, p. 2254–2261, abr. 1977.

CHAN, P.-S.; CARON, J. P.; ORTH, M. W. Short-term gene expression changes in cartilage explants stimulated with interleukin beta plus glucosamine and chondroitin sulfate. **The Journal of rheumatology**, v. 33, n. 7, p. 1329–40, jul. 2006.

CHAN, P. S. et al. Glucosamine and chondroitin sulfate regulate gene expression and synthesis of nitric oxide and prostaglandin E2 in articular cartilage explants. **Osteoarthritis and Cartilage**, v. 13, n. 5, p. 387–394, maio 2005.

CHIU, H.-W. et al. Glucosamine inhibits IL-1β expression by preserving mitochondrial integrity and disrupting assembly of the NLRP3 inflammasome. **Scientific Reports**, v. 9, n. 1, p. 5603, 3 dez. 2019.

CHOU, M. M. et al. Effects of Chondroitin and Glucosamine Sulfate in a Dietary Bar Formulation on Inflammation, Interleukin-1β, Matrix Metalloprotease-9, and Cartilage Damage in Arthritis. **Experimental Biology and Medicine**, v. 230, n. 4, p. 255–262, 29 abr. 2005.

CLEGG, D. O. et al. Glucosamine, chondroitin sulfate, and the two in combination for painful knee osteoarthritis. **N Engl J Med**, v. 354, n. 8, p. 795–808, 2006.

COCHET, F.; PERI, F. The Role of Carbohydrates in the Lipopolysaccharide (LPS)/Toll-Like Receptor 4 (TLR4) Signalling. **International Journal of Molecular Sciences**, v. 18, n. 11, p. 2318, 3 nov. 2017.

COWMAN, M. K.; MATSUOKA, S. Experimental approaches to hyaluronan structure. **Carbohydrate Research**, v. 340, n. 5, p. 791–809, 11 abr. 2005.

CROSS, R. K.; WILSON, K. T. Nitric oxide in inflammatory bowel disease. **Inflamm Bowel Dis**, v. 9, n. 3, p. 179–189, 2003.

CUI, J. et al. Mechanisms and pathways of innate immune activation and regulation in health and cancer. **Human Vaccines & Immunotherapeutics**, v. 10, n. 11, p. 3270–3285, 2 nov. 2014.

DA CUNHA, A. L. et al. Pharmaceutical grade chondroitin sulfate: Structural analysis and identification of contaminants in different commercial preparations. **Carbohydr Polym**, v. 134, p. 300–308, 2015.

DA CUNHA, A. L. et al. Do chondroitin sulfates with different structures have different activities on chondrocytes and macrophages? **International Journal of Biological Macromolecules**, v. 103, p. 1019–1031, out. 2017.

DE BRUYN, M. et al. The molecular biology of matrix metalloproteinases and tissue inhibitors of metalloproteinases in inflammatory bowel diseases. **Critical Reviews in Biochemistry and Molecular Biology**, 2016.

DESAIRE, H.; LEARY, J. A. Detection and quantification of the sulfated disaccharides in chondroitin sulfate by electrospray tandem mass spectrometry. **Journal of the American Society for Mass Spectrometry**, 2000.

DHEER, R. et al. Intestinal Epithelial Toll-Like Receptor 4 Signaling Affects Epithelial Function and Colonic Microbiota and Promotes a Risk for Transmissible Colitis. **Infection and Immunity**, v. 84, n. 3, p. 798–810, 11 mar. 2016.

DIETRICH, C. P. Novel heparin degradation products. Isolation and characterization of novel disaccharides and oligosaccharides produced from heparin by bacterial degradation. **Biochemical Journal**, v. 108, n. 4, p. 647–654, 1 jul. 1968.

DIETRICH, C. P. et al. Changes in the composition of sulfated mucopolysaccharides during neoplastic transformation of cerebral tissue. **Cancer research**, United States, nov. 1978.

DIETRICH, C. P. et al. Heparin in molluscs: chemical, enzymatic degradation and 13C and 1H n.m.r. spectroscopical evidence for the maintenance of the structure through evolution. **Int J Biol Macromol**, v. 11, n. 6, p. 361–366, 1989.

DIETRICH, C. P. et al. Structure of heparan sulfate: identification of variable and constant oligosaccharide domains in eight heparan sulfates of different origins. **Cellular and molecular biology (Noisy-le-Grand, France)**, v. 44, n. 3, p. 417–29, maio 1998.

DIETRICH, C. P.; DIETRICH, S. M. Electrophoretic behaviour of acidic mucopolysaccharides in diamine buffers. **Anal Biochem**, v. 70, n. 2, p. 645–647, 1976.

DIETRICH, C. P.; SAMPAIO, L. O.; TOLEDO, O. M. S. Characteristic distribution of sulfated mucopolysaccharides in different tissues and in their respective mitochondria. **Biochemical and Biophysical Research Communications**, 1976.

DINARELLO, C. A. Biologic basis for interleukin-1 in disease. **Blood**, v. 87, n. 6, p. 2095–147, 15 mar. 1996.

DU SOUICH, P. et al. Immunomodulatory and anti-inflammatory effects of chondroitin sulphate. **J Cell Mol Med**, v. 13, n. 8A, p. 1451–1463, 2009.

ESKO, J. D.; KIMATA, K.; LINDAHL, U. Proteoglycans and Sulfated Glycosaminoglycans. In: VARKI, A. et al. (Eds.). . Cold Spring Harbor (NY): [s.n.].

FENTON, J. I. et al. Glucosamine HCl reduces equine articular cartilage degradation in explant culture. **Osteoarthritis Cartilage**, v. 8, n. 4, p. 258–265, 2000.

FRANSSON, L.-A.; MALMSTROM, A. Structure of Pig Skin Dermatan Suflate. 1. Distribution of D-Glucuronic Acid Residues. **European Journal of Biochemistry**, v. 18, n. 3, p. 422–430, 1 fev. 1971.

FURCHGOTT, R. F.; ZAWADZKI, J. V. The obligatory role of endothelial cells in the relaxation of arterial smooth muscle by acetylcholine. **Nature**, v. 288, n. 5789, p. 373–376, nov. 1980.

GALLAGHER, J. T.; WALKER, A. Molecular distinctions between heparan sulphate and heparin. Analysis of sulphation patterns indicates that heparan sulphate and heparin are separate families of *N* -sulphated polysaccharides. **Biochemical Journal**, v. 230, n. 3, p. 665–674, 15 set. 1985.

GARG, P. et al. Selective ablation of matrix metalloproteinase-2 exacerbates experimental colitis: contrasting role of gelatinases in the pathogenesis of colitis. **J Immunol**, v. 177, n. 6, p. 4103–4112, 2006.

GEMBA, T. et al. Focal adhesion kinase and mitogen-activated protein kinases are involved in chondrocyte activation by the 29-kDa amino-terminal fibronectin fragment. **Journal of Biological Chemistry**, 2002.

GEREMIA, A. et al. Innate and adaptive immunity in inflammatory bowel disease. **Autoimmunity reviews**, v. 13, n. 1, p. 3–10, jan. 2014.

GEROVA, V. A. et al. Increased intestinal permeability in inflammatory bowel diseases assessed by iohexol test. **World Journal of Gastroenterology**, 2011.

GERSEMANN, M.; WEHKAMP, J.; STANGE, E. F. Innate immune dysfunction in inflammatory bowel diseaseJournal of Internal Medicine, 2012.

GOMES, P. B.; DIETRICH, C. P. Distribution of heparin and other sulfated glycosaminoglycans in vertebrates. **Comparative Biochemistry and Physiology -- Part B: Biochemistry and**, 1982.

GOTO, Y.; IVANOV, I. I. Intestinal epithelial cells as mediators of the commensal–host immune crosstalk. **Immunology and Cell Biology**, 2013.

GRISHIN, A. V et al. Lipopolysaccharide induces cyclooxygenase-2 in intestinal epithelium via a noncanonical p38 MAPK pathway. **J Immunol**, v. 176, n. 1, p. 580–588, 2006.

GROSS, A. R.; THEOHARIDES, T. C. Chondroitin sulfate inhibits secretion of TNF and CXCL8 from human mast cells stimulated by IL-33. **BioFactors**, v. 45, n. 1, p. 49–61, jan. 2019.

HAYDEN, M. S.; WEST, A. P.; GHOSH, S. NF-kappaB and the immune response. **Oncogene**, v. 25, n. 51, p. 6758–6780, 2006.

HAYES, A. et al. Biodiversity of CS–proteoglycan sulphation motifs: chemical messenger recognition modules with roles in information transfer, control of cellular behaviour and tissue morphogenesis. **Biochemical Journal**, v. 475, n. 3, p. 587–620, 14 fev. 2018.

HE, Y.; HARA, H.; NÚÑEZ, G. Mechanism and Regulation of NLRP3 Inflammasome Activation. **Trends in Biochemical Sciences**, v. 41, n. 12, p. 1012–1021, 1 dez. 2016.

HERULF, M. et al. Increased luminal nitric oxide in inflammatory bowel disease as shown with a novel minimally invasive method. **Scand J Gastroenterol**, v. 33, n. 2, p. 164–169, 1998.

HILBORN, J. C.; ANASTASSIADIS, P. A. Estimation of the molecular weights of acidic mucopolysaccharides by polyacrylamide gel electrophoresis. **Analytical biochemistry**, v. 39, n. 1, p. 88–92, jan. 1971.

HIMMEL, M. E. et al. Regulatory T-cell therapy for inflammatory bowel disease: More questions than answersImmunology, 2012.

HIROTA, S. A. et al. NLRP3 inflammasome plays a key role in the regulation of intestinal homeostasis. **Inflammatory Bowel Diseases**, v. 17, n. 6, p. 1359–1372, jun. 2011.

HOOPER, L. V.; MIDTVEDT, T.; GORDON, J. I. How host-microbial interactions shape the nutrient environment of the mammalian intestine. **Annual Review of Nutrition**, v. 22, n. 1, p. 283–307, jul. 2002.

HUANG, B.-P. et al. AMPK activation inhibits expression of proinflammatory mediators through downregulation of PI3K/p38 MAPK and NF-kappaB signaling in murine macrophages. **DNA and cell biology**, v. 34, n. 2, p. 133–141, fev. 2015.

HUANG, H. Matrix Metalloproteinase-9 (MMP-9) as a Cancer Biomarker and MMP-9 Biosensors: Recent Advances. **Sensors**, v. 18, n. 10, p. 3249, 27 set. 2018.

HUANG, Y.; CHEN, Z. Inflammatory bowel disease related innate immunity and adaptive immunity. **American journal of translational research**, v. 8, n. 6, p. 2490–2497, 2016.

IGNARRO, L. J. et al. Endothelium-derived relaxing factor produced and released from artery and vein is nitric oxide. **Proceedings of the National Academy of Sciences**, v. 84, n. 24, p. 9265–9269, 1 dez. 1987.

IMADA, K. et al. Anti-arthritic action mechanisms of natural chondroitin sulfate in human articular chondrocytes and synovial fibroblasts. **Biol Pharm Bull**, v. 33, n. 3, p. 410–414, 2010.

IMAGAWA, K. et al. The epigenetic effect of glucosamine and a nuclear factor-kappa B (NF-kB) inhibitor on primary human chondrocytes – Implications for osteoarthritis. **Biochemical and Biophysical Research Communications**, v. 405, n. 3, p. 362–367, 18 fev. 2011.

IOVU, M.; DUMAIS, G.; DU SOUICH, P. Anti-inflammatory activity of chondroitin sulfate. **Osteoarthritis Cartilage**, v. 16 Suppl 3, p. S14-8, 2008.

IOZZO, R. V.; SCHAEFER, L. Proteoglycan form and function: A comprehensive nomenclature of proteoglycans. **Matrix Biology**, v. 42, p. 11–55, mar. 2015.

IOZZO, R. V. Matrix proteoglycans: from molecular design to cellular function. **Annu Rev Biochem**, v. 67, p. 609–652, 1998.

ITO, Y.; HABUCHI, O. Purification and characterization of N-acetylgalactosamine 4-sulfate 6-O-sulfotransferase from the squid cartilage. **The Journal of biological chemistry**, v. 275, n. 44, p. 34728–34736, nov. 2000.

IWASAKI, A.; MEDZHITOV, R. Toll-like receptor control of the adaptive immune responses. **Nature Immunology**, v. 5, n. 10, p. 987–995, 28 out. 2004.

JACKSON, P. The use of polyacrylamide-gel electrophoresis for the high-resolution separation of reducing saccharides labelled with the fluorophore 8-aminonaphthalene-1,3,6-trisulphonic acid. Detection of picomolar quantities by an imaging system based on a cooled charge-coupled device. **Biochemical Journal**, v. 270, n. 3, p. 705–713, 15 set. 1990.

JACKSON, P. Polyacrylamide gel electrophoresis of reducing saccharides labeled with the fluorophore 2-aminoacridone: Subpicomolar detection using an imaging system based on a cooled charge-coupled device. **Analytical Biochemistry**, v. 196, n. 2, p. 238–244, ago. 1991.

JACKSON, P. The Analysis of Fluorophore-Labeled Glycans by High-Resolution Polyacrylamide-Gel Electrophoresis. **Analytical Biochemistry**, v. 216, n. 2, p. 243–252, 1 fev. 1994.

JACKSON, R. L.; BUSCH, S. J.; CARDIN, A. D. Glycosaminoglycans: molecular properties, protein interactions, and role in physiological processes. **Physiol Rev**, v. 71, n. 2, p. 481–539, 1991.

JANEWAY, C. A.; GOODNOW, C. C.; MEDZHITOV, R. Danger - pathogen on the premises! Immunological tolerance. **Current biology : CB**, v. 6, n. 5, p. 519–22, 1 maio 1996.

JOMPHE, C. et al. Chondroitin sulfate inhibits the nuclear translocation of nuclear factor-kappaB in interleukin-1beta-stimulated chondrocytes. **Basic Clin Pharmacol Toxicol**, v. 102, n. 1, p. 59–65, 2008.

JORDAN, K. M. et al. EULAR Recommendations 2003: an evidence based approach to the management of knee osteoarthritis: Report of a Task Force of the Standing Committee for International Clinical Studies Including Therapeutic Trials (ESCISIT). **Ann Rheum Dis**, v. 62, n. 12, p. 1145–1155, 2003.

KALLIOLIAS, G. D.; IVASHKIV, L. B. TNF biology, pathogenic mechanisms and emerging therapeutic strategies. **Nature Reviews Rheumatology**, v. 12, n. 1, p. 49–62, 10 jan. 2016.

KANG, S.; TANAKA, T.; KISHIMOTO, T. Therapeutic uses of anti-interleukin-6 receptor antibody. **International Immunology**, v. 27, n. 1, p. 21–29, 1 jan. 2015.

KARAMANOS, N. K. et al. Determination of 24 variously sulfated galactosaminoglycan- and hyaluronan-derived disaccharides by high-performance liquid chromatography. **Analytical Biochemistry**, 1994.

KAWAGOE, T. et al. Sequential control of Toll-like receptor–dependent responses by IRAK1 and IRAK2. **Nature Immunology**, v. 9, n. 6, p. 684–691, 27 jun. 2008.

KHOR, B.; GARDET, A.; XAVIER, R. J. Genetics and pathogenesis of inflammatory bowel disease. **Nature**, v. 474, n. 7351, p. 307–317, 2011.

KIESSLICH, R. et al. Local barrier dysfunction identified by confocal laser endomicroscopy predicts relapse in inflammatory bowel disease. **Gut**, 2012.

KJELLEN, L.; LINDAHL, U. Proteoglycans: structures and interactions. **Annu Rev Biochem**, v. 60, p. 443–475, 1991.

KOSLOWSKI, M. J. et al. Innate antimicrobial host defense in small intestinal Crohn's diseaseInternational Journal of Medical Microbiology, 2010.

KRUKENBERG, C. Die chemischen Bestandteile des Knorpels. **Z Biol**, v. v. 20, p. 307–326, 1884.

LAMARI, F. N. et al. Metabolism and biochemical/physiological roles of chondroitin sulfates: analysis of endogenous and supplemental chondroitin sulfates in blood circulation. **Biomed Chromatogr**, v. 20, n. 6–7, p. 539–550, 2006.

LAMARI, F. N.; KARAMANOS, N. K. Structure of Chondroitin Sulfate. In: NICOLA, V. (Ed.). . **Advances in Pharmacology**. [s.l.] Academic Press, 2006. v. Volume 53p. 33–48.

LAMAS, S. et al. Endothelial nitric oxide synthase: molecular cloning and characterization of a distinct constitutive enzyme isoform. **Proceedings of the National Academy of Sciences**, v. 89, n. 14, p. 6348–6352, 15 jul. 1992.

LARGO, R. et al. Glucosamine inhibits IL-1beta-induced NFkappaB activation in human osteoarthritic chondrocytes. **Osteoarthritis Cartilage**, v. 11, n. 4, p. 290–298, 2003.

LARMONIER, C. B. et al. T Lymphocyte Dynamics in Inflammatory Bowel Diseases: Role of the Microbiome. **BioMed Research International**, 2015.

LAURENT, T. C.; FRASER, J. R. Hyaluronan. FASEB journal : official publication of the Federation of American Societies for Experimental Biology, v. 6, n. 7, p. 2397–404, abr. 1992.

LEE, M. et al. Immunobiology of Nitric Oxide and Regulation of Inducible Nitric Oxide Synthase. In: **Results and problems in cell differentiation**. [s.l: s.n.]. v. 62p. 181–207.

LEE, S.-I. et al. Muramyl dipeptide activates human beta defensin 2 and pro-inflammatory mediators through Toll-like receptors and NLRP3 inflammasomes in human dental pulp cells. **Clinical Oral Investigations**, v. 19, n. 6, p. 1419–1428, 3 jul. 2015.

LI, S. et al. Synthesis of chondroitin sulfate magnesium for osteoarthritis treatment. **Carbohydrate Polymers**, v. 212, p. 387–394, 15 maio 2019.
LI, Y. et al. Anti-inflammatory effects in a mouse osteoarthritis model of a mixture of glucosamine and chitooligosaccharides produced by bi-enzyme single-step hydrolysis. **Scientific Reports**, v. 8, n. 1, p. 5624, 4 dez. 2018.

LIEVIN-LE MOAL, V.; SERVIN, A. L. The Front Line of Enteric Host Defense against Unwelcome Intrusion of Harmful Microorganisms: Mucins, Antimicrobial Peptides, and Microbiota. **Clinical Microbiology Reviews**, v. 19, n. 2, p. 315–337, 1 abr. 2006.

LINDAHL, U.; AXELSSON, O. Identification of iduronic acid as the major sulfated uronic acid of heparin. **The Journal of biological chemistry**, v. 246, n. 1, p. 74–82, 10 jan. 1971.

LOWENSTEIN, C. J. et al. Cloned and expressed macrophage nitric oxide synthase contrasts with the brain enzyme. **Proceedings of the National Academy of Sciences**, v. 89, n. 15, p. 6711–6715, 1 ago. 1992.

MAINRECK, N. et al. Rapid characterization of glycosaminoglycans using a combined approach by infrared and Raman microspectroscopies. **Journal of Pharmaceutical Sciences**, 2011.

MALOY, K. J.; POWRIE, F. Intestinal homeostasis and its breakdown in inflammatory bowel disease, **Nature**, 2011.

MANN, E. R.; LI, X. Intestinal antigen-presenting cells in mucosal immune homeostasis: Crosstalk between dendritic cells, macrophages and B-cells. **World Journal of Gastroenterology**, 2014.

MARLETTA, M. A. et al. Macrophage oxidation of L-arginine to nitrite and nitrate: nitric oxide is an intermediate. **Biochemistry**, v. 27, n. 24, p. 8706–8711, nov. 1988.

MARTEL-PELLETIER, J. et al. Cartilage in normal and osteoarthritis conditions. **Best Pract Res Clin Rheumatol**, v. 22, n. 2, p. 351–384, 2008.

MARTEL-PELLETIER, J. et al. Discrepancies in Composition and Biological Effects of Different Formulations of Chondroitin Sulfate. **Molecules**, v. 20, n. 3, p. 4277–4289, 6 mar. 2015.

MATHEWS, M. B.; CIFONELLI, J. A. Comparative biochemistry of keratosulfates. **The Journal of biological chemistry**, v. 240, n. 11, p. 4140–5, nov. 1965.

MATIJASIC, M. et al. Modulating Composition and Metabolic Activity of the Gut Microbiota in IBD Patients. **International journal of molecular sciences**, v. 17, n. 4, abr. 2016.

MEDINA, C. et al. Increased activity and expression of matrix metalloproteinase-9 in a rat model of distal colitis. **Am J Physiol Gastrointest Liver Physiol**, v. 284, n. 1, p. G116-22, 2003.

MEDINA, C.; RADOMSKI, M. W. Role of matrix metalloproteinases in intestinal inflammation. **J Pharmacol Exp Ther**, v. 318, n. 3, p. 933–938, 2006.

MEDZHITOV, R. Origin and physiological roles of inflammation. **Nature**, v. 454, n. 7203, p. 428–435, 23 jul. 2008.

MENEGHETTI, M. C. Z. et al. Heparan sulfate and heparin interactions with proteins. **Journal of The Royal Society Interface**, v. 12, n. 110, p. 20150589, 6 set. 2015.

MEYER, B. N. et al. Brine Shrimp - a Convenient General Bioassay for Active-Plant Constituents. **Planta Med**, v. 45, n. 1, p. 31–34, 1982.

MICHELACCI, Y. M. et al. Chondroitin sulfates and proteoglycans from normal and arthrosic human cartilage. **Connect Tissue Res**, v. 7, n. 1, p. 29–36, 1979.

MICHELACCI, Y. M.; DIETRICH, C. P. A comparative study between a chondroitinase B and a chondroitinase AC from Flavobacterium heparinum: Isolation of a chondroitinase AC-susceptible dodecasaccharide from chondroitin sulphate B. **Biochemical Journal**, 1975.

MICHELACCI, Y. M.; DIETRICH, C. P. Chondroitinase C from Flavobacterium heparinum. **Journal of Biological Chemistry**, 1976a.

MICHELACCI, Y. M.; DIETRICH, C. P. Structure of chondroitin sulfates analyses of the products formed from chondroitin sulfates A and C by the action of the chondroitinases C and AC from Flavobacterium heparinum. **Biochimica et Biophysica Acta (BBA) - General Subjects**, v. 451, n. 2, p. 436–443, 21 dez. 1976b.

MICHELACCI, Y. M.; DIETRICH, C. P. Structure of chondroitin sulphate from whale cartilage: distribution of 6- and 4-sulphated oligosaccharides in the polymer chains. **International Journal of Biological Macromolecules**, v. 8, n. 2, p. 108–113, 1 abr. 1986.

MICHELACCI, Y. M.; HORTON, D. S. P. Q. Proteoglycans from the Cartilage of Young Hammerhead Shark Sphyrna-Lewini. **Comparative Biochemistry and Physiology B-Biochemistry & Molecular Biology**, v. 92, n. 4, p. 651–658, 1989.

MIKAMI, T.; KITAGAWA, H. Biosynthesis and function of chondroitin sulfateBiochimica et Biophysica Acta - General Subjects, 2013.

MITROPOULOU, T. N.; STAGIANNIS, K. D. Variation in sulfation pattern of galactosaminoglycan containing proteoglycans is associated with the development of uterine leiomyoma. **Biomedical Chromatography**, 2004.

MIURA, R. O. et al. Analysis of glycosaminoglycan-degrading enzymes by substrate gel electrophoresis (zymography). **Anal Biochem**, v. 225, n. 2, p. 333–340, 1995.

MOGENSEN, T. H. Pathogen Recognition and Inflammatory Signaling in Innate Immune Defenses. **Clinical Microbiology Reviews**, v. 22, n. 2, p. 240–273, 1 abr. 2009.

MOSMANN, T.; METHODS, J. I. Rapid colorimetric assay for cellular growth and survival: application to proliferation and cytotoxicity assays. **J Immunol Methods**, v. 65, n. 1–2, p. 55–63, 1983.

MUCCI, A.; SCHENETTI, L.; VOLPI, N. 1H and 13C nuclear magnetic resonance identification and characterization of components of chondroitin sulfates of various origin. **Carbohydrate Polymers**, v. 41, n. 1, p. 37–45, 1 jan. 2000.

MULLOY, B.; GRAY, E.; BARROWCLIFFE, T. W. Characterization of unfractionated heparin: comparison of materials from the last 50 years. **Thrombosis and haemostasis**, v. 84, n. 6, p. 1052–6, dez. 2000.

MUZES, G. et al. Changes of the cytokine profile in inflammatory bowel diseases. **World Journal of Gastroenterology**, 2012.

NADER, H. B. Characterization of a heparan sulfate and a peculiar chondroitin 4-sulfate proteoglycan from platelets. Inhibition of the aggregation process by platelet chondroitin sulfate proteoglycan. **Journal of Biological Chemistry**, 1991.

NATHAN, C. Nitric oxide as a secretory product of mammalian cells. **FASEB journal : official publication of the Federation of American Societies for Experimental Biology**, v. 6, n. 12, p. 3051–64, set. 1992.

NELL, S.; SUERBAUM, S.; JOSENHANS, C. The impact of the microbiota on the pathogenesis of IBD: Lessons from mouse infection modelsNature Reviews Microbiology, 2010.

NEMOTO, H. et al. Reduced diversity and imbalance of fecal microbiota in patients with ulcerative colitis. **Digestive Diseases and Sciences**, 2012.

NEURATH, M. F. Cytokines in inflammatory bowel disease. **Nature reviews. Immunology**, v. 14, n. 5, p. 329–342, maio 2014.

OEBEN, M. et al. Constant and variable domains of different disaccharide structure in corneal keratan sulphate chains. **The Biochemical journal**, v. 248, n. 1, p. 85–93, 15 nov. 1987.

OHTAKE, K. et al. Oral nitrite ameliorates dextran sulfate sodium-induced acute experimental colitis in mice. **Nitric Oxide**, v. 23, n. 1, p. 65–73, 2010.

OLIVEIRA, L. G. Avaliação da atividade anti-inflamatória de condroitim sulfato e glucosamina em modelo experimental de colite ulcerativa em ratos. [s.l.] Universidade Federal de Juiz de Fora, 2013.

OONUKI, Y. et al. Application of fluorophore-assisted carbohydrate electrophoresis to analysis of disaccharides and oligosaccharides derived from glycosaminoglycans. **Analytical Biochemistry**, 2005.

ORLOWSKY, E. W. et al. Monosodium urate crystal induced macrophage inflammation is attenuated by chondroitin sulphate: pre-clinical model for gout prophylaxis? **BMC Musculoskeletal Disorders**, v. 15, n. 1, p. 318, 27 dez. 2014.

OTTE, J.-M.; CARIO, E.; PODOLSKY, D. K. Mechanisms of cross hyporesponsiveness to toll-like receptor bacterial ligands in intestinal epithelial cells☆. **Gastroenterology**, v. 126, n. 4, p. 1054–1070, abr. 2004.

PALMER, R. M. J.; FERRIGE, A. G.; MONCADA, S. Nitric oxide release accounts for the biological activity of endothelium-derived relaxing factor. **Nature**, v. 327, n. 6122, p. 524–526, jun. 1987.

PARK, K.-I. et al. Regulation of Proinflammatory Mediators via NF-kappaB and p38 MAPK-Dependent Mechanisms in RAW 264.7 Macrophages by Polyphenol Components Isolated from Korea Lonicera japonica THUNB. **Evidence-based complementary and alternative medicine : eCAM**, v. 2012, p. 828521, 2012.

PETERSON, L. W.; ARTIS, D. Intestinal epithelial cells: Regulators of barrier function and immune homeostasisNature Reviews Immunology, 2014.

POBLACIÓN, C. A.; MICHELACCI, Y. M. Structural differences of dermatan sulfates from different origins. **Carbohydrate research**, v. 147, n. 1, p. 87–100, 1 mar. 1986.

PRYDZ, K.; DALEN, K. T. Synthesis and sorting of proteoglycans. **Journal of cell science**, 2000.

RAVI, A.; GARG, P.; SITARAMAN, S. V. Matrix metalloproteinases in inflammatory bowel disease: boon or a bane? **Inflamm Bowel Dis**, v. 13, n. 1, p. 97–107, 2007.

REN, K.; TORRES, R. Role of interleukin-1β during pain and inflammation. 2009.

ROGLER, G. et al. Nuclear factor kappaB is activated in macrophages and epithelial cells of inflamed intestinal mucosa. **Gastroenterology**, v. 115, n. 2, p. 357–369, 1998.

SAMPAIO, L. O.; NADER, H. B. Emergence and Structural Characteristics of Chondroitin Sulfates in the Animal Kingdom. In: NICOLA, V. (Ed.). . **Advances in Pharmacology**. [s.l.] Academic Press, 2006. v. Volume 53p. 233–251.

SATOH, T.; AKIRA, S. Toll-Like Receptor Signaling and Its Inducible Proteins. **Microbiology Spectrum**, v. 4, n. 6, 1 dez. 2016.

SCOTT, J. E. Supramolecular organization of extracellular matrix glycosaminoglycans, in vitro and in the tissues. **FASEB journal : official publication of the Federation of American Societies for Experimental Biology**, 1992.

SCOTTO D'ABUSCO, A. et al. Glucosamine and its N-acetyl-phenylalanine derivative prevent TNF-alpha-induced transcriptional activation in human chondrocytes. **Clinical and experimental rheumatology**, v. 25, n. 6, p. 847–52, 2007.

SEIBEL, M. J.; ROBINS, S. P.; BILEZIKIAN, J. P. **Dynamics of Bone and Cartilage Metabolism**. [s.l: s.n.].

SHA, S. et al. The biodiversity and composition of the dominant fecal microbiota in patients with inflammatory bowel disease. **Diagnostic Microbiology and Infectious Disease**, 2013.

SHAPIRO, S. D.; KELLEY, D.; KOBAYASHI, D. Measurement of metalloproteinases. **Methods Mol Med**, v. 56, p. 383–390, 2001.

SIEGMUND, B.; ZEITZ, M. Innate and adaptive immunity in inflammatory bowel disease. **World journal of gastroenterology**, v. 17, n. 27, p. 3178–3183, jul. 2011.

SILBERT, J. E.; SUGUMARAN, G. Biosynthesis of chondroitin/dermatan sulfate. **IUBMB life**, v. 54, n. 4, p. 177–186, out. 2002.

SILVA, M. E.; DIETRICH, C. P. Structure of heparin. Characterization of the products formed from heparin by the action of a heparinase and a heparitinase from Flavobacterium heparinum. **The Journal of biological chemistry**, v. 250, n. 17, p. 6841–6, 10 set. 1975.

SOMEYA, A. et al. Glucosamine Downregulates the IL-1β-Induced Expression of Proinflammatory Cytokine Genes in Human Synovial MH7A Cells by O-GlcNAc Modification-Dependent and -Independent Mechanisms. **PLOS ONE**, v. 11, n. 10, p. e0165158, 24 out. 2016.

STABLER, T. V. et al. Chondroitin sulphate inhibits NF-κB activity induced by interaction of pathogenic and damage associated molecules. **Osteoarthritis and Cartilage**, v. 25, n. 1, p. 166–174, jan. 2017.

STROBER, W. Impact of the gut microbiome on mucosal inflammationTrends in Immunology, 2013.

STYLIANOU, M.; TRIANTAPHYLLIDOU, I. -E; VYNIOS, D. H. Advances in the Analysis of Chondroitin/Dermatan Sulfate. In: NICOLA, V. (Ed.). . **Advances in Pharmacology**. [s.l.] Academic Press, 2006. v. Volume 53p. 141–166.

SUGAHARA, K. et al. Novel sulfated oligosaccharides containing 3-O-sulfated glucuronic acid from king crab cartilage chondroitin sulfate K: Unexpected degradation by chondroitinase ABC. **Journal of Biological Chemistry**, 1996.

SUGAHARA, K.; YAMADA, S. Structure and function of oversulfated chondroitin sulfate variants: Unique sulfation patterns and neuroregulatory activities. **Trends Glycosci. and Glycotech.**, 2000.

SUZUKI, S. et al. Formation of three types of disulfated disaccharides from chondroitin sulfates by chondroitinase digestion. **The Journal of biological chemistry**, v. 243, n. 7, p. 1543–1550, abr. 1968.

TAIPALE, J.; KESKI-OJA, J. Growth factors in the extracellular matrix. **FASEB J.**, 1997.

TAKEDA, K.; AKIRA, S. Toll-like receptors in innate immunity. **International Immunology**, v. 17, n. 1, p. 1–14, 22 nov. 2004.

TAKEDA, K.; AKIRA, S. Toll-Like Receptors. In: **Current Protocols in Immunology**. Hoboken, NJ, USA: John Wiley & Sons, Inc., 2015. p. 14.12.1-14.12.10.

TAKEUCHI, O.; AKIRA, S. Toll-like receptors; their physiological role and signal transduction system. **International immunopharmacology**, v. 1, n. 4, p. 625–35, abr. 2001.

TAKEUCHI, O.; AKIRA, S. Pattern Recognition Receptors and Inflammation. **Cell**, v. 140, n. 6, p. 805–820, 19 mar. 2010.

TANAKA, T. et al. Regulation of IL-6 in Immunity and Diseases. In: **Advances in experimental medicine and biology**. [s.l: s.n.]. v. 941p. 79–88.

TANAKA, T.; NARAZAKI, M.; KISHIMOTO, T. Therapeutic Targeting of the Interleukin-6 Receptor. **Annual Review of Pharmacology and Toxicology**, v. 52, n. 1, p. 199–219, 10 fev. 2012.

TANAKA, T.; NARAZAKI, M.; KISHIMOTO, T. IL-6 in Inflammation, Immunity, and Disease. **Cold Spring Harbor Perspectives in Biology**, v. 6, n. 10, p. a016295–a016295, 1 out. 2014.

TERENCIO, M. C. et al. Chondroprotective effects of the combination chondroitin sulfate-glucosamine in a model of osteoarthritis induced by anterior cruciate ligament transection in ovariectomised rats. **Biomedicine & Pharmacotherapy**, v. 79, p. 120–128, abr. 2016.

TOLEDO, O. M. S.; DIETRICH, C. P. Tissue specific distribution of sulfated mucopolysaccharides in mammals. **BBA - General Subjects**, 1977.

TSIKAS, D. Analysis of nitrite and nitrate in biological fluids by assays based on the Griess reaction: Appraisal of the Griess reaction in the l-arginine/nitric oxide area of research. **Journal of Chromatography B**, v. 851, n. 1–2, p. 51–70, 15 maio 2007.

UEBELHART, D. et al. Treatment of Knee Osteoarthritis with Oral Chondroitin Sulfate. In: NICOLA, V. (Ed.). . **Advances in Pharmacology**. [s.l.] Academic Press, 2006. v. Volume 53p. 523–539.

VERMEIREN, J. et al. Intrarectal nitric oxide administration prevents cellular infiltration but not colonic injury during dextran sodium sulfate colitis. **Dig Dis Sci**, v. 57, n. 7, p. 1832–1837, 2012.

VOLPI. **Chondroitin sulfate safety and quality Molecules.** Multidisciplinary Digital Publishing Institute, ,12 abr. 2019.

VOLPI, N. Analytical aspects of pharmaceutical grade chondroitin sulfates. **J Pharm Sci**, v. 96, n. 12, p. 3168–3180, 2007a.

VOLPI, N. Analytical aspects of pharmaceutical grade chondroitin sulfates. **Journal of Pharmaceutical Sciences**, v. 96, n. 12, p. 3168–3180, dez. 2007b.

VOLPI, N. Quality of different chondroitin sulfate preparations in relation to their therapeutic activity. **Journal of Pharmacy and Pharmacology**, v. 61, n. 10, p. 1271–1280, 1 out. 2009.

VOLPI, N. Anti-inflammatory activity of chondroitin sulphate: new functions from an old natural macromolecule. **Inflammopharmacology**, v. 19, n. 6, p. 299–306, 2011.

WULLAERT, A.; BONNET, M. C.; PASPARAKIS, M. NF-kappaB in the regulation of epithelial homeostasis and inflammation. **Cell research**, v. 21, n. 1, p. 146–158, jan. 2011.

XIA, Z.-P. et al. Direct activation of protein kinases by unanchored polyubiquitin chains. **Nature**, v. 461, n. 7260, p. 114–119, 12 set. 2009.

XU, X.-R. et al. Dysregulation of mucosal immune response in pathogenesis of inflammatory bowel disease. **World journal of gastroenterology**, v. 20, n. 12, p. 3255–3264, mar. 2014.

YAMADA, S.; SUGAHARA, K.; ÖZBEK, S. Evolution of glycosaminoglycans: Comparative biochemical studyCommunicative and Integrative Biology, 2011.

YU, C. G.; HUANG, Q. Recent progress on the role of gut microbiota in the pathogenesis of inflammatory bowel disease. **Journal of digestive diseases**, v. 14, n. 10, p. 513–517, out. 2013.

ZHANG, W. et al. Electrophoretic Separation of Alginic Sodium Diester and Sodium Hexametaphosphate in Chondroitin Sulfate that Interfere with the Cetylpyridinium Chloride Titration Assay. **Journal of AOAC International**, v. 97, n. 6, p. 1503–1513, 1 nov. 2014.

ZINGARELLI, B.; SHEEHAN, M.; WONG, H. R. Nuclear factor-kappaB as a therapeutic target in critical care medicine. **Crit Care Med**, v. 31, n. 1 Suppl, p. S105-11, 2003.

ANEXOS

ANEXO 1

ARQGA/1710

POSITIVE CORRELATION BETWEEN DISEASE ACTIVITY INDEX AND MATRIX METALLOPROTEINASES ACTIVITY IN A RAT MODEL OF COLITIS

Luiz Gustavo de **OLIVEIRA**[1], André Luiz da **CUNHA**[1], Amaury Caiafa **DUARTE**[1], Maria Christina Marques Nogueira **CASTAÑON**[2], Júlio Maria Fonseca **CHEBLI**[3] and Jair Adriano Kopke de **AGUIAR**[1]

ABSTRACT - ***Context*** - Inflammatory bowel disease, including ulcerative colitis and Crohn's disease, comprising a broad spectrum of diseases those have in common chronic inflammation of the gastrointestinal tract, histological alterations and an increased activity levels of certain enzymes, such as, metalloproteinases. ***Objective*** - Evaluate a possible correlation of disease activity index with the severity of colonic mucosal damage and increased activity of metalloproteinases in a model of ulcerative colitis induced by dextran sulfate sodium. ***Methods*** - Colitis was induced by oral administration of 5% dextran sulfate sodium for seven days in this group (n=10), whereas control group (n=16) received water. Effects were analyzed daily by disease activity index. In the seventh day, animals were euthanized and hematological measurements, histological changes (hematoxylin and eosin and Alcian Blue staining), myeloperoxidase and metalloproteinase activities (MMP-2 and MMP-9) were determined. ***Results*** - Dextran sulfate sodium group showed elevated disease activity index and reduced hematological parameters. Induction of colitis caused tissue injury with loss of mucin and increased myeloperoxidase (P<0.001) and MMP-9 activities (45 fold) compared to the control group. ***Conclusion*** - In this study, we observed a disease activity index correlation with the degree of histopathological changes after induction of colitis, and this result may be related mainly to the increased activity of MMP-9 and mieloperoxidase.

HEADINGS - Colitis. Crohn disease. Metalloproteinases.

INTRODUCTION

Inflammatory bowel diseases (IBD) have in common chronic inflammation of the digestive tract, which may or may not have a cause or specific pathogen[5, 7]. Its etiology is multifactorial and complex, it is believed to have genetic involvement, environmental, immune and intestinal microbiota[26, 30].

For many years, studies on the understanding of the pathogenesis of IBD have been delayed by the lack of experimental models that corresponded to the disease[10]. But now more than 30 models have been developed, with the most varied clinical manifestations of IBD[4, 18]. These models contribute to important advances in understanding the mechanisms of inflammation, the pathogenesis and the treatment of possible discoveries[11]. Among the models used, stands the induction of colitis by dextran sulfate sodium (DSS), due to its good reproducibility and also for presenting clinical symptoms, inflammatory markers and histopathological features similar to IBD in humans[17, 21]. The exact mechanism by which the DSS induced colitis is unknown but it is known that this compound is toxic to intestinal epithelial cells with a probable mechanism that has direct action on intestinal permeability allowing entry of luminal antigens resulting in an inflammatory response[22, 29].

Changes in the activity and expression of extracellular matrix metalloproteinases (MMPs) were described in IBD patients suggesting that these enzymes are involved in tissue degradation process[16, 20]. MMPs are endopeptidases dependent of calcium and zinc and are considered the main enzymes involved in the control of the homeostasis of extracellular matrix (ECM) at various levels, including growth, division and cell function, regulation of immune response, controlled synthesis and matrix remodeling by cleavage of almost all of its components such as collagen, proteoglycans, fibronectin, elastin, and laminin[15, 24].

Declared conflict of interest of all authors: none.
Research performed at: Laboratório de Análise de Glicoconjugados do Departamento de Bioquímica, Instituto de Ciências Biológicas, UFJF, Juiz de Fora, MG, Brasil.
[1] Laboratório de Análise de Glicoconjugados, Departamento de Bioquímica, Instituto de Ciências Biológicas, Universidade Federal de Juiz de Fora - UFJF; [2] Departamento de Morfologia, Instituto de Ciências Biológicas, UFJF. [3] Disciplina de Gastroenterologia, Faculdade Medicina, UFJF, Juiz de Fora, MG, Brasil.
Correspondence: Dr. Jair Adriano Kopke de Aguiar. Universidade Federal de Juiz de Fora. Departamento de Bioquímica/ICB - Rua José Lourenço Kelmer, s/n - Campus Universitário - Bairro São Pedro - 36036-900 - Juiz de Fora, MG, Brasil. E-mail: jair.aguiar@ufjf.edu.br

Several MMPs (MMP-1, MMP-2, MMP-3, MMP-8, MMP-9, MMP-12) have their activity increased in a variety of animal models colitis and in patients with inflammatory bowel disease. Thus, the present study investigated a possible correlation of DAI in the model of ulcerative colitis induced by DSS with the severity of colonic mucosal damage and increased activity of MMP-2 and MMP-9.

METHODS

Materials

Dextran sodium sulfate (DSS - MW: 36-50 kDa, MP Biomedicals, Solon, OH, USA), hexadecyltrimethylammonium bromide (HTAB, Sigma-Aldrich Co., St. Louis, MO, USA), *o*-dianisidine hydrochloride (Sigma-Aldrich Co., St. Louis, MO, USA); Acrylamide (Ludwig Biotechnology Ltd., Porto Alegre, RS, Brazil); *N*,*N'*-methylenebisacrylamide (Neon Comercial Ltda., São Paulo, SP, Brazil); Tris(hydroxymethyl)aminomethane (Biosolve Valkenswaard, Netherlands); Triton x-100 (Vetec Fine Chemicals Ltda., Duque de Caxias, RJ, Brazil); Gelatin (Sigma-Aldrich Co., St. Louis, MO, USA).

Animals

Male Wistar rats (6-8 weeks old) were obtained from the Center of Biology for Reproduction (CBR) at Federal University of Juiz de Fora (UFJF, Juiz de Fora, MG, Brazil) for induction of colitis by DSS. The animals were kept in a bioterium of Laboratório de Análise de Glicoconjugados in the Biochemistry Department (UFJF), throughout the experiment in individual plastic boxes under, "Guide for the Care and Use of Laboratory Animals". The procedures were approved by the Ethics Committee on Animal Experimentation UFJF (002/2010-CEEA UFJF).

DSS induced colitis

The induction of colitis DSS was done according Okayasu et al. with modifications. The animals were randomized into two groups: control group (n = 16), which was given water and the DSS group (n = 10) given only a solution of 5% DSS *ad libitum* for 7 days. The total volume of DSS consumed *per* rat was about 40 ml/day per group. At the end of the experiment (seventh day), rats were euthanized by deepening anesthesia with administration of sodium pentobarbital (100 mg/kg) and the colon was completely removed from the colon-cecal junction to the anal canal.

Assessment of disease activity index

All the rats were observed once a day. The disease activity index (DAI) was determined by scoring body weight loss, trait of stool, and occult blood in stool or hematochezia from day 0 to day 7 in colitis induction according to the classic scoring system by Cooper in the process of modeling: body weight loss (0, none; 1, 1%-5%; 2, 5%-10%; 3, 10%- 20%; 4, >20%), stool consistency (0, normal; 2, loose stool; 4, diarrhea), and stool blood (0, negative; 2, fecal occult blood test positive; 4, gross bleeding)[6]

Hematological Evaluation

Blood samples were analyzed for the number of erythrocyte, hematocrit and hemoglobin for the evaluation of hematological parameters. The analysis was performed at the Center for Reproductive Biology (CBR/UFJF) using the veterinary hematology analyzer Poch 100i V-Diff (Sysmex).

Histopathologic analysis

Initially, each colon segment was washed in 0.1 M phosphate buffer, pH 7.4, and its length and weight measured to evaluate the ratio length/weight. After the colon was opened longitudinally, using the technique of swiss roll, fixed with paraformaldehyde solution 10% in 0.05 M phosphate buffer, pH 7.4, for at least 24 hours, embedded in paraffin and processed so that cuts of 5 mm thick were performed. Besides the normal staining (hematoxylin and eosin, HE) it was also used a specific one mucopolysaccharides alcian blue at pH 2.5. The sections were graded histopathologically and evaluated as described by Cooper et al.[6].

Myeloperoxidase activity (MPO)

The tissue MPO activity was measured according to the technique described by Bradley et al.[2]. The absorbance was determined at a wavelength of 450 nm. The MPO activity was calculated using the molar extinction coefficient ($e = 11.48\ mM^{-1}.cm^{-1}$)[8]. 1UE (enzyme unit) of myeloperoxidase was considered as amount of enzyme that degrades 1μmol/min of hydrogen peroxide at 25 °C. The results were expressed in mUE/mg protein.

Extraction of metalloproteinases

Fragments of the colon were macerated in liquid nitrogen and then added 1 ml of Tris-HCl 50 mM pH 7.4, containing 100 mM $CaCl_2$ and 1 ml of Triton X-100 0.2% (v/v) for extraction the enzymes. The samples were centrifuged for 10 minutes at 12,000 xg, and the supernatant aliquoted. Protein was quantified by BCA kit (Thermo Scientific).

Zymograms

Colon homogenates (10 μg protein) were submitted to a electrophoresis on polyacrylamide gels (10% acrylamide-bisacrylamide solution T 30% C 2.7% gelatin containing 2 mg/ml) in Tris-glycine (25 mM / 192 mM) pH 8.3 containing sodium dodecyl sulphate (0.1%). After the migration, gels were washed with Triton X-100 (2%) and incubated with 50 mM Tris-HCl, pH 8.2, containing 5 mM $CaCl_2$, 1μM $ZnCl_2$ and for 24h at 37°C. The gels were stained by Coomassie Brilliant Blue R-250 (0.5% dye, 30% methanol, 10% acetic acid) and destained (30% methanol, 10% acetic acid)[19, 27]. The activity of gelatinases was evidenced as bright regions (bleached) in the gel. To measure the intensities of the bands a program was used, TotalLab Quant®. The activities were corrected for protein content.

Statistical analysis

Values are expressed as mean ± standard error. Statistical analysis was performed using SPSS for Windows, version 19.

We evaluated the data normality by the Shapiro-Wilk test, the comparison of data distributed on the curve of normality was performed by t test student. $P<0.05$ was considered statistically significant.

RESULTS

The clinical signs of DSS-induced colitis in rats were determined by assessing the disease activity index (DAI). This index is composed of three parameters (stool consistency, presence of rectal bleeding and weight variation of the animals) and provides the degree of severity of the inflammatory process that can be correlated with damage to the intestinal mucosa. We observed an increase in the DAI for the DSS group after the first day of induction with a significant increase from the fourth to the seventh day, in addition, significant weight loss during all days of the experiment (Figure 1. A, B), for the control group there was a gain of weight and no clinical changes. Weight loss was the first symptoms observed from the third day on showed changes in stool consistency, while the presence of blood was viewed from the fifth day (Figure 1 C). Macroscopically, there was also a reduction in the length of the colon group DSS (Figure 1 D).

The DSS-induced colitis caused hematological decreasing of erythrocyte count ($P<0.01$), hematocrit ($P<0.05$) and hemoglobin ($P<0.01$), indicating severe loss of blood compared to the control group (Table 1).

TABLE1. Hemathological parameters analysis with blood (EDTA) in the animals of both control and DSS group

Groups	Erythrocyte (x 10^6/mm^3)	Hematocrit (%)	Hemoglobin (g/dL)
Control	8.88 ± 0.17	48.0 ± 1.0	17.7 ± 0.4
DSS	[a]6.75 ± 0.58	[b]39.3 ± 2.6	[a]13.1 ± 1.0

Data represents the values of the mean ± standard error
Significant statistical diferences are shown with [a]$P<0,01$ and [b]$P<0,05$ compared to the control

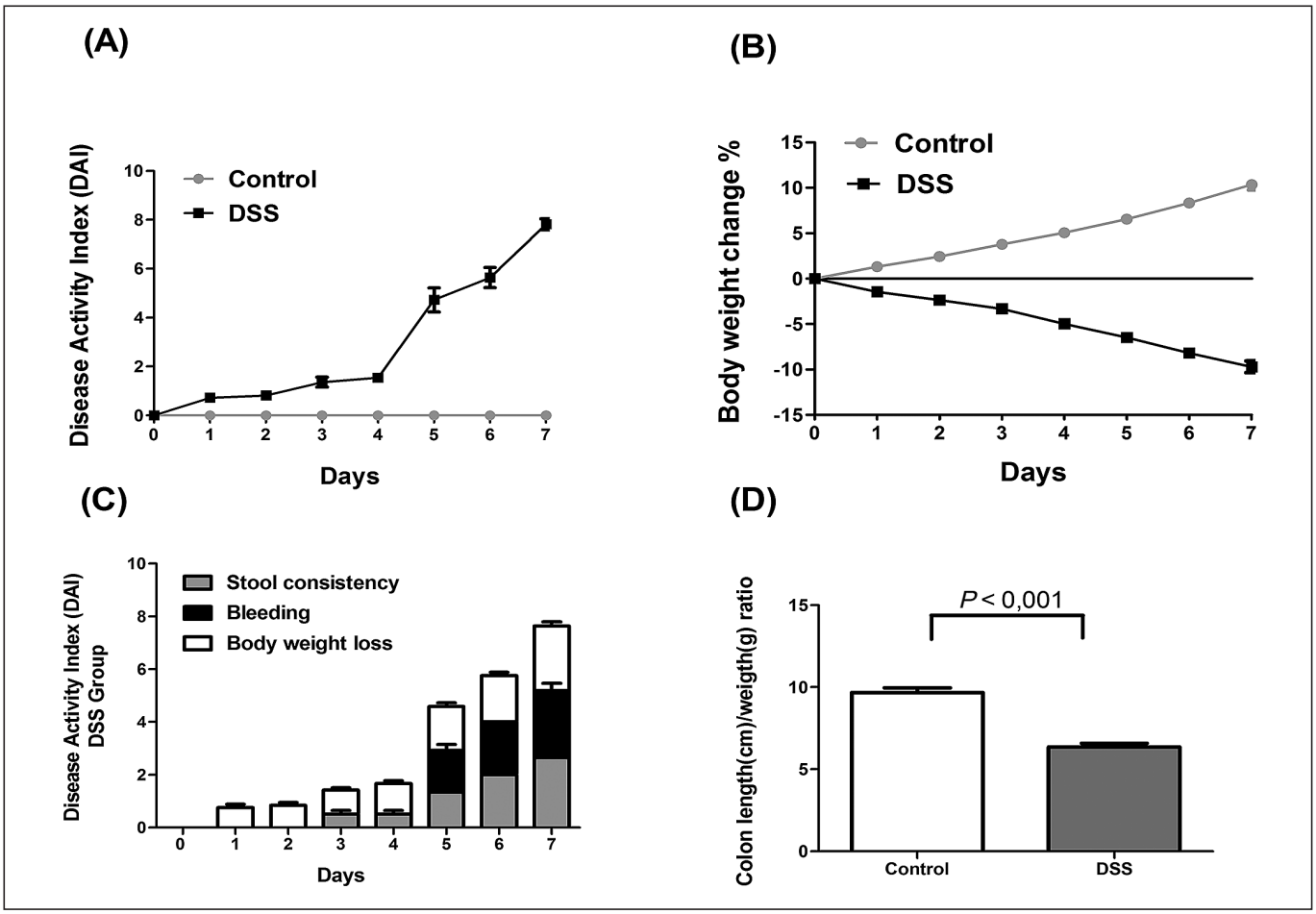

FIGURE 1. Assessment of disease activity index (DAI) in dextran sulfate sodium DSS-induced colitis model.
(A) The DAI of the DSS group presented a difference from the first day of the experiment and (B) a reduction in weight loss when compared to the control group. (C) DSS group began to demonstrate alterations in the consistence of their stool from the third day, and bleeding was noticed after the fifth day of the experiment while no alterations were observed on the control group. (D) The use of DSS caused shortening of the colon of the animals when compared to the control group. The data is demonstrated by the mean± standard error. DSS- dextran sulfate sodium

Histological analysis of colonic mucosa of animals in the DSS group showed multifocal areas of erosion and ulcers as well as regions of loss of more than 2/3 of the crypts. It was also observed vascular congestion, edema in the lamina propria and inflammatory infiltrate (Figure 2. A). Animals in the control group the colonic mucosa remained normal, with the epithelium and crypts intact (Figure 2. A). This result also observed in the analysis reflects the histological score (Figure 2. B, $P<0.001$). For alcian blue staining, we found out that the DSS group (Figure 2. A), had significant decreases in the number of goblet cells and mucin production while in the control group these numbers of crypts and goblet cells were maintained.

The activity of myeloperoxidase (MPO), a marker widely used to assess the tissue infiltration of neutrophils showed an increase in MPO activity compared to the control group (Figure 2. C). This result is consistent with the histopathological changes observed.

There is good evidence of the involvement of matrix metalloproteinases in inflammatory bowel disease, among them are two gelatinases (MMP-2 and 9). To evaluate changes in the activity of MMP-2 and MMP-9 in both controlled and induced group, densitometric analysis of zymograms was performed as described in materials and methods. It was observed in healthy animals only the activity of MMP-2 (Figure 3. A) while for the induced animals, besides the in-

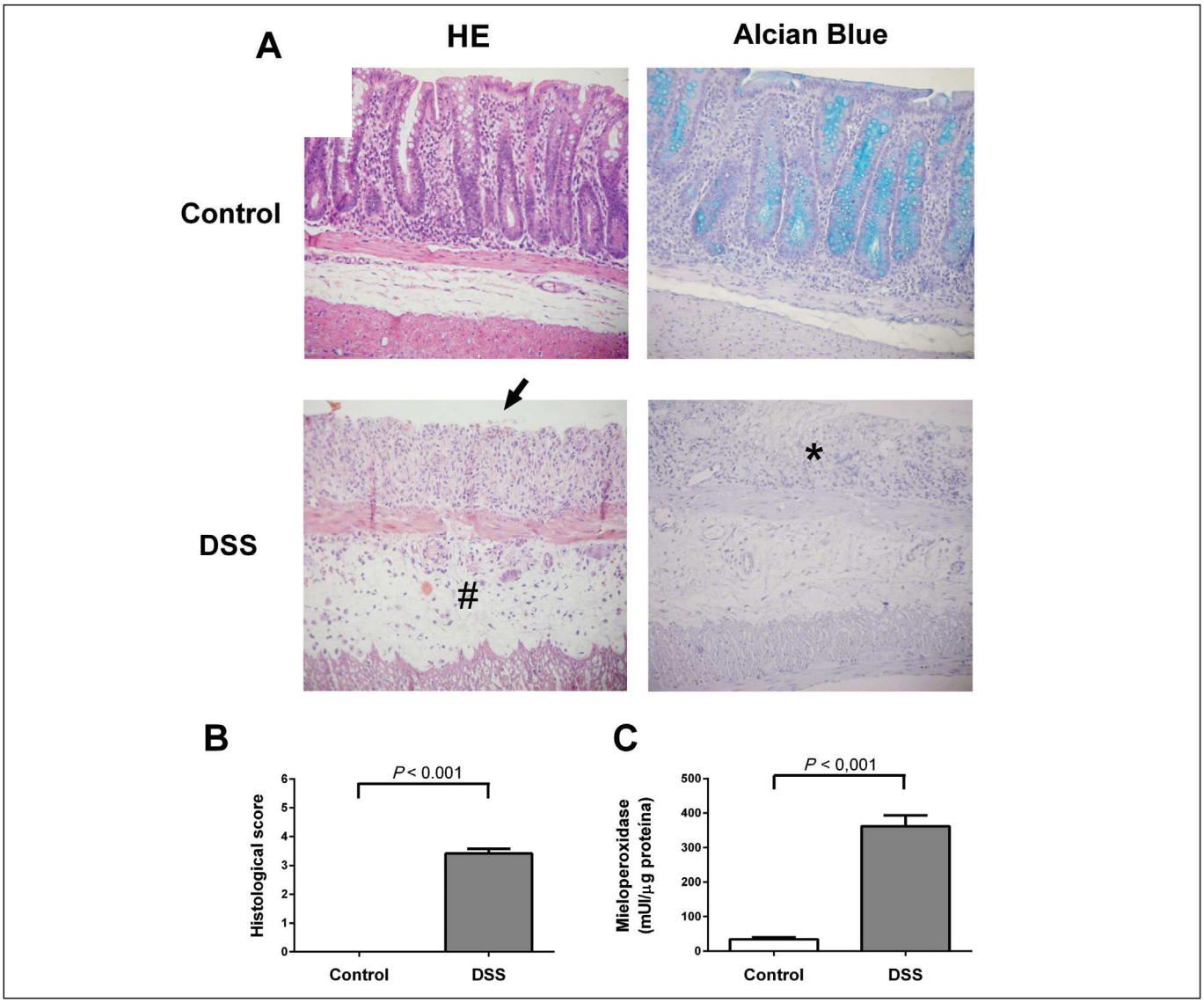

FIGURE 2. Histophatological changes and enzymatic activity present in the colon of the dextran sulfate sodium DSS-induced colitis model. (A) Control group maintained normal colon, whereas DSS group shows the multifocal areas of the mucosal erosions with loss of epithelial cells (black arrow), goblet cell depletion (*), crypt loss, inflammatory cell infiltration, edema and vascular congestion. (B) The histophatologic score demonstrated a significant increase in the DSS group compared to the control, (C) the same result was observed for the Myeloperoxidase activity (MPO) tissue activity. The colon was fixed and stained with HE and alcian blue pH 2,5, original magnification 10x).

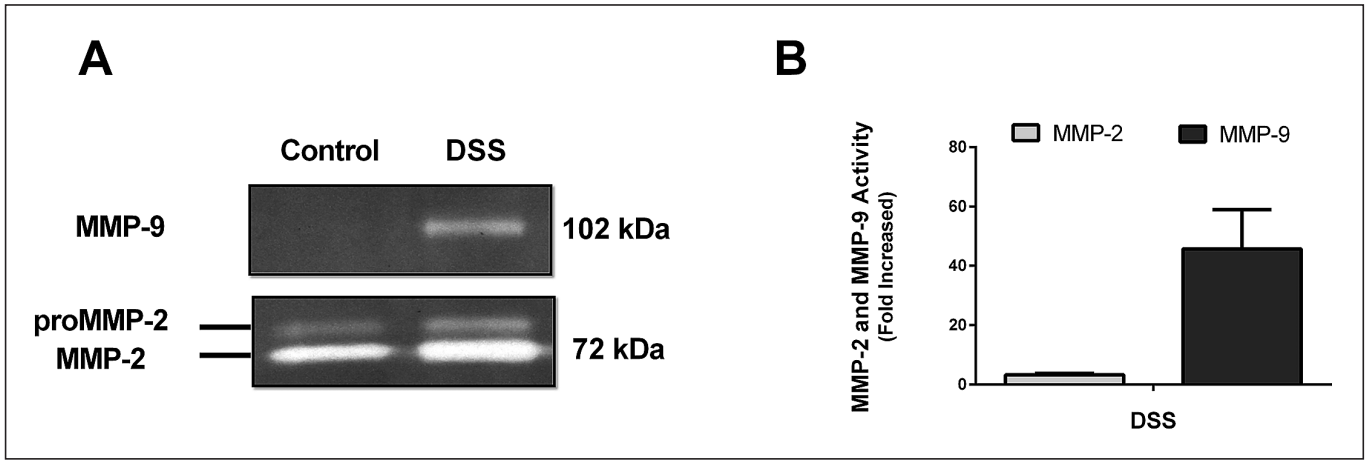

FIGURE 3. A representative zymogram of matrix metalloproteinases in the colon of the DSS-induced colitis model.
Aliquots (10 µg of protein) were submitted to electrophoresis in poliacrilamida gel at 10%, containing gelatine 2 mg/mL, as substrate. The activities of the metalloproteinase activities MMP-2 and MMP-9 were quantified by densitometry of the bands in gel slabs (A) and compared to the control (B). The data represents the mean ± standard error.

creased activity of MMP-2 compared to the control group (3 fold), we noticed the onset of the activity of MMP- 9 (Figure 3. A, B).

DISCUSSION

The experimental model using DSS has as main clinical manifestations: diarrhea, bloody stools, weight loss, bleeding, and anemia[29]. The histological changes in the colon most commonly found are the decrease mucin, epithelial degeneration, presence of erosions, infiltration of neutrophils and crypt abscesses[22]. These manifestations and histopathological changes were also observed in our study, in addition to shortening of the length of the colon evaluated macroscopically. The diarrhea observed in the animals of group DSS from the third day may be due to increased permeability of the intestinal cells or by hyperosmolarity in the lumen caused by DSS[31]. The weight loss observed and shortening of the colon shows high correlation with the histological and pathological changes of colitis and are good markers of the severity of bowel inflammation[29, 31]. Allied to these factors, the worsening of the disease occurs in the presence of acute bleeding evaluated by DAI and hematological measurements[12, 29]. We observed a significant reduction in erythrocyte count, hematocrit and hemoglobin in the group DSS, indicating that these animals suffer large losses of blood.

The histopathological features observed in this animal model are very similar to the disease in humans[22]. In DSS colitis it was observed the presence of edema and inflammatory infiltrate in the lamina propria, loss of crypts and goblet cells (loss of mucins observed by alcian blue) along with multifocal areas of erosions and ulcerations demonstrating great tissue damage in the colon. The inflammatory infiltrate was observed and histologically confirmed by myeloperoxidase activity (MPO), a marker of inflammatory infiltrate often used in the model of colitis by DSS. MPO is a major enzyme found in the granules of neutrophils, it primarily catalyzes the oxidation of Cl^- to hypochlorous acid and its increase is involved in tissue damage[23]. In our study, we observed a high activity of MPO in the DSS group compared to the control group ($P<0.001$). Recent studies also showed that reduction in the degradation of matrix present in the intestinal mucosa can be related to a reduction in MPO activity and improves the course of the disease in an experimental model of colitis[13, 14].

Activity of extracellular matrix metalloproteinases is currently discussed in terms of its involvement with inflammatory bowel diseases. These enzymes and their inhibitors are produced by cells in the gastrointestinal tract, and a change in this balance can cause some inflammatory conditions in the intestine[15]. Within this group of enzymes stands, MMP-2 and MMP-9, known as gelatinases. MMP-2 is constitutively expressive while MMP-9 is absent in major human tissues[9]. Some lines of research suggests that these enzymes are involved in the process of destruction and tissue remodeling in inflammatory conditions[3, 28].

Our study shows a high activity of MMP-9 (45 fold increase) in the group DSS, while there was a slight increase in MMP-2 (three fold increase). Studies in patients with ulcerative colitis showed greater activity of MMP-9 compared to the control patients[1]. Studies on experimental models have already shown that animals deficient on MMP-9 attenuated colitis demonstrating that gelatinase is involved in inflammatory processes and its inhibition can reduce inflammation[25]. This increase in MMP-9 may relate to the high neutrophil infiltration observed by tissue MPO activity as well as by high tissue damage visualized in histological analysis since these enzymes are involved in the degradation of ECM.

CONCLUSIONS

Our results demonstrate that there is a correlation between the DAI and the degree of pathological alterations in the colon of the animals in the induced by DSS group, and these changes can be caused principally by increased expression/activity mainly on the MMP-9 and myeloperoxidase produced by inflammatory cells. Being these enzymes a possible therapeutic target for the reduction of tissue injury in treating IBD.

Oliveira LG, Cunha AL, Duarte AC, Castañon MCMN, Chebli JMF, Aguiar JAK. Correlação positiva entre índice de atividade de doença e metaloproteinase de matriz em modelo de colite em ratos. Arq Gastroenterol. 2014,51(2):107-12.

RESUMO - ***Contexto*** **-** Doenças inflamatórias intestinais, entre elas colite ulcerativa e doença de Crohn, compreendem um amplo espectro de doenças que apresentam em comum inflamação crônica do trato gastrointestinal, alterações histológicas e um aumento de atividade de determinadas enzimas, tais como, metaloproteinases. ***Objetivo*** **-** Avaliar possível correlação do índice de atividade de doença em modelo de colite ulcerativa induzida por dextran sulfato de sódio com o grau de severidade de danos na mucosa colônica e aumento de atividade de metaloproteinases. ***Métodos*** **-** Colite foi induzida por administração oral de dextran sulfato de sódio 5% durante sete dias no grupo (n = 10), enquanto que o grupo controle (n = 16) recebeu água. Efeitos foram analisados diariamente pelo índice de atividade de doença. No sétimo dia, os animais foram sacrificados e as medições hematológicas, alterações histológicas (hematoxilina e eosina e coloração de azul Alcian), mieloperoxidase e atividades de metaloproteinases (MMP-2 e MMP-9) foram determinados. ***Resultados*** - Grupo dextran sulfato de sódio mostrou elevação no índice de atividade de doença e redução dos parâmetros hematológicos. A indução da colite causa lesão no tecido, com perda de mucina e aumento da mieloperoxidase (P<0,001) e as atividades MMP-9 (45 vezes) em comparação com o grupo de controle. ***Conclusão*** **-** Neste estudo, observamos uma correlação do índice de atividade de doença com o grau de alterações histopatológicas após indução da colite por dextran sulfato de sódio, podendo associar este resultado ao aumento principalmente da atividade de MMP-9 e de mieloperoxidase.

DESCRITORES - Colite. Doença de Crohn. Metaloproteinase.

REFERENCES

1. Baugh MD, Perry MJ, Hollander AP, Davies DR, Cross SS, Lobo AJ, et al. Matrix metalloproteinase levels are elevated in inflammatory bowel disease. Gastroenterology. 1999;117:814-22.
2. Bradley PP, Priebat DA, Christensen RD, Rothstein G. Measurement of cutaneous inflammation: estimation of neutrophil content with an enzyme marker. J Invest Dermatol. 1982;78:206-9.
3. Burrage PS, Mix KS, Brinckerhoff CE. Matrix metalloproteinases: role in arthritis. Front Biosci. 2006;11:529-43.
4. Byrne FR, Viney JL. Mouse models of inflammatory bowel disease. Curr Opin Drug Discov Devel. 2006;9:207-17.
5. Colli MV, Amaro TA, Pinto ALT, Gaburri PD, Chebli JMF. Toxicidade da azatioprina na doença de Crohn: incidência, abordagem e evolução. Rev Ass Med Bras. 2008;54:415-21.
6. Cooper HS, Murthy SN, Shah RS, Sedergran DJ. Clinicopathologic study of dextran sulfate sodium experimental murine colitis. Lab Invest. 1993;69:238-49.
7. Danese S, Fiocchi C. Ulcerative colitis. N Engl J Med. 2011;365:1713-25.
8. Fietz S, Bondzio A, Moschos A, Hertsch B, Einspanier R. Measurement of equine myeloperoxidase (MPO) activity in synovial fluid by a modified MPO assay and evaluation of joint diseases - an initial case study. Res Vet Sci. 2008;84:347-53.
9. Garg P, Vijay-Kumar M, Wang L, Gewirtz AT, Merlin D, Sitaraman SV. Matrix metalloproteinase-9-mediated tissue injury overrides the protective effect of matrix metalloproteinase-2 during colitis. Am J Physiol Gastrointest Liver Physiol. 2009;296:G175-84.
10. Gaudio E, Taddei G, Vetuschi A, Sferra R, Frieri G, Ricciardi G, Caprilli R. Dextran sulfate sodium (DSS) colitis in rats: clinical, structural, and ultrastructural aspects. Dig Dis Sci. 1999;44:1458-75.
11. Jurjus AR, Khoury NN, Reimund JM. Animal models of inflammatory bowel disease. J Pharmacol Toxicol Methods. 2004;50:81-92.
12. Kullmann F, Messmann H, Alt M, Gross V, Bocker T, Scholmerich J, Ruschoff J. Clinical and histopathological features of dextran sulfate sodium induced acute and chronic colitis associated with dysplasia in rats. Int J Colorectal Dis. 2001;16:238-46.
13. Lee B, Lee JH, Lee HS, Bae EA, Huh CS, Ahn YT, Kim DH. Glycosaminoglycan degradation-inhibitory lactic acid bacteria ameliorate 2,4,6-trinitrobenzenesulfonic acid-induced colitis in mice. J Microbiol Biotechnol. 2009;19:616-21.
14. Lee HS, Han SY, Ryu KY, Kim DH. The degradation of glycosaminoglycans by intestinal microflora deteriorates colitis in mice. Inflammation. 2009;32:27-36.
15. Medina C, Radomski MW. Role of matrix metalloproteinases in intestinal inflammation. J Pharmacol Exp Ther. 2006;318:933-8.
16. Medina C, Videla S, Radomski A, Radomski MW, Antolin M, Guarner F, et al. Increased activity and expression of matrix metalloproteinase-9 in a rat model of distal colitis. Am J Physiol Gastrointest Liver Physiol. 2003;284:G116-22.
17. Melgar S, Karlsson A, Michaelsson E. Acute colitis induced by dextran sulfate sodium progresses to chronicity in C57BL/6 but not in BALB/c mice: correlation between symptoms and inflammation. Am J Physiol Gastrointest Liver Physiol. 2005;288:G1328-38.
18. Melgar S, Karlsson L, Rehnstrom E, Karlsson A, Utkovic H, Jansson L, Michaelsson E. Validation of murine dextran sulfate sodium-induced colitis using four therapeutic agents for human inflammatory bowel disease. Int Immunopharmacol. 2008;8:836-44.
19. Miura RO, Yamagata S, Miura Y, Harada T, Yamagata T. Analysis of glycosaminoglycan-degrading enzymes by substrate gel electrophoresis (zymography). Anal Biochem. 1995;225:333-40.
20. Naito Y, Yoshikawa T. Role of matrix metalloproteinases in inflammatory bowel disease. Mol Aspects Med. 2005;26:379-90.
21. Okayasu I, Hatakeyama S, Yamada M, Ohkusa T, Inagaki Y, Nakaya R. A novel method in the induction of reliable experimental acute and chronic ulcerative colitis in mice. Gastroenterology. 1990;98:694-702.
22. Perse M, Cerar A. Dextran sodium sulphate colitis mouse model: traps and tricks. J Biomed Biotechnol. 2012;2012:718617.
23. Prokopowicz Z, Marcinkiewicz J, Katz DR, Chain BM. Neutrophil myeloperoxidase: soldier and statesman. Arch Immunol Ther Exp (Warsz). 2012;60:43-54.
24. Ravi A, Garg P, Sitaraman SV. Matrix metalloproteinases in inflammatory bowel disease: boon or a bane? Inflamm Bowel Dis. 2007;13:97-107.
25. Santana A, Medina C, Paz-Cabrera MC, Diaz-Gonzalez F, Farre E, Salas A, et al. Attenuation of dextran sodium sulphate induced colitis in matrix metalloproteinase-9 deficient mice. World J Gastroenterol. 2006;12:6464-72.
26. Sartor RB. Mechanisms of disease: pathogenesis of Crohn's disease and ulcerative colitis. Nat Clin Pract Gastroenterol Hepatol. 2006;3:390-407.
27. Shapiro SD, Kelley D, Kobayashi D. Measurement of metalloproteinases. Methods Mol Med. 2001;56:383-90.
28. Siasos G, Tousoulis D, Kioufis S, Oikonomou E, Siasou Z, Limperi M, et al. Inflammatory mechanisms in atherosclerosis: the impact of matrix metalloproteinases. Curr Top Med Chem. 2012;12:1132-48.
29. Solomon L, Mansor S, Mallon P, Donnelly E, Hoper M, Loughrey M, Kirk S, Gardiner K. The dextran sulphate sodium (DSS) model of colitis: an overview. Comparative Clinical Pathology. 2010;19:235-9.
30. Xavier RJ, Podolsky DK. Unravelling the pathogenesis of inflammatory bowel disease. Nature. 2007;448:427-34.
31. Yan Y, Kolachala V, Dalmasso G, Nguyen H, Laroui H, Sitaraman SV, Merlin D. Temporal and Spatial Analysis of Clinical and Molecular Parameters in Dextran Sodium Sulfate Induced Colitis. PLoS One. 2009;4:e6073.

Received 18/9/2013.
Accepted 10/12/2013.

ANEXO 2

Carbohydrate Polymers 134 (2015) 300–308

Contents lists available at ScienceDirect

Carbohydrate Polymers

journal homepage: www.elsevier.com/locate/carbpol

Pharmaceutical grade chondroitin sulfate: Structural analysis and identification of contaminants in different commercial preparations

André Luiz da Cunha[a,c], Luiz Gustavo de Oliveira[a], Lenize Fernandes Maia[b], Luiz Fernando Cappa de Oliveira[b], Yara M. Michelacci[c], Jair Adriano K. de Aguiar[a,c,*]

[a] Departamento de Bioquímica, Instituto de Ciências Biológicas, UFJF, Juiz de Fora, MG 36036-900, Brazil
[b] Departamento de Química, Instituto de Ciências Exatas, UFJF, Juiz de Fora, MG 36036-900, Brazil
[c] Departamento de Bioquímica, Escola Paulista de Medicina, Unifesp, São Paulo, SP 04044-020, Brazil

ARTICLE INFO

Article history:
Received 25 June 2015
Received in revised form 3 August 2015
Accepted 5 August 2015
Available online 8 August 2015

Keywords:
Chondroitin sulfate
FACE
Raman spectroscopy
Contaminants
Maltodextrin
Lactose

ABSTRACT

The aim of the present study was to characterize 16 pharmaceutical grade chondroitin sulfate (CS) samples, concerning the structure and presence of contaminants, in comparison to USP and analytical grade CS. Agarose gel electrophoresis has shown that only 5 samples were >90% CS, while 11 contained less than 15% CS. FACE (fluorophore-assisted carbohydrate electrophoresis) revealed that maltodextrin was the main contaminant in nine of them, and lactose in two. Raman spectroscopy corroborated these results. Concerning the structure of the CS present in the five CS-rich samples, the ratios 4-sulfated:6-sulfated disaccharides varied from 0.9 to 1.7, and their modal molecular weight was 20–29 kDa. Also, they were all contaminated by small amounts of keratan sulfate (<1%). In conclusion, our findings indicate that the composition of CS preparations not always corresponds to the manufacturers' descriptions, and indicate that further characterization should be required for the registry and license of pharmaceutical grade CS.

1. Introduction

Osteoarthritis is a major public health problem for which there are few effective medical remedies. In the 1990s, chondroitin sulfate (CS) and glucosamine (GlcN) were introduced as "nutraceutical agents" for treatment of osteoarthritis (Reginster, Gillot, Bruyere, & Henrotin, 2000), and soon it was shown that these compounds also present anti-inflammatory and chondroprotective activities (Iovu, Dumais, & du Souich, 2008; Vallières & du Souich, 2010). Because they are extracted from natural sources, and due to their safety, treatment with CS and GlcN acquired substantial popularity. They are absorbed from the gastrointestinal tract (Ronca, Palmieri, Panicucci, & Ronca, 1998), and are excreted in the urine, part as intact polymers and part as partial degradation products (Baccarin, Machado, Lopes-Moraes, Vieira, & Michelacci, 2012; Michelacci, Boim, Bergamaschi, Rovigatti, & Schor, 1992), indicating their systemic distribution. Furthermore, they were tested in a number of clinical trials, which demonstrated their efficacy in osteoarthritis (review in McAlindon, LaValley, Gulin, & Felson, 2000).

CS and GlcN are currently recommended by The European League Against Rheumatism (EULAR) as a "SYSADOA" – symptomatic slow-acting drug for the treatment of osteoarthritis. It means that they provide pain relief and increased joint mobility only after a relatively long period of regular administration (1–2 months), despite the fact that their effects last long after the end of treatment (2–3 months).

It is well established that CSs are composed of alternating 1,3-*N*-acetyl-β-D-galactosamine and 1,4-β-D-glucuronic acid units, which bear 4-*O*- and/or 6-*O*-sulfations at the *N*-acetylgalactosamine units. Most CS polymers are hybrid structures, composed of two or more types of disaccharide units, disposed in specific patterns (Michelacci & Dietrich, 1976, 1986). Depending on the disaccharide unit that predominates, CS receive different names, and may have different biological activities. For instance, it was shown that the CS of human adult articular cartilage is predominantly 6-sulfated, while in human growth cartilage it is 50% 4-sulfated and 50% 6-sulfated (Michelacci, Mourão, Laredo, & Dietrich, 1979). The distribution of these units in the polymer is very specific and well defined.

In fact, some authors report that CS has little symptom-modifying activities (Distler & Anguelouch, 2006), while others include CS in the guidelines for osteoarthritis treatment (Cutolo, Berenbaum, Hochberg, Punzi, & Reginster, 2015). These different

* Corresponding author at: Instituto de Ciências Biológicas, UFJF, Brazil.
E-mail address: jair.aguiar@ufjf.edu.br (J.A.K. de Aguiar).

http://dx.doi.org/10.1016/j.carbpol.2015.08.006
0144-8617/

activities described by different authors could be due either to differences in the CS structures or to the presence of contaminants (or both).

CSs are isolated and purified from animal sources and, as already mentioned, have complex structures. Hence, it is very important to ensure the quality of the pharmaceutical grade CSs commercially available, which are currently used as raw materials by compounding pharmacies to prepare remedies to fit the unique need of each patient. Thus, the first aim of this study was to analyze the structure of the pharmaceutical grade CSs available in local compounding pharmacies (Juiz de Fora, MG, Brazil).

These compounds were submitted to agarose gel electrophoresis, which has shown that 11, out of 16 samples, contained much less CS than declared by their respective "Certificates of Analysis". Consequently, our second aim was to identify the main contaminants. Fluorophore-assisted carbohydrate electrophoresis (FACE), Raman spectroscopy, immunoblotting, and paper chromatography were used to identify the main contaminants.

FACE is a method introduced in 1990 for the analysis of the carbohydrate moiety of glycoconjugates (Jackson, 1990). This method is based on the separation, by polyacrylamide gel electrophoresis, of saccharides that have been labeled with a suitable fluorophore. In principle, carbohydrates that have a reducing aldehydic carbon are reacted with a fluorophore that has a primary amino group. The resulting Schiff base is stabilized by reductive amination with sodium cyanoborohydride forming the stable fluorescently labeled derivatives, which are separated by high resolution PAGE.

Raman spectroscopy is a vibrational technique based on scattered radiation, which has been successfully applied to investigate structure of different carbohydrates (Almeida et al., 2010; Mainreck et al., 2012). It has been applied to the analysis of both sulfated and non-sulfated polysaccharides, including heparin (Beni, Limtiaco, & Larive, 2011). It is a non-destructive technique that requires small amount of sample and is not time consuming. In the present study, Raman spectroscopy was used to confirm the identification of CS and contaminants.

Immunoblotting was used to identify keratan sulfate, and paper chromatography to identify and quantify inorganic sulfate.

2. Experimental

2.1. Materials

Sixteen samples of pharmaceutical grade CS raw material were obtained from seven pharmaceutical dealers in Juiz de Fora, MG, Brazil. These samples were numbered – samples #1–16 – and, according to the "Certificate of Analysis" of each product, all are extracted from bovine trachea. These samples came from the following countries: sample #6 from Brazil; samples #1, 2, 5, 7, 8, 9, 10, 11, and 14 from USA; samples #3, 4, 12 and 16 from China; and samples #13, and 15 from Germany.

United States Pharmacopeia standard CS (USP-CS) was obtained from the United States Pharmacopeia (Rockville, MD; cat. 1133570, Lot H1K241). Analytical grade chondroitin 4-sulfate (Ch4S, from bovine trachea), chondroitin 6-sulfate (Ch6S, from shark cartilage), dermatan sulfate (DS, from porcine mucosa), maltodextrin, lactose, and sodium sulfate were purchased from Sigma–Aldrich Co (St. Louis, MO, USA). Heparan sulfate (HS, from bovine pancreas) and chondroitin sulfate lyases AC and B (from *Flavobacterium heparinum*) were prepared by methods previously described (Aguiar, Lima, Berto, & Michelacci, 2003; Dietrich & Nader, 1974). Agarose (standard, low Mr), nitrocellulose and Zeta-Probe membranes were purchased from Bio-Rad Laboratories (Richmond, CA, USA). MST1 anti-KS monoclonal antibody was obtained as previously described (Alves, Straus, Takahashi, & Michelacci, 1994). 2-Aminoacridone (AMAC), mercuric acetate, sodium cyanoborohydride, glycine, *N*,*N*,*N*′,*N*′-tetramethylenediamine (TEMED), and Dowex AG50W-X8 (200–400 mesh) were purchased from Sigma–Aldrich Co. Tetramethylbenzidine was from KPL (Gaithersburg, MD, USA), and SuperSignal West Pico chemoluminescent substrate was from Thermo Scientific (Rockford, IL, USA). Standard unsaturated disaccharides ΔDi0S, ΔDi2S, ΔDi4S, and ΔDi6S were from Sigma–Aldrich Co., and standard ΔDi2,6S, ΔDi4,6S, ΔDi2,4,6S were from Seikagaku Kogyo Co. Ltd. (Tokyo, Japan). These disaccharides were a kind gift from Prof. Dr. Mauro Pavão, UFRJ, Rio de Janeiro, RJ, Brazil. Standard ΔDi0S, ΔDi4S, and ΔDi6S were also prepared by methods previously described (Michelacci & Dietrich, 1976).

2.2. Agarose gel electrophoresis of CS samples

All CS samples were submitted to agarose gel electrophoresis as previously described (Dietrich & Dietrich, 1976). Briefly, 1 mg/mL solutions of CS samples were prepared, and aliquots (5 μL) were applied to agarose gel slabs in 0.05 M 1,3-diaminopropane-acetate buffer, pH 9 (PDA). After fixation with cetyltrimethylammonium bromide (cetavlon) and Toluidine Blue staining, the glycosaminoglycans were quantified by densitometry of the gel slabs (Epson Expression 1680 Flatbed Scanner, with QuickScan Win 2000, Helena Laboratories, Beaumont, TX, USA). Analysis was performed in triplicates, using Sigma–Aldrich chondroitin sulfate as standard. These compounds were further characterized by enzymatic degradation with bacterial glycosaminoglycan lyases (chondroitinase AC and chondroitinase B from *Flavobacterium heparinum*), as already described (Petricevich & Michelacci, 1990).

2.3. Analytical data

Aminosugars were determined after acid hydrolysis (4 M HCl for 6 h at 100 °C) by a modified Elson–Morgan reaction (Rondle & Morgan, 1955). Uronic acid was determined by a modification of the carbazole reaction (Di Ferrante et al., 1971). Total sulfate was measured by paper chromatography after acid hydrolysis (8 M HCl for 6 h at 100 °C), as previously described (Nader & Dietrich, 1977), and soluble protein was measured by a modified Lowry procedure with bicinchoninic acid (BCA Protein Kit Assay, Pierce, IL, USA), using bovine serum albumin as standard (Smith et al., 1985). Reducing sugars were measured by the method of 3-5-dinitrosalicylic acid (DNS, Miller, 1959).

2.4. Identification of main contaminants of CS-poor samples by FACE (fluorophore-assisted carbohydrate electrophoresis) and Raman spectroscopy

2.4.1. Treatment of unsaturated disaccharides with mercuric acetate

Aliquots of standard unsaturated disaccharides (<50 nmol) were frozen on dry ice, and lyophilized on a vacuum concentrator until dry. These samples were resuspended in 100 μL of 17.5 mM mercuric acetate, 50 mM sodium acetate, and incubated at room temperature (30 min, Calabro, Benavides, Tammi, Hascall, & Midura, 2000). The mercuric ion was removed by addition of 30 μL of a 50% slurry of Dowex H^+ resin, which was removed by filtration through a glass wool plugged pipette tip. Both the reaction tube and the glass wool were washed with 100 μL of ultrapure water, and the trapped volume was recovered by centrifugation (2000 × g). The samples were again frozen and vacuum dried.

2.4.2. Fluorescent derivatization with 2-aminoacridone (AMAC)

The derivatization was performed as described by Calabro et al. (2000), with modifications. Dried samples (20–200 nmol of saccharides) were derivatized by addition of 5 μL of 50 mM AMAC (250 nmol) in 85% DMSO/15% acetic acid. After 15 min incubation at room temperature, 5 μL of a newly prepared 1 M sodium cyanoborohydride solution was added, incubated for 16 h at 37 °C, and then 30 μL of 30% glycerol were added. One aliquot (2 μL) of each derivatized sample was immediately analyzed, and the remaining was stored in the dark at −80 °C.

2.4.3. Fluorophore-assisted carbohydrate electrophoresis

Electrophoresis were carried out in Mini-Protean Tetra Cell (Bio-Rad Laboratories, Richmond, CA, USA) in two alternative buffer systems: nonborate buffer system (anionic oligosaccharides) and borate-containing buffer system (for neutral sugars).

For nonborate conditions, gels were prepared in Tris–HCl buffer and run in Tris–glycine buffer. Polyacrylamide separating gels (20%) were prepared as described by Oonuki, Yoshida, Uchiyama, and Asari (2005), with some modifications. Acrylamide-bisacrylamide stock solution (40% containing 5% bisacrylamide, 5 mL) plus 1.5 M Tris–HCl buffer, pH 8.9 (1.5 mL) were diluted with 3.5 mL of pure water. This solution was degased for a few minutes, and then mixed with 0.1 mL of 10% APS and 10 μL of TEMED. The gel solution was poured into sets of glass boards with butanol added to the top, and was left until completion of gelling. Then 0.5 mL of the acrylamide–bisacrylamide solution (40%) was mixed with 0.66 mL of 0.5 M Tris–HCl buffer (pH 6.7), and diluted with 3 mL of pure water. Also this "stacking gel solution" was degassed. After the butanol was taken away from the top of the separating gel, 5 μL of TEMED and 50 μL of 10% APS were added to the stacking gel solution, which was poured on top of the separation gel and a sample comb was set into the stacking gel. Stock electrode buffer, 10× was 1.92 M glycine, 0.25 M Tris base, pH 8.3. The run (100–220 V, 70 min) was followed with the aid of an UV-lamp (320–400 nm).

For borate-containing conditions, the stock resolving gel buffer 4× was 0.75 M Tris-0.5 M boric acid, adjusted to pH 7.0 with concentrated HCl; the stock stacking gel buffer, 4× was 0.5 M Tris-0.5 M boric acid, adjusted to pH 6.8 with concentrated HCl, and the stock electrode buffer, 5× was 0.5 M glycine, 0.6 M Tris base, and 0.5 M boric acid, final pH 8.3 (Gao & Lehrman, 2003).

After electrophoresis, gels were removed from the apparatus, illuminated with a UV transilluminator (365 nm), and photographed (GelDoc-It Imaging System, UVP). Quantitative results were obtained with TotalLab TL120 1D v2009 software, Nonlinear Dynamics Ltd.

2.4.4. Raman spectroscopy

Fourier transform Raman measurements were carried out using a Bruker RFS 100 instrument equipped with a Nd:YAG laser, a Germanium detector cooled with liquid nitrogen, operating at 1064 nm. The *in situ* analysis of each solid sample was obtained with 1000 scans collected at resolution of 4 cm^{-1}, with a power of 35 mW. These parameters were selected in order to obtain the best signal-to-noise ratio while the physical and chemical integrity of the samples was maintained; this was achieved by repeating each one of the spectra and observing the possible changes in position and intensity over all the spectrum bands. The FT-Raman spectra in the range of 3500–50 nm were obtained from the reference standard chondroitin 4-sulfate, maltodextrin, lactose, sodium sulfate, and sixteen pharmaceutical chondroitin sulfate samples. The peak assignment was based on Bansil, Yannas, and Stanley (1978) and on Ellis, Green, and Winlove (2009).

2.5. Structural analysis of the CS of the "CS-rich"

Aliquots of CS samples (100 μg, 10 μL of 10 mg/mL solutions) were incubated with 10 mU of chondroitin lyase AC (10 μL) in 0.05 M ethylenediamine-acetate (EDA) buffer, pH 8.0, at room temperature. After 18 h incubation, aliquots (2 μL) were submitted to agarose gel electrophoresis as described in Section 2.2. The remaining 18 μL were applied to Whatman #1 filter paper and submitted to descending chromatography in isobutyric acid: 1.25 M NH_4OH, 5:3, v/v. After 24 h, the reducing products were located by silver nitrate staining.

Alternatively, 20 μg of substrate were incubated with 2 mU of chondroitin lyase AC in EDA buffer, 50 μL final volume. After 18 h incubation at room temperature, the samples were vacuum dried, derivatized with AMAC as described in Section 2.4.2., and submitted to FACE as in Section 2.4.3.

The molecular weight of the chondroitin sulfates was determined by polyacrylamide gel electrophoresis as previously described (Dietrich & Nader, 1974; Hilborn & Anastassiadis, 1971).

2.6. Detection of keratan sulfate by immunoblotting

Keratan sulfate was detected in the samples by immunoblotting probed with MST1, a monoclonal antibody that recognizes keratan sulfate both as free chains and as proteoglycans (Alves et al., 1994; Baccarin et al., 2012; Pereira, Aguiar, Hagiwara, & Michelacci, 2004). After agarose gel electrophoresis, the glycosaminoglycans were transferred to nitrocellulose and Zeta-Probe nylon membranes. After blocking, membranes were probed with MST1. Then, the membranes were incubated with peroxidase-conjugated rabbit anti-mouse IgG secondary antibody, and either tetramethylbenzidine (TMB) or SuperSignal West Pico was used as substrates. Quantitative analysis were performed by ELISA (Alves et al., 1994), using keratan sulfate purified from bovine nucleus pulposus as standard.

3. Results and discussion

3.1. Agarose gel electrophoresis of CS samples

Sixteen pharmaceutical grade CS samples were analyzed by agarose gel electrophoresis in PDA buffer, in comparison to USP-CS and analytical grade Ch4S. USP-CS contained less CS (96.4%) then the analytical grade Ch4S. That is why the analytical grade Ch4S was used as standard in the following experiments. Fig. 1 shows representative agarose gel slabs (B), as well as a standard curve of Ch4S (A). The bands were quantified by densitometry, and the curve was linear (R^2 = 0.9998) between 1 and 8 μg of CS (European Pharmacopoeia, 2007; United States Pharmacopoeia, 2008). For all CS samples, a single band appeared, migrating as the standard Ch4S (Fig. 1B). However, only five samples – #3, 4, 6, 12 and 16 – were more than 90% CS (average 96.5%), while the remaining eleven were less than 15% CS (average 10%) (Table 1). Thus, these samples were classified as "CS-rich" (#3, 4, 6, 12 and 16) and "CS-poor" (#1, 2, 5, 7, 8, 9, 10, 11, 13, 14, 15) samples.

Electrophoretic techniques are recommended by both the European Pharmacopeia (agarose gel electrophoresis in barium acetate buffer) and the United States Pharmacopeia (cellulose acetate electrophoresis in barium acetate buffer) for CS analysis. Not more than 2% of any individual impurity is acceptable. Furthermore, both pharmacopeias describe a photometric titration procedure with cetylpyridinium chloride (CPC), which forms insoluble complexes with CS and precipitate. Nevertheless, this procedure is not specific, since other glycosaminoglycans, nucleic acids, and even inorganic salts interfere with the CS quantification (Sim et al., 2005; Volpi,

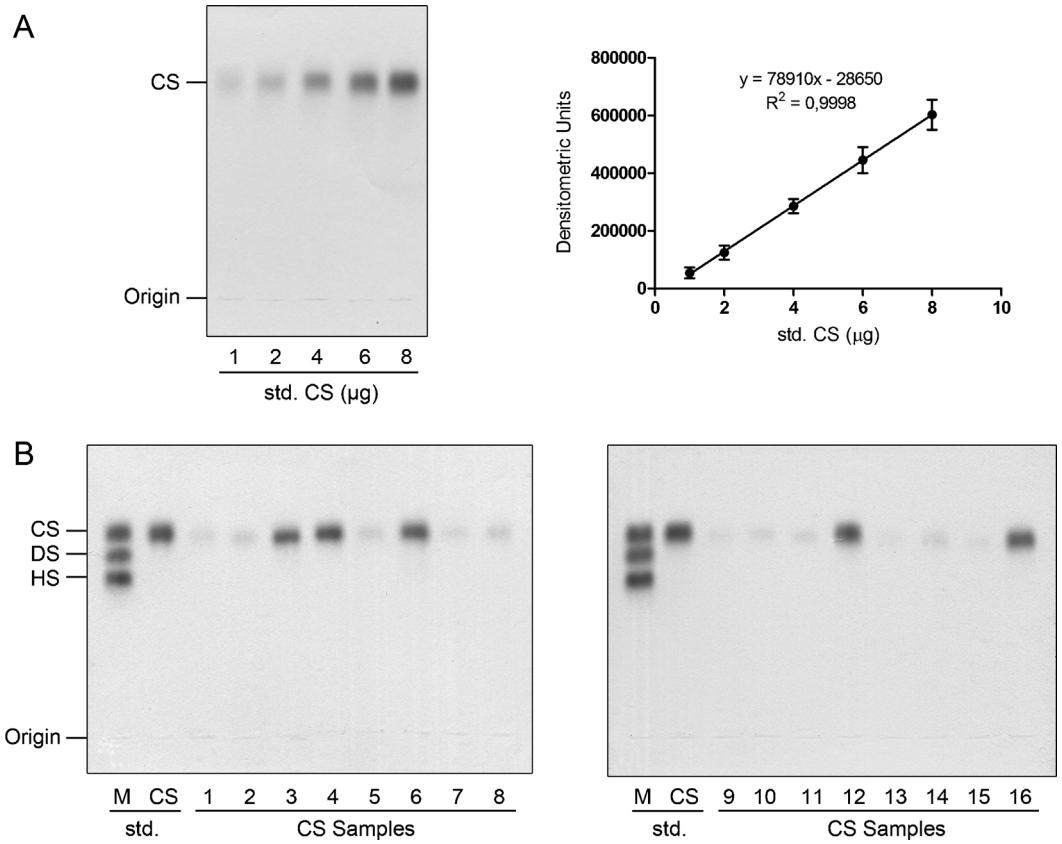

Fig. 1. Agarose gel electrophoresis of CS samples. (A) Calibration curve for CS. Standard chondroitin 4-sulfate (std CS) solutions were prepared: 0.2 mg/mL, 0.4 mg/mL, 0.8 mg/mL, 1.2 mg/mL, 1.6 mg/mL, and 5 μL aliquots of each were applied to 0.55% agarose gel in 0.05 M 1,3-diaminopropane-acetate buffer, pH 9.0 (PDA). After the run, the glycosaminoglycans were precipitated in the gel by 0.1% cetyltrimethylammonium bromide (cetavlon), the gel was dried, and stained by Toluidine Blue, as previously described (Dietrich & Dietrich, 1976). CS was quantified by densitometry, and mean ± standard deviation for three independent determinations are shown. The curve was linear from 1 to 8 μg of CS. A representative gel of the 16 CS samples here analyzed is shown in (B). Aqueous solutions (1 mg/mL) of each CS sample (1–16) were prepared, and 5 μL aliquots were submitted to agarose gel electrophoresis as above described. CS was quantified by densitometry in comparison to standard CS run in the same gel, and also to the CS standard curve. Quantitative results are mean ± standard deviation of three independent determinations. M, mixture of standard glycosaminoglycans containing chondroitin sulfate (CS), dermatan sulfate (DS), and heparan sulfate (HS) (5 μg each).

Table 1
Analytical data of sixteen samples of pharmaceutical grade CS.

	CS #	CS content (%)	Protein (%)	Reducing sugars (μg/100 μg of sample)	GlcUA (μg/100 μg of sample)	GalNAc (μg/100 μg of sample)	Sulfate (μg/100 μg of sample)
CS-rich	3	91.0	3.6	8.3	38.2	33.4	27.3[a]
	4	94.0	3.5	8.1	36.3	29.0	17.9[a]
	6	97.8	1.9	9.0	37.5	32.0	29.3[a]
	12	97.8	3.6	9.7	39.7	40.3	25.5[a]
	16	102.0	3.5	9.2	36.8	33.7	24.6[a]
	Mean ± SD	*96.5 ± 4.2*	*3.2 ± 0.7*	*8.9 ± 0.7*	*37.7 ± 1.3*	*33.7 ± 4.1*	*24.9 ± 4.3*
CS-poor	1	10.4	3.0	33.3	19.0	5.5	–
	2	13.1	3.2	34.8	19.6	6.5	–
	5	12.5	3.5	29.2	21.1	7.3	–
	7	9.6	3.5	32.3	20.9	8.9	–
	8	13.4	3.2	31.2	19.8	11.0	–
	9	7.3	3.4	32.7	20.7	10.4	–
	10	8.9	2.9	29.6	20.3	9.6	–
	11	11.0	3.1	33.3	24.8	6.9	–
	13	5.4	10.5	21.9	6.7	9.5	26.3[b]
	14	11.4	3.1	32.4	23.6	11.8	–
	15	6.8	11.1	19.8	7.9	8.0	26.1[b]
	Mean ± SD	*10.0 ± 2.7*	*4.6 ± 3.1*	*30.0 ± 4.9*	*18.6 ± 5.8*	*8.7 ± 2.0*	*26.2*
Standards	Ch4S	100.0	1.3	8.9	43.0	45.9	27.7[a]
	Ch6S	100.0	0.0	7.5	42.0	39.5	24.0[a]
	Maltodextrin	–	3.4	35.4	17.7	3.3	–
	Lactose	–	9.1	54.5	14.1	3.3	–

Results are given as mean ± standard deviation.
[a] Sulfate detected only after acid hydrolysis (HCl 8 M, 6 h, 100 °C).
[b] Inorganic free sulfate.

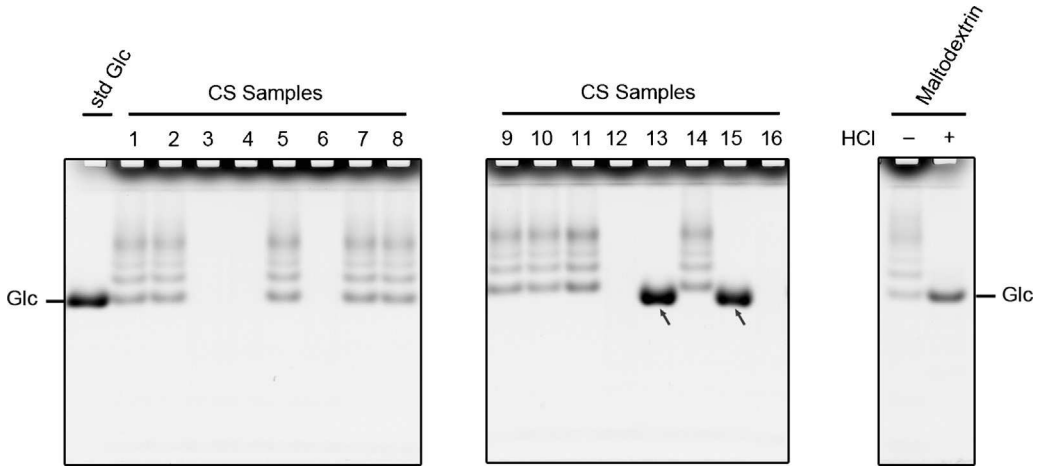

Fig. 2. Fluorophore-assisted carbohydrate electrophoresis (FACE) of CS samples in Tris-borate-glycine buffer. The CS samples were analyzed by FACE in 0.12 M Tris-borate-glycine buffer, pH 8.3, in order to identify the main contaminants. CS samples (50 μg) were derivatized with AMAC, and aliquots (2.5 μg) were submitted to electrophoresis as described in Section 2.4. Gel images were obtained under UV (λ = 365 nm) with a scientific grade CCD Camera (*GelDoc-It Imaging System, equipped with GelCam 310*). For comparison, maltodextrin was equally derivatized with AMAC and analyzed by FACE, under the same conditions. A band patter similar to that of maltodextrin was observed in CS samples 1, 2, 5, 7, 8, 9, 10, 11 and 14, but did not appear in the CS-rich samples (3, 4, 6, 12 and 16), as well as in samples 13 and 15, which presented only one band (arrow).

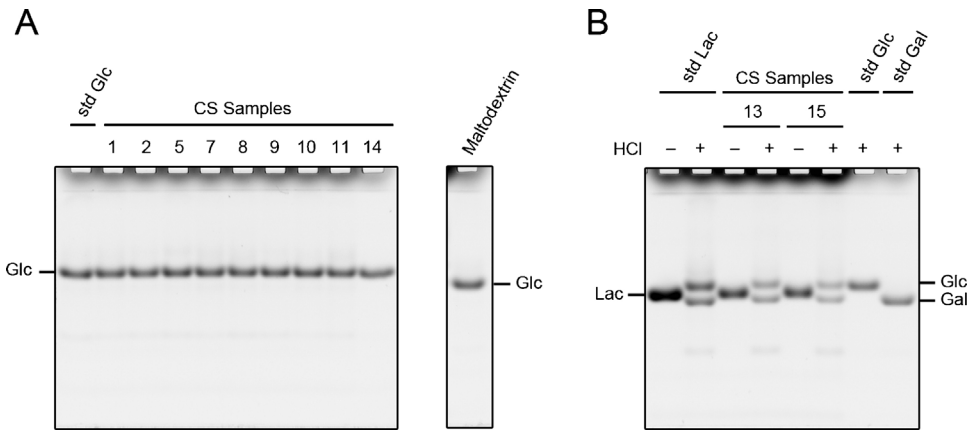

Fig. 3. Acid hydrolysis of CS-poor samples. To further characterize the main contaminants of CS-poor samples (15% CS or less), aliquots (20 μg) were submitted to acid hydrolysis (6 M HCl, 100 °C, 6 h), and then derivatized by AMAC and analyzed by FACE, under the same conditions described in Fig. 2. For comparison, maltodextrin was equally submitted to acid hydrolysis, treated with AMAC and analyzed by FACE, under the same conditions. Now, the electrofluorogram showed a single band for samples 1, 2, 5, 7, 8, 9, 10, 11, 14 and maltodextrin, migrating as glucose (Glc) (A). In contrast, for samples 13 and 15, which have shown only one band, migrating as lactose (Lac) before hydrolysis, two bands appeared after acid hydrolysis, migrating as glucose (Glc) and galactose (Gal) (B). Gel images were obtained as described in Fig. 2.

2007). For instance, it was recently shown that propylene glycol alginate sulfate sodium, also known as alginic sodium diester (ASD), and Zero One (Z1), a water-soluble agent recently identified as sodium hexametaphosphate, are also titratable anions and form ionic pairs with CPC, therefore interfering with the CPC titration (Weiguo et al., 2014). The authors suggest that CPC titration and electrophoresis to be used in combination to detect CS adulterants ASD and Z1.

The agarose gel electrophoresis here used, developed by Jaques, Ballieux, Dietrich, and Kavanagh (1968) and modified by Dietrich and Dietrich (1976), using a special buffer system – PDA – to permit the separation and identification of different glycosaminoglycans, is much more precise and specific. After electrophoresis, the glycosaminoglycans are precipitated in the gel by a cationic detergent (cetavlon), the gel is dried under a sheet of paper and hot air flow to remove excess cetavlon and buffer, and stained by Toluidine Blue. Only metachromatic bands are glycosaminoglycans. These bands are quantified by densitometry.

3.2. Analytical data

Table 1 shows the analytical data of our CS samples, and standards Ch4S, Ch6S, maltodextrin and lactose. Only two of the CS-poor samples – #13 and 15 – contained significant amounts of soluble proteins (~10%). All other samples contained ~3% protein. In contrast, all the "CS-poor" samples contained much more reducing sugars than the "CS-rich" samples (about 3 times), while the amounts of glucuronic acid (GlcUA) and galactosamine (GalNAc) were lower (a half for GlcUA, and one third for GalNAc). These results are in agreement with the findings shown in Fig. 1. It is also important to notice that the GlcUA measurement may be overestimated in some "CS-poor" samples due to the possible presence of neutral sugars (see Table 1 and Section 3.3). Free inorganic sulfate was also detected only in samples #13 and 15 (before acid hydrolysis). In the "CS-rich" samples, as well as in standard Ch4S and Ch6S, sulfate was measured after acid hydrolysis of the polymers (HCl 8 M, 6 h, 100 °C).

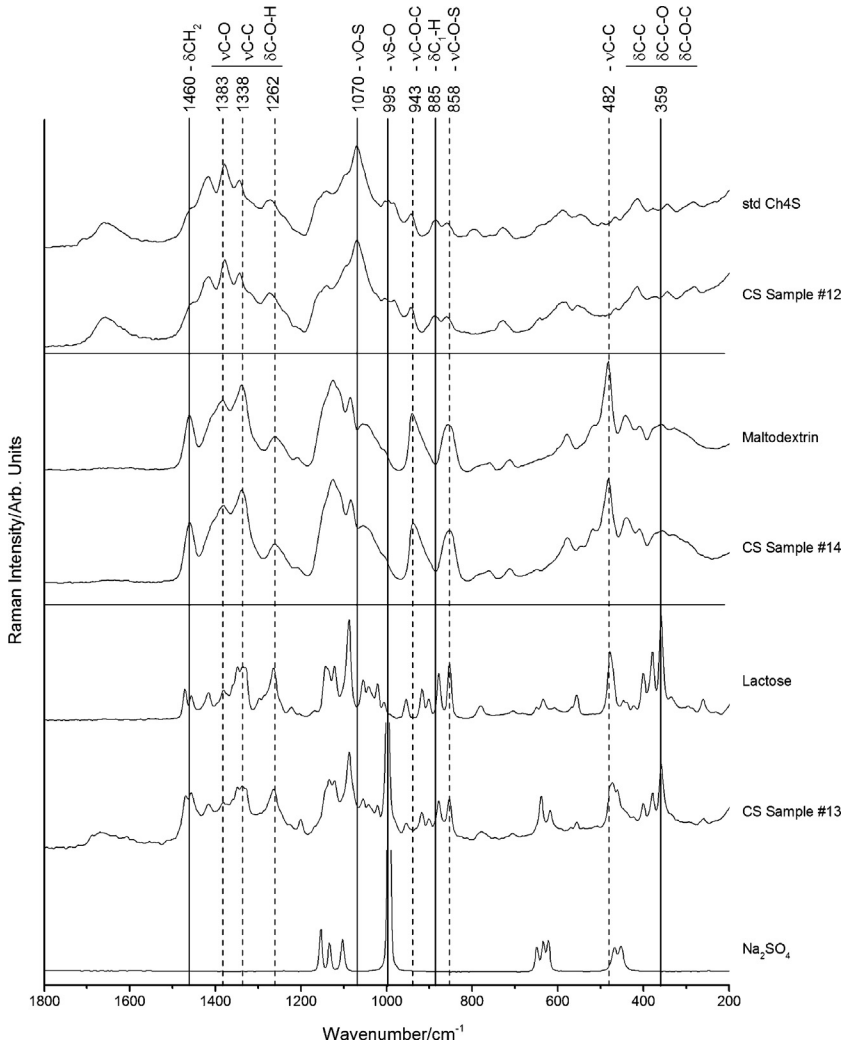

Fig. 4. Raman spectra of CS pharmaceutical samples and standards. *In situ* analysis of reference standards and representative samples by macro-Raman spectroscopy operating at 1064 nm. The spectra were obtained with 1000 scans of powder samples. Fingerprint bands are shown in the region of 1800–200 cm^{-1}.

3.3. *Identification of main contaminants of CS-poor samples by FACE and Raman spectroscopy*

As CS was only a minor component of 11 (out of 16) CS samples, corresponding to only 5–13% of total weight, we decided to investigate the main contaminants. So, the "CS-poor" samples were submitted to FACE in Tris-borate-glycine buffer system (Fig. 2). In 9, out of these 11 "CS-poor" samples – #1, 2, 5, 7–11, 14 – several bands appeared. These bands migrated as those obtained from maltodextrin (Fig. 2). The remaining two "CS-poor" samples – #13 and 15 – presented a single intense band (arrow, Fig. 2). In the "CS-rich" samples, no bands appeared.

In order to further characterize the contaminant carbohydrates, the "CS-poor" samples were again submitted to acid hydrolysis (HCl 6 M, 6 h, 100 °C), and analyzed by FACE in Tris-borate-glycine buffer system (Fig. 3). A single band migrating as glucose was observed in all samples that presented the "maltodextrin-type" band pattern – #1, 2, 5, 7-11, 14, Fig. 3A. In contrast, the "CS-poor" samples that presented only one intense band in Fig. 2, exhibited, after acid hydrolysis, two bands of the same intensity, migrating as glucose and galactose (Fig. 3B). Actually, the single band observed in the non-hydrolyzed material had the same migration of lactose.

These results were confirmed by Raman spectroscopy. Fig. 4 shows representative spectra of standard CS, maltodextrin, lactose, and sodium sulfate, as well as selected CS samples (#12, 13, and 14). The main component of CS #12 presents a Raman profile similar to that of standard CS, while the spectrum of sample #14 is similar to that of maltodextrin, and the sample #13 spectrum resembles that of lactose and sodium sulfate.

So, our data show that the main contaminant of samples #1, 2, 5, 7–11, and 14 was maltodextrin, while samples #13 and 15 contain predominantly lactose (51% and 46%, respectively), sulfate (~26%), and protein (~10%), with only 5–6% CS. This finding is alarming since medicines prepared from these raw materials will not only contain much less of the desired active principle (CS), but also could have serious side effects from the contaminants.

Unconformities regarding CS content in nutraceuticals, as well as the presence of other contaminant sugars and glycosaminoglycans have also been reported by others (Adebowale, Cox, Liang, & Eddington, 2000; Sim et al., 2005; Volpi, 2009).

To our knowledge, this is the first study to describe pharmaceutical preparations having less than 15% CS, and in which the main contaminants of eleven preparations were totally characterized. It is still important to note that these contaminants could not be impurities from the extraction and purification

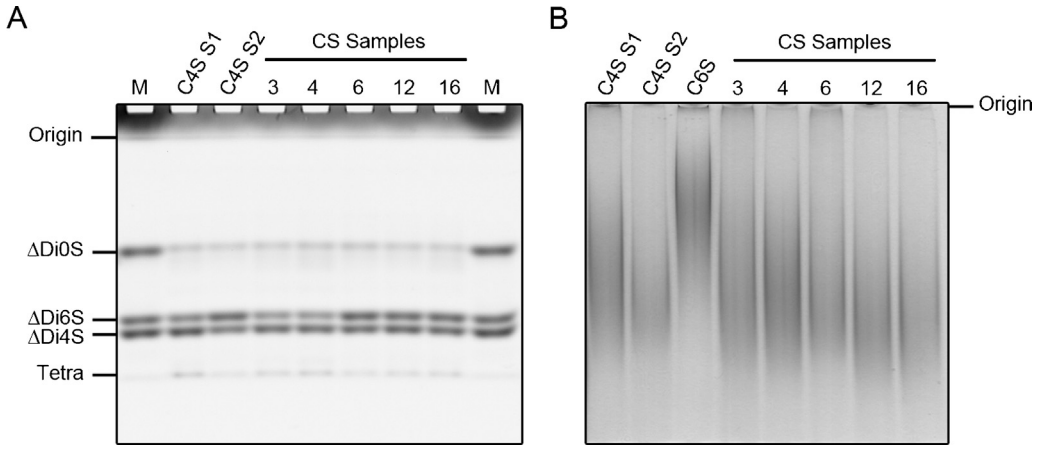

Fig. 5. FACE (Tris-glycine buffer), and PAGE of the five "CS-rich" samples. To access the CS sulfation pattern and modal molecular weight, the "CS-rich" samples were further analyzed by FACE after enzymatic degradation, and by PAGE. Aliquots (20 μg) of each sample were incubated with *Flavobacterium heparinum* chondroitin lyase AC (2 mU). The products formed were derivatized with AMAC, and analyzed by FACE in 0.025 M Tris-glycine buffer, pH 8.3. Gel images were obtained as described in Fig. 2. A representative gel is shown in (A). The bands were quantified by densitometry using TotalLab TL120 software. Two independent derivatizations were made for each sample, and three gels were run for each derivatization. For the determination of CS modal molecular weight, aliquots (10 μg) of CS samples were applied to a 7.5% polyacrylamide gel in 20 mM Tris-HCl buffer, pH 7.4, as previously described (Hilborn & Anastassiadis, 1971; Dietrich & Nader, 1974). After the run (100 V, 50 min) the gels were stained with 0.1% Toluidine Blue in 1% acetic acid (B), and analyzed by densitometry. ΔDi0S, 2-acetamido-2-deoxy-3-*O*-(β-D-gluco-4-enepyranosyluronic acid)-D-galactose; ΔDi6S, 2-acetamido-2-deoxy-3-*O*-(β-D-gluco-4-enepyranosyluronic acid)-6-*O*-sulfo-D-galactose; ΔDi4S, 2-acetamido-2-deoxy-3-*O*-(β-D-gluco-4-enepyranosyluronic acid)-4-*O*-sulfo-D-galactose; Tetra, tetrasaccharides; M, mixture of standard unsaturated disaccharides; Ch4S, standard CS extracted from bovine trachea (Sigma–Aldrich); Ch6S, standard CS from shark cartilage (Sigma–Aldrich); 3, 4, 6, 12 and 16, CS pharmaceutical samples.

procedures, since they are not found in the same animal sources of CS.

3.4. Structural analysis of the CS of the "CS-rich"

Standard disaccharides were characterized by FACE, and also by treatment with mercuric acetate, followed by FACE (nonborate system). The products formed from the "CS-rich" samples were compared to these standards.

Aliquots (20 μg) of the "CS-rich" samples – #3, 4, 6, 12, 16 – were incubated with *F. heparinum* chondroitin lyase AC as described in Section 2.5, and derivatized with AMAC (40 μL final volume). Aliquots (2 μL, containing ~1 μg of CS products) were submitted to FACE, as described in Section 2.4.3. Representative results are shown in Fig. 5, and quantitative data are given in Table 2. All the

Table 2
Disaccharide composition and molecular weight analysis of 5 pharmaceutical CS samples with CS content above 90%.

	Disaccharide composition					Modal molecular weight (kDa)
	Di0S	Di6S	Di4S	4S/6S	SO_3/UA	
Ch4S (standard)	10%	49%	41%	0.8	0.90	25.4
CS sample #3	12%	33%	55%	1.7	0.88	27.6
CS sample #4	13%	34%	53%	1.6	0.87	29.0
CS sample #6	11%	47%	42%	0.9	0.89	24.0
CS sample #12	9%	44%	47%	1.1	0.91	19.6
CS sample #16	10%	44%	46%	1.0	0.90	20.4

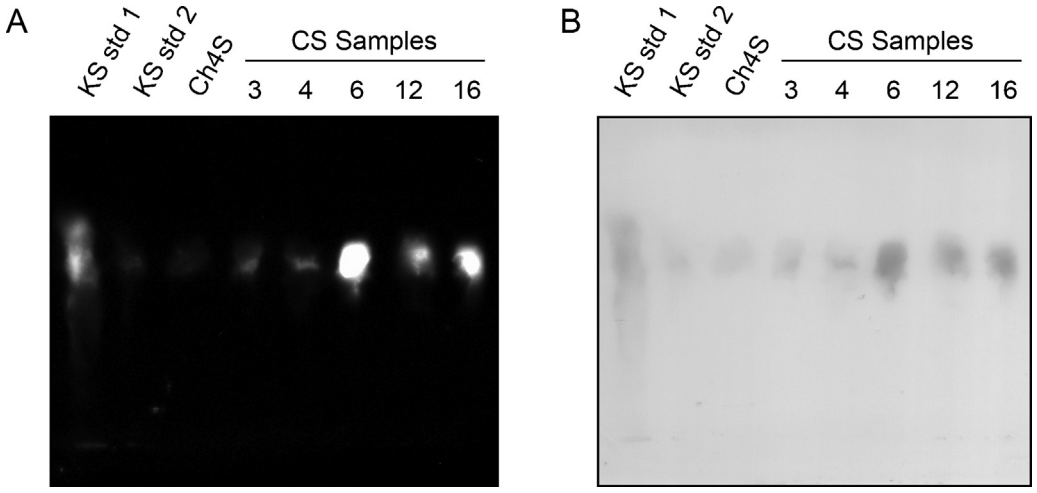

Fig. 6. Immunoblotting of keratan sulfate. Aliquots (5 μg) of the five CS-rich samples (3, 4, 6, 12 and 16) were submitted to agarose gel electrophoresis as described in Fig. 1, except that after the run the glycosaminoglycans were transferred to nitrocellulose membrane, and revealed by an anti-keratan sulfate monoclonal antibody – MST1 (Alves et al., 1994). The blotting was processed as previously described (Pereira et al., 2004). This antibody recognizes keratan sulfate both as free chains and as proteoglycans. Secondary antibody conjugated with horseradish peroxidase (HRP) was used, and two substrates were used in sequence: Super Signal West Pico chemiluminescent substrate (A), and tetramethylbenzidine (TMB) (B). KS std 1, standard keratan sulfate proteoglycan; KS std 2, standard keratan sulfate; Ch4S, standard chondroitin 4-sulfate (Sigma–Aldrich).

CS samples gave three bands migrating as ΔDi0S, ΔDi4S, ΔDi6S, and trace amounts of tetrasaccharide (Tetra). Nevertheless, the relative proportions of disaccharides varied. All of them contained ~10% Di0S, but samples #3 and 4 contained predominantly Di4S (Di4S:Di6S ratios 1.6–1.7), while samples #6, 12, and 16 contained similar amounts of Di4S and Di6S (Di4S:Di6S ratios 0.9–1.1). Fig. 5 also shows a polyacrylamide gel electrophoresis of the same samples, performed to determine the molecular weight of the polymers. All of them were polydisperse polymers, with modal molecular weight ~20 kDa.

Differences in the composition and biological activities of chondroitin sulfates of different origins were also reported by others (Martel-Pelletier, Farran, Montell, Vergés, & Pelletier, 2015; Michelacci & Dietrich, 1976; Michelacci et al., 1979).

3.5. Detection of keratan sulfate by immunoblotting

Although only one band migrating as CS was observed for all "CS-rich" samples in agarose gel electrophoresis (Fig. 1), trace amounts of keratan sulfate appeared on immunoblotting probed with monoclonal antibody (MST1) (Fig. 6). The identification of keratan sulfate was confirmed by incubation with *Pseudomonas* sp. keratanase. Quantitative analysis performed by ELISA using the same primary antibody has shown that keratan sulfate corresponds to less than 1% of total glycosaminoglycan of these samples. It is important to notice that even the standard Ch4S (Sigma–Aldrich) also contained trace amounts of keratan sulfate. This keratan sulfate probably comes from the same biological source – cartilage – and due to its polyanionic nature was not separated from chondroitin sulfate during the purification procedures.

The presence of keratan sulfate in CS preparations was also recently reported by others (Nakano & Ozimek, 2014).

4. Conclusions

In conclusion, our data show that, out of 16 CS samples prepared in different countries all over the world, only 5 contained more than 90% CS and were in conformity to their labels. The remaining 11 CS-poor samples contained maltodextrin or lactose as the main contaminants (both of which are commonly used as pharmaceutical excipients). It is important to reinforce that these "CS" preparations came from diverse locations, and all of them are clearly not in conformity to their label specifications.

This finding could explain, at least in part, the variations reported by different authors in the biological responses of osteoarthritis to CS treatment. In addition, some contaminants could lead to serious side effects, especially in sensible patients (for instance, lactose in intolerant patients).

We strongly suggest that more efficient and strict criteria should be applied to both licensing and quality control of raw materials, as well as to the final pharmacological preparations obtained from them.

The use of agarose gel electrophoresis, as well as FACE and Raman spectroscopy, to determine both the CS contents and the eventual presence/identification of contaminants, is recommended.

Acknowledgements

This research was supported by Fundação de Amparo à Pesquisa do Estado de São Paulo (FAPESP, grant #2010/16022-5), São Paulo, SP, Brazil; Conselho Nacional de Desenvolvimento Científico e Tecnológico (CNPq, grant #308642/2010-4), Brasília, DF, Brazil; and Fundação Coordenação de Aperfeiçoamento de Pessoal de Nível Superior (CAPES), Brasília, SP, Brazil.

References

Adebowale, A. O., Cox, D. S., Liang, Z., & Eddington, N. D. (2000). Analysis of glucosamine and chondroitin sulfate content in marketed products and the Caco-2 permeability of chondroitin sulfate raw materials. *The Journal of The American Nutraceutical Association*, *3*, 37–44.

Aguiar, J. A. K., Lima, C. R., Berto, A. G. A., & Michelacci, Y. M. (2003). An improved methodology to produce *Flavobacterium heparinum* chondroitinases, important instruments for diagnosis of diseases. *Biotechnology and Applied Biochemistry*, *37*, 115–127.

Almeida, M. R., Alves, R. S., Nascimbem, L. B., Stephani, R., Poppi, R. J., & de Oliveira, L. F. (2010). Determination of amylose content in starch using Raman spectroscopy and multivariate calibration analysis. *Analytical Bioanalytical Chemistry*, *397*, 2693–2701.

Alves, M. J. M., Straus, A. H., Takahashi, H. K., & Michelacci, Y. M. (1994). Production and characterization of monoclonal antibodies to shark cartilage proteoglycan. *Brazilian Journal of Medical and Biological Research*, *27*, 2103–2108.

Baccarin, R. Y. A., Machado, T. S. L., Lopes-Moraes, A. P., Vieira, F. A. C., & Michelacci, Y. M. (2012). Urinary glycosaminoglycans in horse osteoarthritis. Effects of chondroitin sulfate and glucosamine. *Research in Veterinary Science*, *93*, 88–96.

Bansil, R., Yannas, I. V., & Stanley, H. E. (1978). Raman spectroscopy: A structural probe of glycosaminoglycans. *Biochimica et Biophysica Acta*, *541*, 535–542.

Beni, S., Limtiaco, J. F., & Larive, C. K. (2011). Analysis and characterization of heparin impurities. *Analytical and Bioanalytical Chemistry*, *399*, 527–539.

Calabro, A., Benavides, M., Tammi, M., Hascall, V. C., & Midura, R. J. (2000). Microanalysis of enzyme digests of hyaluronan and chondroitin/dermatan sulfate by fluorophore-assisted carbohydrate electrophoresis (FACE). *Glycobiology*, *10*, 273–281.

Cutolo, M., Berenbaum, F., Hochberg, M., Punzi, L., & Reginster, J. Y. (2015). Commentary on recent therapeutic guidelines for osteoarthritis. *Seminars on Arthritis and Rheumatism*, *44*, 611–617.

Dietrich, C. P., & Dietrich, S. M. (1976). Electrophoretic behaviour of acidic mucopolysaccharides in diamine buffers. *Analytical Biochemistry*, *70*, 645–647.

Dietrich, C. P., & Nader, H. B. (1974). Fractionation and properties of four heparitin sulfates from beef lung tissue. Isolation and partial characterization of a homogeneous species of heparitin sulfate. *Biochimica et Biophysica Acta*, *343*, 34–44.

Di Ferrante, N., Nichols, B. L., Donnelly, P. V., Neri, G., Hrgovcic, R., & Berglund, R. K. (1971). Induced degradation of glycosaminoglycans in Hurler's and Hunter's syndromes by plasma infusion. *Proceedings of the National Academy of Sciences USA*, *68*, 303–307.

Distler, J., & Anguelouch, A. (2006). Evidence-based practice: review of clinical evidence on the efficacy of glucosamine and chondroitin in the treatment of osteoarthritis. *Journal of American Academy of Nurse Practice*, *18*, 487–493.

Ellis, R., Green, E., & Winlove, C. P. (2009). Structural analysis of glycosaminoglycans and proteoglycans by means of Raman microspectrometry. *Connective Tissue Research*, *50*, 29–36.

European Pharmacopoeia. (2007). *European directorate for the quality of medicines* (6th ed.). France: Strasbourg.

Gao, N., & Lehrman, M. A. (2003). Alternative sources of reagents and supplies for fluorophore-assisted carbohydrate electrophoresis (FACE). *Glycobiology*, *13*, 1G–3G.

Hilborn, J. C., & Anastassiadis, P. A. (1971). Estimation of the molecular weights of acidic mucopolysaccharides by polyacrylamide gel electrophoresis. *Analytical Biochemistry*, *39*, 88–92.

Iovu, M., Dumais, G., & du Souich, P. (2008). Anti-inflammatory activity of chondroitin sulfate. *Osteoarthritis and Cartilage*, *16*, S14–S18.

Jackson, P. (1990). The use of polyacrylamide-gel electrophoresis for the high-resolution separation of reducing saccharides labelled with the fluorophore 8-aminonaphthalene-1,3,6-trisulphonic acid. Detection of picomolar quantities by an imaging system based on a cooled charge-coupled device. *Biochemical Journal*, *270*, 705–713.

Jaques, L. B., Ballieux, R. E., Dietrich, C. P., & Kavanagh, L. W. (1968). A microelectrophoresis method for heparin. *Canadian Journal of Physiology and Pharmacology*, *46*, 351–360.

Mainreck, N., Brézillon, S., Sockalingum, G. D., Maquart, F. X., Manfait, M., & Wegrowski, Y. (2012). Characterization of glycosaminoglycans by tandem vibrational microspectroscopy and multivariate data analysis. *Methods of Molecular Biology*, *836*, 117–130.

Martel-Pelletier, J., Farran, A., Montell, E., Vergés, J., & Pelletier, J. P. (2015). Discrepancies in composition and biological effects of different formulations of chondroitin sulfate. *Molecules*, *20*, 4277–4289.

McAlindon, T. E., LaValley, M. P., Gulin, J. P., & Felson, D. T. (2000). Glucosamine and chondroitin for treatment of osteoarthritis. A systematic quality assessment and meta-analysis. *JAMA*, *283*, 1469–1475.

Michelacci, Y. M., Boim, M. A., Bergamaschi, C. T., Rovigatti, R. M., & Schor, N. (1992). Possible role for chondroitin sulfate in urolithiasis: In vivo studies in an experimental model. *Clinica Chimica Acta*, *208*, 1–8.

Michelacci, Y. M., & Dietrich, C. P. (1976). Structure of chondroitin sulfates. Analyses of the products formed from chondroitin sulfates A and C by the action of the chondroitinases C and AC from *Flavobacterium heparinum*. *Biochimica et Biophysica Acta*, *451*, 436–443.

Michelacci, Y. M., & Dietrich, C. P. (1986). Structure of chondroitin sulphate from whale cartilage: Distribution of 6- and 4-sulphated oligosaccharides in the

polymer chains. *International Journal of Biological Macromolecules*, *8*, 108–113.
Michelacci, Y. M., Mourão, P. A. S., Laredo, J., & Dietrich, C. P. (1979). Chondroitin sulfates and proteoglycans from normal and arthrosic human cartilage. *Connective Tissue Research*, *7*, 29–36.
Miller, G. L. (1959). Use of dinitrosalicylic acid reagent for determination of reducing sugars. *Analytical Biochemistry*, *31*, 426–428.
Nader, H. B., & Dietrich, C. P. (1977). Determination of sulfate after chromatography and toluidine blue complex formation. *Analytical Biochemistry*, *78*, 112–118.
Nakano, T., & Ozimek, L. (2014). Detection of keratan sulfate by immunological methods in commercial chondroitin sulfate preparations. *Carbohydrate Polymers*, *99*, 547–552.
Oonuki, Y., Yoshida, Y., Uchiyama, Y., & Asari, A. (2005). Application of fluorophore-assisted carbohydrate electrophoresis to analysis of disaccharides and oligosaccharides derived from glycosaminoglycans. *Analytical Biochemistry*, *343*, 212–222.
Pereira, D. A., Aguiar, J. A. K., Hagiwara, M. K., & Michelacci, Y. M. (2004). Changes in cat urinary glycosaminoglycans with age and in feline urologic syndrome. *Biochimica et Biophysica Acta*, *1672*, 1–11.
Petricevich, V. L., & Michelacci, Y. M. (1990). Proteoglycans synthesized *in vitro* by nude and normal mouse peritoneal macrophages. *Biochimica et Biophysica Acta*, *1053*, 135–143.
Reginster, J. Y., Gillot, V., Bruyere, O., & Henrotin, Y. (2000). Evidence of nutriceutical effectiveness in the treatment of osteoarthritis. *Current Rheumatology Reports*, *2*, 472–477.
Ronca, F., Palmieri, L., Panicucci, P., & Ronca, G. (1998). Anti-inflammatory activity of chondroitin sulfate. *Osteoarthritis Cartilage*, *6*(Suppl A), 14–21.
Rondle, C. J., & Morgan, W. T. (1955). The determination of glucosamine and galactosamine. *Biochemical Journal*, *61*, 586–589.
Sim, J. S., Jun, G., Toida, T., Choc, S. Y., Choi, D. W., Chang, S. Y., et al. (2005). Quantitative analysis of chondroitin sulfate in raw materials, ophthalmic solutions, soft capsules and liquid preparations. *Journal of Chromatography B*, *818*, 133–139.
Smith, P. K., Krohn, R. I., Hermanson, G. T., Mallia, A. K., Gartner, F. H., Provenzano, M. D., et al. (1985). Measurement of protein using bicinchoninic acid. *Analytical Biochemistry*, *150*, 76–85.
United States Pharmacopoeia. (2008). *United States pharmacopeial convention* (32nd ed.). Rockville, MD, USA: US Pharmacopeia.
Vallières, M., & du Souich, P. (2010). Modulation of inflammation by chondroitin sulfate. *Osteoarthritis and Cartilage*, *18*, S1–S6.
Volpi, N. (2007). Analytical aspects of pharmaceutical grade chondroitin sulfates. *Journal of Pharmaceutical Sciences*, *96*, 3168–3180.
Volpi, N. (2009). Quality of different chondroitin sulfate preparations in relation to their therapeutic activity. *Journal of Pharmaceutical Pharmacology*, *61*, 1271–1280.
Weiguo, Z., Giancaspro, G., Adams, K. M., Neal-Kababick, J., Hildreth, J., Li, A., et al. (2014). Electrophoretic separation of alginic sodium diester and sodium hexametaphosphate in chondroitin sulfate that interfere with the cetylpyridinium chloride titration assay. *Journal of AOAC International*, *97*, 1503–1513.

ANEXO 3

Journal of Ethnopharmacology 198 (2017) 399–406

Contents lists available at ScienceDirect

Journal of Ethnopharmacology

journal homepage: www.elsevier.com/locate/jep

New aspects on the hepatoprotective potential associated with the antioxidant, hypocholesterolemic and anti-inflammatory activities of *Vernonia condensata* Baker

Jucélia Barbosa da Silva[a], Renata de Freitas Mendes[a], Vívian Tomasco[a], Nícolas de Castro Campos Pinto[a], Luiz Gustavo de Oliveira[b], Matheus Nehrer Rodrigues[c], Danielle Maria de Oliveira Aragão[a], Jair Adriano Kopke de Aguiar[b], Maria Silvana Alves[d], Maria Christina Nogueira Marques Castañon[c], Antônia Ribeiro[a], Elita Scio[a,*]

[a] *Laboratory of Bioactive Natural Products, Department of Biochemistry, Biological Sciences Institute, Federal University of Juiz de Fora, Juiz de Fora, MG 36036-900, Brazil*
[b] *Glycoconjugate Analysis Laboratory, Department of Biochemistry, Biological Sciences Institute, Federal University of Juiz de Fora, Juiz de Fora, MG 36036-900, Brazil*
[c] *óDepartment of Morphology, Biological Sciences Institute, Federal University of Juiz de Fora, Juiz de Fora, MG 36036-900, Brazil*
[d] *Molecular and Cellular Bioactivity Laboratory, Department of Pharmaceutical Sciences, Faculty of Pharmacy, Federal University of Juiz de Fora, Juiz de Fora, MG 36036 900, Brazil*

ARTICLE INFO

Chemical compounds studied in this article:
Ethyl Acetate (PubChem CID: 8857)
Apigenin (PubChem CID: 5280443)
Chlorogenic Acid (PubChem CID: 1794427)
Luteolin (PubChem CID: 5280445)
1,5-Dicaffeoylquinic acid (PubChem CID: 6474640)

Keywords:
Hepatoprotective
Anti-inflammatory
Antioxidant
Vernonia condensate
1,5-dicaffeoylquinic acid

ABSTRACT

Ethnopharmacological relevance: *Vernonia condensata* Baker (Asteraceae) is traditionally used in South American Countries as an anti-inflammatory, analgesic and hepatoprotective.
Aim of the study: This study aimed to investigate the *in vivo* hepatoprotective and antioxidant, and the *in vitro* anti-inflammatory activities of the ethyl acetate partition (EAP) from the ethanolic extract of this medicinal plant leaves.
Materials and methods: For the *in vivo* hepatoprotective activity, rats were pretreated orally for seven days with vehicle, silymarin 100 mg/kg or EAP 50, 100 and 200 mg/kg. Then, acetaminophen 3 g/kg was also orally administrated. Animals were euthanatized 24 h after the damage inducement. The levels of the serum enzymes ALT, AST and ALP were determined, as well as the triglycerides, total cholesterol and fractions. The antioxidant activity was evaluated by TBARS assay and by the measurement of glutathione reductase, superoxide dismutase and catalase activities in the rats liver tissue. The *in vitro* anti-inflammatory assay using Raw 264.7 cell line induced by lipopolysaccharide was conducted to verify EAP ability to inhibit pro-inflammatory cytokines.
Results: EAP was able to inhibit all the acute biochemical alterations caused by acetaminophen overdose. EAP inhibited malondialdehyde formation, maintained the catalase and increased the glutathione reductase activities. Also, EAP decreased NO, IL-6 and TNF-α levels at concentrations from 10 to 20 μg/mL. 1,5-dicaffeoylquinic acid was isolated and identified as the major compound in EAP. Apigenin, luteolin, chlorogenic acid were also identified. EAP anti-inflammatory action may be due to its antioxidant activity or its capacity to inhibit the pro-inflammatory cytokines.
Conclusion: These results strongly suggested that *V. condensata* may be useful as a possible therapy against liver damage.

1. Introduction

Drug-induced hepatic injury is a common reason of liver failure and consists of an essential task for new approval medications by regulatory agencies (Kuehn, 2009). Regarding this aspect, liver damages are not due to drugs themselves, but to their toxic metabolites, such as free

Abbreviations: CAT, catalaseCEEA, Ethics Committee on Animal Experimentation; COBEA, Brazilian College of Animal Experimentation; EAP, ethyl acetate partition; EE, ethanolic extract; FCS, fetal calf serum; GSHPx, glutathione peroxidase; GSH, glutathione reductase HDL-c, HDL cholesterol; H & E, hematoxylin and eosin; LDL-c, LDL cholesterol; NAPQI, N-acetyl-p-benzoquinone imine; TC, total cholesterol; TRIGL, triglycerides; SOD, superoxide dismutase; TBARS, thiobarbituric acid reactive substances; VLDL-c, VLDL cholesterol

* Corresponding author.
E-mail address: elita.scio@ufjf.edu.br (E. Scio).

http://dx.doi.org/10.1016/j.jep.2017.01.039
Received 30 November 2016; Received in revised form 16 January 2017; Accepted 19 January 2017
Available online 21 January 2017

radicals, which react mainly with membrane lipids (Madkour and Abdel-Daim, 2013). In general, the liver can combat the free radical damage by biotransformation of these toxic agents in less reactive compounds *via* cytochrome P-450, and glutathione peroxidase (GSHPx) (Hiraganahalli et al., 2012).

Acetaminophen, also known as paracetamol or *N*-acetyl-p-aminophenol (Wang et al., 2015), is an analgesic agent that often induces hepatic intoxication causing serious liver damage, usually associated with unintentional overdose (Kuehn, 2009). N-acetyl-p-benzoquinone imine (NAPQI) is the main toxic metabolite produced after acetaminophen administration, which decreases the hepatic antioxidant system, leading to a cellular oxidative stress (Wang et al., 2015).

The liver damage associated with drugs is also related to the production of pro-inflammatory cytokines, and other mediators, by Kupffer cells, which are the liver macrophages. These cells present important regulatory roles in pathophysiological liver damages due to the production of a variety of modulatory factors that can counteract the inflammatory response, and/or stimulate liver regeneration (Ju et al., 2002).

In spite of the claim for an effective hepatoprotective medicine, there is a lag in the modern pharmacotherapies of a reliable drug with this property. However, there are a large number of traditional plants recommended for liver protection or treatment (Hiraganahalli et al., 2012).

Vernonia condensata Baker, popularly known in Brazil as “alumã”, “figatil” or “necroton”, is a medicinal plant frequently used to treat liver and stomach disorders, as well as an anti-inflammatory remedy by some South American communities (Frutuoso et al., 1994; Risso et al., 2010; Silva et al., 2011; Valverde et al., 2001). The ethyl acetate partition (EAP), obtained from ethanolic extract of the leaves, had been pointed as a promising source of antioxidants (Silva et al., 2013). Several compounds have already been detected in *V. condensata* leaves, as luteolin, apigenin, vernonioside, chlorogenic acid and rutin (Ola et al., 2009; Silva et al., 2013; Valverde et al., 2001).

As species of Vernonia genus was already reported as hepatoprotective (Iwalokun et al., 2006), and EAP was also described with a remarkable antioxidant activity (Silva et al., 2013), this study aimed to investigate EAP ability to prevent hepatic injury on acute acetaminophen-induced liver damage model in rats, by the evaluation of the hepatic enzymes activities in the serum of these animals. The oxidative stress in addition to the cholesterol and fractions measurements were also used as parameters to understand better the EAP hepatoprotective role. Besides, the anti-inflammatory activity was assessed in RAW264.7 murine macrophages. The chemical characterization was also performed, followed by the isolation of the major compound, which was identified by spectrometry methods.

2. Material and methods

2.1. Plant material

Vernonia condensata leaves were collected in the Garden of Medicinal Plants of Faculty of Pharmacy, Federal University of Juiz de Fora (UFJF), Minas Gerais, Brazil, between June and September 2012, in the morning. Local names for this species are “alumã”, “figatil” or “necroton”. The plant name was checked with http://www.theplantlist.org/tpl1.1/record/gcc-133050, site accessed in November, 11th of 2016. The exsiccate (voucher number CESJ No. 52943) was deposited in the UFJF Herbarium Leopoldo Krieger.

2.2. Preparation of EAP

Approximately 2.5 kg of fresh leaves were dried at room temperature, and then crushed and pulverized. The powder (500 g) was extracted by static maceration with ethanol 96%. Then, the ethanolic extract (EE) was concentrated using a rotary evaporator under reduced pressure. Forty five grams of EE were resuspended in water: ethanol (9:1), followed by liquid/liquid partition with organic solvents (3×200 mL, each) of increasing polarity to obtain the hexane, dichloromethane and ethyl acetate (EAP −5.7 g) partitions. All solvents were purchased from Vetec®.

2.3. In vivo *hepatoprotective and antioxidant properties*

2.3.1. Animals

Male Wistar rats (2–3 months old and 200–300 g) were housed in cages and kept under appropriately controlled conditions. The animals were adapted to the environment and handlers for a minimum of 72 h before the beginning of the experiments. The experimental protocols and procedures were in accordance with the Ethical Principles in Animal Experimentation adopted by the Brazilian College of Animal Experimentation (COBEA). The protocol was submitted to the Ethics Committee on Animal Experimentation (CEEA/UFJF – n° 024/2014; October 22nd, 2014).

2.3.2. Inducement of liver damage

The hepatoprotective activity was evaluated by the induction of acute liver injury with acetaminophen in rats (Kuriakose and Kurup, 2010). The animals were divided into six groups (A-F) of six animals each, as follows: Group A: normal control - Vehicle; Group B: negative control - Vehicle; Group C: positive control - Silymarin 100 mg/kg (Legalon, Nycomed® −77,8%); Group D: EAP 50 mg/kg; Group E: EAP 100 mg/kg; Group F: EAP 200 mg/kg. The vehicle consisted of distilled water, sodium lauryl sulfate 0.6% and Tween 80 2% (Sigma®). Each treatment was orally administered for seven days. After this period, the animals from Groups B to F received a single oral dose of acetaminophen (Tylenol®) 3 g/kg, and after 24 h, they were euthanized. The blood and liver were collected for biochemical and histopathological analysis, respectively.

2.3.3. Measurement of the biochemical parameters in the serum

Liver injury was assessed by the determination of the serum enzymatic activities of ALT, AST and ALP. TRIGL, TC, VLDL-c, LDL-c and HDL-c were also evaluated. The analyses were performed using corresponding commercial kits (LABTEST®) according to the manufacturer instructions.

2.3.4. TBARS assay and measurement of enzymes activity in liver homogenates

Liver tissues were homogenized with phosphate buffer pH 7.4 at 1:9 ratio (w/v, tissue, buffer). The homogenates were centrifuged (3000 rpm for 5 min) to collect the supernatants for the subsequent determinations. The evaluation of MDA levels was performed as an index of lipid peroxidation (Buege and Aust, 1978). The activity of GSH (Carlberg and Mannervik, 1985), CAT (Beutler, 1975) and SOD (Kakkar et al., 1984) were also determined in liver homogenates.

2.3.5. Histopathological analysis

Pieces of livers in each group were fixed in a formalin 10% solution, and processed for paraffin embedding. Sections (5 µm thick) were stained with hematoxylin and eosin (H & E) for microscopic evaluation to verify changes of hepatic cells. Photomicrographs of these sections were obtained using the software Image-Pro Plus® 6.0.

2.4. In vitro *anti-inflammatory activity*

2.4.1. Cell line RAW 264.7

The murine macrophages (RAW 264.7) were acquired from the cell bank of Federal University of Rio de Janeiro. The cells were maintained in DMEM purchased from Sigma® supplemented with the antibiotics penicillin (100 IU/mL) and streptomycin (100 µg/mL), both purchased from GIBCO®, and FCS 10% at 37 °C under 5% CO_2 atmosphere.

2.4.2. Cell viability

Cell viability in the presence of EAP was determined using the MTT assay (Mosmann, 1983). Briefly, RAW 264.7 cells (1×10^4 cells/well) were seeded in 96-well microplates and incubated for 24 h before the treatment with EAP. The cells were treated with various EAP concentrations (0.5–40 μg/mL) at 37 °C for 44 h. Next, MTT solution (Sigma, 5 mg/mL in serum-free medium, 20 μL/well) was added to each well and followed by incubation for 4 h. Finally, the MTT solution was removed, and the formazan crystals formed by MTT reduction were solubilized in 200 μL of DMSO. The absorbance was measured at 540 nm using a microplate reader (Thermo Scientific® - MULTISKAN) and values were calculated in comparison to the control cells.

2.4.3. Nitric oxide production

The production of NO was indirectly determined by Griess reaction to measure the concentration of nitrite in the culture medium. RAW 264.7 cells were seeded in 96-well microplates at a density of 8×10^4 cells/well and were incubated for 24 h. Cells were exposed to 100 ng/mL of LPS (Sigma®) with various EAP concentrations (1.0–20 μg/mL) for 48 h. The culture supernatant (100 μL) was mixed with Griess reagent (100 μL, 1% sulphanilamide, 0.1% *N*-[1-naphthyl]-etilenodiamine in 5% phosphoric acid) and incubated at room temperature for 10 min. The absorbance was measured at 540 nm (Thermo Scientific® - MULTISKAN). NO concentration was determined using a standard curve of sodium nitrite ($NaNO_2$).

2.4.4. Analysis of pro-inflammatory cytokines

Anti-inflammatory effects of EAP have also analyzed on the LPS-induced RAW 264.7 cells. Cells were seeded on 96-well microplate at a density of 8×10^4 cells/well and incubated for 24 h. The cells were exposed to LPS 100 ng/mL in the presence or absence of EAP at concentrations from 1.0 to 20 μg/mL for 48 h. Then, the TNF-α and IL-6 levels in the supernatants were analyzed with ELISA kits according to the manufacturer instructions (DuoSet kit, R & D Systems).

2.5. Phytochemical analysis

2.5.1. HPLC-DAD phytochemical profile

The phytochemical profile was obtained using a HPLC-DAD Agilent 1200 series® and a Zorbax SB-C18 column (5 μm×4.6×150 mm). Twenty μL of EAP was injected. The mobile phase used was a linear gradient of solvents A (MeOH:H_2O, 5:95, v/v, pH=3 with H_3PO_4) and B (MeOH); 0 a 100% of B in 30 min; a flow rate of 0.6 mL/min was used. The chromatogram was obtained at 330 nm. Solvents were purchased from Tedia.

2.5.2. Isolation of EAP major compound

EAP (2 g) was fractionated using a Sephadex® LH 20, purchased from Sigma® (250 g) column chromatography (4×74 cm), eluted with MeOH, and the fractions were grouped in accordance to their thin layer chromatography profile, so that five fractions were obtained and named according to their elution order (FA, FB, FC, FD and FE). The major compound was isolated from the most purified fraction (FD) using HPLC-DAD with a semi-preparative Zorbax CN column (5 μm×9.4×250 mm). An isocratic 70% A (MeOH: H_2O, 5:95, v/v, pH=3 with H_3PO_4) and 30% B (MeOH), 0–10 min was used as mobile phase at a flow rate of 2.5 mL/min to yield 7.4 mg of the major EAP compound.

2.5.3. Spectroscopic studies

EAP major compound was identified by ^{1}H NMR (500 MHz), ^{13}C NMR (125 MHZ), DEPT-135, and ^{2}D NMR (COSY, HMBC, HSQC) spectra, which were recorded on a Bruker AVANCE III spectrometer in MeOD solution at 25 °C, using TMS (δ=O) as internal standard. Chemical shifts are reported in ppm on the δ scale and referenced to the residual solvent peak resonances.

For chemical analysis by mass spectrometry, 4 μg of EAP major compound was diluted in methanol for the negative mode. The solution was infused directly into the ESI source using a syringe pump at a flow rate of (10 μL/min). ESI (-)-MS and tandem ESI-MS/MS were acquired using a hybrid high-resolution and high accuracy Xevo® G2-S Q-Tof (Waters®). For data acquisition and processing, MassLynx V4.1 software (Waters®) was used. The data were collected in the m/z range of 50–1000 at the speed of 1 scan per second.

1,5-di-*O*-caffeoylquinic acid: $C_{25}H_{24}O_{12}$, amorphous white powder. ESI-MS/MS *m/z* (rel. int.): 515 [M-H] (75); 353[M-H-$C_9H_6O_3$]$^-$ (100); 335 [M-H-$C_9H_6O_3$-H_2O]$^-$ (7); 191 [M- H- 2x$C_9H_6O_3$]$^-$ (20). NMR (500 MHz, CD_3OD): δ2.09 (H-6ax; dd, $J_{6ax\text{-}6eq}$=13,7 Hz, $J_{5\text{-}6ax}$=8.6 Hz); 2.58 (H-6eq, dd, $J_{6ax\text{-}6eq}$=13,7 Hz and $J_{5\text{-}6eq}$=3.9 Hz); 5.41 (H-5, td, J_{4-5}=8.2 Hz; $J_{5\text{-}6eq}$=3.9 Hz, $J_{5\text{-}6ax}$=8.6 Hz); 3.80 (H-4; dd, J_{3-4}=3.6 and J_{4-5}=8.2 Hz); 4.32 (H-3, m); 2.46 (2 H,m, H-2ax and H-2eq),(quinic acid moiety); 7.08 (2 H, H-2′ and H-2″; d, $J_{2'/2''-6'/6''}$=2 Hz); 6.80 (2 H, H-5′ and H-5″; d, $J_{5'/5''-6'/6''}$=8.0 Hz); 6.98 (2 H, H-6′ and H-6″; dd, $J_{2'/2''-6'/6''}$ =2 Hz and $J_{5'/5''-6'/6''}$=8.0 Hz); 7.60 (2 H, H-7′ and H-7″; d, $J_{7'/7''-8'/8''}$=15.1 Hz); 6.30 (2 H, H-8′ and H-8″; d, $J_{7'/7''-8'/8''}$=15.1 Hz); 6.28 (H-8″, d, $J_{7''-8''}$=15.1 Hz),(caffeoyl group).^{13}C NMR (125 MHz, CD_3OD): δ 79.48 (C-1); 34.22 (C-2); 67.96 (C-3); 71.35 (C-4); 70.15 (C-5); 35.45 (C-6), 173.37 (COOH) (quinic acid moiety); 126.40 (C-1′/C-1″); 113,84/113,83 (C-2′/C-2″); 145,42 (C-3′ e C-3″); 148.26/148.23 (C-4′/C-4″); 115.11/115.08 (C-5′/C-5″); 121.70/121.63 (C-6′/C-6″); 146.13/145.92 (C-7′/C-7″); 113.76/113.70(C-8′/C-8″); 166,61/167.23/(C-9′/C9″), (caffeoyl group).

2.5.4. EAP chemical characterization

EAP chemical biomarkers quantification was conducted in HPLC-DAD as previously described (item 3.5.1) using the external standards apigenin (purity ≥95%), luteolin purity ≥98%) and chlorogenic acid (purity ≥95%) all of them were purchased from Sigma®, in addition to an internal standard (the major compound isolated from EAP). These compounds were quantified by the calibration curve construction using 0.5; 0.25; 0.125; 0.0625–0.0312 mg/mL in triplicate of each standard.

2.6. Statistical analysis

The results were expressed as a mean ± standard deviation. The software GraphPad Prism® 5.0 was used for one-way ANOVA followed by Tukey test for all experiments ($p < 0.05$ was considered significant).

3. Results and discussion

3.1. In vivo *EAP hepatoprotective activity*

Acetaminophen overdose can induce hepatotoxicity and acute liver failure (Kuriakose and Kurup, 2010). For this reason, a pretreatment with EAP followed by the acetaminophen administration (3 g/kg, v.o.) was used to evaluate its hepatoprotective capacity. As shown in Table 1, the relative liver weights for EAP 100 and 200 mg/kg (group E and F) were close to the normal group. An increase of the liver weight may be associated with an inflammatory process induced by the hepatic toxicity (Wang, 2015).

In acute liver injury induced by acetaminophen or other compounds with similar metabolism, it is possible to detect changes in certain biochemical parameters. The intracellular enzymes aspartate aminotransferases (AST) and alanine aminotransferases (ALT) are important indicators of liver damage. AST and ALT are normally present in the cytoplasm; however, after liver injury their levels increase in blood serum due to alterations in hepatic cells membrane permeability (Giannini et al., 2005; Vargas-Mendoza et al., 2014). Alkaline phosphatase (ALP) is another important hepatic parameter and high serum levels of this enzyme indicate cholestasis (Vargas-Mendoza et al., 2014). The levels of these enzymes in the serum of

Table 1
Relative body and liver weight after the pretreatment with EAP.

Animals group	Relative body weight (g)			Livers weight (g)
	First day	8th day	% change	
A	212.8 ± 5.0	232.2 ± 4.9	9.15	8.32 ± 0.25[a]
B	211.8 ± 2.1	234.6 ± 1.7	10.80	9.71 ± 0.15[b]
C	225.6 ± 4.4	226.4 ± 5.8	0.3	9.62 ± 0.43[b]
D	269.4 ± 8.71	269.0 ± 8.44	0.1	9.68 ± 0.27[b]
E	229.4 ± 6.5	232.6 ± 7.2	1.3	8.00 ± 0.31[a]
F	226.6 ± 8.3	229.8 ± 7.4	1.4	8.98 ± 0.43[c]

Group A: normal group; Group B: negative control; Group C: silymarin, 100 mg/kg; Group D, E and F: EAP 50, 100 and 200 mg/kg, respectively. The values represent the mean ± standard deviation. One-way ANOVA followed by Tukey test ($p < 0.001$). Groups with the same letter indicate no statistical differences.

animals pretreated with EAP are shown in Fig. 1. All EAP doses reduced AST level; however, at 200 mg/kg, AST achieved normal levels (Fig. 1A). Also, all pretreatments reduced ALT levels (Fig. 1B). Pretreatment with EAP, at all doses, was able to maintain the ALP levels close to normal values (Fig. 1C). Taken together, these results suggested that EAP pretreatment was able to prevent liver damage.

Acetaminophen was capable to increase triglycerides and cholesterol serum levels (Özsoy and Pabuçcuoğlu, 2007; Buttar et al., 1976), which explains why total cholesterol (TC), and VLDL (c-VLDL) and LDL cholesterol (c-LDL) fractions, in addition to triglycerides (TRIGL), were increased in the negative control group (Group B). Nevertheless, HDL cholesterol (c-HDL) levels decreased. In contrast, EAP 50, 100 and 200 mg/kg caused significant reduction of TC and c-LDL. At 200 mg/kg, EAP also reduced TRIGL and c-VLDL levels to normal values (Group A). It is important to point out that, under acetaminophen effect, animals pretreated with EAP 100 and 200 mg/kg (Groups E and F) showed high levels of c-HDL when compared to Groups B and C (Table 2).

The ability of *V. condensata* aqueous extract to inhibit the *in vitro* activity of HMG-CoA reductase, a key enzyme involved in the biosynthesis of endogenous cholesterol, was already published (Arantes et al., 2016). Thus, the present data reinforced the hypocholesterolemic effect reported in the literature and showed that EAP pretreatment can prevent the hypercholesterolemia commonly caused after liver damages induced by acetaminophen (Arantes et al., 2016; Koppes et al., 2005).

In order to evaluate EAP ability to prevent oxidative stress, thiobarbituric acid reactive substances assay (TBARS) and GSH, CAT and SOD activities were performed. NAPQI and other free radicals induce macromolecules peroxidation, leading to an MDA increase and a failure in the hepatocyte antioxidant system (Pareek et al., 2013; Wang et al., 2015). Oxidative stress induced by NAPQI is the major cause for the deleterious acetaminophen action (Wang et al., 2015). NAPQI is converted to harmless water-soluble metabolites by the GSH action, so that the increasing of GSH levels is fundamental for more efficient NAPQI elimination (Iwalokun et al., 2006). Fig. 2 (A and B) shows the effect of EAP pretreatment in the production of MDA and in the GSH enzyme activity in the hepatic tissue, respectively. The oxidative stress caused by NAPQI was evidenced in the animals of Group B due to the high levels of MDA and the low GSH activity. On the other hand, EAP in all doses, was able to inhibit MDA formation and to increase the GSH activity.

In acetaminophen intoxications, CAT and SOD activities are normally compromised (Adam et al., 2016; Wang et al., 2015). The negative control group (Group B) showed a decrease in CAT activity, unlike the animals pretreated with EAP (100 and 200 mg/kg), which showed CAT levels similar to the normal group (Group A) (Fig. 2C). EAP 100 and 200 mg/kg also increased SOD activity (Fig. 2D). Therefore, EAP strongly prevented the oxidative stress caused by acetaminophen administration, reaffirming its protective capacity, which is a relevant finding, as the antioxidant activity is usually related to a hepaprotective role (Sabir et al., 2012; Wang et al., 2015).

Histopathological studies confirmed the liver damage caused by acetaminophen. Untreated animals (negative control) presented de-

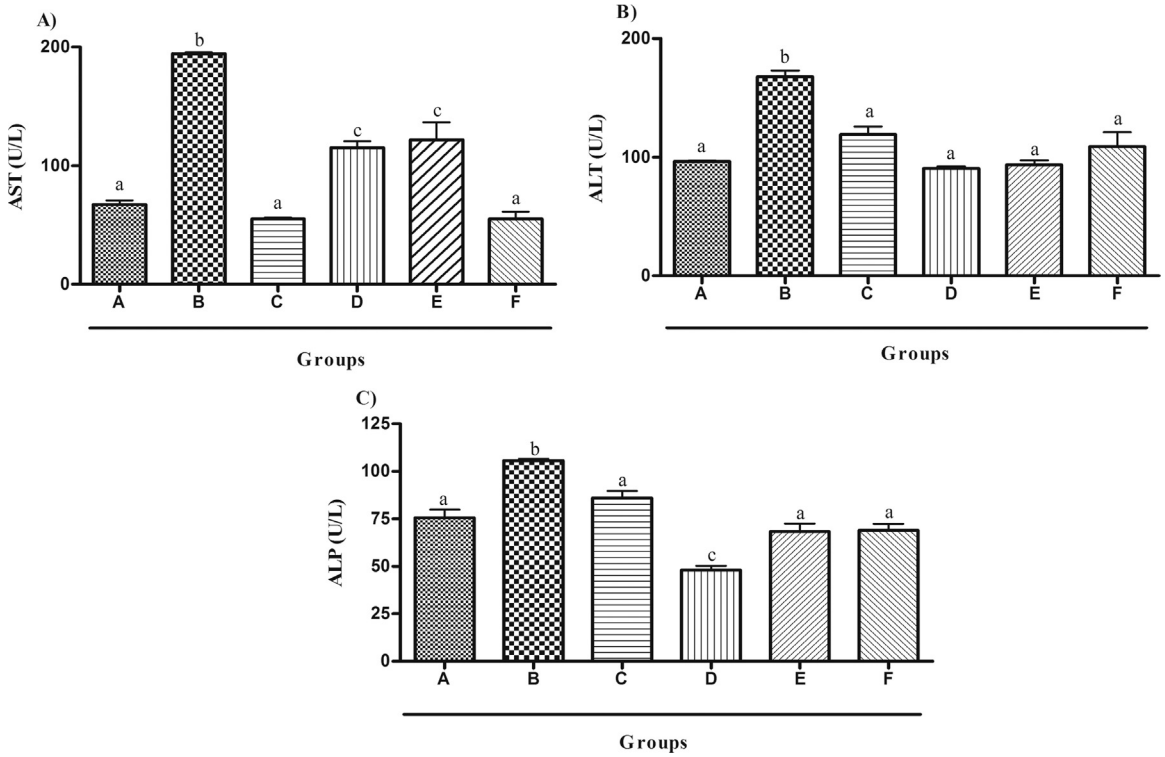

Fig. 1. Effects of EAP pretreatment on AST (A), ALT (B) and ALP (C) serum levels after acetaminophen-induced acute liver toxicity in rats. Group A: normal group; Group B: negative control; Group C: silymarin, 100 mg/kg; Group D, E and F: EAP 50, 100 and 200 mg/kg, respectively. The values represent the mean ± standard deviation. One-way ANOVA followed by Tukey test ($p < 0.01$). Groups with the same letter indicate no statistical difference.

Table 2
Effect of EAP on lipidic parameters after acute acetaminophen damage in pretreated rats.

Animals groups	TRIGL mg/dL	TC mg/dL	c- VLDL mg/dL	c-LDL mg/dL	c-HDL mg/dL
A	88.99 ± 9.16[a]	88.40 ± 4.34[a]	17.80 ± 1.83[a]	62.28 ± 3.55[a]	11.88 ± 4.67[a]
B	123.1 ± 13.76[b]	122.4 ± 14.62[b]	20.57 ± 4.67[b]	86.49 ± 11.47[b]	3.59 ± 1.14[b]
C	116.5 ± 16.58[c]	84.27 ± 9.98[a]	23.29 ± 3.12[c]	57.10 ± 4.40[a]	3.57 ± 0.57[b]
D	117.8 ± 15.87[c]	81.54 ± 7.42[a]	24.98 ± 6.8[c]	50.10 ± 5.49[c]	7.57 ± 1.19[c]
E	125.1 ± 19.17[b]	81.04 ± 2,50[a]	25.01 ± 3.83[c]	43.56 ± 3.94[c]	10.36 ± 2.90[d]
F	84.22 ± 3.48[a]	83.06 ± 3.68[a]	16.40 ± 0.70[a]	53.88 ± 2.01[a]	11.06 ± 0.67[a]

Group A: normal group; Group B: negative control; Group C: silymarin, 100 mg/kg; Group D, E and F: EAP 50, 100 and 200 mg/kg, respectively. The values represent the mean ± standard deviation. One-way ANOVA followed by Tukey test ($p < 0.01$). Groups with the same letter indicate no statistical differences.

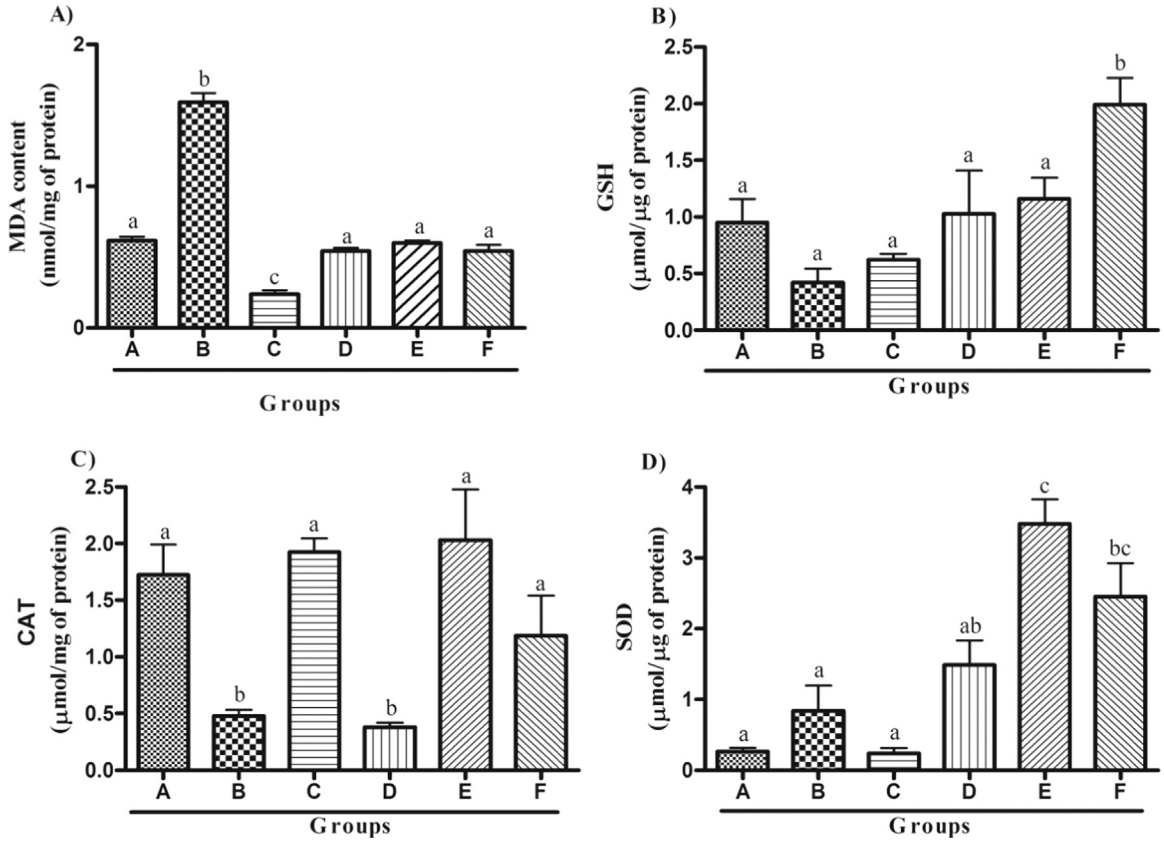

Fig. 2. Effects of EAP on MDA (A) content and GSH (B), CAT (C) and SOD (D) activity in hepatic tissue of acetaminophen-induced acute liver toxicity in rats. Group A: normal group; Group B: negative control; Group C: sylimarin, 100 mg/kg; Group D, E and F: EAP 50, 100 and 200 mg/kg, respectively. The values represent the mean ± standard deviation. One-way ANOVA followed by Tukey test ($p < 0.05$). Groups with the same letter indicate no statistically difference.

generative changes such as vacuolization and pycnotic nuclei in the parenchymal cells in the centrolobular areas, congestion and sinusoidal dilation, mild degree of lymphocytic infiltrate and bleeding (Fig. 3B). On the other hand, the liver of the rats pretreated with EAP did not present degenerative changes maintaining a quite normal histological aspect, with only few areas of congestion and mild lymphocytic infiltrate.

3.2. In vitro *EAP anti-inflammatory activity*

The anti-inflammatory activity of EAP was evaluated by the measurement of nitric oxide (NO), and interleukin-6 (IL-6) and tumor necrosis factor alfa (TNF-α) cytokines. LPS-induced RAW 264.7 cell line, which presents a good correlation with the Kupffer cells (Kiemer et al., 2002), was used. Initially, MTT assay was performed in order to identify the ideal EAP concentrations to be assessed. Cellular viability was observed below 20 µg/mL.

In cellular injury, NO is produced in large quantities by the enzyme nitric oxide synthase (iNOS) (Yang et al., 2009). NO is a free radical and an intracellular messenger produced by different human and other mammalian cells. It is a mediator in numerous biological actions, including vasodilation, neurotransmission, inhibition of platelet adhesion and aggregation (Oh et al., 2008). The level of NO produced by iNOS can reflect a certain degree of tissue inflammation and also serves as an important indicator in the assessment of inflammatory processes. Large amount of NO inhibits cellular respiration, induces DNA damage and decreases intracellular levels of enzymatic antioxidants (Chen et al., 2002). Thus, it is essential to reduce NO production for the prevention of liver injury (Miki et al., 2015). EAP was able to significantly decrease the NO levels at 10 and 20 µg/mL (Fig. 4A).

LPS, a glycolipid endotoxin from Gram-negative bacteria outer membrane, is recognized by receptors in animal cells, such as macrophages, which activate the innate immune system and stimulates the secretion of cytokines (TNF-α) (Kim et al., 1999). The inhibition of TNF-α expression may attenuate liver injury induced by alcohol (Iimuro et al., 1997). TNF-α is generally produced with IL-6, which

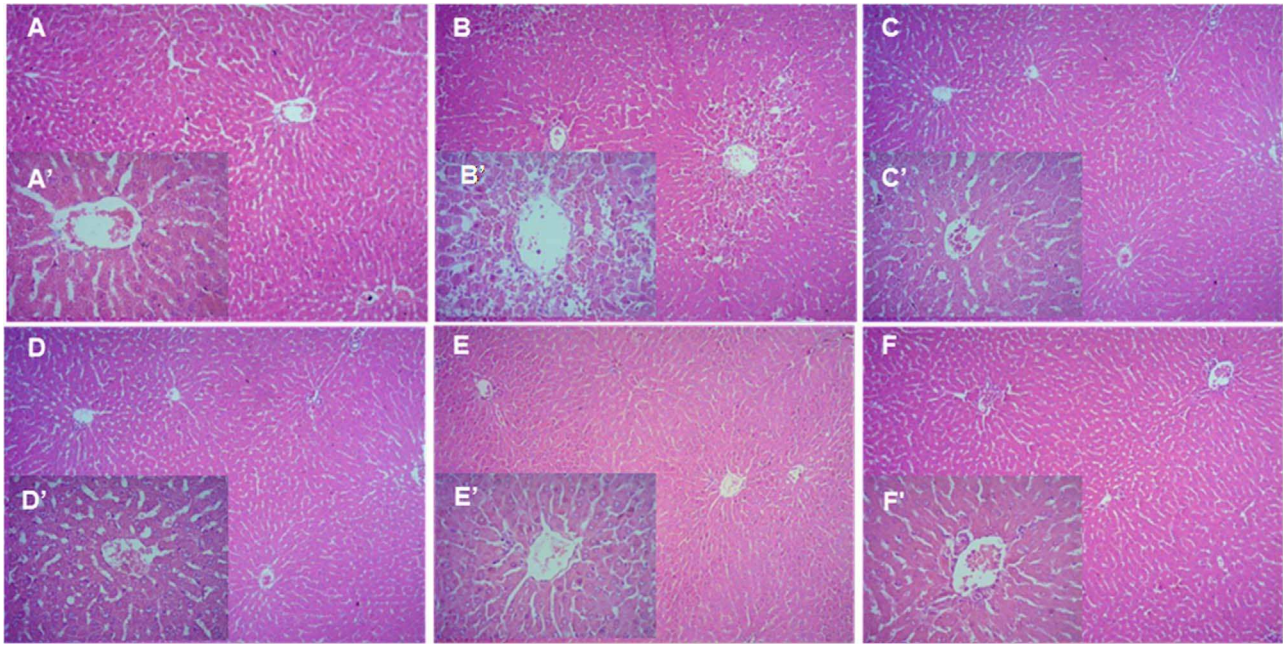

Fig. 3. Representative photomicrographs of longitudinal sections of rat liver after 7 days of pretreatments followed by acetaminophen-induced acute damaged. normal group (A 100x, A′ 400x), negative control (B 100x, B′ 400x), sylimarin (C 100x, C′ 400x), EAP 50 mg/kg (D 100x, D′ 400x), EAP 100 mg/kg (E 100x, E′ 400x) and EAP 200 mg/kg (F 100x, F′ 400x). Images were captured using the Image-Pro Plus® 6.0 software.

exerts an important regulatory role in acute inflammation (local or systemic). Drugs that are capable to reduce or inhibit the expression of both pro-inflammatory cytokines are considered as promising anti-inflammatory agents (Sittisart et al., 2016). IL-6 levels were reduced by EAP at 5, 10 and 20 μg/mL (Fig. 4B). TNF-α levels decreased by EAP at all tested concentrations (Fig. 4C).

3.3. Phytochemical analysis

EAP chemical profile was shown in Fig. 5. Chlorogenic acid, luteolin and apigenin were identified by relative retention times using authentic standards and quantified by a calibration curve (Table 3).

The main compound was isolated in order to better know the chemical profile of EAP. Its structure, showed in Fig. 5, was identified as 1,5-di-*O*-caffeoylquinic acid by analysis of one-dimensional (1D) and two-dimensional (2D) high resolution NMR spectroscopy and by comparison with published data (Merfort, 1992). The molecular mass ($C_{25}H_{24}O_{12}$) was determined by ESI-MS negative spectra that showed the deprotonated molecular peak, [M-H]-, at m/z 515. The ESI-MS/MS fragmentation pattern was identical to that observed by Clifford et al.

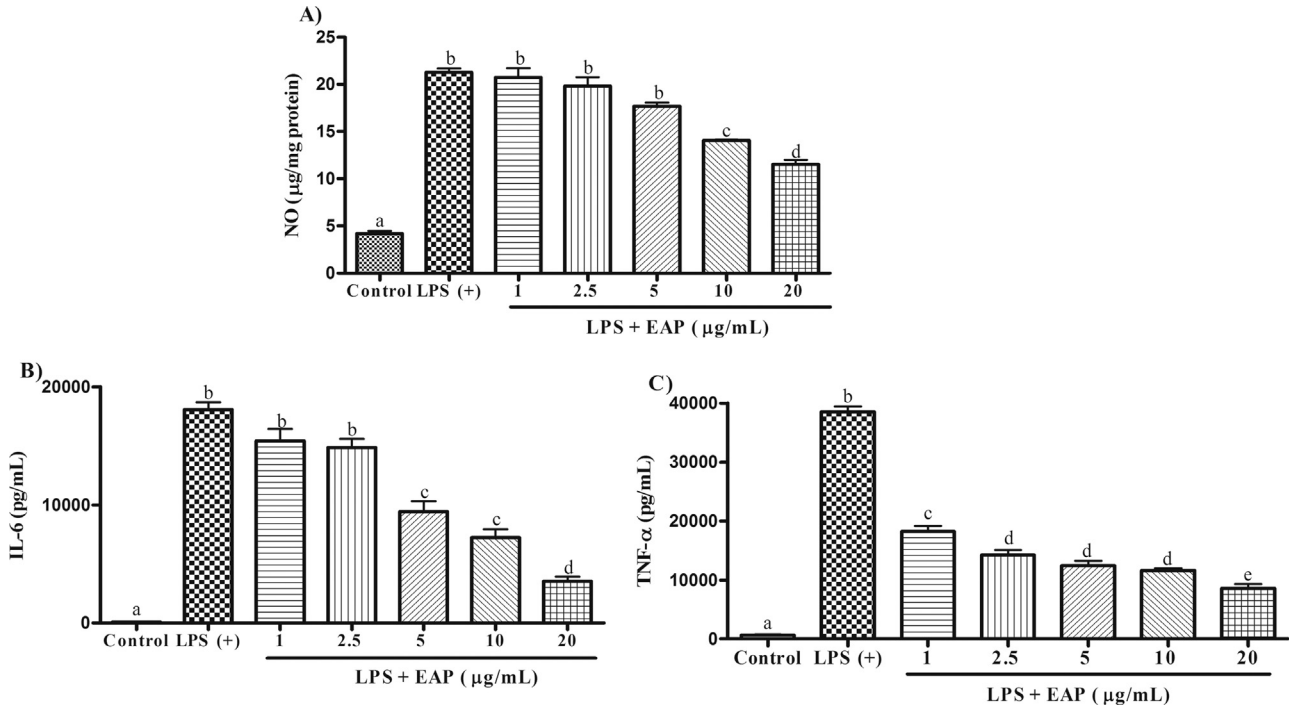

Fig. 4. Effects of EAP on NO (A), IL-6 (B) and TNF-α (C) levels in LPS-induced RAW 264.7 cells;8×10^4 cells/well in 96 wells microplates. The values represent the mean ± standard deviation. Test was performed in hexaplicate. One-way ANOVA followed by Tukey test ($p < 0.05$). Groups with the same letter indicate no statistically difference.

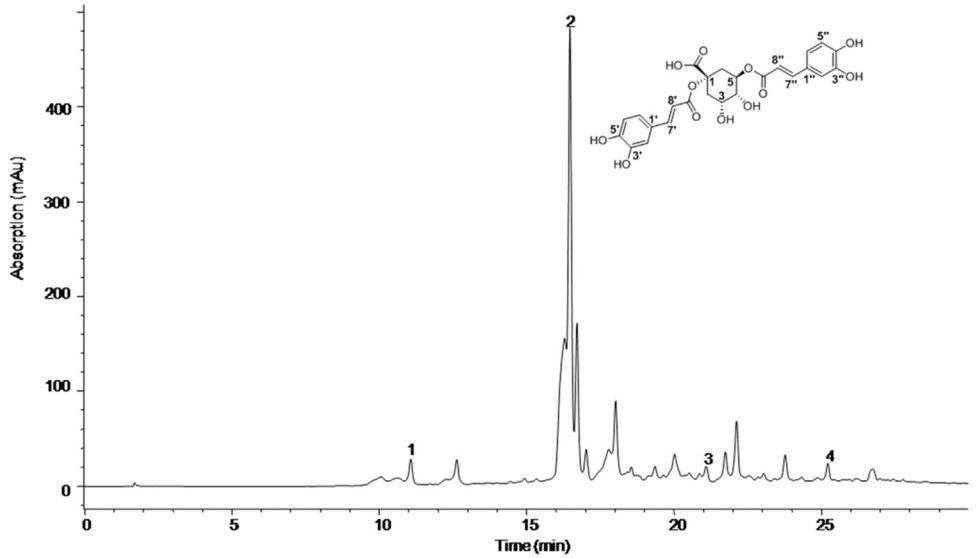

Fig. 5. HPLC-DAD phytochemical profile of EAP. (1) chlorogenic acid, (2) 1,5-di-O-caffeoylquinic acid, (3) luteolin and (4) apigenin. Zorbax SB-C18 column (5 μmx4.6×150 mm).20 μL of EAP was injected. The mobile phase used was a linear gradient of solvents A (MEOH: H2O, 5:95, v/v, pH=3 with H_3PO_4) and B (MEOH); 0 a 100% of B in 30 min; a flow rate of 0.6 mL/min was used. The chromatogram was obtained at 330 nm.

Table 3
Calibration curves and quantification of chlorogenic acid, apigenin, luteolin and 1,5-dicaffeoylquinic acid.

Standard	Curve	Concentration (μg/mL)[a]
Chlorogenic acid	y=7998.6x−31.639 r^2=0.9982	9.23 ± 0.08
1,5-di-*O*-caffeoylquinic acid	y=12012x+688.60 r^2=0.9986	292.00 ± 0.06
Luteolin	y=20233x+419.43 r^2=0.9975	1.87 ± 0.08
Apigenin	y=2918.3x+47.453 r^2=0.9936	25.08 ± 0.01

[a] Values expressed as a mean ± standard error.

(2005) for 1,5-di-*O*-caffeoylquinic acid isomers. Those compounds had previously been detected in *V. condensata* (Arantes et al., 2016).

Chlorogenic acid and the flavonoids luteolin and apigenin are commonly found in several plant species and possess biological activities related to the findings reported in this study. According to the literature, chlorogenic acid is endowed with antioxidant activity (Johnston et al., 2003; Sato et al., 2011; Shimoda et al., 2006). In addition, this compound may inhibit the absorption of lipids, increase their metabolism, and reduce the serum cholesterol levels and steatosis (Khan et al., 2016; Shimoda et al., 2006). Apigenin and luteolin are also an antioxidant, anti-inflammatory and hepatoprotective agents (Rathee et al., 2009; Simeonova et al., 2014). Moreover, there are reports describing the antioxidant activity of dicaffeoylquinic acids (Salem et al., 2015; Zhao et al., 2014). Thus, the presence of these compounds in EAP might contribute for the expressive antioxidant, anti-inflammatory and hepatoprotective properties of *V. condensata* leaves showed in this study.

4. Conclusion

Taken together, all those findings suggested that EAP pretreatment presented a notable hepatoprotective potential associated with antioxidant, hypocholesterolemic, control of triglycerides levels and anti-inflammatory activities. For this reason, EAP should be further evaluated as a future remedy to prevent liver damage, dyslipedemia and inflammatory process.

Conflict of interest

"The authors declare no conflict of interest."

Acknowledgements

This work was supported by the grant from Fundação de Amparo a Pesquisa do Estado de Minas Gerais (FAPEMIG APQ 01403/14 and APQ 01798/14) and Coordenação de Aperfeiçoamento de Profissional de Ensino Superior (CAPES). The authors are grateful to Dr Fátima Salimena for the botanical identification of the species, to Delfino Antônio Campos for technical assistance, to the Reproduction Biology Center of the Federal University of Juiz de Fora for providing the rats, as well as the Chemistry Department of the Institute of Exact Sciences (UFJF) for NMR analysis and Research Center of Pharmaceutical Sciences for mass spectrometry data.

References

Kuehn, B.M., 2009. FDA focuses on drugs and liver damage. JAMA 302 (4), 369–371. http://dx.doi.org/10.1001/jama.2009.1019.

Madkour, F., Abdel-Daim, M., 2013. Hepatoprotective and antioxidant activity of *Dunaliella salina* in paracetamol-induced acute toxicity in rats. Indian J. Pharm. Sci. 75 (6), 642. http://dx.doi.org/10.4103/0250-474X.124747.

Hiraganahalli, D., Chandrasekaran, C., Dethe, S., Mundkinajeddu, D., Pandre, M., Balachandran, J., 2012. Hepatoprotective and antioxidant activity of standardized herbal extracts. Pharmacogn. Mag. 8 (30), 116. http://dx.doi.org/10.4103/0973-1296-96553.

Wang, Y., Li, D., Cheng, N., Gao, H., Xue, X.F., Cao, W., Sun, L., 2015. Antioxidant and hepatoprotective activity of vitex honey against paracetamol induced liver damage in mice. Food Funct. 6, 2339–2349. http://dx.doi.org/10.1039/c5fo00345h.

Ju, C., Reilly, T.P., Bourdi, M., Radonovich, M.F., Brady, J.N., George, J.W., Pohl, L.R., 2002. Protective role of Kupffer cells in acetaminophen-induced hepatic injury in mice. Chem. Res. Toxicol. 15 (12), 1504–1513. http://dx.doi.org/10.1021/tx0255976.

Frutuoso, V.S., Gurjão, M.R.R., Cordeiro, R.S.B., Martins, M.A., 1994. Analgesic and anti-ulcerogenic effects of a polar extract from leaves of *Vernonia condensata*. Planta Med. 60 (1), 21–25. http://dx.doi.org/10.1055/s-2006-959400.

Risso, W.E., Scarminio, I.S., Moreira, E.G., 2010. Antinociceptive and toxicity evaluation of *Vernonia condensata* leaves. Indian J. Exp. Biol. 48 (8), 811–816.

Silva, J.B., Temponi, V.S., Fernandes, F.V., Alves, G.A.D., Matos, D.M., Gasparetto, C.M., Ribeiro, A., Pinho, J.J.R.G., Alves, M.S., Sousa, O.V., 2011. New approaches to clarify antinociceptive and anti-inflammatory effects of the ethanol extract from *Vernonia condensata* leaves. Int. J. Mol. Sci. 12, 8993–9008. http://dx.doi.org/10.3390/ijms12128993.

Valverde, A.L., Cardoso, G.L.C., Pereira, N.A., Silva, A.J.R., Kuster, R.M., 2001. Analgesic

and antiinflammatory activities of vernonioside B2 from *Vernonia condensata*. Phytother. Res. 15 (3), 263–264. http://dx.doi.org/10.1002/ptr.733.
Silva, J.B., Temponi, V.S., Gasparetto, C.M., Fabri, R.L., Aragão, D.M.O., Pinto, N.C.C., Ribeiro, A., Scio, E., Vieira, G.D., Sousa, O.V., Alves, M.S., 2013. *Vernonia condensata* Baker (Asteraceae): a promising source of antioxidants. Oxid. Med. Cell Longev.. http://dx.doi.org/10.1155/2013/698018.
Ola, S.S., Catia, G., Marzia, I., Francesco, V.F., Afolabi, A.A., Nadia, M., 2009. HPLC/DAD/MS characterization and analysis of flavonoids and cynnamoil derivatives in four Nigerian green-leafy vegetables. Food Chem. 115, 1568–1574. http://dx.doi.org/10.1016/j.foodchem.2009.02.013.
Iwalokun, B.A., Efedede, B.U., Alabi-Sofunde, J.A., Oduala, T., Magbagbeola, O.A., Akinwande, A.I., 2006. Hepatoprotective and antioxidant activities of *Vernonia amygdalina* on acetaminophen-induced hepatic damage in mice. J. Med. Food 9 (4), 524–530. http://dx.doi.org/10.1089/jmf.2006.9.524.
Kuriakose, G.C., Kurup, M.G., 2010. Antioxidant and hepatoprotective of *Aphanizomenon flos-aquae* Linn against paracetamol intoxication in rats. Indian J. Exp. Biol. 48 (11), 1123–1130.
Buege, J.A., Aust, S.D., 1978. Microsomal lipid peroxidation. Methods Enzimol. 52, 302–310.
Beutler, E., 1975. Red Cell MetabolismA Manual of Biochemical methods Second ed.. Grune & Stratton, New York.
Carlberg, I., Mannervik, B., 1985. Glutathione reductase. Methods Enzymol. 113, 484–490.
Kakkar, P., Das, B., Viswanathan, P.N., 1984. A modified spectrophotometric assay of superoxide dismutase. Indian J. Biochem. Biophys. 21 (2), 130–132.
Mosmann, T., 1983. Rapid colorimetric assay for cellular growth and survival: application to proliferation and cytotoxicity assays. J. Immunol. Methods 65 (1–2), 55–63.
Giannini, E.G., Testa, R., Savarino, V., 2005. Liver enzyme alteration: a guide for clinicians. CMAJ 3, 367–379. http://dx.doi.org/10.1503/cmaj.1040752.
Vargas-Mendoza, N., Madrigal-Santillàn, E., Morales-Gonzalez, A., Esquivel-Soto, J., Esquivel-Chirino, C., González-Rubio, M.G.L., Gayosso-De-Lucio, J.A., Morales-González-Morales, J.A., 2014. Hepatoprotective effect of silymarin. World J. Hepatol. 6 (3), 144–149. http://dx.doi.org/10.4254/wjh.v6.i3.144.
Özsoy, M.B., Pabuçcuoğlu, A., 2007. The effect of acetaminophen on oxidative modification of low-density lipoproteins in hypercholesterolemic rabbits. J. Clin. Biochem. Nutr. 41 (1), 27–31. http://dx.doi.org/10.3164/jcbn.2007004.
Buttar, H.S., Nera, E.A., Downie, R.H., 1976. Serum enzyme activities and hepatic triglyceride levels in acute and subacute acetaminophen-treated rats. Toxicol 6, 9–20 . http://dx.doi.org/10.1016/0300-483X(76)90003-2.
Arantes, A.A., Falé, P.L., Costa, L.C.B., Pacheco, R., Ascensão, L., Serralheiro, M.L., 2016. Inhibition of HMG-CoA reductase activity and cholesterol permeation through Caco-2 cells by caffeoylquinic acids from *Vernonia condensata*. Braz. J. Pharm. Adv. Online Publ. 28 July 2016. http://dx.doi.org/10.1016/j.bjp.2016.05.008.
Koppes, L.L., Twisk, J.W.R., Van Mechelen, W., Snel, J., Kemper, H., 2005. Cross-sectional and longitudinal relationships between alcohol consumption and lipids, blood pressure and body weight indices. J. Stud. Alcohol. 66 (6), 713–721. http://dx.doi.org/10.15288/jsa.2005.66.713.
Pareek, A., Godavarthi, A., Issarani, R., Nagori, B.P., 2013. Antioxidant and hepatoprotective activity of *Fagoni schweinfurthii* (Hadidi) extract in carbon tetrachoride induced hepatotoxity in HepG2 cell line and rats. J. Ethnopharmacol. 150, 973–981. http://dx.doi.org/10.1016/j.jep.2013.09.048.
Adam, G.O., Rahman, M.M., Lee, S.J., Kim, G.B., Kang, H.S., Kim, J.S., Kim, S.J., 2016. Hepatoprotective effects of *Nigella sativa* seed extract against acetaminophen-induced oxidative stress. Asian Pac. J. Trop. Med. 9 (3), 221–227. http://dx.doi.org/10.1016/j.apjtm.2016.01.039.
Sabir, S.M., Ahmad, S.D., Hamid, A., Khan, M.Q., Athayde, M.L., Santos, D.B., Santos, D.B., Boligon, A.A., Rocha, J.B.T., 2012. Antioxidant and hepatoprotective activity of ethanolic extract of leaves of *Solidago microglossa* containing polyphenolic compounds. Food Chem. 131, 741–747. http://dx.doi.org/10.1016/j.foodchem.2011.09.026.
Kiemer, A.K., Müller, C., Vollmar, A.M., 2002. Inhibition of LPS-induced nitric oxide and TNF-α production by α-lipoic acid in rat Kupffer cells and in RAW 264.7 murine macrophages. Immunol. Cell Boil. 80 (6), 550–557. http://dx.doi.org/10.1046/j.1440-1711.2002.01124.x.
Yang, E.J., Yim, E.Y., Song, G., Kim, G.O., Hyun, C.G., 2009. Inhibition of nitric oxide production in lipopolysaccharide-activated RAW 264.7 macrophages by Jeju plant extracts. Interdiscip. Toxicol. 2 (4), 245–249. http://dx.doi.org/10.2478/v10102-009-0022-2.
Oh, J.H., Lee, T.J., Park, J.W., Kwon, T.K., 2008. Withaferin A inhibits iNOS expression and nitric oxide production by Akt inactivation and down-regulating LPS-induced activity of NF-kappaB in RAW 264.7 cells. Eur. J. Pharmacol. 599, 11–17. http://dx.doi.org/10.1016/j.ejphar.2008.09.017.
Chen, G.G., Lau, W.Y., Lai, P., Chun, Y.S., Chak, E.C., Leung, B., Chui, A.K., 2002. Activation of Kupffer cells inhibits tumor growth in a murine model system. Int. J. Cancer 99 (5), 713–720. http://dx.doi.org/10.1002/ijc.10412.
Miki, H., Tokuhara, K., Oishi, M., Nakatake, R., Tanaka, Y., Kaibori, M., Kon, M., 2015. Japanese Kampo Saireito has a liver-protective effect through the inhibition of inducible nitric oxide synthase induction in primary cultured rat hepatocytes. J. Parenter. Enter. Nutr.. http://dx.doi.org/10.1177/0148607115575035.
Kim, H.K., Cheon, B.S., Kim, Y.H., Kim, S.Y., Kim, H.P., 1999. Effects of naturally occurring flavonoids on nitric oxide production in the macrophage cell line RAW 264.7 and their structure-activity relationships. Biochem. Pharmacol. 58, 759–765. http://dx.doi.org/10.1016/s0006-2952(99)00160-4.
Iimuro, Y., Gallucci, R.M., Luster, M.I., Kono, H., Thurman, R.G., 1997. Antibodies to tumor necrosis factor alfa attenuate hepatic necrosis and inflammation caused by chronic exposure to ethanol in the rat. Hepatology 26, 1530–1537. http://dx.doi.org/10.1002/hep.510260621.
Sittisart, P., Chitsomboon, B., Kaminski, N.E., 2016. *Pseuderanthemum palatiferum* leaf extract inhibits the proinflammatory cytokines, TNF-α and IL-6 expression in LPS-activated macrophages. Food Chem. Toxicol. 97, 11–22. http://dx.doi.org/10.1016/j.fct.2016.08.021.
Merfort, I., 1992. Caffeoylquinic acids from flowers of *Arnica montana* and *Arnica chamissonis*. Phytochemistry 31 (6), 2111–2113.
Clifford, M.N., Knight, S., Kuhnert, N., 2005. Discriminating between the six isomers of dicaffeoylquinic acid by LC-MS. J. Agric. Food Chem. 53, 3821–3832.
Johnston, K.L., Clifford, M.N., Morgan, L.M., 2003. Coffee acutely modifies gastrointestinal hormone secretion and glucose tolerance in humans: glycemic effects of chlorogenic acid and caffeine. Am. J. Clin. Nutr. 78 (4), 728–733.
Sato, Y., Itagaki, S., Kurokawa, T., Ogura, J., Kobayashi, M., Hirano, T., Iseki, K., 2011. *In vitro* and *in vivo* antioxidant properties of chlorogenic acid and caffeic acid. Int. J. Pharm. 403 (1–2), 136–138. http://dx.doi.org/10.1016/j.ijpharm.2010.09.035.
Shimoda, H., Seki, E., Aitani, M., 2006. Inhibitory effect of green coffee bean extract on fat accumulation and body weight gain in mice. Complement. Altern. Med. 6 (1), 1–9 . http://dx.doi.org/10.1186/1472-6882-6-9.
Khan, J., Saraf, S., Saraf, S., 2016. Preparation and evaluation of luteolin–phospholipid complex as an effective drug delivery tool against GalN/LPS induced liver damage. Pharm. Dev. Technol. 21 (4), 475–486. http://dx.doi.org/10.3109/10837450.2015.1022786.
Rathee, P., Chaudhary, H., Rathee, S., Rathee, D., Kumar, V., Kohli, K., 2009. Mechanism of action of flavonoids as anti-inflammatory agents: a review. Inflamm. Allergy-Drug Targets 8 (3), 229–235. http://dx.doi.org/10.2174/187152809788681029.
Simeonova, R., Kondeva-Burdina, M., Vitcheva, V., Krasteva, I., Manov, V., Mitcheva, M., 2014. Protective effects of the apigenin-O/C-diglucoside saponarin from *Gypsophila trichotoma* on carbone tetrachloride-induced hepatotoxicity *in vitro*/*in vivo* in rats. Phytomedicine 21 (2), 148–154. http://dx.doi.org/10.1016/j.phymed.2013.07.014.
Salem, M.B., Affes, H., Ksouda, K., Dhouibi, R., Sahnoun, Z., Hammami, S., Zeghal, K.M., 2015. Pharmacological studies of Artichoke leaf extract and their health benefits. Plant Foods Hum. Nutr. 70, 441–453. http://dx.doi.org/10.1007/s11130-015-0503-8.
Zhao, Y., Geng, C., Ma, Y., Huang, X., Chen, H., Cao, T., He, K., Wang, H., Zhang, X., Chen, J., 2014. UFLC/MS-IT-TOF guided isolation of anti-HBV active chlorogenic acid analogues from *Artemisia capillaris* as a traditional Chinese herb for the treatment of hepatitis. J. Ethnopharmacol. 156, 147–154.

ANEXO 4

frontiers in Microbiology

ORIGINAL RESEARCH
published: 13 April 2018
doi: 10.3389/fmicb.2018.00724

Antibacterial and Antibiofilm Activities of Psychorubrin, a Pyranonaphthoquinone Isolated From *Mitracarpus frigidus* (Rubiaceae)

*Ari S. O. Lemos[1], Lara M. Campos[1], Lívia Melo[1], Maria C. M. R. Guedes[1], Luiz G. Oliveira[2], Thiago P. Silva[3], Rossana C. N. Melo[3], Vinícius N. Rocha[4], Jair A. K. Aguiar[2], Ana C. M. Apolônio[5], Elita Scio[1] and Rodrigo L. Fabri[1]**

[1] Bioactive Natural Products Laboratory, Department of Biochemistry, Institute of Biological Sciences, Federal University of Juiz de Fora, Juiz de Fora, Brazil, [2] Laboratory of Glycoconjugate Analysis, Department of Biochemistry, Institute of Biological Sciences, Federal University of Juiz de Fora, Juiz de Fora, Brazil, [3] Laboratory of Cellular Biology, Department of Biology, Institute of Biological Sciences, Federal University of Juiz de Fora, Juiz de Fora, Brazil, [4] Department of Veterinary Medicine, Faculty of Medicine, Federal University of Juiz de Fora, Juiz de Fora, Brazil, [5] Laboratory of Bacterial Physiology and Molecular Genetics, Department of Parasitology, Microbiology and Immunology, Institute of Biological Sciences, Federal University of Juiz de Fora, Juiz de Fora, Brazil

OPEN ACCESS

Edited by:
Octavio Luiz Franco, Universidade Católica de Brasília, Brazil

Reviewed by:
Akanksha Singh, Central Institute of Medicinal and Aromatic Plants (CIMAP), India
Fohad Mabood Husain, King Saud University, Saudi Arabia

***Correspondence:**
Rodrigo L. Fabri
rodrigo.fabri@ufjf.edu.br

Specialty section:
This article was submitted to Antimicrobials, Resistance and Chemotherapy, a section of the journal Frontiers in Microbiology

Received: *15 December 2017*
Accepted: *28 March 2018*
Published: *13 April 2018*

Citation:
Lemos ASO, Campos LM, Melo L, Guedes MCMR, Oliveira LG, Silva TP, Melo RCN, Rocha VN, Aguiar JAK, Apolônio ACM, Scio E and Fabri RL (2018) Antibacterial and Antibiofilm Activities of Psychorubrin, a Pyranonaphthoquinone Isolated From Mitracarpus frigidus (Rubiaceae). Front. Microbiol. 9:724. doi: 10.3389/fmicb.2018.00724

Psychorubrin, a natural pyranonaphthoquinone found in different plants, has become an interesting compound in the search for new antimicrobial therapeutic agents. Here, we investigated the potential antagonistic activity of psychorubrin against planktonic and biofilm bacteria. First, psychorubrin was tested against several Gram-positive and Gram-negative bacteria strains by a broth microdilution susceptibility method. Second, bacterial killing assay, bacterial abundance, and membrane viability were evaluated. The nucleotide leakage assay was used to verify membrane destabilization while antibiofilm activities were analyzed by the effect on established biofilm, static biofilm formation, isolation of biofilm matrix assay and scanning electron microscopy. In parallel, the combinatorial effect of psychorubrin and chloramphenicol was evaluated by the checkerboard method. Psychorubrin was active against Gram-positive bacteria, showing rapid time-dependent kinetics of bacterial killing, amplified nucleotide leakage, and greater activity against the methicillin-resistant species (MRSA) *Staphylococcus aureus* 33591 and 33592 and *Staphylococcus pyogenes* 10096. Psychorubrin also interfered with the composition of the biofilm matrix by reducing the total content of carbohydrates and proteins. A synergic effect between psychorubrin and chloramphenicol was observed for *S. aureus* 33592 and *S. pyogenes* 10096 while an additive effect was detected for *S. aureus* 33591. Our findings demonstrate, for the first time, an antagonistic activity of psychorubrin against bacteria not only in their planktonic forms but also in biofilms, and identify bacterial membranes as primary targets for this compound. Based on these observations, psychorubrin has a good potential for the design of novel antimicrobial agents.

Keywords: psychorubrin, antibacterial activity, MRSA, *Mitracarpus frigidus*, biofilm control

INTRODUCTION

Staphylococcus aureus is a major human pathogen that can cause varied diseases, ranging from minor skin infections to severe systemic diseases such as septicemia and pneumonia (reviewed in Kobayashi et al., 2015). Moreover, new resistant strains of *S. aureus* have arisen with tentative treatments of the pathologies caused by this bacterium (Choo, 2017; Oestergaard et al., 2017). The bacteremia caused by methicillin-resistant *S. aureus* (MRSA), for example, is associated with increased morbidity and mortality in adults and its frequency has become greater in hospital institutions (Wilson et al., 2017). In 2004, the Center for Disease Control showed that MRSA proportion was higher than 50% in intensive care unit patients, considering the hospitals that integrated the National Nosocomial Infections Surveillance System [NNIS] (2004). However, multidrug-resistant organisms have not emerged only in the hospital environment. In recent years, due to the exacerbated use of antibiotics, MRSA has also been increasingly found in community-onset infections (Choo, 2017). MRSA is widely prevalent worldwide, with rates highest than 50% reported in North and South America, Asia, and Malta (Stefani et al., 2012). Diverse antimicrobial classes including the β-lactams, the glycopeptides, and the fluoroquinolones have been recognized as a major problem in public health because of their resistance (Mai et al., 2017).

Streptococcus pyogenes (group A streptococcus) is another common human pathogen. Although most infections caused by *S. pyogenes* are benign and have short duration, this agent may cause late sequelae such as post-streptococcal acute glomerulonephritis, rheumatic fever, streptococcal toxic shock syndrome, necrotizing fasciitis, and other localized or systemic infections, which may present a fulminate evolution (reviewed in Carapetis et al., 2005; Imohl et al., 2017). The global impact of invasive *S. pyogenes* disease is high with, at least, 663,000 new cases and 163,000 deaths worldwide each year (Carapetis et al., 2005).

Although resistant bacteria in their free-living forms have been a major concern for the health system, when they congregate in large numbers to form a biofilm, the problem is even bigger (Ribeiro et al., 2016). In fact, biofilms, densely packed communities of microbial cells growing in a living or inert surface and surrounded by a self-produced polymeric matrix, requires much higher doses of antibiotics (10–1000 times) for bacterial killing and can lead to chronic and persistent infections (Mishra and Wang, 2017). This occurs because biofilm protects bacteria against several physicochemical aggressions, including ultraviolet light, heavy metals, acidity, modulation in hydration or salinity, and phagocytosis (Lebeaux et al., 2014). Thus, bacteria growing in a biofilm are highly resistant to antibiotic treatment and host immune defense and, once established, a biofilm becomes difficult to eradicate (Wu et al., 2015).

Because antimicrobial resistance and biofilm formation are a global public health challenge, there is a striking need of development of new biologically active molecules against multidrug-resistant bacteria and the adoption of medicinal crude extracts of plants to treat infectious diseases (Subramani et al., 2017). In this context, our group has been studying different potential bioactive antibacterial compounds (Pinto et al., 2017a,b), including a natural product termed psychorubrin, a napthoquinone commonly found in a variety of plants (Fabri et al., 2009, 2012).

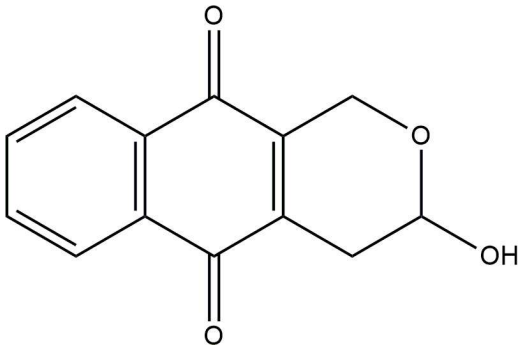

FIGURE 1 | Chemical structure of psychorubrin.

Psychorubrin (**Figure 1**) has been associated with diverse biological activities, such as antitumoral (Hayashi et al., 1987; Fabri et al., 2012), cytotoxic (Hayashi et al., 1987), leishmanicidal (Fabri et al., 2012), and antiplasmodial (Endale et al., 2012) actions. In a previous work, we isolated psychorubrin from *Mitracarpus frigidus* (Fabri et al., 2009), a native species of Brazil (Pereira et al., 2006) and identified a promising potential antimicrobial property for this compound (Fabri et al., 2012). Here, the planktonic antibacterial activities of psychorubrin were investigated in detail as well as the potential bacterial biofilm control by this agent. By using different approaches, we found a consistent antagonistic activity for psychorubrin, which affects both bacterial forms and biofilms of Gram-positive bacteria, especially the multidrug-resistant *S. aureus* 33591 and 33592 in addition to *S. pyogenes* 10096. We also identified that the antimicrobial action of psychorubrin is linked with disruption of the bacterial cell membrane structure.

MATERIALS AND METHODS

Plant Material

The aerial parts of *Mitracarpus frigidus* (Willd. Ex Roem. & Schult.) K. Shum (Rubiaceae) were collected in Juiz de Fora, Minas Gerais State, Brazil, in May 2011. The plant was identified by Dr. Tatiana Konno from the Ecological and Socio environmental Core of Macaé/UFRJ. A voucher specimen (CESJ 46076) was deposited at the Leopoldo Krieger Herbarium at the Federal University of Juiz de Fora (Brazil).

Extraction and Reisolation

A crude dichloromethane (CH_2Cl_2) extract was prepared from *Mitracarpus frigidus* as before (Fabri et al., 2009). The isolation and structural elucidation of psychorubrin were performed as previously described in Fabri et al. (2012).

Microbial Strains

The psychorubrin extract was screened by serial dilution assay against the following Gram-positive microorganisms: *Staphylococcus aureus* ATCC 25923, *Staphylococcus aureus* ATCC 33591 (Gentamicin and methicillin-resistant *Staphylococcus aureus* – MRSA), *Staphylococcus aureus* ATCC 33592 (Methicillin-resistant *Staphylococcus aureus* – MRSA) and *Streptococcus pyogenes* ATCC 10096 as well as the Gram-negative microorganisms *Escherichia coli* ATCC 10536, *Klebsiella pneumoniae* ATCC 4532 and *Pseudomonas aeruginosa* ATCC 9027. For subsequent tests, only *S. aureus* ATCC 33591, *S. aureus* ATCC 33592 and *S. pyogenes* ATCC 10096 were selected. The strains were cultured overnight at 37°C in Mueller Hinton agar (MHA) before each experiment.

Serial Dilution Assay for Determination of the Minimal Inhibitory Concentration (MIC)

The minimal inhibitory concentration (MIC) of psychorubrin was determined by microdilution techniques in Mueller Hinton broth (MHB) as described (CLSI, 2014). Bacteria were cultured at 37°C for 24 h in MHA. The psychorubrin stock solution was twofold diluted ranging from 320 to 2.5 $\mu g\ mL^{-1}$ (final volume = 80 μL) with final dimethyl sulfoxide (DMSO) concentration $\leq$ 1%. Then, 100 μL of MHB and 20 μL of 10^8 CFU mL^{-1} (according to McFarland turbidity standards) bacterial suspensions were inoculated onto microplates, and the test was performed in a 200 μL final volume. Plates were incubated at 37°C for 24 h. Experiments were performed simultaneously for bacterial growth control (MHB + bacteria + psychorubrin vehicle) and sterility control (MHB + psychorubrin vehicle) as well as for the positive controls with chloramphenicol (100–0.2 $\mu g\ mL^{-1}$) and ciprofloxacin (500–0.24 $\mu g\ mL^{-1}$). MIC values were calculated from the highest dilution showing a complete inhibition of the tested strain. Analyses were done in triplicate. Compounds were considered significantly active when the MIC values were $\leq$ 10 $\mu g\ mL^{-1}$ (Kuete, 2017).

Studies of Planktonic Bacteria

Bacterial Growth Curve

Psychorubrin was tested to determine the time-kill kinetics of strains. Saline suspensions of freshly grown bacterial strains (10^8 CFU mL^{-1}) were inoculated with different concentrations of psychorubrin (MIC, 0.5MIC, and 0.25MIC values) supplemented with MHB. Optical density (OD) at 600 nm was recorded in a spectrophotometer (Multiskan Go, Thermo Scientific, Waltham, MA, United States) at 2, 4, 6, 8, and 24 h of bacterial growth at 37°C as before (Pinto et al., 2017a,b). Graphs of turbidity versus incubation time were plotted. As a positive control, chloramphenicol was added. For bacterial growth control, groups consisting of MHB medium containing psychorubrin vehicle plus strains were used. Experiments were performed in triplicate (Babii et al., 2016).

Bacterial Abundance

Slides prepared in a cytocentrifuge were used to quantitate bacteria as before (Silva et al., 2014). Bacterial strains maintained in saline were inoculated into MHB containing psychorubrin (MIC value) and incubated at 37°C during 24 h. As a positive and negative control for this assay, chloramphenicol and psychorubrin vehicle at MIC values were added, respectively, to the groups containing bacterial strains. After diluting 10 times (1 mL) in saline, samples were fixed with sterile free-particle 37% formaldehyde to a final concentration of 2%, stained with 4′,6-Diamidino-2-Phenylindole (DAPI) (Vector Laboratories, Burlingame, CA, United States) for DNA recognition (final concentration of 0.01 $\mu g\ mL^{-1}$) and placed in mega funnels (Shandon Mega Funnel, Thermo, United Kingdom) for immediate centrifugation in a cytocentrifuge (Shandon Cytospin 4, Thermo, United Kingdom), at 452 *g* at high acceleration during 10 min. Acceleration and speed were determined as the Cytospin manufacturer manual. Cells were analyzed under a fluorescence microscope (BX-60, Olympus, Melville, NY, United States) with a U-MWU2 filter (330–385 nm excitation wavelengths). For bacteria quantification, 20 random fields were counted for each sample at 1,000x magnification using an ocular grid. By applying a dilution factor (10x), the total bacterial count was obtained.

Bacteria Viability

Cell membrane integrity was investigated by using a fluorescent probe as an indicator for cell viability (Boulos et al., 1999). Bacterial samples (10 fold-diluted) were stained with the BacLight viability kit (Molecular Probes, Inc, Thermo Fisher Scientific, Eugene, OR, United States) and the proportion of live/viable and dead/non-viable cells was determined. This kit contains a mixture of fluorescent dyes, SYTO® 9 and propidium iodide, which differ both in their spectral features and their ability to penetrate healthy bacterial cell membranes. Cells with intact membranes (live cells) stain green and those with damaged membranes (dead cells) stain red (Joux and Lebaron, 2000; Silva et al., 2014). Saline bacterial strains were inoculated into MHB containing psychorubrin at MIC value and incubated at 37°C during 24 h. Bacterial strains inoculated into MHB with psychorubrin vehicle or incubated with chloramphenicol (MIC values) served as negative and positive controls, respectively. For bacterial staining, samples were mixed with Baclight (1 mL of each sample to 3 μL of BacLight), placed in megafunnels (Shandon Mega funnel, Thermo, United Kingdom), cytocentrifuged as above and evaluated under a fluorescence microscope (BX-60, Olympus, Melville, NY, United States) at 450–480 nm excitation wavelengths (U-MWB filter) for simultaneous imaging of live and dead cells. For each sample, bacteria were directly counted in 10 random fields using an ocular grid at 1,000x magnification, and the average percentage of live/dead bacteria was obtained for each slide sampled.

Nucleotide Leakage

Nucleotide release was evaluated as before (Tang et al., 2008) with some modifications. Overnight bacterial cultures at 37°C were washed and resuspended in 10 mM PBS (pH 7.4), reaching a final

density of nearly 10^8 cells mL^{-1}. Strains were then incubated with psychorubrin at MIC value during different times (2, 4, 6, and 8 h) while strains incubated with 10 mM PBS (pH 7.4) served as control groups. After incubation, cell suspensions were centrifuged at 10,000 *g* for 10 min; the supernatants were diluted appropriately, and the OD at 260 nm was recorded in a spectrophotometer (Multiskan Go, Thermo Scientific, Waltham, MA, United States) at room temperature (25°C). Experiments were performed in triplicate.

Checkerboard Test

The potential synergistic activity of psychorubrin and chloramphenicol was investigated by the checkerboard test (Pillai et al., 2005), which enables calculation of the fractional inhibitory concentration (FIC) index (FICI), that is the sum of the FICs (ΣFIC) of both agents. FICI values were interpreted as follows: FICI $\leq$ 0.5 synergy; 0.5 $<$ FICI $\leq$ 1 additivity; 1 $<$ FICI $\leq$ 2 indifference or no effect; and FICI $\geq$ 2 antagonism (Božić et al., 2014). The MIC of the two assayed agents was used for the FICI tested dilutions.

Assays were done using 96-well polystyrene microtiter plates with MHB, psychorubrin and chloramphenicol in twofold serial concentrations. Bacterial suspensions were prepared at a final concentration of 10^8 CFU mL^{-1}, incubated overnight at 37°C and read in a spectrophotometer (Multiskan Go, Thermo Scientific, Waltham, MA, United States). Tests were done in triplicate.

Biofilm Studies

Effect on Established Biofilms

The effect of psychorubrin on established biofilms was tested as before (Nostro et al., 2007) with some alterations. Briefly, biofilms of *S. aureus* 33591, *S. aureus* 33592 and *S. pyogenes* 10096 strains were generated with each of these organisms using 96-well polystyrene microtiter plates filled with MHB, 1% glucose and cells (conc 10 $cells^7$/mL) during 24 h at 37°C. Then, the planktonic cells were gently removed and, after washing with saline (three times), the wells were filled with 200 μL of psychorubrin (twofold dilutions), with MIC in the range of four-fold dilution. Incubation was performed at 37°C during 24 h. OD was evaluated at 492 nm at time 0 and at 24 h after incubation. As a positive control for this assay, chloramphenicol was added. For biofilm growth control, groups consisting of MHB medium plus strains were used. All experiments were performed in triplicate. To calculate the percentage of biofilm inhibition, the OD values of the growth control group for each strain were compared with that of the treated group using the following equation:

$$[(\mathrm{OD(control)} - \mathrm{OD(treatment)}/\mathrm{OD(control)}] \times 100$$

Effect on Adherence of Biofilms

Inhibition of biofilm formation was performed by spectrophotometric assay according to (Plyuta et al., 2013). Cell suspensions (100 μL) of *S. aureus* 33591, *S. aureus* 33592 and *S. pyogenes* 10096 (10^8 CFU/mL) and different concentrations of psychorubrin and chloramphenicol (MIC, 0.5 MIC, and 0.25 MIC) were incubated at 37°C during 24 h. The suspensions were then removed, and the wells were washed with 200 μL of PBS to remove free-floating bacteria. Biofilms formed by adherent cells in the plate were stained with 200 μL of 0.1% crystal violet and incubated at room temperature for 30 min. Excess stain was rinsed off by thorough washing with PBS, plates were fixed with 200 μl of 96% ethanol and incubated for 15 min. The resulting reaction was read spectrophotometrically at 590 nm. All experiments were performed in triplicate. The percentage of biofilm inhibition was calculated using the following equation:

$$[(\mathrm{OD(control)} - \mathrm{OD(treatment)}/\mathrm{OD(control)}] \times 100$$

Effect on Biofilm Matrix Composition

The biochemical composition of the biofilm matrix from *S. aureus* 33591, *S. aureus* 33592, and *S. pyogenes* 10096 was studied by using the bicinchoninic acid method for proteins (Smith et al., 1985) and the phenol-sulphuric acid method for total carbohydrates (Dubois et al., 1956). Briefly, adherent biofilms were transferred to screw cap bottles containing 2 mL of distilled water. The bottles were sonicated for 5 min in an ultrasonic water bath and vortexed vigorously for 1 min to disrupt the biofilms. Cell suspensions were then pooled, centrifuged and the supernatants collected for subsequent evaluation of the total content of proteins and carbohydrates.

Scanning Electron Microscopy (SEM)

Staphylococcus aureus 33591, *S. aureus* 33592, and *S. pyogenes* 10096 strains were seeded in MH agar, incubated for 24 h at 37°C, and inoculated into a tube containing 5 mL of BHI broth with 1% glucose. Then, 500 μL of the inoculated broth (10^8 UFC mL^{-1}) was added in plated of 24 wells containing round glass coverslips (13 mm, Glasscyto®). The treatment (n = 3 wells) was done by adding 500 μL of the psychorubrin (final concentration per well = MIC). For negative (n = 3) and positive (n = 3) controls 500 μL of sterile water or chloramphenicol (MIC) were added, respectively. Biofilms on glass coverslips (13 mm, Glasscyto®) were cultured for 24 h at 37°C and fixed in 2.5% glutaraldehyde for 30 min at room temperature (Riedel-de-Haen, Germany) in 0.1 M cacodylate buffer (pH 7.2). Coverslip-adherent cells were post-fixed with osmium tetroxide, and dehydrated through a graded series of ethanol solutions (30, 50, 70, 90% and twice in 100%) for 15 min at each concentration. Cells were then critical point dried in carbon dioxide. Coverslips were mounted on aluminum holders, sputtered with 5 nm gold, and analyzed in a scanning electron microscope (JEOL JSM-6390LV, Tokyo, Japan) for observation of the biofilms and bacterial morphology.

Statistical Analysis

Results are expressed as mean values with the standard error. The statistical analyses were performed using ANOVA test followed by Bonferroni to compare the controls and treated groups at a significance level of 5%

RESULTS

Minimal Inhibitory Concentration (MIC)

Psychorubrin showed a broad spectrum of antibacterial activity, with clear effectiveness against both Gram-negative and

Gram-positive bacteria. However, the three bacteria species most susceptible to psychorubrin according to MIC values were *S. aureus* 33591, *S. aureus* 33592, and *S. pyogenes* 10096, in this order (**Table 1**). Psychorubrin was more effective than chloramphenicol and less effective than ciprofloxacin for *S. aureus* 33591, *S. aureus* 33592, and *S. pyogenes* 10096. Based on these observations, these three bacteria strains were selected for further investigation of the psychorubrin activity.

Bacterial Killing Assay

The psychorubrin vehicle did not affect the bacterial growth curve for all species. ON the other hand, all tested bacteria showed a dose-dependent growth decrease when exposed to psychorubrin (**Figure 2**). All the concentrations evaluated (MIC, 0.5 MIC, and 0.25 MIC) inhibited the growth cycle curve of the three tested bacteria in comparison to the vehicle-treated control. For *S. aureus* 33591 and *S. pyogenes* 10096

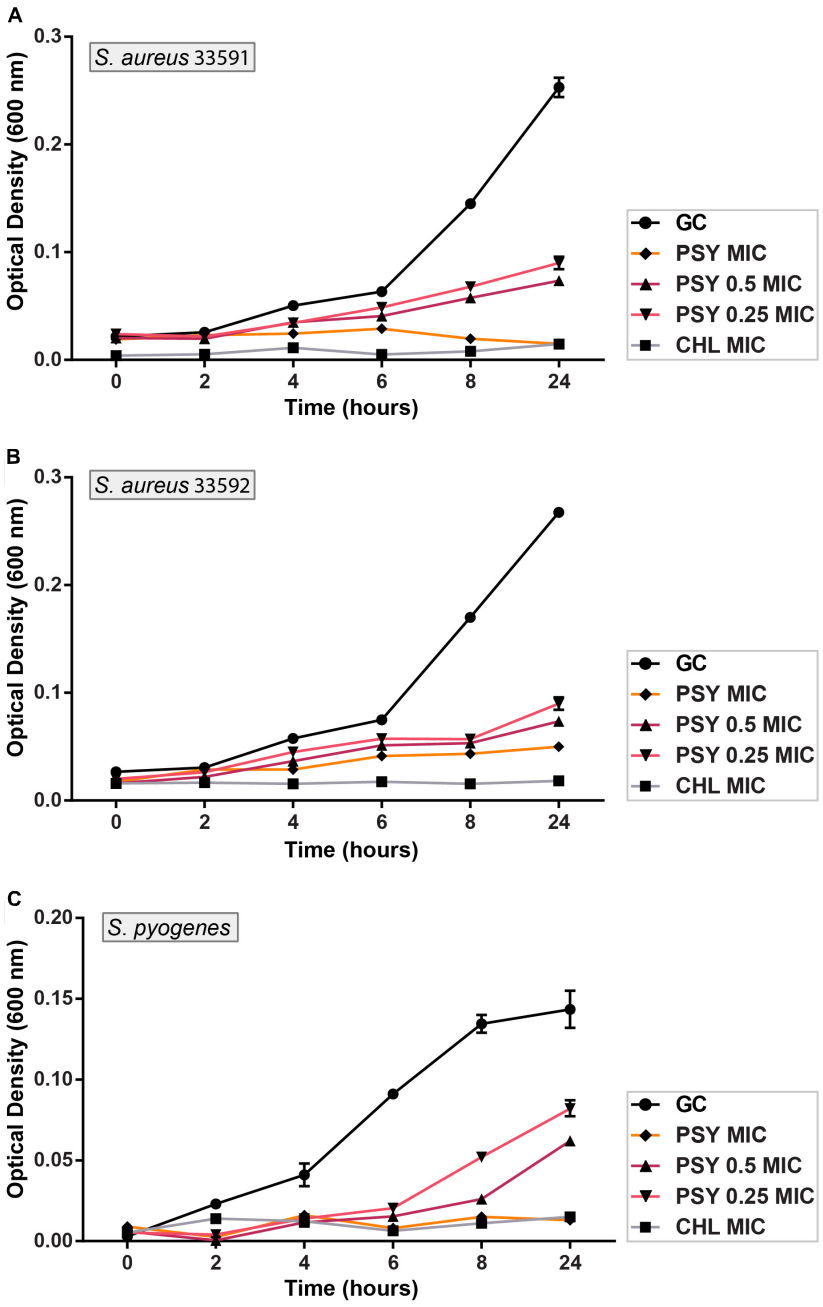

FIGURE 2 | Activity kinetics of psychorubrin (PSY) against *S. aureus* 33591 **(A)**; *S. aureus* 33592 **(B);** and *S. pyogenes* 10096 **(C).** Chloramphenicol (CHL) was used as positive control, and bacteria inoculated in MHB with psychorubrin vehicle was used as bacteria growth control (GC). The experiments were carried out in triplicate, and data represent the mean ± SD.

TABLE 1 | Antibacterial activity of the psychorubrin.

	PSY	CHL	CIP
	MIC*	MIC*	MIC*
Staphylococcus aureus 25923	80	12.5	2.5
Staphylococcus aureus 33591	5	25	0.16
Staphylococcus aureus 33592	5	25	0.08
Streptococcus pyogenes 10096	10	12.5	0.63
Klebsiella pneumoniae 4352	20	0.78	0.31
Escherichia coli 10536	20	3.13	0.08
Pseudomonas aeruginosa 9027	160	25.0	0.63

*PSY, psychorubrin; CHL, chloramphenicol; CIP, ciprofloxacin; *Values in μg mL^{-1}.*

(**Figures 2A,C**) psychorubrin extended the lag phase by 4 h (0.5 MIC and 0.25 MIC), and inhibited fully bacterial growth at MIC value similar to chloramphenicol. For *S. aureus* 33592, all concentration for psychorubrin extended the phase lag by 2 h (**Figure 2B**).

Bacterial Abundance and Viability

Fluorescence microscopy after DAPI staining showed that psycorubrin inhibited the bacterial abundance compared to the control group, reducing bacterial growth by 52, 50, and 96% for *S. aureus* 33591, *S. aureus* 33592 and *S. pyogenes* 10096, respectively (**Figure 3A**). Psychorubrin treatment produced decrease of cell density and increase of cell death.

The cytocentrifuge preparations of the cell viability probe test (Live/Dead® BacLight) revealed the presence of live (green) and dead (red) bacteria in all psychorubrin-treated and control groups (**Figures 3B,C**). Psychorubrin treatment (MIC value for 24 h) led to an increase of the dead cell numbers for *S. aureus* 33591, *S. aureus* 33592, and *S. pyogenes* 10096, corresponding to 37, 28, and 28% of dead cells, respectively, in comparison to the vehicle-treated group (*S. aureus* 33591 = 94.91%, *S. aureus* 33592 = 95.68%, *S. pyogenes* 10096 = 96.40%). Chloramphenicol showed 9, 7, and 1.3% of dead cells, respectively.

Nucleotide Leakage

The efflux of nucleotides from the intracellular compartment was significant for the three Gram-positive bacteria. As shown in (**Figures 4A–D**) psychorubrin increased at 19, 41, and 30% the nucleotide release in *S. aureus* 33591, *S. aureus* 33592, and *S. pyogenes* 10096 respectively, compared to the controls.

Checkerboard

The checkerboard assay showed a decrease in the MIC values for both psychorubrin and chloramphenicol, suggesting possible interactions between these substances. The results demonstrated a synergistic action between psychorubrin and chloramphenicol for *S. aureus* 33592 and *S. pyogenes* 10096, and an additive effect between psychorubrin and chloramphenicol for *S. aureus* 33591 (**Table 2**).

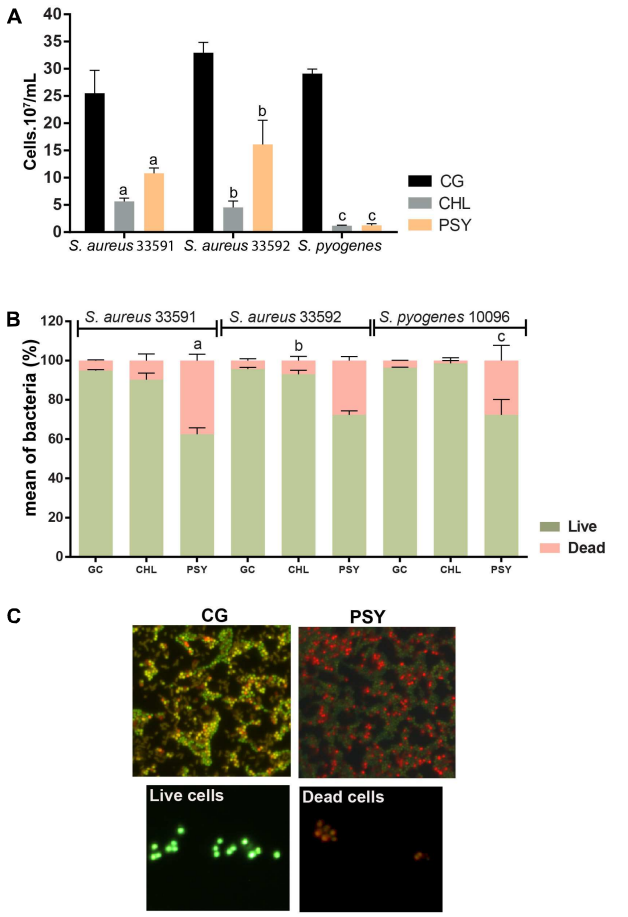

FIGURE 3 | Effect of psychorurin (PSY) on the growth of *S. aureus* 33591, *S. aureus* 33592 and *S. pyogenes* 10096. Cultured bacteria were stained with DAPI or LIVE/ DEAD® BacLight™ and counted under fluorescence microscopy for evaluation of cell density **(A)** and viability **(B,C)**, respectively. Psychorubrin treatment induced both decrease of cell density **(A)** and increase of cell death **(B)** compared to control groups treated with psychorubrin vehicle. **(C)** Representative images from *S. aureus* 33501 show dead cells in red and live cells in green after baclight staining. Letters indicate statistical difference from controls treated with psychorubrin vehicle for *S. aureus* 33591 (^{a}), *S. aureus* 33592 (^{b}), *S. pyogenes* 10096 (^{c}) (ANOVA followed by Bonferroni, $P < 0.05$). Chloramphenicol (CHL) was used as a positive control. All experiments were carried out in triplicate, and data represent the mean ± SD of bacteria counted.

Effect on Established Biofilms and on Their Adhesion

To investigate if psychorubrin was able to disrupt pre-formed biofilms and to affect their adhesion capability, samples were evaluated at the MIC and 0.5MIC (**Figure 5**). The disruption and adhesion of biofilm at MIC and 0.5MIC were significantly effective when compared to positive controls. In these concentrations, the inhibition of pre-formed biofilms of psychorubrin was about 56 and 46% for *S. aureus* 33591, 84 and 85% for *S. aureus* 33592, 57 and 35% for *S. pyogenes* 10096, respectively. Psychorubrin also decreased the adhesion of biofilms with percentages of inhibition of 49 and 12% for

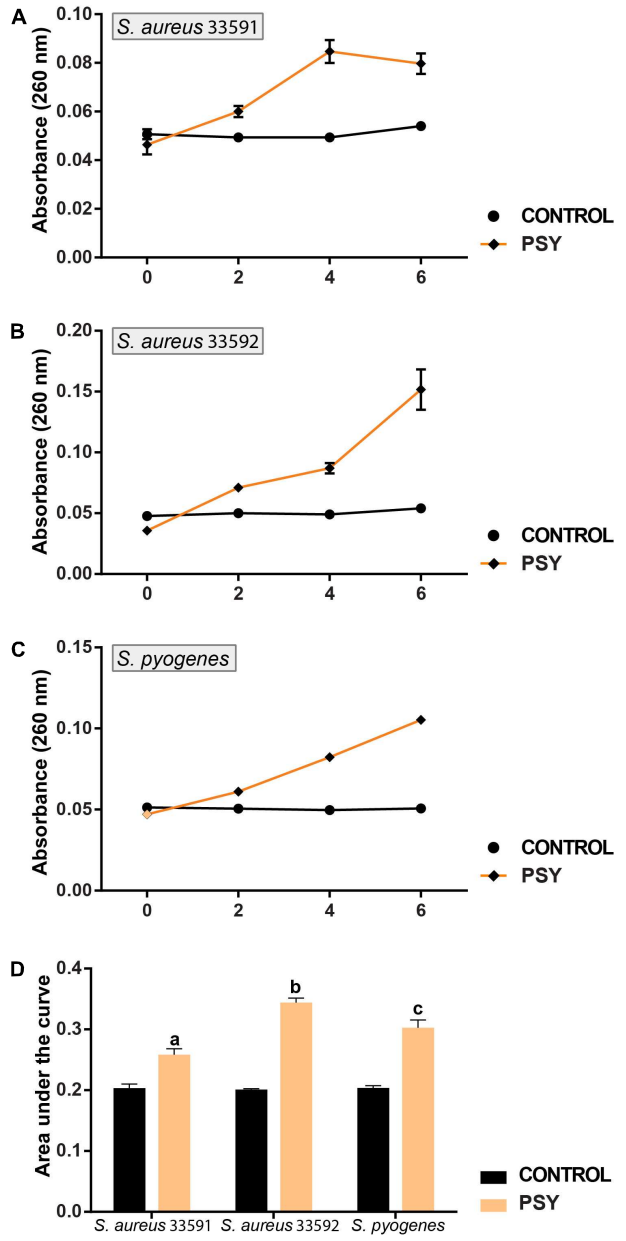

FIGURE 4 | Mode of action of psychorubrin (PSY). Effect of psychorubrin on the amount of the total nucleotide released from *S. aureus* 33591 **(A)**, *S. aureus* 33592 **(B)**, and *S. pyogenes* 10096 **(C)**. Area under the curve in PSY-treated and controls are showed in **(D)**. Letters indicate statistical difference from controls treated with psychorubrin vehicle for S. aureus 33591 ([a]), *S. aureus* 33592 ([b]), *S. pyogenes* 10096 ([c]) (ANOVA followed by Bonferroni, $P < 0.05$). All experiments were carried out in triplicate, and data represent the mean ± SD.

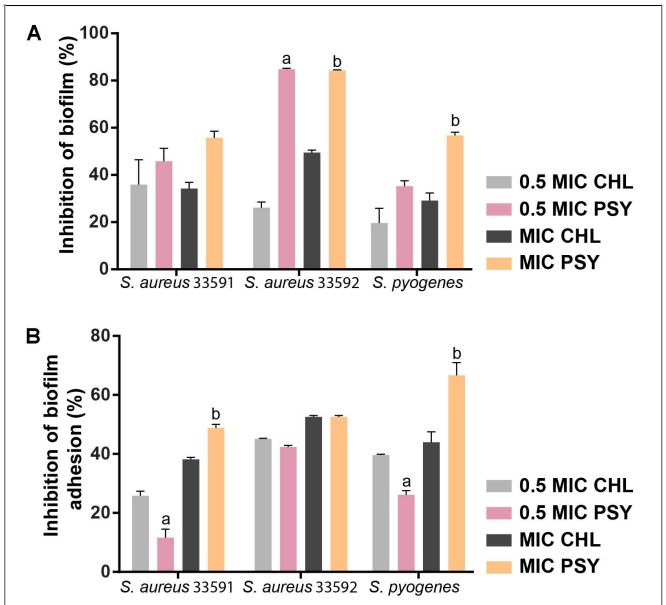

FIGURE 5 | The effect of psychorubrin (PSY) on established biofilms **(A)** of *S. aureus* 33591, *S. aureus* 33592, and *S. pyogenes* 10096 and on their adherence ability **(B)**. Choramphenicol (CHL) was used as positive control. Each data point represents mean ± SD from at least two independent experiments performed in triplicate. [a]Statistically different from chloramphenicol (MIC value). [b]Statistically different from chloramphenicol (0.5 MIC value) (ANOVA followed by Bonferroni, $P < 0.05$).

S. aureus 33591, 52 and 42% for *S. aureus* 33592, 67 and 26% *S. pyogenes* 10096, respectively with MIC and 0.5MIC values.

Effect on Biofilm Matrix Composition

Table 3 shows the total content of carbohydrates and proteins of formed biofilms by *S. aureus* 33591, *S. aureus* 33592 and *S. pyogenes* 10096. Psychorubrin and chloramphenicol (MIC values) significantly reduced carbohydrate and protein contents, being the maximum reduction observed for total content of proteins.

SEM Observations

Ultrastructural analyses by SEM revealed the surface structure and morphology of biofilms formed by different bacterial strains with or without antimicrobial treatment (**Figure 6**). The control group showed the typical multilayer growth of bacterial biofilms (**Figures 6A,D,G**) while the group treated with chloramphenicol exhibited a significant reduction of biofilms only for the *S. aureus* 33592 and *S. pyogenes* 10096 strains (**Figures 6B,E,H**). Remarkably, psychorubrin led to a significant reduction of biofilm formation in all strains (**Figures 6C,F,I**), with loss of the

TABLE 2 | Fractional inhibitory concentration (FIC) indices.

Microorganisms	PSY	CHL	ΣFIC	Effect
	MIC*	MIC*		
Staphylococcus aureus 33591	0.078	12.5	0.52	Additive
Staphyloccocus aureus 33592	0.078	3.13	0.14	Synergy
Streptococcus pyogenes 10096	0.312	1.95	0.14	Synergy

*PSY, psychorubrin; CHL, chloramphenicol; *MIC in a combination of psychorubrin and chloramphenicol (μg/mL). ΣFIC: sum of fractional inhibitory concentrations – the combinatory effect is evaluated as follows: synergy ΣFIC ≤ 0.5; additive ΣFIC > 0.5 and ≤ 1; indifferent ΣFIC > 1 and ≤ 2.*

TABLE 3 | Biochemical composition of biofilms treated with psychorubrin and chloramphenicol.

Microorganims	GBC		PSY		CHL	
	TP	TC	TP	TC	TP	TC
Staphylococcus aureus 33591	145.1 ± 0.2	0.628 ± 0.02	1.2 ± 0.01	0.148 ± 0.01	5.3 ± 0.07	0.077 ± 0.001
Staphyloccocus aureus 33592	153.7 ± 0.7	0.654 ± 0.01	6.7 ± 0.02	0.148 ± 0.03	7.0 ± 0.1	0.106 ± 0.005
Streptococcus pyogenes 10096	67.2 ± 0.5	0.624 ± 0.03	0.2 ± 0.01	0.135 ± 0.04	1.0 ± 0.001	0.104 ± 0.06

GBC, growth biofilm control; PSY, psychorubrin; CHL, chloramphenicol; TP, total protein in μg mL^{-1}; TC, total carbohydrate in μg mL^{-1}.

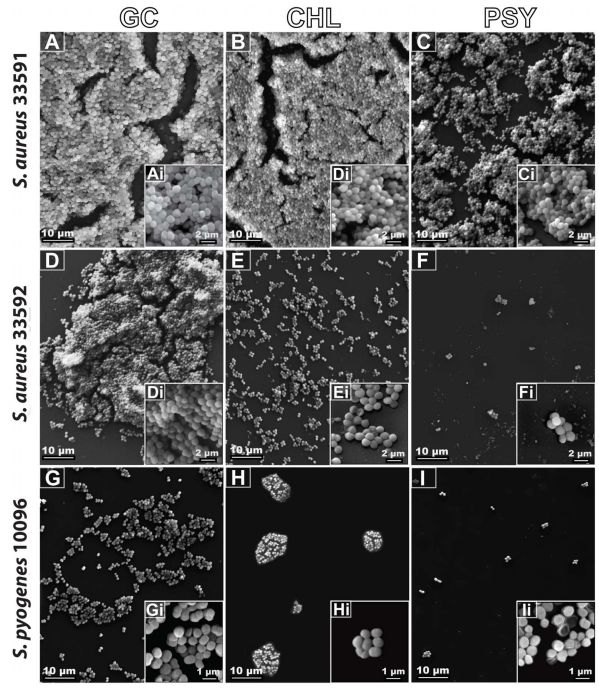

FIGURE 6 | Biofilm scanning electron micrographs of the different bacterial strains with or without antimicrobial treatment. GC, growth control **(A,D,G)**; CHL, chloramphenicol **(B,E,H)**; PSY, psychorubrin **(C,F,I)**. Note in high magnification (inset), the morphological external structure of the different bacterial strains.

bacterial original shape as evidenced by a distorted and irregular bacterial cell wall (**Figure 6I**). Altogether, our findings provide evidence that psychorubrin has a potent antimicrobial action against the different strains analyzed.

DISCUSSION

New antimicrobial compounds are greatly needed to treat infections caused by bacteria resistant to currently available agents. Here, we provided direct evidence that the bioactive compound psychorubrin has a broad spectrum of antibacterial activity being effective against both bacterial forms and biofilms of Gram-positive bacteria. We demonstrated a strong inhibitory activity of this agent for *S. pyogenes* and *S. aureus* including multiresistant strains. Therefore, the present study expands previous findings (Fabri et al., 2012) highlighting the use of psychorubrin as a possible strategy to treat the infections caused by these microorganisms.

The time-kill curves can monitor bacterial growth and death over a wide range of antimicrobial concentrations and have been frequently used to evaluate the effect of antimicrobials over time (Foerster et al., 2016). A time-dependent bactericidal effect happens when the concentration of the antibacterial drug surpasses the MIC for the microorganism, while the concentration-dependent bactericidal effect takes place when an antibiotic has a high concentration at the binding site to eradicate the microorganism (Anantharaman et al., 2010). Our time-kill kinetics analyses showed that psychorubrin presented a rapid time-dependent kinetics of bacterial killing for all tested bacteria, mainly at MIC value. Comparing the activity of the psychorubrin with chloramphenicol at MIC concentration, we observed a similar action starting at initial hours (**Figure 2**).

Psychorubrin prolonged the lag phase for the three tested bacteria (*S. aureus* 33591, *S. aureus* 33592, and *S. pyogenes* 10096) with 0.5 MIC and 0.25 MIC values. Since the lag phase is a response during the adaptation period by first division of the bacterial cell, this process could involve the repair of macromolecular damage that occurred in the ambient that the cell came from and the synthesis of cellular components necessary for growth (Baty and Delignette-Muller, 2004; Rolfe et al., 2012). Therefore, one of the possible psychorubrin targets might be the synthesis of macromolecules, since pyranonaphthoquinones and naphthoquinones can act in the redox cycle generating a pro-oxidant state that favors the occurrence of oxidative lesions in macromolecules and cellular structures thus resulting in cell death (Silva et al., 2003). In fact, we found a efficient inhibition of bacterial growth by psycorubrin during 24 h indicating a bactericidal effect of this compound, especially for *S. pyogenes* 10096. Moreover, the efficiency of psychorubrin was a little better than chloramphenicol.

To investigate the effect of psychorubrin on bacterial density and viability, we performed two additional approaches. By using fluorescent probes for DNA (DAPI staining) and membrane integrity (*Backlight*) (Gamalier et al., 2017), we showed that the psychorubrin treatment was able to reduce cell density and increase cell death, thus corroborating our bacterial killing assay results. The psychorubrin-elicited bacterial death may be related with a potential inhibitory effect of this compound on bacterial growth and/or a direct effect on bacterial cells, leading to cell death. Because the marker for cell viability enables the detection of compromised plasma membranes, dead

cells can be directly identified before complete cell lysis (Gamalier et al., 2017). Indeed, when cells exhibiting damaged membranes are not able to keep an electrochemical potential, they are considered dead (Joux and Lebaron, 2000). Thus, our approach was helpful to recognize bacterial viability at a single-cell level (Joux and Lebaron, 2000; Silva et al., 2014; Gamalier et al., 2017).

The significant increase of dead cells induced by psychorubrin is in accordance with previous studies, which demonstrated bactericidal activity after treatment with compounds through viability analyses using *Baclight* (You et al., 2013; Yuan and Yuk, 2018). Additionally, the bacteriostatic effect from chloramphenicol (Bernatová et al., 2013), showed a very low proportion of dead cells, statistically different from psychorubrin. Overall, our viability results support the potential bactericidal effect of psychorubrin for the three bacteria tested, indicating the occurrence of membrane damage. Therefore, the microscopic approaches used in the present study were especially revealing in demonstrating the mode of action of psychorubrin.

Our results showed that psychorubrin is effective against Gram-positive bacteria, but the antimicrobial activity is organism-dependent. In this context, nucleotide leakage assay was used to clarify how psychorubrin is able to inhibit proliferation of these bacteria (Hao et al., 2009). As DNA and RNA are released after membrane disruption, these nucleotides were quantified by monitoring the absorbance at 260 nm. The results of nucleotide leakage assay confirm the occurrence of membrane destabilization triggered by psychorubrin (**Figure 4**).

Considering antimicrobial therapy, drug combination has many advantages compared with the use of individual agents. It can be used to prevent the emergence of resistant organisms, to minimize toxicity due to the need of lower drug concentrations, and to obtain synergistic antimicrobial activity (Ocampo et al., 2014). The association of psychorubrin and chloramphenicol was important to optimize the antimicrobial effect of both. However, future studies are needed to test antimicrobial resistance to other clinical choice drugs.

One interesting observation from the present study was the efficiency of psychorubrin in disrupting pre-formed biofilms and decreasing biofilm adhesion for different bacterial species (**Figure 5**). These results combined with our findings showing the psychorubrin effect on biofilm matrix composition, indicate that this compound leads to the inhibition of exopolysaccharide synthesis and especially to the interference of protein formation. Altogether, our data demonstrated that psychorubrin limited the formation of biofilm. Considering that the matrix exopolysaccharide is one of the most distinctive features of a microbial biofilm, forming a three dimensional, gel-like, highly hydrated and locally charged environment in which the microorganisms are largely immobilized (Namasivayam and Roy, 2013), biofilm reduction must be considered the first step for its control by an antimicrobial agent. Furthermore, the restriction of the biochemical composition of the biofilm matrix leads to weakening of the biofilm thus facilitating the entry of the drugs (Joseph, 2003). Our SEM analyses reinforced the action of psychorubrin over the strains tested, both in biofilm form reducing the multilayer growth, and free living cells by affecting the integrity of cell wall.

CONCLUSION

Taken together, our findings identify, for the first time that psychorubrin is active against all tested Gram-positive and Gram-negative bacteria, especially *S. pyogenes* and *S. aureus*, including multi-resistant strains. Considering these two species, this compound has a bactericidal effect, targeting the bacterial synthesis of macromolecules and rapidly (2 h) destabilizing their membranes. The efficacy of psychorubrin showed to be better than chloramphenicol for *S. pyogenes* 10096 and the association of these agents showed at least an additive effect. The bioactivities of psychorubrin identified in this study include both planktonic and biofilm growing Gram-positive bacteria. Psychorubrin was able to reduce bacteria biofilms by interfering with protein formation and inhibiting exopolysaccharide synthesis. These results are promising. Given the potential of psychorubrin as an antibiofilm drug against *S. aureus* and *S. pyogenes*, and the possible combination with chloramphenicol, this compound could be used to reduce the development of resistance to these microorganisms and improve the outcome of the therapies for infections caused by these pathogens. This is of great relevance in hospital services, especially considering the multi-resistance of MRSA.

AUTHOR CONTRIBUTIONS

AL, LC, AA, and RF designed the study. AL, LC, TS, LO, MG, and VR performed the field work and laboratory work. RM, JA, AA, and RF analyzed the data. RM, VR, ES, and RF wrote the manuscript. All authors reviewed the manuscript.

FUNDING

This work was supported by grants from Conselho Nacional de Desenvolvimento Científico e Tecnológico (CNPq, Brazil) e Fundação de Amparo à Pesquisa do Estado de Minas Gerais (Grant Number: APQ-01059-14 for RF and CBB-APQ-03647-16 for RM). Scholarships were provided by Federal University of Juiz de Fora (UFJF/Brazil and Coordenação de Aperfeiçoamento de Pessoal de Nível Superior (CAPES, Brazil).

ACKNOWLEDGMENTS

We gratefully thank Plataforma de Microscopia Eletrônica Rudolf Barth/FIOCRUZ and Dr. Vinícius Antônio de Oliveira Dittrich (Department of Botany/UFJF) for the botanical identification of the species.

REFERENCES

Anantharaman, A., Rizvi, M. S., and Sahal, D. (2010). Synergy with rifampin and kanamycin enhances potency, kill kinetics, and selectivity of de novo-designed antimicrobial peptides. *Antim. Agents Chem.* 54, 1693–1699. doi: 10.1128/AAC.01231-09

Babii, C., Bahrin, L. G., Neagu, A. N., Gostin, I., Mihasan, M., Birsa, L. M., et al. (2016). Antibacterial activity and proposed action mechanism of a new class of synthetic tricyclic flavonoids. *J. Appl. Microb.* 120, 630–663. doi: 10.1111/jam.13048

Baty, F., and Delignette-Muller, M. L. (2004). Estimating the bacterial lag time: which model, which precision? *Int. J. Food Microb.* 91, 261–277. doi: 10.1016/j.ijfoodmicro.2003.07.002

Bernatová, S., Samek, O., Pilát, Z., Šerý, M., Ježek, J., and Jákl, P. (2013). Following the mechanisms of bacteriostatic versus bactericidal action using Raman spectroscopy. *Molecules* 18, 13188–13199. doi: 10.3390/molecules181113188

Boulos, L., Prevost, M., Barbeau, B., Coallier, J., and Desjardins, R. (1999). LIVE/DEAD® *Bac*Light™: application of a new rapid staining method for direct enumeration of viable and total bacteria in drinking water. *J. Microb. Met.* 37, 77–86. doi: 10.1016/S0167-7012(99)00048-2

Božić, D. D., Milenković, M., Ivković, B., and Ćirković, I. (2014). Antibacterial activity of three newly-synthesized chalcones & synergism with antibiotics against clinical isolates of methicillin-resistant *Staphylococcus aureus*. *Indian J. Med. Res.* 140, 130–137.

Carapetis, J. R., Steer, A. C., Mulholland, E. K., and Weber, M. (2005). The global burden of group a streptococcal diseases. *Lancet Infect. Dis.* 5, 685–694. doi: 10.1016/S1473-3099(05)70267-X

Choo, E. J. (2017). Community-associated methicillin-resistant *Staphylococcus aureus* in nosocomial infections. *Infect. Chemother.* 49, 158–159. doi: 10.3947/ic.2017.49.2.158

CLSI (2014). *Performance Standards for Antimicrobial Susceptibility Testing; Twenty-Fourth Informational Supplement. Twenty-Fourth Informational Supplement*. Wayne, PA: Clinical and Laboratory Standards Institute.

Dubois, M., Gilles, K. A., Hamilton, J. K., Rebers, P. A., and Smith, F. (1956). Colorimetric method for determination of sugars and related substances. *Anal. Chem.* 28, 350–356. doi: 10.1021/ac60111a017

Endale, M., Alao, J. P., Akala, H. M., Rono, N. K., Eyase, F. L., and Derese, S. (2012). Antiplasmodial quinones from *Pentas longiflora* and *Pentas lanceolata*. *Planta Med.* 78, 31–35. doi: 10.1055/s-0031-1280179

Fabri, R. L., Grazul, R. M., Carvalho, L. O., Coimbra, E. S., Cardoso, G. M. M., and Souza-Fagundes, E. S. (2012). Antitumor, antibiotic and antileishmanial properties of the pyranonaphthoquinone psychorubrin from *Mitracarpus frigidus*. *An. Acad. Bras. Ciênc.* 84, 1081–1089. doi: 10.1590/S0001-37652012005000064

Fabri, R. L., Nogueira, M. S., Braga, F. G., Coimbra, E. S., and Scio, E. (2009). Mitracarpus frigidus aerial parts exhibited potent antimicrobial, antileishmanial, and antioxidant effects. *Bioresour. Technol.* 100, 428–433. doi: 10.1016/j.biortech.2008.05.053

Foerster, S., Unemo, M., Hathaway, L. J., Low, N., and Althaus, C. L. (2016). Time-kill curve analysis and pharmacodynamic modelling for in vitro evaluation of antimicrobials against *Neisseria gonorrhoeae*. *BMC Microb.* 16:216. doi: 10.1186/s12866-016-0838-9

Gamalier, J. P., Silva, T. P., Zarantonello, V., Dias, F. F., and Melo, R. C. N. (2017). Increased production of outer membrane vesicles by cultured freshwater bacteria in response to ultraviolet radiation. *Microbiol. Res.* 194, 38–46. doi: 10.1016/j.micres.2016.08.002

Hao, G., Shi, Y. H., Tang, Y. L., and Le, G. W. (2009). The membrane action mechanism of analogs of the antimicrobial peptide Buforin 2. *Peptides* 30, 1421–1427. doi: 10.1016/j.peptides.2009.05.016

Hayashi, T., Smith, F. T., and Lee, K. H. (1987). Antitumor agents. 89. Psychorubrin, a new cytotoxic naphthoquinone from *Psychotria rubra* and its structure-activity relationships. *J. Med. Chem.* 30, 2005–2008. doi: 10.1021/jm00394a013

Imohl, M., Fitzner, C., Perniciaro, S., and van der Linden, M. (2017). Epidemiology and distribution of 10 superantigens among invasive *Streptococcus pyogenes* disease in Germany from 2009 to 2014. *PLoS One* 12:e0180757. doi: 10.1371/journal.pone.0180757

Joseph, R. L. (2003). Prosthetic joint infections: bane of orthopedists. *Clin. Infect. Dis.* 36, 1157–1161. doi: 10.1086/374554

Joux, F., and Lebaron, P. (2000). Use of fluorescent probes to assess physiological functions of bacteriaat single-cell level. *Microbes. Infect.* 2, 1523–1535. doi: 10.1016/S1286-4579(00)01307-1

Kobayashi, S. D., Malachowa, N., and DeLeo, F. R. (2015). Pathogenesis of Staphylococcus aureus abscesses. *Am. J. Pathol.* 185, 1518–1527. doi: 10.1016/j.ajpath.2014.11.030

Kuete, V. (ed.) (2017). "African medicinal spices and vegetables and their potential in the management of metabolic syndrome," in *Medicinal Spices and Vegetables from Africa*, (Amsterdam: Elsevier), 315–327. doi: 10.1016/B978-0-12-809286-6.00012-1

Lebeaux, D., Ghigo, J. M., and Beloin, C. (2014). Biofilm-related infections: bridging the gap between clinical management and fundamental aspects of recalcitrance toward antibiotics. *Microbiol. Mol. Biol. Rev.* 78, 510–543. doi: 10.1128/MMBR.00013-14

Mai, B., Gao, Y., Li, M., Wang, X., Zhang, K., Liu, Q., et al. (2017). Photodynamic antimicrobial chemotherapy for *Staphylococcus aureus* and multidrug-resistant bacterial burn infection in vitro and in vivo. *Int. J. Nanomed.* 12, 5915–5931. doi: 10.2147/IJN.S138185

Mishra, B., and Wang, G. (2017). Individual and combined effects of engineered peptides and antibiotics on *Pseudomonas aeruginosa* biofilms. *Pharmaceuticals* 10:E58. doi: 10.3390/ph10030058

Namasivayam, S. K. R., and Roy, E. A. (2013). Anti biofilm effect of medicinal plant extracts against clinical isolate of biofilm of *Escherichia coli*. *Int. J. Pharm. Pharm. Sci.* 5, 486–489.

National Nosocomial Infections Surveillance System [NNIS] (2004). National nosocomial infections surveillance (NNIS) System report, data summary from January 1992 through June 2004, issued October 2004. *Am. J. Infect. Control* 32, 470–485. doi: 10.1016/j.ajic.2004.10.001

Nostro, A., Sudano Roccaro, A., Bisignano, G., Marino, A., Cannatelli, M. A., and Pizzimenti, F. C. (2007). Effects of oregano, carvacrol and thymol on *Staphylococcus aureus* and *Staphylococcus epidermidis* biofilms. *J. Med. Microb.* 56, 519–523. doi: 10.1099/jmm.0.46804-0

Ocampo, P. S., Lázár, V., Papp, B., Arnoldini, M., Wiesch, P. A., and Busa-fekete, R. (2014). Antagonism between bacteriostatic and bactericidal antibiotics is prevalent. *Antim. Agents Chem.* 58, 4573–4582. doi: 10.1128/AAC.02463-14

Oestergaard, L. B., Schmiegelow, M. D., Bruun, N. E., Skov, R. L., Petersen, A., and Andersen, P. S. (2017). The associations between socioeconomic status and risk of *Staphylococcus aureus* bacteremia and subsequent endocarditis–a Danish nationwide cohort study. *BMC Infect. Dis.* 17:589. doi: 10.1186/s12879-017-2691-3

Pereira, Z. V., Carvalho-Okano, R. M., and Garcia, F. C. P. (2006). Rubiaceae juss. da reserva florestal mata do paraíso, viçosa, MG, Brasil. *Acta Bot. Brasilica* 20, 207–224. doi: 10.1590/S0102-33062006000100020

Pillai, S. K., Moellering, R. C., and Eliopoulos, G. M. (2005). "Antimicrobial combinations," in *Antibiotics in Laboratory Medicine*, ed. V. Lorian (Philadelphia, PA: Lippincott Williams and Wilkins), 365–440.

Pinto, N. C. C., Campos, L. M., Evangelista, A. C. S., Lemos, A. S. O., Silva, T. P., and Melo, R. C. N. (2017a). Antimicrobial *Annona muricata* L. (soursop) extract targets the cell membranes of Gram-positive and Gram-negative bacteria. *Ind. Crops Prod.* 107, 332–340. doi: 10.1016/j.indcrop.2017.05.054

Pinto, N. C. C., Silva, J. B., Menegati, L. M., Guedes, M. C. M. R., Marques, L. B., Silva, T. P., et al. (2017b). Cytotoxicity and bacterial membrane destabilization induced by *Annona squamosa* L. extracts. *An. Acad. Bras. Ciênc.* 89, 2053–2073. doi: 10.1590/0001-3765201720150702

Plyuta, V., Zaitseva, J., Lobakova, E., Zagoskina, N., Kuznetsov, A., and Khmel, I. (2013). Effect of plant phenolic compounds on biofilm formation by *Pseudomonas aeruginosa*. *APMIS* 121, 1073–1081. doi: 10.1111/apm.12083

Ribeiro, S. M., Felício, M. R., Boas, E. V., Gonçalves, S., Costa, F. F., and Samy, R. P. (2016). New frontiers for anti-biofilm drug development. *Pharmacol. Ther.* 160, 133–144. doi: 10.1016/j.pharmthera.2016.02.006

Rolfe, M. D., Rice, C. J., Lucchini, S., Pin, C., Thompson, A., and Cameron, A. D. S. (2012). Lag phase is a distinct growth phase that prepares bacteria for exponential growth and involves transient metal accumulation. *J. Bacteriol.* 194, 686–701. doi: 10.1128/JB.06112-11

Silva, M. N., Ferreira, V. F., and Souza, M. C. B. V. (2003). Um panorama atual da química e da farmacologia de naftoquinonas, com ênfase na β-lapachona e derivados. *Quim. Nova* 26, 407–416. doi: 10.1590/S0100-40422003000300019

Silva, T. P., Noyma, N. P., Duque, T. L. A., Gamalier, J. P., Vidal, L. O., Lobão, L. M., et al. (2014). Visualizing aquatic bacteria by light and transmission electron microscopy. *Antonie Van Leeuwenhoek* 105, 1–14. doi: 10.1007/s10482-013-0047-6

Smith, P. K., Krohn, R. I., Hermanson, G. T., Mallia, A. K., Gartner, F. H., and Provenzano, M. D. (1985). Measurement of protein using bicinchoninic acid. *Anal. Biochem.* 150, 176–185. doi: 10.1016/0003-2697(85)90442-7

Stefani, S., Chung, D. R., Lindsay, J. A., Friedrich, A. W., Kearns, A. M., Westh, H., et al. (2012). Meticillin-resistant *Staphylococcus aureus* (MRSA): global epidemiology and harmonisation of typing methods. *Int. J. Antimic. Agents* 39, 273–282. doi: 10.1016/j.ijantimicag.2011.09.030

Subramani, R., Narayanasamy, M., and Feussner, K. D. (2017). Plant-derived antimicrobials to fight against multi-drug-resistant human pathogens. *3 Biotech* 7:172. doi: 10.1007/s13205-017-0848-9

Tang, Y. L., Shi, Y. H., Zhao, W., Hao, G., and Le, G. W. (2008). Insertion mode of a novel anionic antimicrobial peptide MDpep5 (Val-Glu-Ser-Trp-Val) from Chinese traditional edible larvae of housefly and its effect on surface potential of bacterial membrane. *J. Pharm Biom. Anal.* 48, 1187–1194. doi: 10.1016/j.jpba.2008.09.006

Wilson, S. E., Graham, D. R., Wang, W., Bruss, J. B., and Castaneda-Ruiz, B. (2017). Telavancin in the treatment of concurrent *Staphylococcus aureus* bacteremia: a retrospective analysis of ATLAS and ATTAIN studies. *Infect. Dis. Ther.* 6, 413–422. doi: 10.1007/s40121-017-0162-1

Wu, H., Moser, C., Wang, H. Z., Hoiby, N., and Song, Z. J. (2015). Strategies for combating bacterial biofilm infections. *Int. J. Oral Sci.* 7, 1–7. doi: 10.1038/ijos.2014.65

You, Y. O., Choi, N. Y., Kang, S. Y., and Kim, K. J. (2013). Antibacterial activity of Rhus javanica against methicillin-resistant *Staphylococcus aureus*. *Evid. Based Complement. Alternat. Med.* 2013, 1–8. doi: 10.1155/2013/549207

Yuan, W., and Yuk, H. G. (2018). Antimicrobial efficacy of *Syzygium antisepticum* plant extract against *Staphylococcus aureus* and methicillin-resistant *S. aureus* and its application potential with cooked chicken. *Food Microbiol.* 72, 176–184. doi: 10.1016/j.fm.2017.12.002

Conflict of Interest Statement: The authors declare that the research was conducted in the absence of any commercial or financial relationships that could be construed as a potential conflict of interest.

ANEXO 5

Hindawi
Evidence-Based Complementary and Alternative Medicine
Volume 2019, Article ID 8263934, 9 pages
https://doi.org/10.1155/2019/8263934

Research Article

Cecropia pachystachya Leaves Present Potential to Be Used as New Ingredient for Antiaging Dermocosmetics

Maria Fernanda Fernandes,[1] Jessica Leiras Mota Conegundes,[1] Nícolas de Castro Campos Pinto,[1] Luiz Gustavo de Oliveira,[2] Jair Adriano Kopke de Aguiar,[2] Elaine Maria Souza-Fagundes,[3] and Elita Scio[1]

[1]*Laboratory of Bioactive Natural Products, Department of Biochemistry, Federal University of Juiz de Fora, 36036-900 Juiz de Fora, MG, Brazil*
[2]*Glycoconjugate Analysis Laboratory, Department of Biochemistry, Biological Sciences Institute, Federal University of Juiz de Fora, 36036-900 Juiz de Fora, MG, Brazil*
[3]*Department of Physiology and Biophysics, Biological Sciences Institute, Federal University of Minas Gerais, 31270-901 Belo Horizonte, MG, Brazil*

Correspondence should be addressed to Elita Scio; elita.scio@ufjf.edu.br

Received 31 August 2018; Revised 21 February 2019; Accepted 24 March 2019; Published 3 April 2019

Academic Editor: Fatima Martel

Several biological activities have been reported for leaf extracts of *Cecropia pachystachya* species, including antioxidant and wound healing activities. This study aims to report, for the first time, the antiaging potential of the hydroethanolic (HE) and the ethanolic (EE) extracts obtained from the leaves of *C. pachystachya* using different *in vitro* assays. Both HE and EE presented relevant antioxidant capacity in different models, including phosphomolybdenum, 1,1-diphenyl-2-picryl-hydrazyl (DPPH), carotene/linoleic acid bleaching, and thiobarbituric acid reactive substances (TBARS) assays. Their ability to prevent the production of advanced glycation end products (AGEs) was also evaluated, and both extracts showed important activity, especially HE. The extracts also stimulated the fibroblasts proliferation *in vitro*, specialized cells that produce several mediators which maintain the skin integrity and youthfulness. Cytotoxicity of the extracts was not observed for this lineage or HEK-293, human embryonic kidney cells widely used to evaluate cytotoxicity of chemical compounds. HE also exhibited the ability to inhibit the collagenase (metalloproteinase MMP-2) and elastase activities. The total phenolic and flavonoids contents were also determined. HPLC analysis revealed the presence of the flavonoids orientin and iso-orientin, which were quantified to be used as chemical markers. The results suggested that the extracts of *C. pachystachya* leaves present the potential to be used in dermocosmetic formulations to prevent the skin aging process, which attracts the attention of pharmaceutical companies and researchers interested in the development of novel ingredients likely to be used as active principles in antiaging products.

1. Introduction

The normal functions and the natural appearance of the skin are severely affected by age and by many factors from the external environment which accelerate the skin aging, including ultraviolet radiation and pollution [1]. Nowadays, the search for new dermocosmetics capable of preventing and treating the skin aging process is gaining attention due to the increase in life expectancy and to the people concern in order to maintain a young appearance [2].

The harmful central mechanism that promotes skin aging is associated with the continuous solar ultraviolet radiation exposure which induces a complex and specific sequence of cellular responses, especially related to the synthesis of reactive oxygen species (ROS), which lead to noxious stimulus to the connective skin tissue [3]. Oxidative stress is also capable of altering the regulation of cellular mediators associated with the increase of metalloproteases expression, which are enzymes responsible for the degradation of extracellular matrix constituents, including collagen and elastin [4]. Also,

ROS may promote direct oxidative damage in several cellular components, including organelle, nucleic acids, and plasmatic and mitochondrial membranes [5].

It is noteworthy mentioning that some histological changes are consequences of protein modifications secondary to oxidative reactions, including glycation reaction. For instance, dicarbonyl compounds produced by oxidative stress can bind to dermal matrix proteins, as collagen and elastin, which leads to the production of advanced glycation end products (AGEs). These chemical complexes may accumulate and accelerate the process of fibroblast apoptosis, aggravating the aging phenomenon [6, 7].

There is considerable interest in searching for new cosmetic ingredients that can be used as antiaging agents, notably those derived from natural sources [8]. In this context, the species *Cecropia pachystachya* Trécul have shown relevant potential to be used in many pharmaceutical formulations. The plant is popular known in Brazil as "embaúba","embaúva","imbaúba","umbaúba", and "tore", where the leaves are traditionally used to treat hypertension, diabetes, and pulmonary and cardiac disorders [9, 10]. Several pharmacological studies have reported the biological activities for different *C. pachystachya* leaves extracts. For instance, the methanolic extract showed significant hypotensive and anti-inflammatory activities [11, 12]. Besides, the ethyl acetate extract demonstrated strong wound healing effects [13]. It is worthy pointing out that both extracts showed significant antioxidant capacity [12, 13]. As the antiaging potential of natural substances is at least in part related to their antioxidant activity, those results are particularly impressive, as they encourage novel studies aimed to identify new extracts capable of reducing the aging process. Also, Duque et al. [13] reported that gel formulations containing ethyl acetate extract obtained from *C. pachystachya* crude extract increased the collagen deposition in rat skin wounds, which would be a relevant mode of action for a cosmetic principle.

Thus, the primary objective of this study was to assess the antiaging potential of *C. pachystachya* extract by evaluating its antioxidant, antiglycant, and its capacity to inhibit enzymes involved in skin aging like elastin and collagen. Ethanol and a mixture of ethanol-water were used as solvents as they are more feasible for dermal application in human skin, due to the lack of toxicity.

2. Materials and Methods

2.1. Reagents and Standards. Folin–Ciocalteu phenol reagent, 1,1-diphenyl-2-picrylhydrazyl (DPPH), 2,6-di-tert-butyl-4-methylphenol (BHT), β-carotene, linoleic acid, Tween 20, quercetin, orientin, iso-orientin, aminoguanidine, fructose, elastase, N-succinyl-Ala-Ala-Ala-p-nitroaniline, and collagenase were purchased from Sigma (St. Louis, MO, USA). Thiobarbituric acid (TBA) was purchased from Acros Organics (New Jersey, NJ, USA). All solvents used for HPLC analysis were HPLC grade from Tedia Company (Fairfield, OH, USA). Commercial chow was from Nuvital (Colombo, PR, Brazil). All other reagents were of the highest quality available.

2.2. Plant Material. *C. pachystachya* leaves were collected in Juiz de Fora, Minas Gerais state, Brazil, in August 2016. The plant was identified by a botanical specialist. A voucher specimen (CESJ 46591) was deposited at the Leopoldo Krieger Herbarium for future evidence (Federal University of Juiz de Fora).

2.3. Extract Preparation. Before the extraction process, the leaves were dried at 40°C and powdered using a knife mill (Marconi MA048, Piracicaba, SP, Brazil). The chemical constituents were extracted by maceration using two extractive solvents (ethanol 98% or ethanol: H_2O 75:25) at a ratio of 1 g of powdered leaves to 10.5 ml of extractive solvent. For the ethanolic extract (EE), a maceration was accomplished for four days at room temperature, and then the solvent was evaporated using a rotatory evaporator (Tecnal, Araras, SP, Brazil) at 40°C. The hydroethanolic extract (HE) was obtained by heating the maceration system at 60°C for 30 min and then freeze-dried. Both extracts were kept in tightly stoppered bottles under refrigeration until the experimental procedures.

2.4. Total Phenolic Content. The total phenolic content was determined by the Folin–Ciocalteu method with some modifications [15]. This assay is based on a colorimetric oxidation/reduction reaction of phenolic compounds [16]. Both EE and HE were diluted in methanol in order to obtain a 500μg/mL solution. Then, 120 μL of Folin–Ciocalteu reagent, 100 μL of calcium carbonate (4% m/v), and 30 μL of the extract solutions were added in a 96-well plate. After 30 min of incubation time, the absorbance was measured at 770 nm using a spectrophotometer (Thermo Fisher Scientific, Waltham, MA, USA). The phenolic content was calculated using a calibration curve of tannic acid standard solutions (0.0075–0.2 mg/mL) and expressed as μg of tannic acid equivalents (TAEs) per milligram of extract. All measurements were performed in triplicate.

2.5. Total Flavonoids Content. The amount of flavonoids was determined by aluminum chloride reagent assay, as described by Dowd [17], with slight modifications. Briefly, aliquots of 0.25 mg/ml of EE, HE, or reference standards were added to 0.25 ml of 2% aluminum chloride solubilized in a 0.5 ml of 5% acetic acid ethanolic solution. Then, 250 μL was added to a 96-well plate (EE and HE at final concentration of 0.0625 μg/mL). After 30 min of incubation time at room temperature, the absorbance was measured at 415 nm in a spectrophotometer (Thermo Fisher Scientific, Waltham, MA, USA). Water was used as blank control. Quercetin was used as reference standard for a calibration curve, which was constructed with seven points (1-320 μg /mL). The total flavonoids content was determined in triplicate, and the results were expressed as the total amount of flavonoids (mg/g extract) in quercetin equivalents (QE).

2.6. HPLC Analyses. High-performance liquid chromatography was accomplished for orientin and iso-orientin quantification, using HPLC Agilent 1200 Series (Agilent Technologies, Santa Clara, CA, USA) at 25°C. An automatic injector and a Zorbax SB-C18 column 50 mm x 4.6 mm x 5 μm were used. The mobile phase was consisted of a gradient elution of

Table 1: Gradient elution used as the mobile phase for HPLC analysis.

Elution time (min)	Solvent		Flow rate
	Methanol	Water	
0	5%	95%	
5	33%	67%	0.8 mL/min
30	37%	63%	

methanol: H_2O, as described in Table 1. The flow rate used was 0.8 ml/min, and the detection was performed using a DAD 254 nm detector. The injection (20 μl) was performed in triplicate.

2.7. Antioxidant Activity

2.7.1. Phosphomolybdenum Method. The total antioxidant activity was evaluated by the phosphomolybdenum method according to Pierto et al. [18] with slight modification. Aliquots of 0.3 mL of EE and HE at 2 mg/mL was combined with 2 mL of a reagent solution (3 M sulfuric acid, 100 mM sodium phosphate, and 30mM ammonium molybdate). The absorbance was read at 695 nm after 90 min of incubation time at 95°C in a spectrophotometer (Thermo Fisher Scientific, Waltham, MA, USA). Ascorbic acid was used as the reference standard. The total antioxidant capacity was expressed as milligrams of HE or EE equivalent to 1 mg of ascorbic acid, using a seven-point standard calibration curve (50-300 mg/mL),

2.7.2. DPPH Assay. The radical 1,1-diphenyl-2-picryl-hydrazyl (DPPH) was used for the determination of free radical-scavenging activity of both extracts [19]. Fifty microliters of HE or EE diluted in methanol at different concentrations (0.49–250 μg/mL) were added to a 50 μL of a methanolic DPPH solution (20 μg/mL). After 30 min of incubation time, the absorbance was measured at 517 nm. The experiment was carried out in triplicate. Ascorbic acid was used as the reference standard. IC_{50} values were calculated using the software GraFit Version 5 (Erithacus Software, Horley, UK) and indicated the concentration of extract required to scavenge 50% of DPPH free radicals.

2.7.3. Carotene/Linoleic Acid Bleaching Assay. Antioxidant activity was also determined by using the β-carotene bleaching assay according to Marco [20] with slight modifications. A stock solution of β-carotene-linoleic acid mixture was prepared as follows: 100 μLβ -carotene (10 mg/mL in dichloromethane HPLC grade), 30 μL linoleic acid, and 265 μL Tween 40 were dissolved in 500 μL dichloromethane HPLC grade. Then, the dichloromethane was evaporated entirely using nitrogen gas. Also, 40 mL of oxygenated distilled water was added with vigorous shaking. Then, 250 μL of this reaction mixture was dispersed to a 96-well plate. Finally, blank, HE, EE, or quercetin (74 μg/mL), used as the reference standard, was added. The emulsion system was incubated for 2h at 45°C. The absorbance was read at 470 nm. The antioxidant activity (AA) was calculated regarding inhibition percentage relative to the control using

$$\mathrm{AA} = \left[\frac{\mathrm{R}\ control - \mathrm{R}\ extract}{\mathrm{R}\ control}\right] \times 100 \quad (1)$$

R *control* and R *extract* mean rate blanching of control (quercetin) and extract, respectively.

2.7.4. Thiobarbituric Acid Reactive Substances (TBARS) Assay. Oxidation products' synthesis was quantified using TBA reactive substances (TBARS) assay, as described by Sørensen and Jørgensen [21] with some modifications. Briefly, a mixture of 100 g of ground meat and 67 ml of distilled and deionized water with 7.5 mg/mL of each extract dissolved in methanol was thoroughly blended at room temperature until a smooth homogenate was formed. The mixture containing only meat, water, and methanol was used as the control. BHT 7.5 mg/mL dissolved in methanol was used as reference drug. Each mixture was transferred to amber jars and stored in a 5°C cold room over a period of 4 days. After this time, the percentage of meat oxidation was measured by the absorbance at 535 nm, using a spectrophotometer (Thermo Fisher Scientific, Waltham, MA, USA). The results were expressed in % oxidation inhibition. A calibration curve was prepared using malondialdehyde (MDA) standard, reacting with the TBA/phosphoric acid solution.

2.8. Antiglycant Activity. Antiglycant activity was *in vitro* determined using fructose-induced protein glycation models. The method was performed as described by Suzuki et al. [22] with some modifications proposed by Farsi et al. [23]. Stock solutions of fructose (1.6 M) and BSA (10 mg/mL) were prepared in 100 mM sodium phosphate monobasic monohydrate buffer (pH 7.4). Each solution was sterilized by vacuum filtration using Nalgene cellulose nitrate membrane filters (Fisher Scientific Ltd., Nepean, ON, CAN) before use. Incubation media containing BSA (10 mg/mL), fructose (1.6 M), sodium phosphate buffer (100mM), sodium azide (8g/L), and EE or HE at 12.5 μg/mL) were prepared. Also, solutions containing aminoguanidine or quercetin, used as reference standards, or vehicle (75% EtOH: 25% H_2O or 100% EtOH v/v) were prepared in 100 mM sodium phosphate.

After the incubation time at 37°C for 7 days, the amount of fluorescent AGEs formed was determined using a fluorimeter. The fluorescent intensity was measured at 330 nm (excitation) and 410 nm (emission). The antiglycant activity

was expressed as percentage of fluorescent inhibition, using the vehicle as control:

$$\text{AGE}(\%) = \left[\frac{(\text{F } control - \text{F } sample)}{(\text{F } control)}\right] \times 100 \quad (2)$$

F *control* and F *sample* mean fluorescence rate of control (vehicle) and extract or reference standards, respectively.

2.9. Enzymatic Activity

2.9.1. Metalloproteinase-2 Inhibition. HE was incubated with matrix metalloproteinase-2 (MMP-2) obtained from RAW 264.7 supernatant culture for 10 minutes. Inhibition of MMP-2 was achieved by zymogram (10% acrylamide-bisacrylamide solution T 30% C 2.7% and gelatin 2 mg/ml) in Tris-glycine (25 mM/192 mM) pH 8.3 containing sodium dodecyl sulphate (SDS, 0.1%). Incubation mixture (v/v) was mixed with equal amounts of 2× SDS-sample buffer containing 125 mMTris-HCl, 4% SDS, 20% glycerol, and 0.001% bromophenol blue in the absence of the nonreducing agent. After the migration, gels were washed with Triton X-100 (2%) and incubated with 50 mMTris-HCl, pH 8.2, containing 5 mM CaCl2 and 1μM ZnCl2 and for 24h at 37°C. The gels were stained by Coomassie Brilliant Blue R-250 (0.5% dye, 30% methanol, and 10% acetic acid) and destained (30% methanol and 10% acetic acid) [14]. The activity of gelatinases was evidenced as bright regions (bleached) in the gel. The software Total Lab Quant® was used to measure the intensities of the bands.

2.9.2. Elastase Inhibition. Elastase inhibition activity was determined according to the method of Bieth et al. [24] with some modifications. Two hundred microliters of 100 Mmtris-HCl buffer, 13μL of 4,4 Mm N-succinyl-ala-ala-pro-val-4-nitroanilide (MAAPVN) and 20 μL of HE were mixed and incubated for 15 min. Then, 5 μL of 0.03 units/mL elastase (optimum reactivity of the enzyme) was added and incubated for another 15 min. The absorbance was read at 410 nm in a microplate. The inhibition rate was measured by the angular coefficient of the curves related to time x substrate concentration.

2.10. Cell Proliferation Assay

2.10.1. Cell Lines. Cell line (BALBc/3T3) was acquired from the cell bank of Federal University of Rio de Janeiro. The cells were maintained in Dulbecco's modified Eagle's medium (DMEM) supplemented with the antibiotics penicillin (100 IU/mL) and streptomycin (100 μg/mL), in addition to sterile fetal calf serum (FCS) 10% at 37°C under 5% CO_2 atmosphere. The human embryonic kidney lineage, HEK293, was provided by Dr. Marcel Leist (University of Konstanz, Germany). Cells were cultured in DMEM medium (Dulbecco's Modified Eagle's medium) supplemented with 100 U/mL^{-1} penicillin and 100 mg/mL^{-1} streptomycin, and enriched with 2 mM of L-glutamine and 10% fetal bovine serum.

All lineages were incubated at 37°C in a humidified atmosphere containing 5% CO2 and split twice weekly. The cells were regularly examined regarding mycoplasma contamination and used until 20 passages.

2.10.2. Cell Viability. Cell viability in the presence of HE and EE was determined using the MTT assay [25]. Briefly, BALBc/3T3 cells (1 x 10^4 cells/well) were seeded in 96-well microplates and incubated for 24 h before the treatment. The cells were treated with various extracts concentrations (16.75; 32.5; 75; 150; and 300 μg/mL) at 37°C, 5% CO2. Assays to evaluate cytotoxicity against HEK-293 cells were performed with the same cell density/well, but with a range of seven twofold concentration dilutions (1.56-100 μg/mL). At the end of 44h of the incubation period, MTT solution (5 mg/mL in serum-free medium, 20 μL/well) was added in each well and followed by incubation for 4 h. Finally, the MTT solution was removed, and the formazan crystals formed by MTT reduction were solubilized in 200 μL of DMSO (BalBc/3T3 cells) or 200uL of 0.04M isopropanol. The absorbance was measured at 540 and 595 nm (respectively, to DMSO and isopropanol used to dissolve the formazan salt) using a microplate reader (Thermo Scientific, Waltham, MA, USA) and values were calculated in comparison to the control cells. At least, two experiments in triplicate were performed.

2.11. Statistical Analysis. The results obtained for each extract were analyzed statistically using one-way ANOVA followed by Tukey test for phosphomolybdenum, DPPH, carotene/linoleic acid bleaching, and enzymatic activity assays. Bonferroni test was used for lipid peroxidation and antiglycation activity. Results were presented as a mean± standard error. The GraphPad Prism 7.0 (GraphPad, San Diego, CA, USA) was used. Differences were considered statistically significant with $p < 0.05$.

3. Results and Discussion

3.1. Phenolic and Flavonoids Contents. Due to their antioxidant capacity, including the ability to chelate metallic ions and to scavenge free radicals, the phenolic compounds, especially flavonoids, are nowadays considered as indispensable components in a variety of nutraceutical, pharmaceutical, medicinal, and cosmetic products, including those destined to prevent the aging phenomenon [26]. Thus, for better positioning of any herbal drug intended to be used as the active principle of topical pharmaceutical formulations, it is interesting to verify its phenolic and flavonoid contents.

Although EE showed the highest total phenolic content, HE exhibited the highest total flavonoid content and higher yield (Table 2).

Flavonoids like orientin, iso-orientin, vitexin, isoquercetin, apigenin, and catechin were already identified in *C. pachystachya* leaves [27], which encouraged the HPLC analysis in the search for chemical markers.

3.2. HPLC Analysis. Although other studies have reported the identification of different flavonoids in *C. pachystachya* leaves, the HPLC analysis detected only the presence of orientin and iso-orientin. Probably, other flavonoids are present in quite small quantities in EE and HE, which may

Table 2: Yield and phenolic and flavonoids contents of the ethanolic (EE) and hydroethanolic (HE) extracts from *Cecropia pachystachya* leaves.

Extract	Yield (%)[a]	Phenolics (μg ETA/mg DE)[b]	Flavonoids (μg QE/mg DE)[c]
EE	10.37%	962.90 ±19.14	18.73± 0.12
HE	14.08%	656.16 ± 22.03	72.71± 0.92

[a]Data expressed as g of dry extract per 100 g of dried plant material.
[b]Total phenolic content was expressed as tannic acid equivalents (μg of tannic acid per mg of dried extract).
[c]Total flavonoids content was expressed as quercetin equivalents (μg quercetin equivalent/mg of extract powder).

Table 3: Amounts of orientin and iso-orientin in EE and HE.

Extract	Orientin[a] (mg/g)	Iso-orientin[b] (mg/g)
EE	23.5 ± 0.5	31.8 ± 0.9
HE	35.5 ± 1.1	64.3 ± 1.6

[a]Line equation: $y = 3611.2x - 47.859$. $R^2 = 0.9946$.
[b]Line equation: $y = 2001.4x - 0.7367$. $R^2 = 0.9997$.

Table 4: Antioxidant activity of EE and HE by phosphomolybdenum, DPPH, β carotene/linoleic acid bleaching, and TBARs assays.

Sample	TAC (EAA)	DPPH (IC_{50})	β-Carotene/Linoleic Acid Bleaching Assay (%inhibition)	MDA (%inhibition)
EE	0.49 ± 0,07	[a]1.07 ± 0.05	[a]50.82± 0.65	[a]62.65±0.38
HE	0.53± 0,08	[a]1.07 ± 0.06	[b]65.18±5.82	[b]56.08±0.51
AA	-	[b]0.28 ± 0.05	-	-
Q	-	-	[b]71.28±3.42	-
BHT	-	-	-	[c]76.80±0.67

Values expressed as mean ± standard error (n = 3). Means with equal letters in the same column are statistically the same ($p<0.05$). AA: ascorbic acid; EE: ethanolic extract; EAA: equivalent to ascorbic acid; HE: hydroethanolic extract; MDA: malonaldehyde; TAC: total antioxidant capacity.

explain why they were not detected by the HPLC DAD detector. For this reason, only orientin and iso-orientin were used as chemical markers. Both were quantified in EE and HE, as shown in Table 3.

3.3. Antioxidant Activity. It is well known that the antioxidant activities of plant extracts are commonly related to the presence of phenolic compounds. Also, flavonoids are recognized as tissue protector against reactive oxygen species (ROS) [28]. The oxidative stress may lead to harmful cellular modifications, affecting the whole body, causing a variety of disorders, including diabetes, cancer, neurodegenerative diseases, and aging acceleration [26]. As a part of the natural aging process, endogenous defense mechanisms decrease, while the production of reactive oxygen species increases, resulting in an accelerated skin aging [29].

The free radical-induced aging theory, as proposed by Harman [30], suggests that aging and aging-associated degenerative diseases could be attributed to deleterious effects of ROS on various cell components [31]. Thus, it is intuitive to hypothesize that the topical application of antioxidant compounds may, at least in part, neutralize the skin aging process, and consequently decrease or prevent the external signs of skin aging [32]. Several methods have been employed for the assessment of antioxidant activities of plant extracts; however, the efficiency cannot be accurately evaluated by a single assay [33]. For this reason, four different methods were used to evaluate the antioxidant activity of EE and HE. The results showed that both extracts presented a significant antioxidant effect, as described in Table 4.

The IC_{50} values for EE and HE obtained by DPPH test were the same, and showed a rather high radical-scavenging activity, assuming that EE and HE are crude extracts endowed with several different chemical constituents at minor concentrations, unlike ascorbic acid, which is a pure compound. The TAC test [34], performed to evaluate the total antioxidant capacity of plant extracts, also reflected the strength of both extracts as antioxidants. The β-carotene/linoleic acid bleaching and TBARs methods were used to evaluate the ability of the extracts in preventing lipid peroxidation. The results clearly demonstrated that both extracts presented a relevant activity. EE was more effective in inhibiting MDA production, while HE presented more efficacy in the β-carotene/linoleic acid bleaching assay. Those results are quite relevant, as products of lipid peroxidation may react with cell macromolecules to form adducts with significant irreversible effects on cellular functions, which promotes the aging process [35].

3.4. Inhibitory Effect on BSA Glycation. In recent years, the anti-AGE potential of natural or synthetic compounds has gained particular attention by pharmaceutical companies

Table 5: Effect of EE and HE on BSA glycation at five different concentrations.

Extract or reference standard (12.5 μg/mL)	Glycation Inhibition of BSA (%)
EE	[a]33.10% ± 0.17
HE	[b]51.30% ± 1.21
Quercetin	[c]8.01 % ± 1.26
Aminoguanidine	[d]23.79 % ± 2.68

Values are expressed as mean ± standard error of the mean (n = 3). Means with different letters in the same column shows statistical differences ($p<0.001$). BSA: bovine serum albumin; EE: ethanolic extract; HE: hydroethanolic extract.

interested in the development of novel antiaging products, as scientific studies have reported the substantial role of AGEs for the aging process [36].

AGEs are proteins to which a sugar molecule is bound, which can induce widespread tissue and cellular damage [37], as the original protein functions are inhibited. As skin contains several proteins, including collagen, the formation of these AGEs could be a viable explanation for the skin diminished functioning in aging [38]. Moreover, ROS and redox active transition metals accelerate AGEs formation [39].

The consequences of AGEs accumulation on the skin are a subject of interest in recent literature aiming at finding the causes for the old aspect of the skin and the decreased skin functions over the age. As in all organs, long-lived proteins are particularly prone to oxygenation. In the skin, this process affects mainly the dermal extracellular matrix proteins, including collagen, fibronectin, and elastin [40]. In addition, studies performed in synthetic skin revealed that the glycation process interferes with dermis metabolism, inducing to structural changes in elastic fibers, which reduce skin elasticity and increase MMPs activities [41]

In this study, the ability of EE and HE to inhibit AGEs formation was evaluated using the BSA-fructose assay, in which the bovine serum albumin is bound to fructose, leading to a glycated protein-sugar complex. The results showed that both EE and HE were capable of preventing the production of the protein-sugar complex. As described in Table 5, the extracts activities were expressive higher when compared to the reference standards (aminoguanidine and quercetin).

The antiglycation activity of the extracts, aligned to their antioxidant actions, reinforces the potential of HE and EE as possible active principle in pharmaceutical formulations intended to prevent skin aging.

3.5. Cell Viability. Dermal fibroblasts play critical functions at dermic homeostasis. Furthermore, fibroblasts can produce molecules which maintain skin integrity and youthfulness, so that substances capable of stimulating the fibroblasts proliferation may be used as ingredients in pharmaceutical formulations aimed to prevent cutaneous aging [42]. Thus, this study intended to evaluate whether the extracts are capable of inducing fibroblasts proliferation or cause any cytotoxic effects towards these cells. Cytotoxicity of the extracts was not observed for this lineage or for HEK-293 (data not shown), a human embryonic kidney cell that is

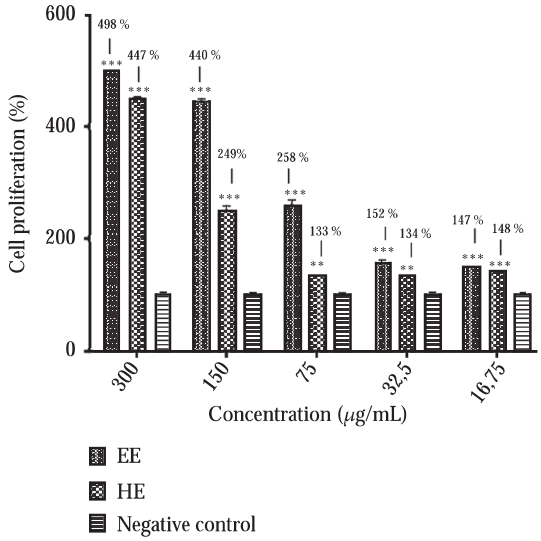

Figure 1: Percentage of $BALB_C$/3T3 fibroblasts proliferation at different concentrations (16.15 to 300 μg/mL) of EE (ethanolic extract) and HE (hydroethanolic extract) after a period of 24 h.

widely used to evaluate the cytotoxicity of compounds [43]. EE and HE were investigated over a range of concentrations (16.75 to 300 μg/mL). As shown in Figure 1, both extracts stimulated the fibroblast proliferation expressively, especially at high concentrations.

The results indicated that both extracts did not present cytotoxicity, at least at the concentrations tested, and stimulate notably the fibroblasts growth. These data corroborate to the study performed by Duque et al. [13], which reported that gels containing the ethyl acetate extract of *C. pachystachya* leaves stimulated fibroblasts proliferation and collagen deposition in rats.

3.6. Enzymatic Activity. The accumulation of free radicals in the skin is considered an inducing agent for collagenase, metalloproteinases, and elastase expression, accelerating dermal disruption [44]. Also, excessive exposure to sunlight, environmental pollution, and modern lifestyle habits, including smoking, accelerates the production of these skin enzymes, stimulating the degradation of the main components of the dermis extracellular matrix, as elastin and collagen [45].

Collagen is the most abundant protein in the extracellular matrix of the connective tissue of the human dermis [46].

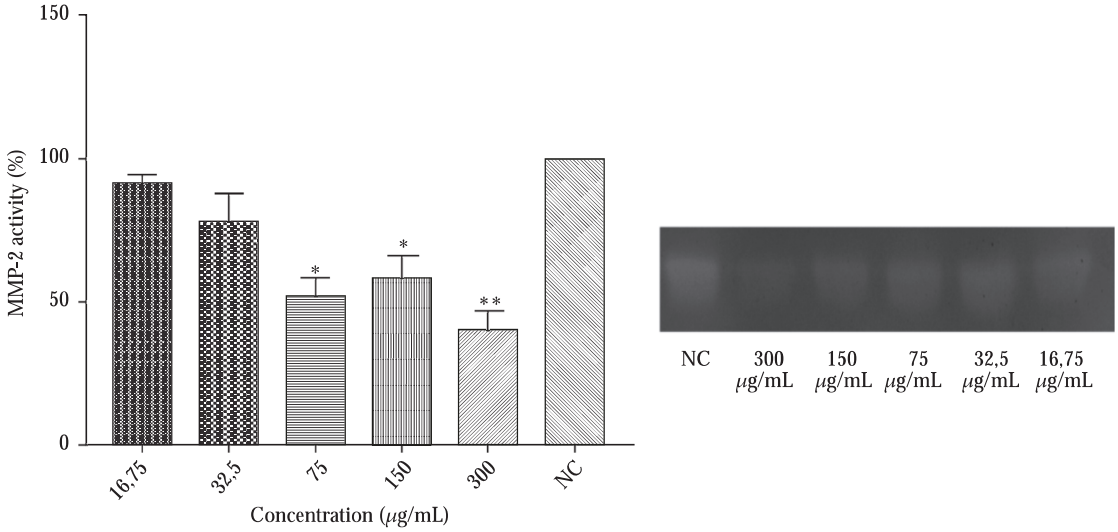

Figure 2: Inhibitory effects of hydroethanolic leaf extract (HE) on MMP-2 activity. A representative zymogram of MMP-2 activity obtained from RAW 264.7 is also shown. Electrophoresis in polyacrylamide gel at 7.5%, containing gelatin was performed. The metalloproteinase MMP-2 activities were quantified by bands densitometry and compared to the control [14]. Values expressed as mean ± standard error of the mean (n = 3). ∗ Statistically different from NC ($p<0.05$); ∗∗ statistically different from NC ($p<0.01$). NC: negative control (DMSO 0.05%).

This protein contributes to both skin strength and elasticity [47]. Elastase is a member of the chymotrypsin proteases family, which is primarily responsible for the breakdown of elastin, which is the main responsible for skin elasticity [47, 48]. Thus, compounds that can inhibit elastase and collagenase activities present potential to be used as cosmetic ingredients in pharmaceutical formulation developed to prevent skin aging, as they may reduce wrinkles formation [49].

In this context, plant extracts endowed with phenolic compounds have shown the ability to promote collagenase and elastase inhibition [44]. Flavonoids derived from plants have also the potential to bind metalloenzymes, due to their capacity to complex with metal ions [50]. Besides, Sim et al. [51] reported the structure-activity relationship of several flavonoids on collagenase (MMP-1) gene expression in UVA-irradiated human dermal fibroblasts and demonstrated that the inhibitory effect, at both the protein and mRNA level, became stronger with the increasing of OH groups on the B-ring of flavonoids.

Although EE and HE presented quite similar results in the chromatographic analysis, HE showed a total antioxidant capacity greater than EE. Besides, HE presented higher ability to inhibit AGEs production. The cell viability assay reported that at minor concentrations HE and EE showed very similar results. However, assuming that the use of low concentration of any chemical compound or natural product in pharmaceutical formulations is preferable to reduce adverse reactions and that HE showed higher TAC values and more potential to suppress AGEs production, the enzymatic assays were accomplished to evaluate the ability of HE to inhibit elastase and collagenase (matrix metalloproteinase-2, MMP-2) enzymes.

As the use of low concentrations of any active principle reduces the possibility of adverse reactions, it is reasonable to test the lowest possible concentrations in *in vitro* or *in vivo* preclinical assays. The lowest HE concentration that inhibited the elastase activity was 0.8 μg/mL; however, the lowest concentration able to inhibit MMP-2 activity was 75 μg/mL. As shown in Figure 2, HE reduced about 50% of the MMP-2 activity at 75, 150, and 300 μg/mL. HE also inhibited elastase at all tested doses, as described in Figure 3; nevertheless, the activity notably increases at 4 μg/mL, and it is only moderately higher at 8 and 16 μg/mL.

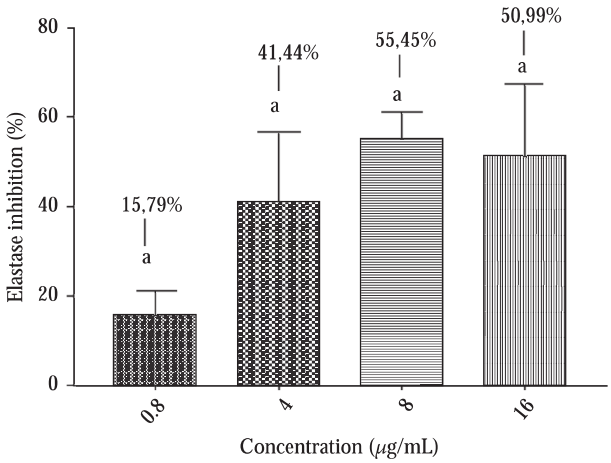

Figure 3: Inhibitory effects of hydroethanolic leaf extract (HE) on elastase activity. Gelatin zymography of MMP-2 was incubated for 24 h in the absence and presence of HE at different concentrations. Values expressed as mean ± standard error of the mean (n = 3). Equal letters represent no statistical difference ($p < 0.05$).

4. Conclusion

The antiaging potential of *C. pachystachya* leaves is reported here for the first time. The results suggested that both

ethanolic and hydroethanolic extracts are likely to be used in dermocosmetic formulations developed to prevent the skin aging process, as both extracts showed significant antioxidant and antiglycation activities. Those properties have been considered as an effective strategy to slow down human aging. Besides, the extracts were capable of inducing the proliferation of fibroblasts, which produce molecules that maintain the skin integrity and youthfulness. In addition, the hydroethanolic extract expressively reduced the activity of collagenase (MMP-2) and inhibited the elastase enzyme, which may be useful to prevent the extracellular matrix degeneration associated with the aging phenomenon.

Data Availability

No data were used to support this study.

Conflicts of Interest

The authors declare that there are no conflicts of interest regarding the publication of this paper.

Acknowledgments

The authors are grateful to FAPEMIG, CAPES, and Federal University of Juiz de Fora for scholarships and to Delfino Antônio Campos for technical assistance. This work was supported by the grant from Fundação de Amparo à Pesquisa do Estado de Minas Gerais [FAPEMIG-CEX APQ 00487-16].

References

[1] T. Quan and G. J. Fisher, "Role of age-associated alterations of the dermal extracellular matrix microenvironment in human skin aging: A mini-review," *Gerontology*, vol. 61, no. 5, pp. 427–434, 2015.

[2] M. Ramos-e-Silva, L. R. Celem, S. Ramos-e-Silva, and A. P. Fucci-da-Costa, "Anti-aging cosmetics: Facts and controversies," *Clinics in Dermatology*, vol. 31, no. 6, pp. 750–758, 2013.

[3] G. J. Fisher, S. Kang, J. Varani et al., "Mechanisms of photoaging and chronological skin aging," *JAMA Dermatology*, vol. 138, no. 11, pp. 1462–1470, 2002.

[4] T. M. Callaghan and K.-P. Wilhelm, "A review of ageing and an examination of clinical methods in the assessment of ageing skin. Part I: Cellular and molecular perspectives of skin ageing," *International Journal of Cosmetic Science*, vol. 30, no. 5, pp. 313–322, 2008.

[5] A. Han, A. L. Chien, and S. Kang, "Photoaging," *Dermatologic Clinics*, vol. 32, no. 3, pp. 291–299, 2014.

[6] R. Katta and S. P. Desai, "Diet and dermatology: The role of dietary intervention in skin disease," *Journal of Clinical and Aesthetic Dermatology*, vol. 7, no. 7, pp. 46–51, 2014.

[7] S. Radjei, M. Gareil, M. Moreau et al., "The glyoxalase enzymes are differentially localized in epidermis and regulated during ageing and photoageing," *Experimental Dermatology*, vol. 25, no. 6, pp. 492–494, 2016.

[8] N. K. Nema, N. Maity, B. Sarkar, and P. K. Mukherjee, "*Cucumis sativus* fruit-potential antioxidant, anti-hyaluronidase, and anti-elastase agent," *Archives of Dermatological Research*, vol. 303, no. 4, pp. 247–252, 2011.

[9] D. O. Souza, S. R. Tintino, F. G. Fegueredo et al., "Atividade antibacteriana e moduladora de *Cecropiapachystachya* Trécul sobre a ação de aminoglicosídeos," *Revista Cubana de Plantas Medicinales*, vol. 19, no. 1, pp. 121–132, 2014.

[10] C. D. De Souza and J. M. Felfili, "Uso de plantas medicinais na região de Alto Paraíso de Goiás, GO, Brasil," *Acta Botanica Brasilica*, vol. 20, no. 1, pp. 135–142, 2006.

[11] A. P. De Almeida, J. C. Quintela, D. S. A. Chaves, J. F. Barbosa, M. Pinto, and M. Pedroa, "The cytotoxic effect of extracts obtained from Cecropia catharinensis cuatrec (Urticaceae)," *Revista Virtual de Química*, vol. 8, no. 1, pp. 27–34, 2016.

[12] N. R. Pacheco, N. D. C. C. Pinto, J. Mello Da Silva et al., "*Cecropia pachystachya*: A species with expressive in vivo topical anti-inflammatory and in vitro antioxidant effects," *BioMed Research International*, vol. 2014, Article ID 301294, 10 pages, 2014.

[13] A. P. D. N. Duque, N. D. C. C. Pinto, R. D. F. Mendes et al., "In vivo wound healing activity of gels containing Cecropia pachystachya leaves," *Journal of Pharmacy and Pharmacology*, vol. 68, no. 1, pp. 128–138, 2016.

[14] L. G. de Oliviera, A. L. da Cunha, A. C. Duarte, M. C. M. N. Castañon, J. M. F. Chebli, and J. A. K. de Aguiar, "Positive correlation between disease activity index and matrix metalloproteinases activity in a rat model of colitis," *Arquivos de Gastroenterologia*, vol. 51, no. 2, pp. 107–112, 2014.

[15] V. L. Singleton and J. A. Rossi, "Colorimetry of total phenolics with phosphomolybdicphosphotungstic acid reagents," *American Journal of Enology and Viticulture*, vol. 16, no. 3, pp. 144–158, 1965.

[16] E. A. Ainsworth and K. M. Gillespie, "Estimation of total phenolic content and other oxidation substrates in plant tissues using Folin-Ciocalteu reagent," *Nature Protocols*, vol. 2, no. 4, pp. 875–877, 2007.

[17] L. E. Dowd, "Spectrophotometric determination of quercetin," *Analytical Chemistry*, vol. 31, no. 7, pp. 1184–1187, 1959.

[18] P. Prieto, M. Pineda, and M. Aguilar, "Spectrophotometric quantitation of antioxidant capacity through the formation of a phosphomolybdenum complex: specific application to the determination of vitamin E," *Analytical Biochemistry*, vol. 269, no. 2, pp. 337–341, 1999.

[19] M. S. Blois, "Antioxidant determinations by the use of a stable free radical," *Nature*, vol. 181, no. 4617, pp. 1199-1200, 1958.

[20] G. J. Marco, "A rapid method for evaluation of antioxidants," *Journal of the American Oil Chemists' Society*, vol. 45, no. 9, pp. 594–598, 1968.

[21] G. SØrensen and S. S. JØrgensen, "A critical examination of some experimental variables in the 2-thiobarbituric acid (TBA) test for lipid oxidation in meat products," *Zeitschrift für Lebensmittel-Untersuchung und - ForschungA*, vol. 202, no. 3, pp. 205–210, 1996.

[22] R. Suzuki, Y. Okada, and T. Okuyama, "Two flavone C-glycosides from the style of Zea mays with glycation inhibitory activity," *Journal of Natural Products*, vol. 66, no. 4, pp. 564-565, 2003.

[23] D. A. Farsi, C. S. Harris, L. Reid et al., "Inhibition of non-enzymatic glycation by silk extracts from a Mexican land race and modern inbred lines of maize (Zea mays)," *Phytotherapy Research*, vol. 22, no. 1, pp. 108–112, 2008.

[24] J. Bieth, B. Spiess, and C. G. Wermuth, "The synthesis and analytical use of a highly sensitive and convenient substrate of elastase," *Biochemical Medicine*, vol. 11, no. 4, pp. 350–357, 1974.

[25] T. Mosmann, "Rapid colorimetric assay for cellular growth and survival: application to proliferation and cytotoxicity assays," *Journal of Immunological Methods*, vol. 65, no. 1-2, pp. 55–63, 1983.

[26] A. N. Panche, A. D. Diwan, and S. R. Chandra, "Flavonoids: An overview," *Journal of Nutritional Science*, vol. 5, 2016.

[27] E. D. M. Cruz, E. R. Da Silva, C. D. C. Maquiaveli et al., "Leishmanicidal activity of Cecropia pachystachya flavonoids: Arginase inhibition and altered mitochondrial DNA arrangement," *Phytochemistry*, vol. 89, pp. 71–77, 2013.

[28] D. de Beer, E. Joubert, W. Gelderblom, and M. Manley, "Phenolic compounds: a review of their possible role as in vivo antioxidants of wine," *South African Journal of Enology & Viticulture*, vol. 23, no. 2, pp. 48–61, 2017.

[29] I. B. Allemann and L. Baumann, "Hyaluronic acid gel (Juvéderm™) preparations in the treatment of facial wrinkles and folds," *Clinical Interventions in Aging*, vol. 3, no. 4, pp. 629–634, 2008.

[30] D. Harman, "Aging: a theory based on free radical and radiation chemistry," *Journal of Gerontology*, vol. 11, no. 3, pp. 298–300, 1956.

[31] T. H. Fleming, P. M. Humpert, P. P. Nawroth, and A. Bierhaus, "Reactive metabolites and AGE/RAGE-mediated cellular dysfunction affect the aging process - A mini-review," *Gerontology*, vol. 57, no. 5, pp. 435–443, 2011.

[32] P. K. Mukherjee, N. Maity, N. K. Nema, and B. K. Sarkar, "Bioactive compounds from natural resources against skin aging," *Phytomedicine*, vol. 19, no. 1, pp. 64–73, 2011.

[33] A. Aktumsek, G. Zengin, G. O. Guler, Y. S. Cakmak, and A. Duran, "Antioxidant potentials and anticholinesterase activities of methanolic and aqueous extracts of three endemic *Centaurea* L. species," *Food and Chemical Toxicology*, vol. 55, pp. 290–296, 2013.

[34] G. Zengin, C. Sarikurkcu, A. Aktumsek, R. Ceylan, and O. Ceylan, "A comprehensive study on phytochemical characterization of Haplophyllum myrtifolium Boiss. endemic to Turkey and its inhibitory potential against key enzymes involved in Alzheimer, skin diseases and type II diabetes," *Industrial Crops and Products*, vol. 53, pp. 244–251, 2014.

[35] A. Ayala, M. F. Muñoz, and S. Argüelles, "Lipid peroxidation: production, metabolism, and signaling mechanisms of malondialdehyde and 4-hydroxy-2-nonenal," *Oxidative Medicine and Cellular Longevity*, vol. 2014, Article ID 360438, 31 pages, 2014.

[36] P. Gkogkolou and M. Böhm, "Advanced glycation end products: keyplayers in skin aging?" *Dermato-Endocrinology*, vol. 4, no. 3, pp. 259–270, 2012.

[37] R. D. Semba, E. J. Nicklett, and L. Ferrucci, "Does accumulation of advanced glycation end products contribute to the aging phenotype?" *The Journals of Gerontology. Series A, Biological Sciences and Medical Sciences*, vol. 65, no. 9, pp. 963–975, 2010.

[38] L. Van Putte, S. De Schrijver, and P. Moortgat, "The effects of advanced glycation end products (AGEs) on dermal wound healing and scar formation: a systematic review," *Scars, Burns & Healing*, vol. 2, Article ID 2059513116676828, 2016.

[39] N. Ahmed, "Advanced glycation end productsrole in the pathology of diabetic complications," *Diabetes Research and Clinical Practice*, vol. 67, no. 1, pp. 3–21, 2005.

[40] R. Bucala and A. Cerami, "Advanced glycosylation: chemistry, biology, and implications for diabetes and aging," *Advances in Pharmacology*, vol. 23, pp. 1–34, 1992.

[41] I. Sadowska-Bartosz and G. Bartosz, "Effect of glycation inhibitors on aging and age-related diseases," *Mechanisms of Ageing and Development*, vol. 160, pp. 1–18, 2016.

[42] D. H. Kim, Y. J. Je, C. D. Kim et al., "Can platelet-rich plasma be used for skin rejuvenation? Evaluation of effects of platelet-rich plasma on human dermal fibroblast," *Annals of Dermatology*, vol. 23, no. 4, pp. 424–431, 2011.

[43] S. J. Shukla, R. Huang, C. P. Austin, and M. Xia, "The future of toxicity testing: A focus on in vitro methods using a quantitative high-throughput screening platform," *Drug Discovery Therapy*, vol. 15, no. 23-24, pp. 997–1007, 2010.

[44] M. Soares, L. Velter, L. Gonzaga et al., "Evaluation of antioxidant activity and identification of phenolic acids present in the pomace of Gala variety apples," *Food Science and Technology*, vol. 28, no. 3, pp. 727–732, 2008.

[45] T. D. N. Pedrosa, A. O. Barros, J. R. Nogueira et al., "Anti-wrinkle and anti-whitening effects of jucá (*Libidibia ferrea* Mart.) extracts," *Archives of Dermatological Research*, vol. 308, no. 9, pp. 643–654, 2016.

[46] M. Masuda, K. Murata, S. Naruto, A. Uwaya, F. Isami, and H. Matsuda, "Matrix metalloproteinase-1 inhibitory activities of *Morinda citrifolia* seed extract and its constituents in UVA-irradiated human dermal fibroblasts," *Biological & Pharmaceutical Bulletin*, vol. 35, no. 2, pp. 210–215, 2012.

[47] J. Varani, R. L. Warner, M. Gharaee-Kermani et al., "Vitamin A antagonizes decreased cell growth and elevated collagen-degrading matrix metalloproteinases and stimulates collagen accumulation in naturally aged human skin," *Journal of Investigative Dermatology*, vol. 114, no. 3, pp. 480–486, 2000.

[48] N. Azmi, P. Hashim, D. M. Hashim, N. Halimoon, and N. M. Nik Majid, "Anti-elastase, anti-tyrosinase and matrix metalloproteinase-1 inhibitory activity of earthworm extracts as potential new anti-aging agent," *Asian Pacific Journal of Tropical Biomedicine*, vol. 4, pp. S348–S352, 2014.

[49] S. Jadoon, S. Karim, M. H. H. B. Asad et al., "Anti-aging potential of phytoextract loaded-pharmaceutical creams for human skin cell longetivity," *Oxidative Medicine and Cellular Longevity*, vol. 2015, Article ID 709628, 17 pages, 2015.

[50] T. S. A. Thring, P. Hili, and D. P. Naughton, "Anti-collagenase, anti-elastase and anti-oxidant activities of extracts from 21 plants," *BMC Complementary and Alternative Medicine*, vol. 9, no. 1, p. 27, 2009.

[51] G.-S. Sim, B.-C. Lee, S. C. Ho et al., "Structure activity relationship of antioxidative property of flavonoids and inhibitory effect on matrix metalloproteinase activity in UVA-irradiated human dermal fibroblast," *Archives of Pharmacal Research*, vol. 30, no. 3, pp. 290–298, 2007.